# THE INFLUENCE OF 'NANOCLUSTER' REINFORCEMENT ON THE MECHANICAL PROPERTIES OF A RESIN-BASED COMPOSITE MATERIAL

By

ANDREW RAYMOND CURTIS

A thesis submitted to the
Faculty of Medicine and Dentistry
of the
University of Birmingham
for the degree of
**DOCTOR OF PHILOSOPHY**

Biomaterials Unit
School of Dentistry
St. Chad's Queensway
Birmingham B4 6NN

April 2008

## SYNOPSIS

The introduction of innovative filled methacrylate resin composites has revolutionised the field of aesthetic restorative dentistry and provided a clinically viable alternative to amalgam-based restorations. The mechano-physical properties and resultant clinical longevity of these materials was insufficient. To improve these properties the on-going development of resin-based composites (RBCs) has sought to modify the filler size and morphology and to improve the loading and distribution of constituent filler particles. This has resulted in the introduction of so-called 'nanofills' which possess a combination of nano- and micro-sized filler to produce a hybrid material. A variation to this approach was the introduction of 'nanocluster' particles, which are essentially an agglomeration of nano-sized silica and zirconia particles. Although these materials have demonstrated a degree of clinical and experimental success debate remains as to their specific benefit compared with existing conventionally filled systems.

Following placement RBC restorations are exposed to masticatory loading (repeated sub-critical stresses) which are typically detrimental to the clinical longevity of the material. The current study determined that RBCs reinforced with the 'nanocluster' particles possessed statistically similar or significantly increased bi-axial flexure strengths and associated Weibull moduli following pre-loading regimes which produced catastrophic failure of conventionally filled RBCs. This was attributed to the unique reinforcement provided by the 'nanocluster' particle, which were identified by a novel micromanipulation technique to possess distinctive fracture mechanisms, in addition to possessing an IPC-like structure. These acted in combination to absorb and dissipate loading stresses and to provide enhanced damage tolerance.

Near-infra-red spectroscopy was also employed to determine the water sorption and it did not identify any direct correlation between water content and extent of strength reduction. However, immersion of the materials in water and also in sodium hydroxide or ethanol highlighted that the long-term hydrolytic stability of the 'nanoclusters' was limited. This suggested that degradation of the interfacial silane layer weakened the 'nanocluster' particle causing them to act as defect centres within the resin matrix and to consequently generate a greater loss of strength. Therefore, whilst the 'nanocluster' reinforced RBCs have the potential to provide enhanced damage tolerance and improved clinical longevity the limited long-term hydrolytic stability suggests further development of hydrophilic silane coupling agents and resin monomers is required to realize these properties.

## ACKNOWLEDGEMENTS

First and foremost I would like to extent my warmest thanks to Dr Will Palin for his exceptional supervision, extensive knowledge and genuine passion for dental materials and also for his continuing encouragement throughout the course of this PhD. I am extremely grateful to Dr Adrian Shortall for his supervision and aptitude for statistics and also to Professor Peter Marquis for his supervision and providing me with the opportunity to study at the University of Birmingham. I would also like to extent my thanks to Dr Garry Fleming for his first-rate supervision during my MPhil(Qualifying) year.

I am extremely grateful to the University of Birmingham School of Dentistry for funding this PhD and to 3M ESPE and Voco for supplying the materials and the opportunity to study at the forefront of dental materials.

I would also like to express my gratitude to Dr Mike Hofmann for his rambunctious sense of humour, Mrs Sue Fisher and Dr John Wilson for their technical assistance and to Mrs Carol Liston and Mrs Carinna Chilton for their assistance dealing with the associated bureaucracy

I would like to express my thanks to Drs Liam Grover, Kevin Lily and Owen Addison who as post-graduate students introduced me to the day-to-day life of a PG student and provided those numerous and seemingly inconsequential pointers essential to completing a PhD. I would also like to thank all the PG students in the Biomaterials Unit whose friendship over the years has provided numerous moments of hilarity.

It isn't possible to complete a PhD without a close group of friends to support you, I'll not name them each individually for fear of missing someone out but needless to say they have provided distraction, laughter and a friendly face whenever needed. Finally, to Angela who has remained patient and steadfast throughout.

## TABLE OF CONTENTS

## LIST OF FIGURES

## LIST OF TABLES

# CHAPTER 1 THE DEVELOPMENT OF RESTORATIVE DENTAL MATERIALS

## 1.1 Historical Development

Modern aesthetic restorative dentistry is said to have begun in 1728 when Dr. Pierre Fauchard (1678-1761) published a discourse entitled 'The surgeon dentist: a treatise on the teeth', which in addition to describing the oral anatomy, oral pathology and operative techniques to remove carious decay also described tooth transplantation and the replacement of missing dentition [Philips 1991; Wahl, 2005]. From this point dentistry began to develop as a recognised science, with the introduction in 1756 by Dr. Philip Pfaff (1715-1767) of wax impressions of the dentition from which plaster of Paris models were produced [Wahl, 2005]. Whilst, in 1792 Dr. Nicholas Dubois de Chemant (1753-1824), following collaboration with the Parisian pharmacist Alexis Duchateau (1714-1792), patented a production process for porcelain dentures. This was followed by the introduction of the porcelain inlay in the early nineteenth century [Sugden, 1983; Philips 1991]. However, despite these advances a wide assortment of esoteric materials and techniques remained in use until the mid-nineteenth century, such techniques frequently included the complete removal of dentition. This led to the common use of dentures, although the materials used varied to a great extent and included animal teeth, ivory, Wedgwood porcelains and transplanted human teeth, which became known as 'Waterloo teeth' and originated from the Napoleonic battlefields of Europe (1803-1815). However, the use of such materials was limited as a consequence of poor fit, intrinsic staining and failure under masticatory loads [Hillam, 1990; Engelmeier, 2003a; 2003b].

The nineteenth century saw a technical revolution in dentistry with the introduction of formal training and regulation of dentistry as a profession. The development of new materials, such as vulcanised rubber in 1853 were combined with existing porcelain teeth to produce the first removable dentures [Rueggeberg et al., 2002] and the introduction and development of amalgam-based restorations in the early and mid-nineteenth century revolutionised restorative dentistry [Philips, 1991; Gelbier, 2005]. The extensive work of Dr. Greene Vardiman Black (1836-1915) during this time influenced and advanced nearly all aspects of dental research, including the production of porcelain and gold foil restorations in 1895 and the development in 1896 of a silver-amalgam alloy [Black, 1896; Cannon et al., 1985].

The pioneering work of Dr. Rafael Bowen in the mid-twentieth century led to the production of an innovative tooth-coloured, particle filled methacrylate resin-matrix which has since formed the cornerstone of modern aesthetic restorative dentistry [Bowen, 1956; 1958; 1962a; 1962b; 1964]. Modern dental techniques have subsequently stressed the retention of natural dentition whilst improved adhesive techniques and the introduction of acid-etching has improved restoration retention [Bunoincore et al., 1955; Yip & Samaranayaka, 1998]. The ensuing development and refinement of resin-based composite (RBC) materials for aesthetic restorative dentistry in the late-twentieth and early twenty-first centuries has led to a wide diversity of materials. These have included Universal RBCs intended for both anterior and posterior placement [Cobb et al., 2000], RBCs containing 'nano-sized' filler particles and described as so-called 'nanofills' [Mitra et al., 2003], highly viscous 'packable' RBCs [Leinfelder et al., 1998; Manhart et al., 2001] and also 'flowable' RBCs [Braga et al., 2005]. In addition, recent modifications to the resin matrix have sought to reduce polymerization shrinkage stresses, such materials have included, siloranes [Weinmann et al., 2005], Ormocers [Moszner et al., 2007a], thiol-ene step-growth polymers [Carisocia et al., 2005] and spiro-orthocarbonates which expand during polymerization [Ferracane, 1995] (Section 1.4.1.1).

## 1.2 Amalgam Dental Restoratives

Amalgam-based restorations have a long history as arguably the most successful and ubiquitous dental restorative material ever produced [Eley, 1997]. The first silver/mercury-amalgam was developed either in 1816 by Dr. Auguste Taveau or in 1819 by Dr. Benjamin Bell and was first recorded as being placed in 1826 by Dr. Taveau. Amalgam was the first standard filling material, consisting of a hand-mixed 'silver paste', although it was commercially introduced as the 'Royal Mineral Succedaneum' in 1833 by the itinerant Crawcour brothers in New York who advertised "cheap, painless and fast fillings" [Pain, 2001]. Unfortunately early amalgams engendered a poor reputation as a consequence of inconsistencies in the mixing technique, post-operative pain following placement over existing untreated carious teeth and the unscrupulous behaviour of some practitioners. Consequently, in 1845 the placement of amalgam was prohibited by the American Dental Association (ADA) due to poor technique, lack of regulation and toxicity concerns related to mercury [Eley, 1997]. This instigated the first

'amalgam war' (1841-1855) and lead to stringent testing of clinical efficacy and eventual standardisation of amalgams. The prohibition of amalgam was gradually rescinded as the threatened adverse health effects failed to occur [Roulet, 1997; Eley, 1997; Meskin, 2001]. In 1855, the work of Dr. J. Foster Flagg (1828-1903) in testing different amalgam formulations for posterior restorations [Hyson, 2006] and later of Dr. Black in 1896 resulted in a standardized formula of 67% silver, 27% tin, 5% copper and 1% zinc by mass [Black, 1896]. The second amalgam war began in 1926 when Dr. Alfred Stock expressed concern regarding the health of dental practitioners due to mercury vapour released during preparation of the amalgam for placement. It would appear that this concern was vindicated as a new amalgam formulation was subsequently introduced which removed the hazardous requirement to heat the original amalgam formulation prior to placement [Dodes, 2001]. The third amalgam war began in the late 1970s when Dr. Hal Huggins attributed a wide variety of systemic and chronic illnesses to mercury release from amalgam, the subsequent debate was especially intense in Scandinavia, the USA and Germany [Dodes, 2001]. In 1997 the FDI World Dental Federation and the World Health Organisation (WHO) and also in 1998 the ADA's Council on Scientific Affairs stated that amalgam was a safe and effective restorative material [7$^{th}$ ICMGP, 2004].

### 1.2.1 Constituents of amalgams

The low-copper conventional amalgam introduced by Dr. Black in 1896 has been rendered redundant by the introduction of the 'modern' high-copper amalgam in 1963 which eliminates the presence of the tin-mercury $\gamma_2$ phase known to cause excessive marginal fracture described as 'ditching', inferior corrosion resistance and strength loss [Jørgensen, 1970; Mahler, 1997; Eley, 1997; Fleming et al., 2001]. The main constituent of the amalgam alloy was $Ag_3Sn$($\gamma$ phase), which was triturated with mercury to produce a plastic mass that set by the formation of $\gamma_1$ and $\gamma_2$ phases, although residual $\gamma$ phase particles remained embedded within the $\gamma_1$ and $\gamma_2$ phase matrix of the set amalgam (Equation 1.1) [Philips, 1991; Eley, 1997],

$$Ag_3Sn_{(\gamma\ phase)} + Hg \rightarrow Ag_2Hg_{3(\gamma 1\ phase)} + Sn_{7\text{-}8}Hg_{(\gamma 2\ phase)} + Ag_3Sn_{(\gamma\ phase)} \qquad \text{Equation 1.1.}$$

High-copper amalgams contained an alloy powder of spherical Ag-Cu and lathe-cut Ag-Sn particles [Youdelis, 1967], with a copper content of 13-20%. High-copper amalgams were

identified to posses improved mechanical properties, corrosion resistance and marginal integrity in clinical trials compared with the preceding low-copper amalgams [Eley et al., 1997] (Table 1.1).

| | **Low-copper amalgams** | **High-copper amalgams** |
|---|---|---|
| **Compressive strength (MPa)** | 227-366 | 340-516 |
| **Tensile strength (MPa)** | 51-55 | 43-56 |
| **Creep (%)** | 1.5-6.3 | 0.09-0.45 |
| **Dimensional change (µm/cm)** | -10.6-19.7 | -1.9-8.8 |

**Table 1.1. The mechanical properties (MPa), creep (%) and dimensional change (µm/cm) of the now defunct low-copper amalgam compared with high-copper amalgam, following 1 week setting. Table adapted from Malhotra & Asgar (1978).**

Two types of high-copper amalgam are available, namely 'admixed' consisting of silver and silver-tin or 'single composition' consisting of a ternary silver-copper-tin alloy. The 'admixed' amalgam contains high-copper spherical silver-copper particles consisting of silver-rich and copper-rich phases and low-copper lathe-cut particles. The initial setting reaction of 'admixed' amalgam is the same as that of low-copper (Equation 1.1) whilst the secondary solid-state reaction occurs according to Equation 1.2.

$$Sn_8Hg_{(\gamma 2\ phase)} + Ag_5Cu_{2(eutectic)} + Hg \rightarrow Ag_2Hg_{3(\gamma 1\ phase)} + Cu_6Sn_{5(\eta\ phase)} \qquad \text{Equation 1.2.}$$

The high-copper 'single composition' amalgam contains a high quantity of spherical $Cu_3Sn$(ε phase) dispersed throughout the $Ag_3Sn$(γ phase). Following mixing with liquid mercury the ε and γ phases diffuse onto the surface of the mercury particles and $Ag_2Hg_3$(γ1 phase) and $Cu_6Sn_5$(η phase) are formed (Equation 1.3),

$$Ag_3Sn_{(\gamma\ phase)} + Cu_3Sn_{(\varepsilon\ phase)} + Hg \rightarrow Ag_2Hg_{3(\gamma 1\ phase)} + Cu_6Sn_{5(\eta\ phase)} \qquad \text{Equation 1.3.}$$

The reaction of mercury in either 'admixed' or 'single composition' high-copper amalgam results in the $Cu_6Sn_5$(η) phase rather than the $Sn_{7\text{-}8}Hg(\gamma_2)$ phase produced during trituration of low-copper amalgams. However, small quantities of both residual $\gamma_2$ phase (<1%) and mercury,

prompting toxicity concerns, remain within high-copper amalgams [Eley, 1997; Powers & Sakaguchi, 2007]. The mechanical trituration of the alloy powder and liquid mercury standardized the amalgamation process and ensured homogeneous distribution of alloy particles, although completion of the setting reaction takes several days to a week and subsequently the mechanical properties improve with time (Table 1.2) [Mitchell & Okabe, 1996].

| | **Low-copper amalgams** | | **High-copper amalgams** | |
|---|---|---|---|---|
| | **1h** | **1 week** | **1h** | **1 week** |
| **Compressive strength (MPa)** | 45-141 | 227-366 | 118-292 | 340-516 |
| **Tensile strength (MPa)** | 3.2-4.7 | 51-55 | 3.0-8.5 | 43-56 |

**Table 1.2. The compressive and tensile strength (MPa) of low- and high-copper amalgams following 1h and 1 week setting time, highlighting that mechanical properties change with time. Table adapted from Malhotra & Asgar (1978).**

The alloy particles possess either an irregular or spheroidal morphology and respectively are produced by lathe-cutting or gas-atomization. The lathe-cut particles are cut and ball milled to produce particles of 60-120μm length, 10-70μm width and 10-35μm thickness which are subsequently described as 'fine-cut'. In contrast, spheroidal particles are produced by melting of the alloy which is sprayed under a high pressure inert gas, such as argon, through a fine crack, to form particles with a diameter of 2-43μm [Powers & Sakaguchi, 2007]. Following setting the alloy particles are embedded within a mercury matrix forming an intermetallic metal-matrix composite [Mitchell & Okabe, 1996], the particles are covered by a 2-3μm thick reaction layer, described as the 'Asgar-Mahler reaction zone', which consists of ultrafine $\gamma_1$ and $\eta$ phase crystals [Johnson et al., 1969; Mitchell & Okabe, 1996]. In high-copper amalgams the addition of spherical silver-copper particles to the irregular lathe-cut particles were identified to act as strong fillers, consequently strengthening the amalgam matrix and thus improving the mechanical properties compared with the low-copper amalgams [Philips, 1991; Mahler, 1997].

### 1.2.2 The gradual demise of amalgam

Despite the clinical success of amalgam-based restorations their routine placement is gradually decreasing due to continuing concern regarding alleged mercury toxicity and environmental considerations arising from disposal [Hörsted-Bindslev, 2004]. In addition, patient

driven demand for aesthetic restorations which mimic the appearance of natural dentition has risen dramatically [Whitters et al, 1999; Burke, 2004; Roeters et al., 2004; Opdam et al., 2007]. Subsequently, the use of amalgam is decreasing annually across the globe, albeit at different rates [Roeters et al., 2004; Opdam et al., 2007]. A comparison between UK and Australian dental practitioners highlighted that the use of amalgam decreased 9% faster in Australia (59%) compared with the UK (50%) over the same five year period [Burke, 2004]. The placement of amalgam restorations is generally not restricted, although Sweden, Norway, Austria and Germany recommend that amalgam not be placed in pregnant women, whilst Sweden has stated its aim to phase out the use of amalgam [Burke, 2004]. This suggests that a considerable shift away from the use of amalgam has occurred. An extensive study of Norwegian clinicians also reported a reduction in the previously widespread placement of amalgam to 32% compared with an increase in RBC restorations to 40% of placements [Mjör et al., 1999]. Furthermore, from 1st January 2008 the Norwegian government has enacted a ban on the production, import, export, sale and use of mercury containing substances including dental amalgam, due to concerns regarding environmental mercury pollution. Unsurprisingly many eminent dental material researchers have been appalled at this apparent travesty, pointing out that 50% of environmental mercury pollution comes from natural sources and 42% from burning fossil fuels whilst only 0.2% at most originates from sources related to dental amalgam [Jones, 2008].

#### 1.2.2.1 Toxicity of amalgam

A number of systemic and chronic illnesses have been attributed to the alleged toxicity of mercury-based amalgams, however no sound scientific evidence of this association exists [Roulet, 1997; Meskin, 2000]. These toxicity concerns have arisen as mercury in high concentrations is neurotoxic and nephrotoxic and adversely affects the respiratory, cardiovascular, reproductive and gastrointestinal systems [Horsted-Bindslev, 2004]. The release of mercury from amalgams has been identified to occur in three main forms, namely as vapour, mercury-oxide and as methyl mercury compounds. However, whilst the occurrence of mercury release is accepted, dispute exists as to whether the quantity released is significant [Langworth et al., 1997; Mackert & Burglund, 1997; Whitters et al., 1999]. A recent review by Horsted-Bindslev, (2004) highlighted that mercury concentration in the urine of dental practitioners who routinely place amalgam restorations ranged from 3-40µg/l, compared with the considerably

lower range of 1-5µg/l for members of the general public, although it was not stated whether the general public included those with or without amalgam restorations or their occupation. WHO guidelines stipulate an occupational mercury exposure limit of 80µg/l so levels remain below toxicological concentrations, however it has been suggested that cumulative exposure may prove detrimental [Langworth et al., 1997; Meskin, 2000; Spencer et al., 2000; Horsted-Bindslev, 2004].

It is also interesting to note that psychosomatic studies have highlighted a psychological 'fear' of amalgam, identifying that the vast majority of patients complaining of amalgam related health problems suffered pre-existing psychiatric disorders. Also, no correlation was identified between the severity of symptoms reported by these patients and the measured mercury levels [Bratel et al., 1997a; 1997b]. However, despite the lack of any vigorous scientific study highlighting a link between amalgam restorations and chronic illnesses attributed to mercury release, the use of amalgam has continued to decline [Meskin, 2000].

#### 1.2.2.2 Clinical longevity

The clinical longevity of amalgam and RBC restorations has been identified to vary greatly between studies and to be influenced by the presence of occluding surfaces and also technique sensitivity and operator induced variability [Mjör et al., 1997; Manhard et al., 2004; Lucarotti et al., 2005]. An extensive review conducted by Mjör et al. (1997) of the reasons for replacement of amalgam and RBC restorations carried out by Swedish general dental practitioners (GDPs), irrespective of the class of restoration, highlighted a median clinical longevity of nine years for amalgam restorations and six years for RBCs. The study concluded that the principle reason for restoration failure was secondary caries and that this diagnosis was significantly higher for amalgam than RBCs, which generally failed due to bulk fracture [Mjör et al., 1997]. Furthermore, a comprehensive review conducted by Lucarotti et al. (2005) involving 80,000 patients and 503,965 directly placed restorations, concluded that 58% of small amalgam surface restorations survived following 10 years service, whilst only 43% of RBC restorations placed in posterior Class V lesions on the gingival third of the tooth surface survived the same period. It is also interesting to note that only 43% of the comparatively much larger mesial-occusal-distal (MOD) amalgam restorations survived following 10 years service, suggesting that size and position of the restoration will influence its longevity [Lucarotti et al., 2005]. In contrast,

Manhart et al. (2004) highlighted that whilst the range of annual survival rates of amalgam and RBC restorations placed in posterior teeth was 0.0-7.4 and 0.0-9.0% respectively, the mean annual failure rate of RBCs were lower (2.2±2.0) than that of amalgam (3.0±1.9%), although statistical analysis highlighted no significant difference between the materials [Manhart et al., 2004].

The apparently superior clinical longevity [Bogacki et al., 2002] and ease of manipulation attributed to 'packability' and 'condensability' [Cunningham et al., 1990; Tyas et al., 1998] of amalgam compared with RBC restorations may be attributed to the previous dental curriculum which emphasised the teaching of amalgam over adhesive techniques [Roeters et al., 2004; Opdam et al., 2007]. However, as dental schools reduce or eliminate the teaching of amalgam in favour of posterior RBC restorations [Roeter et al., 2004; Wilson et al., 2004; Lucarotti et al., 2005; Mitchell et al., 2007], a new generation of dental practitioners may be expected to favour the placement of RBC restorations which possess equivalent or improved clinical longevity compared with amalgams [Opdam et al., 2007].

## 1.3 The Development of Resin Based Composite Restoratives

The precursor of RBCs were acrylic resins, particularly polymethyl methacrylate (PMMA), which was introduced to the dental profession in 1936 as Vernonite and was employed for inlays, crowns and fixed partial dentures [Rueggeberg, 2002]. However, the use of PMMA-based restorations was limited due to volumetric shrinkage during polymerization, a large difference in the thermal expansion coefficient between PMMAs and the surrounding tooth, lack of colour stability, low adhesion and 'ditching'. As a consequence of these limitations a high incidence of marginal staining and recurrent caries was identified at the restoration/tooth interface [Paffenbarger et al., 1953; Rueggeberg, 2002].

The pioneering work of Dr. Rafael Bowen in the 1950s developed novel organic high molecular weight epoxy resin and methacrylate derivatives that incorporated inorganic filler particles and sought to reduce the detrimental polymerization shrinkage of the preceding PMMAs. This work resulted in a patent in 1958 of a material composed of 75% by weight of quartz or aluminosilicate glass filler and 25% by weight polymerizable resin monomer, namely the dimethacrylate formulation 2,2-bis[4-(2-hydroxy-3-methacryloxypropoxy)phenyl]propane

(bisphenol-A glycidyl methacrylate; BisGMA). Subsequently, the large molecular size and chemical structure of the difunctional BisGMA resulted in decreased polymerization shrinkage compared with PMMAs and improved the elastic modulus, tensile and compressive strengths [Bowen, 1956; Braden, 1974].

The high viscosity of BisGMA limited the filler particle loading necessitating the introduction of a lower molecular weight monomer, namely triethylene glycol dimethacrylate (TEGDMA) to reduce the viscosity of the paste and allow for increased filler loading and appropriate handling characteristics. A silane coupling agent was used to coat the glass filler particles prior to incorporation into the resin matrix to promote adhesion between the glass filler and the BisGMA/TEGDMA comonomer. Early RBCs were chemically cured via a reduction-oxidation reaction (redox) to initiate free radical polymerization [Bowen, 1956; 1958; 1962a; 1962b; 1964]. As RBCs were developed, light-activated polymerization was introduced and subsequently a photo-initiator, such as camphoroquinone, was added to promote the curing reaction, whilst the addition of an inhibitor, such as hydroquinone, was also required to increase both the shelf-life of the material and working time available to the dental practitioner during placement [Rueggeberg, 2002].

The ongoing development of RBCs has coincided with the decline in placement of amalgam restorations (Section 1.2.2) and resulted in an extensive range of polymer-based dental restorative materials of which RBCs have become seen as the dominant alternative to amalgam for the direct restoration of posterior teeth [Whitters et al., 1999].

### 1.3.1 Classification of RBCs according to filler type

RBCs are commonly classified according to the mean size of the inorganic filler particles or volume percent of filler [Lang et al., 1992; Willems et al., 1992]. The first classification system was based on the mean size of filler particles, manufacturing techniques and chemical composition of the filler [Lutz & Philips, 1983]. RBCs are frequently experimentally classified by filler extraction from the unpolymerized paste using either thermogravimetric analysis, ashing or chemical decomposition of the resin and subsequent scanning electron microscopy to determine filler load and morphology or energy dispersed x-ray spectroscopy to determine filler composition [Marshall et al., 1988; Hosoda et al., 1990; Khan et al., 1992; Lang et al., 1992; Kim & Shim, 2001; Sabbagh et al., 2004; Beun et al., 2007]. The classification of RBCs according to

filler type has produced a wide variety of classifications and sub-classifications as new RBCs have been developed and existing materials refined, although the system developed by Lutz & Philips (1983) remains the most widely accepted.

#### 1.3.1.1 Traditional

The original RBCs contained macro-sized filler particles with a mean size distribution of 10-100μm [Bowen, 1962; Lutz & Philips (1983)] and were classified as either conventional [Bowen, 1962] or traditional [Lutz & Philips (1983); Hosoda et al., 1990] RBCs, dependent upon the literature. The inorganic filler particulates were quartz, borosilicate, ceramic or glass manufactured by milling which produced particles with a splintered and irregular morphology (Figure 1.1; page 13). These particles were added to the BisGMA/TEGDMA resin matrix at approximately 70-80 weight percent (wt%) or 55-65 volume percent (vol%), to produce a paste that exhibited flexural strengths of 110-135MPa following chemical polymerization [McCabe et al., 1998]. Traditional RBCs included Concise (3M, St. Paul, MN, US) and Adaptic (Johnson & Johnson, Windsor, NJ, US) which contained a particle size range of 1-40μm [Willems et al., 1992; Sabbagh et al., 2004]. However, traditional RBCs possessed a low wear resistance as a consequence of differential wear whereby the resin loss occurred more rapidly than that of the filler. This produced large wear facets, a high degree of surface roughness and a 'dull' appearance where particles protruded from the surrounding matrix [Willems et al., 1992; Sabbagh et al., 2004]. Traditional RBCs have been replaced with products possessing improved particle distribution and which generally possess a reduced filler size [Lutz & Philips, 1983].

#### 1.3.1.2 Small particle

Small particle RBCs include both "intermediate" and "midifill" materials which possess a mean filler size range of 1-10μm [Marshall et al., 1988; Lang et al., 1992] and a filler loading of ~80wt% (60vol%) [Yap et al., 2002; Xu & Burgess, 2003]. The smaller particle size (Figure 1.1; page 13) compared with traditional RBCs sought to improve filler loading and distribution. Subsequently, small particle RBCs possessed a flexure strength of 91-102MPa [Adabo et al., 2003; Lohbauer et al., 2003a; 2003b] and a compressive strength of 285MPa [Xu & Burgess, 2003] (values taken for Ariston pHc, Vivadent, Schann, Liectenstein and classified by Yap et al. (2002) as a midifill). The first RBC indicated for posterior placement was the small particle RBC

P-10 (3M, St. Paul, MN, US), which was a development of the earlier traditional RBC Concise and possessed improved wear resistance [Leinfelder, 1995].

#### 1.3.1.3 Microfilled

Microfilled RBCs were introduced in the late 1970s and contained finely dispersed radiolucent glass spheres (Figure 1.1; page 13) with a mean size of 0.04-0.1μm produced using a chemical hydrolysis and precipitation reaction known as a sol-gel technique (Section 1.3.3) to produce colloidal silica particles [Lutz & Philips, 1983; Lang et al., 1992]. An alternative process known as flame hydrolysis was also available to produce pyrogenic silica particles, also described as fumed silica, although the particle size is higher (~0.1μm) compared with colloidal silica [Lutz & Philips, 1983; Lang et al., 1992]. Despite the high aesthetic appearance and polish retention of 'homogeneous microfills', these materials possessed a maximum filler loading of only 50-65wt% (20vol%) due to the high surface-area-to-volume ratio of the microfill particles which increased the filler surface wettability with resin. Subsequently, the admixture of higher microfill loads rapidly produced an extremely viscous paste which limited the rheological properties and ease of manipulation [Lutz & Philips, 1983; Roulet, 1987].

In order to increase the maximum attainable filler load 'hetergeneous microfills' were introduced which consisted of microfill complexes produced by grinding a pre-polymerized resin containing colloidal silica to 20-50μm sized particles which were then admixed into a resin filled with submicron colloidal silica prior to polymerization (Figure 1.1; page 13) [Lutz & Philips, 1983]. However, the maximum achievable filler loading (~50vol%) remained considerably lower than traditional RBCs [Lang et al., 1992] and microfills were identified to possess a flexural strength of 60-80MPa, subsequently contraindicating their use for posterior restorations [Lutz & Philips, 1983; Roulet, 1987; Lang et al., 1992]. The three microfill complexes were described by Lutz & Philips (1983) and Roulet, (1987) as;

- Splintered pre-polymerized: Pre-polymerized particles containing pyrogenic or colloidal silica particles were milled to produce a size distribution of 1-200μm prior to incorporation in a filled methacrylate matrix.
- Spherical polymer-based: Silica particles were incorporated into partially cured polymer spheres with a mean diameter of 20-30μm, which are loaded into the resin matrix.

- Agglomerated: Silica filler particles with a mean size distribution of 1-100nm were agglomerated into complexes via hydrolysis or precipitation and heat treated at 600°C, to produce agglomerated particles with a size distribution of 0.5-50μm described as an 'agglomerated microfill complex' (AMC) [Roulet, 1987].

A recognised contributor to the degradation and premature clinical failure of microfills was that these pre-polymerized particles were not well bonded into the matrix, as adequate covalent bonding failed to occur due to lack of available surface methacrylate groups, resulting in particle debonding under high stresses [Ferracane et al., 1995]. Furthermore, the properties of microfills remained limited by the inability to incorporate a particularly high filler loading, regardless of the presence of pre-polymerized particles, when compared with traditional RBCs.

#### 1.3.1.4 Hybrid

The development of hybrid materials has increased filler loading of RBCs and has aimed to combine the improved mechano-physical properties of microfills with higher filler loading achieved in traditional RBCs [Lutz & Philips, 1983]. Bimodal 'hybrid' materials contain two distinct filler size distributions in the same matrix (Figure 1.1) consisting of micro- or submicron-sized colloidal silica (0.01-0.05μm) particles and larger macro-sized (15-20μm) particles [Lang et al., 1992; van Noort, 2007]. A carefully graded distribution of filler size minimises gaps between particles, theoretically allowing them to fit together more efficiently and therefore maximising packing density [Darvell, 2006]. Gladys et al. (1997) identified that hybrid RBCs contain a wide diversity of filler particle sizes and distributions, suggesting that dental manufacturers load the resin matrix with one of three filler ratios, namely either an equal quantity of large and small particles or either a greater quantity of large or small particles compared with a smaller quantity of the remaining particle size. The classification of 'hybrid' is largely redundant as the majority of modern RBCs contain two distinct particle size ranges, one of which is typically colloidal silica to improve rheological properties, instead the term 'microhybrid' is routinely used to describe the majority of modern RBCs [Ferracane, 1995].

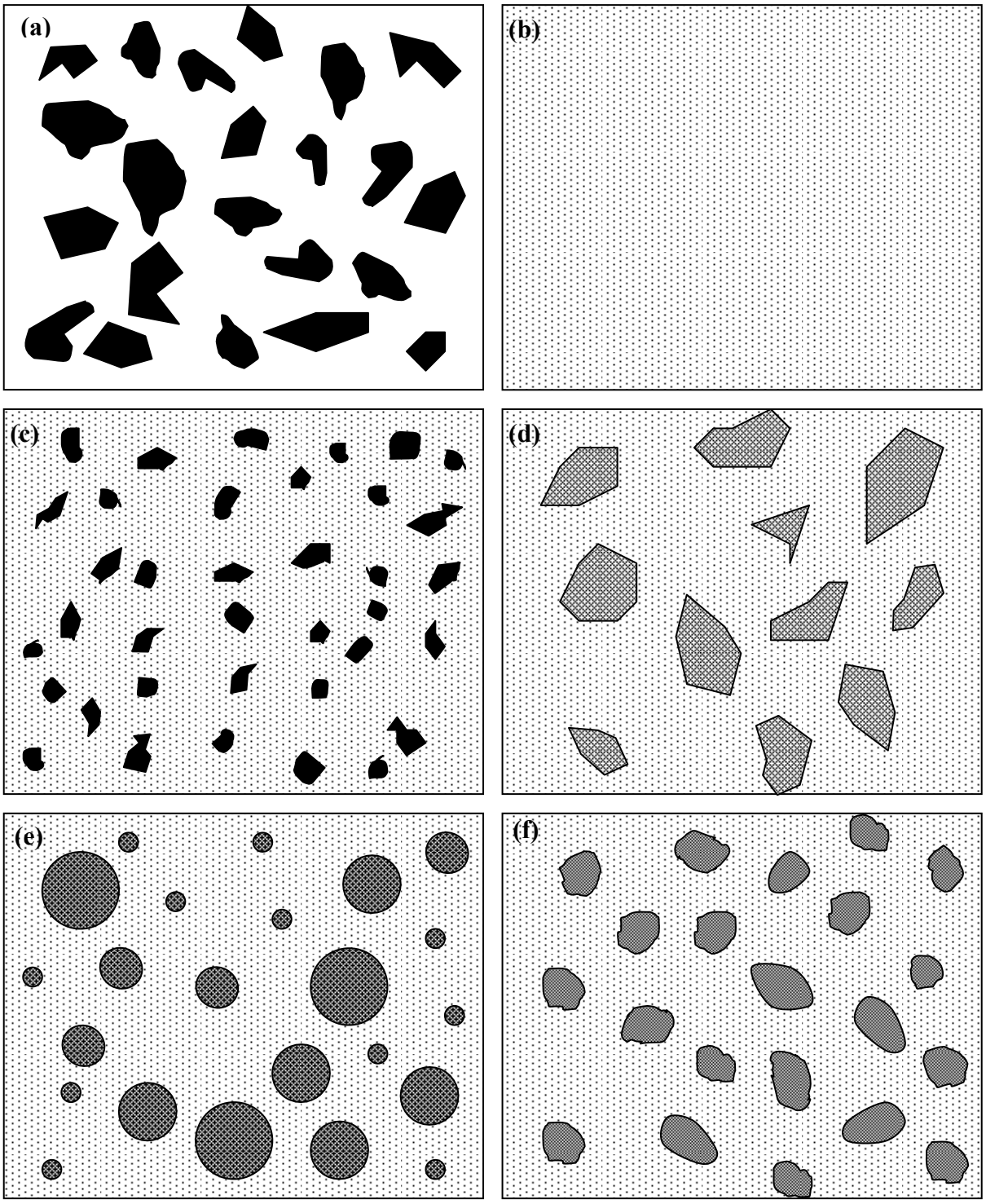


**Figure 1.1. Schematic representations adapted from Lutz & Philips, (1983), highlighting (a) traditional, (b) homogeneous microfill RBCs, (c) a hybrid containing traditional macrofills and microfills, (d) a heterogeneous microfill containing splintered pre-polymerized microfill complexes, (e) a heterogeneous microfill containing 'suspension cured' particles and (f) a heterogeneous microfill containing agglomerated microfill complexes.**

#### 1.3.1.5 Fibre-reinforced

Fibre-reinforced composite (FRC) materials offered an alternative to particulate reinforced methacrylate resin materials and have been available to restorative dentistry since the 1960s in the form of methacrylate resins reinforced with whiskers, glass fibres [Smith, 1962; Grant & Greener, 1967] or carbon fibres [Schreiber, 1971]. The fibre length has been reported to vary widely from 300µm [Willems et al., 1992] to 3mm [Garoushi et al., 2007]. However, FRCs exhibited a high degree of surface roughness and wear as a consequence of loss of fibres from the matrix [Willems et al., 1992]. Subsequently, modern FRCs have been described for use as endodontic-posts as an alternative to metal posts which cause root fractures, compromise aesthetics and risk allergic reactions [Torbjorner et al., 1995]. FRC posts contain unidirectional glass-, silica- or carbon-fibres (~60vol%) embedded in a polymer matrix, such as epoxy, to a fibre density of ~32/mm$^2$ and possess an elastic modulus of 16-40GPa [Seefeld et al., 2007; Kececi et al., 2008]. Such materials include DT Light (Vereinigte, Dentalwerke, Munich, Germany), FRC Postec Plus (Ivoclar Vivadent, Schaan, Liechtenstein) and Everstick (StickTeck Ltd., Turku, Finland).

| | Filler Particle | | Material Properties | | |
|---|---|---|---|---|---|
| | **Size (µm)** | **Volume (%)** | **Flexural Modulus (GPa)** | **Flexure Strength (MPa)** | **Compressive Strength (MPa)** |
| **Traditional** | 10-100 | 55-65 | 8.0-15.0 | 110-135 | 260 |
| **Small** | 1.0-10 | 56-61 | 10.6 | 91-102 | 285 |
| **Microfill** | 0.04 | 20-55 | 3.0-6.0 | 60-80 | 240-300 |
| **Hybrid** | 0.01-0.05 & 15-20 | 60-65 | 7.0-14.0 | 75-150 | 300 |
| **FRC** | - | 40-75 | 6.5-15.0 | 130-200 | 260-300 |

**Table 1.3. The filler size and loading and mechanical properties of traditional, small, microfill, hybrid and FRC RBCs [McCabe et al., 1998; Yap et al., 2002; Adabo et al., 2003; Lohbauer et al., 2003a; 2003b; Xu & Burgess, 2003].**

### 1.3.2 Modern RBCs

The classification of RBC materials in modern restorative dentistry has proven to be increasingly difficult. Incremental changes in both particle morphology and size [Willems et al., 1992; Beun et al., 2006] have complicated previous classifications of conventional RBCs

described in this Chapter (Section 1.3.1). Furthermore, some modern RBCs possess resin matrix chemistries modified from the original BisGMA introduced by Dr. Bowen [Asmussen & Peutzfeldt, 1998; Weinmann et al., 2005], although RBCs are not classified with regard to the resin. The continuing development, modification and refinement of the filler particles have resulted in the majority of improvements to the mechano-physical properties of RBCs, either in an attempt to improve clinical longevity or handling properties to assist placement [Ferracane, 1995; Lu et al., 2006].

#### 1.3.2.1 Universal

Modern microhybrids have also been described as 'universal' or 'all-purpose' RBCs and have been indicated for both anterior and posterior placement [Cobb et al., 2000; Manhert et al., 2001]. Universal RBCs possess appropriate filler distributions to attain a maximum loading in excess of 80wt% with a non-uniform size distribution of less than or equal to 1μm, providing flexural strengths of up to 160MPa [Mitra et al., 2003; Sabbagh et al., 2004; Lohbauer et al., 2006; Lu et al., 2006]. In addition, Cobb et al. (2000) identified that universal RBCs exhibited an increased resistance to wear and improved surface polishability compared with preceding materials. The first so-called 'universal' RBC was Herculite XR (Kerr Manufacturing Co., Bioggio, Switzerland) which consisted of barium silicate filler with a mean size of 0.6μm, an extensive range of universal materials followed including Filtek™ Z250 (3M ESPE, St Paul, MN, US) and Tetric (Vivadent Ivoclar) [Leinfelder, 1995].

#### 1.3.2.2 Packable

The introduction of high viscosity 'packable', or incorrectly termed 'condensable', RBCs has sought to provide handling properties similar to the condensability and ease of manipulation reported for amalgams (Section 1.2.2.2) [Leinfelder et al., 1998]. Commercial packable RBCs, such as SureFil (Dentsply, York, PA, US), Alert (Pentron Clinical Technologies, Wallingford, CT, US) and Solitaire (Heraeus Kulzer Inc., Armonk, MY, US), possess a filler loading in excess of 86wt% and possess a wide filler size distribution (0.04-10μm). The irregular filler morphology maximises packing efficiency and restricts flow of smaller particles to achieve the requisite viscosity higher than that of conventional RBCs [Combe et al., 2000; Nash et al., 2001]. Packable RBCs are considered by some to allow more convenient placement in posterior cavities and

produce a placement technique similar to that of amalgam [Leindfelder et al., 1999; Manhart et al., 2001]. However, whilst the mechanical properties, namely compressive strength, flexural strength and diametral tensile strength, of packable RBCs has been identified to be comparable with conventional RBCs (Table 1.3; page 14), the larger particle size was suggested by Cobb et al. (2000) to produce increased wear and surface roughness. Furthermore, syringable RBCs where shown by Opdam et al. (2002) to introduce less porosity compared with packable RBCs, whilst Loomans et al. (2006) suggests that the proximal contact tightness of Class II restorations depends more on the matrix separation technique used than the RBC viscosity.

#### 1.3.2.3 Flowable

A directly contrasting approach to high viscosity packable RBCs has been the introduction of low viscosity materials, described as 'flowable' RBCs, which contain a filler loading of 50-68wt% (<50vol%) [Combe et al., 2000]. Flowable materials have been developed and introduced to meet specific clinical requirements, such as pit and fissure sealants, repair of marginal defects, as liners in deep previously difficult to access cavities and as stress absorbing layers [Combe et al., 2000; Sabbagh et al., 2004]. Filtek™ Flow (3M, ESPE, St Paul, MN, US) contains a 68wt% (47vol%) filler loading of 0.01-6.0μm particles and has been described as possessing pseudo-plasticity prior to photoactivated polymerization [3M ESPE, Filtek™ Flow]. An alternative approach to obtaining flowable RBCs is modification of the resin matrix chemistry in addition to lower filler loading, Grandio Flow (Voco, Cruxhaven, Germany) possesses a higher filler loading of 80.2wt (65.6vol%) with a resin matrix containing a 5-ethyl-1,3-dioxane-5-yl methyl methacrylate (HEDMA) monomer. Interestingly, the addition of nanosized filler particles to some flowable RBCs, namely Grandio Flow (Voco) has been identified to produce mechanical properties, such as flexural strength, Vickers surface hardness and elastic modulus, comparable with or superior to some universal RBCs [Sabbagh et al., 2002; Beun et al., 2007].

#### 1.3.2.4 "Nanofills"

The current trend in modern RBCs of minimising filler size whilst aiming to improve the filler loading has sought to optimise the resultant mechano-physical properties and clinical performance [Ferracane, 1995]. The introduction of so-called 'nanofilled' and 'nano-hybrid' materials therefore appears a logical continuation of this trend and a number of dental material

manufacturers have marketed these as the advancement of dental materials into the field of nanotechnology [Mitra et al., 2003]. By definition, a 'nano-material' possesses components and/or structural features, such as fibres or particles, with at least one dimension in the range of 1-100nm and subsequently demonstrates novel and distinct properties [Harris et al., 2006; Lui & Webster, 2007]. However 'nano' is not a recognised classification and a considerable degree of debate and speculation exists amongst researchers [Harris et al., 2006; Curtis et al., 2008] and manufacturers [CARE, 2003] as to whether 'nano' RBCs exhibit improvements to mechano-physical properties compared with pre-existing RBCs. Notwithstanding the unremitting hype and often aggressive marketing of manufacturers, it is interesting to note that the size of fillers present in microfilled RBCs (Section 1.3.1.3) do not differ vastly from 'nano-hybrid' RBCs (Figure 1.2).

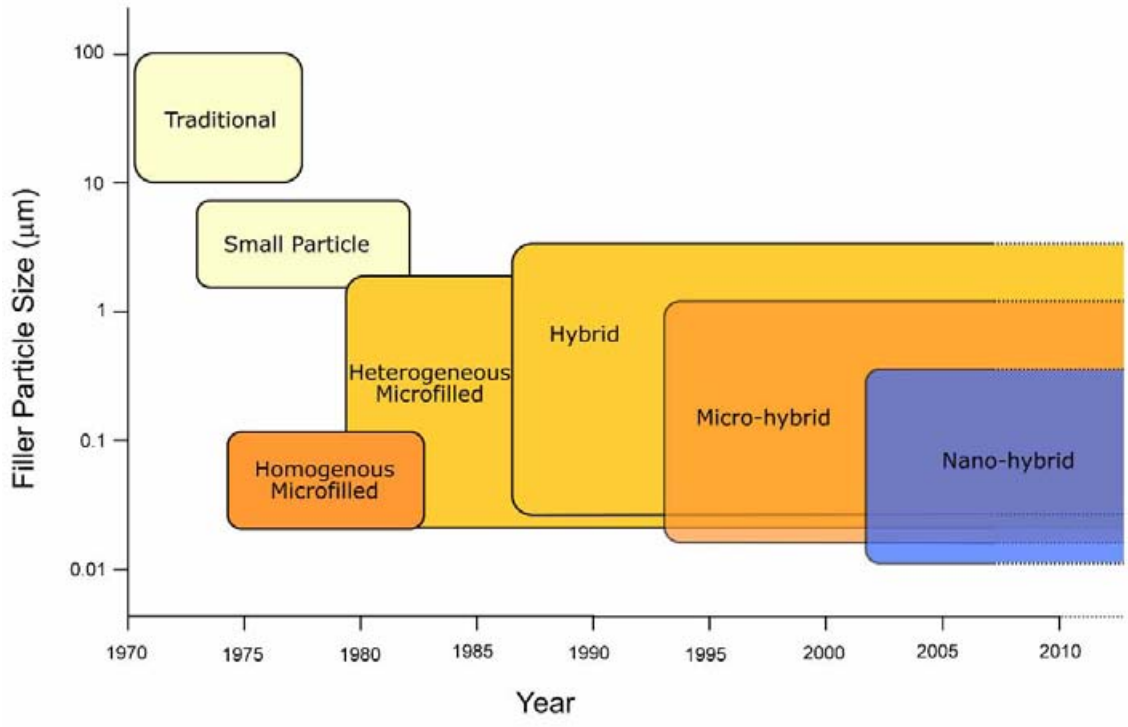


**Figure 1.2 Diagrammatic representation of the development of RBCs employed by restorative dentistry and classified according to the size of the filler particles. It is interesting to note that the size of fillers present in homogeneous microfilled RBCs do not differ vastly from that of modern nano-hybrids.**

Several approaches have been adopted by manufacturers to produce 'nanofilled' RBCs. The introduction of 'nano-hybrid' RBCs was an approach chosen by several manufactures to produce what have been described as low shrinkage and high wear resistant RBCs [Grandio

Product Specification, 2006; Tetric EvoCeram, Scientific Documentation, 2006]. Nano-hybrid RBCs contain a mixture of colloidal silica particles with a size distribution of 0.02-0.06µm (20-60nm) in addition to micron-sized filler particles of 0.1-2.5µm, such as borosilicate, admixed with a methacrylate-based resin matrix [Grandio Product Specification, 2006]. An alternative novel approach to the clinical application of 'nanofill' technology in dental restorative materials has been an RBC containing a combination of individually dispersed filler particles of 0.005-0.075µm (5-75nm) and agglomerated nanosized particles of 1.3µm, described as 'nanoclusters' [Filtek Supreme; 3M ESPE, St. Paul, MN, US] (Figure 1.3).

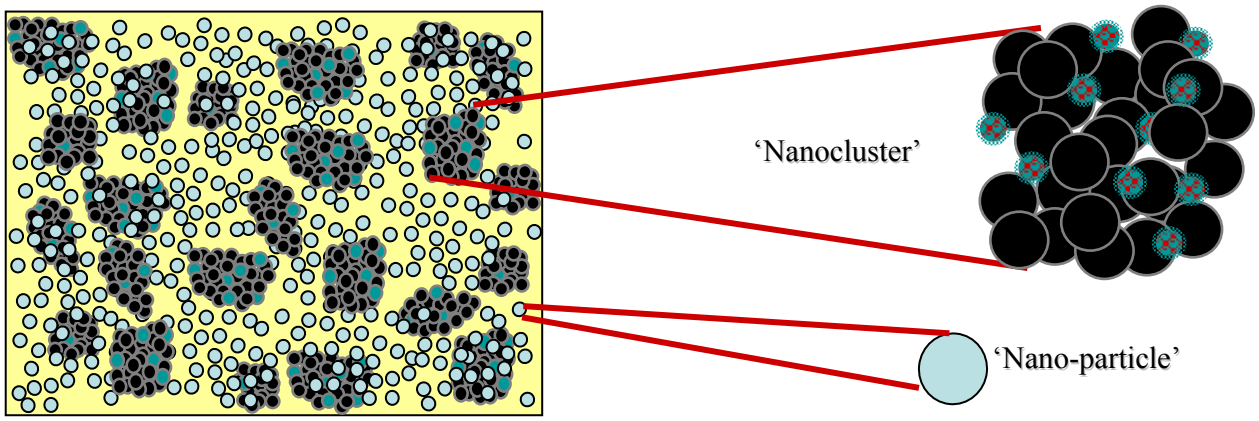


**Figure 1.3. Schematic representation of silica-zirconia nanoclusters and individually dispersed nano-sized filler particles embedded in the methacrylate resin matrix of Filtek Supreme (3M ESPE, St Paul, MN, US). Image courtesy of B. Holmes, 3M ESPE.**

The agglomerated porous clusters are partially calcined and infiltrated with a dilute silane coupling agent to ensure infiltration of the silane into the cluster interstices, a second undilute silane coupling agent was then admixed with the 'nanoclusters' prior to incorporation into the resin matrix [Private communication, S. Mitra, 3M ESPE at IADR 2007 New Orleans, US]. This material has been claimed to "possess polish retention similar to that of microfills and also to exhibit mechanical and physical properties comparable with hybrid composites" [Mitra et al., 2003]. The term 'nanocluster' may appear misleading as the agglomerated particle complexes are micron-sized and subsequently may be considered by some [Junior et al., 2008] to act as conventional microhybrid fillers.

The presence of nanosized filler particles in RBC materials have been identified to produce distinct improvements to the material, such as increased filler loading in hybrid-type materials as nano-sized particles pack more efficiently between larger particles and also a subsequent reduction in polymerization shrinkage [Grandio Product Specification, 2006]. An extensive study conducted by Beun et al. (2007) compared the flexural strength, elastic modulus, Vickers microhardness and degree of conversion of several nanofills with universal and microfill RBCs. The study concluded that the nanofills Filtek™ Supreme (3M ESPE) and Grandio (Voco) exhibited superior flexure strengths, surface hardness values and elastic moduli compared with the other RBCs tested, with the exception of Filtek™ Z100 (3M ESPE). Subsequently, both nanofill materials were indicated for posterior and anterior placement [Beun et al., 2007].

The addition of even small quantities of nano-sized silica particles has been identified to improve the mechanical properties. Tian et al. (2008) highlighted that the addition of 1 and 2.5% mass of nano-sized fibrillar silica to a BisGMA/TEGDMA resin significantly improved the flexure strengths (128 and 130MPa) compared with conventionally filled RBCs, (110 and 120MPa respectively). This was suggested to occur as a consequence of the reinforcing effect of highly separated and uniformly distributed nano-fibrillar silica, whilst the formation of agglomerates of fibrillar silica may weaken the resulting material [Tian et al., 2008]. Nanoparticles produce a more homogeneous filler distribution in low viscosity materials, such as bonding agents, which restricts 'filler settling', namely filler-rich regions within the matrix [Wilson et al., 2005]. The incorporation of nanosized filler in bonding agents also produced a more structured bond at the tooth/bonding agent interface as filler penetrates the dentine tubules to reinforce the hybrid zone [Breschi et al., 2008].

A further phenomenon contributing to the aesthetic appearance of nanofill RBCs was that such materials appear translucent as a consequence of the small size of the dispersed nano-sized filler particles [Grandio Product Specification, 2006]. This occurs as the particle size is smaller than the wavelength of incident light (400-700nm), the subsequent scattering coefficient is reduced enabling light to pass through the RBC without refraction at the interface between the resin matrix and inclusions, such as filler particles and porosity voids [Ruyter & Øysæd, 1982; Van Dijk et al., 2006; Lee, 2007].

| | Filler Particle | | Material Properties | | |
|---|---|---|---|---|---|
| | Distribution (μm) | Volume (%) | Flexural Modulus (GPa) | Flexure Strength (MPa) | Compressive Strength (MPa) |
| **Universal** | 0.2-3.0 | 60-70 | 8.8-13.0 | 80-161 | 240-290 |
| **Packable** | 0.04-10 | 59-80 | 9.0-12.0 | 85-110 | 220-300 |
| **Flowable** | 0.04-3.0 | 42-62 | 2.6-6.0 | 70-125 | 210-300 |
| **Nanofill** | 0.002-0.075 | 78.5 | 8.3-16.2 | 60-177 | 460 |

**Table 1.4. Summary of the filler size distribution and loading present in modern universal, packable, flowable and nanofill RBCs and the resulting mechanical properties [Mitra et al., 2003; Lohbauer et al., 2006].**

### 1.3.3 Filler particle production

A top-down milling technique has been widely used to produce filler particles to a minimum size of 0.1μm from larger particles [Lutz & Philips 1983]. Such particles have included quartz (silicon dioxide) which was widely available and possessed a refractive index comparable with the resin matrix. However, large quartz particles, such as ~4μm in Clearfil Photoposterior (Kuraray Dental, NY, US) caused excessive wear of the enamel of opposing teeth. Quartz is also radiolucent and early quartz fillers possessed a high level of surface roughness due to filler size which compromised aesthetics (Section 1.3.1.3). Milling of radiopaque silicate-based glasses of oxides of barium, strontium, aluminium, zirconium or zinc reduced particles to a mean size of 0.6-1.0μm [Hosoda et al., 1990; Khan et al., 1992].

The production of nano-sized fillers for conventional microfill (Section 1.3.1.3), microhybrid (Section 1.3.1.4) and modern nano-hybrid (Section 1.3.2.4) materials has required a shift from traditional top-down milling techniques to a bottom-up synthetic chemical sol-gel process. A synthetic sol-gel technique has been used to produce silicon dioxide ($SiO_2$) particles, known as colloidal silica, although the high surface-area-to-volume-ratio and subsequent low surface monomer wettability limited the filler loading of early microfills (Section 1.3.1.3). The specific sol-gel techniques used to produce dental fillers generally remain proprietary to the manufacturer, although several generic sol-gel methods are available to produce submicron colloidal silica particles. Firstly, the reaction of sodium silicate with hydrochloric acid produces sodium chloride and the formation by crystallisation of silicon dioxide particles. Secondly, burning tetrachloride in a mixture of hydrogen and oxygen gases produces colloidal silicon dioxide, also described as pyrogenic or fumed particles (‘aerosil’), with a mean size of 0.05μm

[Lang et al., 1992; Leinfelder et al., 1995]. Despite the generally proprietary nature of sol-gel techniques the 0.01-3.5μm zirconia-silica filler in Filtek™ Z100 (3M, ESPE, St. Paul, MN, US) was reported to be produced by mixing a metal carboxylate and metal oxide sol to form a gel by dehydration which was heated and then ball-milled to produce spherical fillers [Ferracane, 1995; Filtek™ Z100 Product Specification]. It is also interesting to note that the inorganic filler used in Filtek™ Z250 (3M ESPE) employed a refinement of this technique to produce a less coarse filler with an improved particle distribution [Filtek™ Z250 Product Report, 1998].

#### 1.3.3.1 Modification of filler surface

The inorganic filler particles incorporated in early RBCs were frequently not chemically bonded within the resin matrix and consequently defects were present, which resulted in the premature failure of these materials [Standford et al., 1971]. Subsequently, the surface of filler particles are coated with an organofunctional silane coupling agent prior to incorporation with the resin matrix to promote interfacial adhesion between these two otherwise incompatible constituents via a chemical bonding process known as silanization [Johannson et al., 1967; Ishida & Koenig, 1978]. The silane interface is the weakest part of RBCs as the extent of adhesion is dependent upon 'areal density', namely the number of covalent bonds per unit area, and also the uniformity of coverage of the filler surface with silane coupling agent [Darvell, 2006].

The silane coupling agent is based on methacrylate chemistry and possesses an amphilic bifunctionality, consisting of a methoxyl silane (Si-$OCH_3$) or silanol group (Si-OH) on one end and a functional methacrylate group on the other [Ferracane, 1995; Hooshmand et al., 2004]. The functionality of silane coupling agents and subsequent interfacial adhesion has been identified to be dependent upon the presence of particular functional groups, such as alkoxyl, amine or methacrylic groups [Mohsen & Craig, 1995; Matinlinna et al., 2004]. The most commonly used silane in RBCs is γ-methacryloxypropyltrimethoxysilane (γ-MPS), although other silanes, such as γ-glycidoxypropyltrimethoxysilane (γ-GPS), have also been used in some materials [Luo et al., 1997; Daniels & Francis, 1998; Debnath et al., 2004; Sabbagh et al., 2004].

Filler particles were coated with the silane coupling agent via either dry-blending of the filler and coupling agent or deposition from solution onto the particle. The functionalised filler was then blended into the methacrylate resin [Venhoven et al., 1994; Torry et al., 2006]. A study by Mohsen & Craig (1995) demonstrated that increased silane concentrations of three times that

required to provide a minimum uniform coverage, which is dependent on filler size and morphology, improved the hydrolytic stability, tensile and transverse strengths of the resulting RBC. An alternative silanization technique from the routinely employed pre-treatment of filler with silane prior to incorporation in the resin matrix required in situ filler silanization, whereby untreated filler was admixed with a silane-functional methacrylate resin [Venhoven et al., 1994]. However, this technique may produce a non-uniform or absence of silane coating on the fillers limiting the amount and absorption of silane and subsequent interfacial adhesion and clinical longevity [Nishiyama et al., 1991]. Venhoven et al. (1994) also highlighted that the advantage of silanization compared with other available coupling techniques, such as grafting or micromechanical coupling, was that the bond formation is reversible and subsequently generated less deleterious internal stresses [Venhoven et al., 1994].

The interfacial silane layer between the silica filler and silane coupling agent forms via a condensation reaction between silanol groups (Si-OH) on the silica surface and the hydrolysed silane coupling agent. Subsequent formation of siloxane bridge bonds (Si-O-Si) results in chemisorption of the silane coupling agent and the formation of a highly crosslinked siloxane film (Figure 1.5) [Söderholm & Shang, 1993; Daniels & Francis, 1998; Matinlinna et al., 2005].

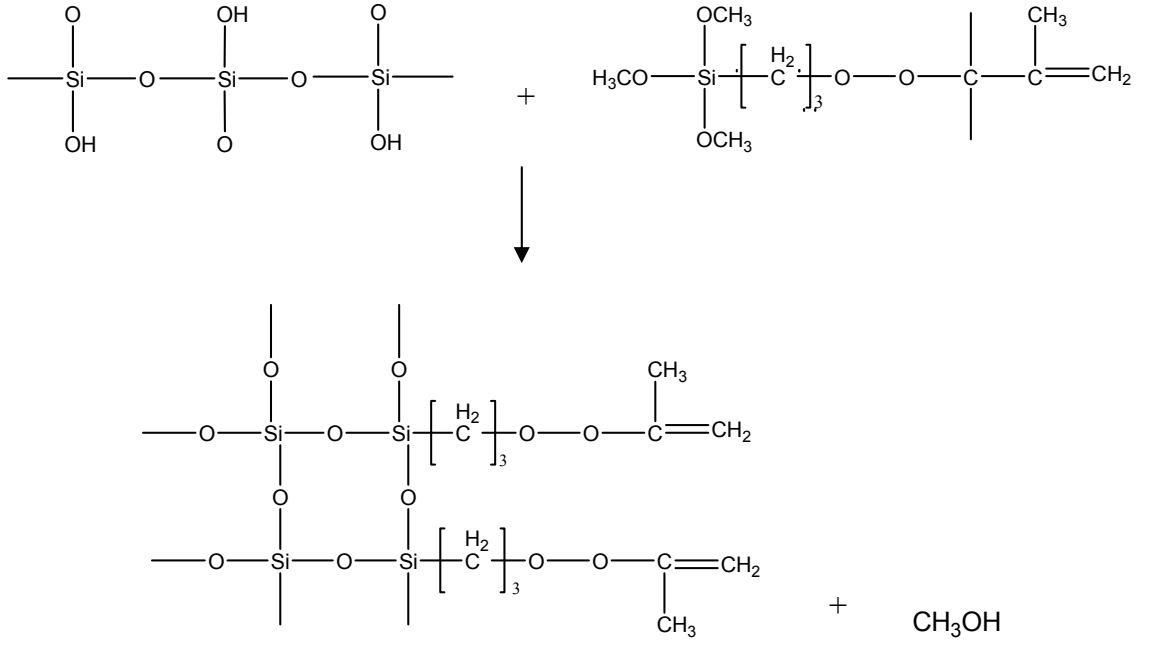


**Figure 1.4. Diagrammatic representation of silanization between the silanol groups on the filler surface and the silane coupling agent, highlighting the subsequent formation of siloxane bridge bonds between the filler and silane coupling agent.**

Simultaneously, the carbonyl group of the silane coupling agent initiates formation of hydrogen and covalent bonds with the resin constituents, producing an interpenetrating silanated network at the filler/resin interface [Söderholm & Shang, 1993; Daniels & Francis, 1998]. The silanated interfacial layer forms a multi-layered polymeric structure of variable thickness and orientation of the silane molecule, with differing extents of chemisorption and physisorption occurring throughout the interfacial layer (Section 2.1.2) [Söderholm et al., 1984; Söderholm & Shang, 1993]. Subsequently, the stability of the silane layer is also influenced by the adhesive and cohesive strength between the silane molecules themselves, whereby the propensity for hydrogen-bonding influences hydrolytic stability [Mohsen & Craig, 1995; Nishiyama et al., 1995]. In addition to improving the mechanical properties of RBCs containing silanated filler particles, silanization also improves particle dispersion and wetting [Kim & Shim, 2001; Ikejima et al., 2003; Matinlinna et al., 2004]. The silane layer has also been identified to inhibit the propagating crack-tip through the polymerized RBC structure as a consequence of absorption of masticatory loads through the silane interface [Shirai et al., 2000]. Furthermore, silane coupling agents have also been identified to increase the hydrolytic stability of RBCs [Nishiyama et al., 1991; Mohsen & Craig, 1995] due to the formation of a highly crosslinked siloxane film between the filler and resin [Matinlinna et al., 2006].

### 1.3.4 Resin matrix chemistry

The original organic resin matrix patented by Bowen, (1962a) consisted of the high molecular weight BisGMA admixed with the low molecular weight TEGDMA monomer to produce workable viscosities (Section 1.3). Modification of type, ratio and quantity of the monomers present in the resin formulation can provide specific rheological and mechanical properties to both the unpolymerized paste and the final restoration. The organic matrix is initially ‘plastic’ enabling the paste to be moulded at ambient temperature in the oral environment and following placement in a prepared cavity a free-radical addition polymerization reaction produces a rigid crosslinked structure [McCabe & Walls, 1990a].

The majority of modern RBCs are based on a BisGMA/TEGDMA matrix, although additional organic monomers have been incorporated. 1,6-bis(methacryloxy-2-ethoxycarbonylamino)-2,4,4-trimethylhexane (urethane dimethacrylate; UDMA) is a high

molecular weight methacrylate monomer which may be incorporated in place of BisGMA to modify the mechanical and rheological properties of the material [Asmussen et al., 1984; Asumssen & Peutzfeldt, 2001a; Floyd & Dickens, 2006]. Floyd & Dickens (2006) highlighted that the incorporation of UDMA produced a higher degree of monomer conversion compared with BisGMA monomers. In contrast, the 2,2-bis[4-(2-methacrlyloxyethoxy)phenyl]propane (bisphenol-A hexaethoxylated dimethacrylate; BisEMA) monomer is a lower viscosity analogue of BisGMA, although the molecular weight is dependent upon the presence of different functional groups, which influences polymerization shrinkage and rheology [Bagheri et al., 2007; Ogliari et al., 2008]. An extensive study of BisEMA monomers highlighted that aromatic dimethacrylates with increased chain extender lengths, namely additional ethylene oxide units in $BisEMA_4$, $BisEMA_{10}$, and $BisEMA_{30}$ monomers, increased the degree of conversion and crosslink density [Ogliari et al., 2008]. However, the $BisEMA_6$ monomer has been identified to be more hydrophilic and demonstrated a greater susceptibility to solvent degradation [Bagheri et al., 2007].

#### 1.3.4.1 Photo-polymerization

The resin matrix also contains an initiator and a co-initiator to ensure rapid polymerization of the methacrylate matrix, the activating agent used is dependent on whether a chemical or light cure is required. Early RBCs (Section 1.3) consisted of a two-paste system containing a benozyl peroxide initiator and a tertiary amine activator, which upon mixing underwent a chemical, or auto-polymerization, reaction [Philips, 1991; Darvell, 2006]. However, the use of chemical polymerization was limited by decreased colour stability of the initiator chemistry, reduced mechanical properties due to increased porosity produced on mixing of the two components [Leinfelder, 1987], inconsistent extent of polymerization and also clinically unacceptable times to realise cure [Lutz & Philips, 1983]. The development of “on demand” photo-activated resin matrix formulations during the 1970s containing a benzoin methyl ether that initiated polymerization via ultra-violet (UV) light at a wavelength of 340-380nm was a major advancement in dental technology [McCabe& Walls, 1990a]. UV polymerization was rendered redundant due to significant concerns regarding UV-induced tissue damage, poor light transmission through both the tooth and RBC structure producing a low monomer conversion and also instability of the light output intensity [Lutz & Philips, 1983].

The majority of modern RBCs consist of a diketone-amine system which absorbs visible (blue) light irradiation at a wavelength of 450-500nm to initiate a free-radical addition polymerization reaction which results in the formation of a rigid three-dimensional polymer structure [Cook, 1992]. Camphoroquinone (CQ) is a commonly used diketone-based photo-initiating molecule which contains a conjugated dicarbonilic group (Figure 1.4a), whilst photolysis of the C-C bond within CQ produces carboxyl radicals [Alvin et al., 2007]. CQ is present at approximately 0.05-0.50wt% in standard resin formulations [Cook, 1992; Asmussen & Peutzfeldt, 2002; Alvin et al., 2007] to reduce the energy level required to initiate polymerization to correspond with radiation within the visible range. In addition to CQ, a tertiary amine, such as dimethylaminoethylmethacrylate (DMAEMA), is incorporated into the resin matrix to provide a source of free radicals during polymerization (Figure 1.4b) [Cook, 1992; Asmussen & Peutzfeldt, 2002].

**(a)** **(b)**


**Figure 1.5. The chemical structure of the light-initiator (a) camphorquinone (CQ) and co-initiator amine activator (b) dimethylaminoethylmethacrylate (DMAEMA) routinely used in the visible-light polymerization of modern RBC.**

Photo-polymerization of RBCs occurs as the diketone, usually CQ, absorbs visible light within a specific wavelength of 450-500nm (with an absorbance maxima of approximately 470nm) and is subsequently promoted to an excited-state, known as a 'triplet'. The triplet then reacts with a tertiary amine, DMAEMA, to form an eciplex, or 'excited-state-complex' following proton transfer [Cook, 1992]. The eciplex then undergoes rapid decay by fluorescence or radiationless transition which releases free-radicals due to proton and electron transfer which initiates chain polymerization [Cook, 1992; Kim & Shim, 2001; Darvell, 2006]. The presence of an inhibitor, such as hydroquinone, in the resin matrix (0.1%) ensures adequate shelf-life and

prevents premature polymerization during placement under ambient light [Asmussen & Peutzfeldt, 2002]. Consequently a threshold level of light exposure must be exceeded to eliminate the inhibitor molecule and enable the progression of free-radical polymerization.

During polymerization the epoxy ring in BisGMA monomers opens on combination with available hydrogen to produce hydroxyl radicals, forming crosslinkages in chain or branched structures [Bowen, 1956]. Subsequently polymerization occurs from these growth centres, described as foci, which initially generate discontinuous microgel regions and as polymerization progresses the foci expand and encounter other regions of gelation, the polymers merge and congregate to produce a highly crosslinked structure [Darvell, 2006]. As gelation continues the resin becomes increasingly viscous and develops a rigid highly crosslinked structure which impedes the continuing diffusion of free-radicals and unreacted monomer molecules through the resinous mass. The mobility of the propagating system continues to decrease as the viscosity of the material increases and the gel-point is reached. Subsequently, post-gel shrinkage occurs where residual stress with the polymerizing material is no longer mitigated as a consequence of flow of the resin in its pre-gel state [Darvell, 2006].

The extent of crosslinking and associated degree of conversion (DC) of the methacrylate monomers to a rigid crosslinked polymeric structure influences the resulting mechano-physical properties of the RBC [Ferracane et al., 1998; Peutzfeldt et al., 2000]. The extent of DC is restricted as a rapid increase in viscosity occurs during polymerization, generating a relatively high concentration of unreacted pendent double bonds and unreacted methacrylate groups as only 35-80% of the methacrylate monomers react [Asmussen & Peutzfeldt, 2001a; 2002]. Also, high viscosity monomers, such as BisGMA, restrict migration of reactive methacrylate groups and diffusion of free-radicals during irradiation [McCabe & Walls, 1990a; Asmussen & Peutzfeldt, 2002]. Previous studies have highlighted that DC may be optimised by modification of CQ concentration. Asmussen & Peutzfeldt (2001a) identified that higher quantities (1.0wt%) of CQ generated additional foci of polymerization and consequently a greater crosslink density. However, excess CQ limits DC where a threshold concentration required to optimise polymerization was exceeded. This threshold was identified as 0.5mol% CQ where concentrations exceeding this caused DC to plateau at 75-77% [Yoshida & Greener, 1994]. Subsequently, unreacted molecules are unable to react with the amine and return to the ground state, thereby limiting free radical formation deeper within the structure [Yoshida & Greener,

1994]. The DC is also influenced by light intensity and the polymerization technique employed. The initiation of multiple foci of polymerization and subsequent increased crosslink density have been realised where a high intensity irradiation method was used, although this generated increased polymerization shrinkage stress [Oberholzer et al., 2003; Petrovic & Atanackovic, 2008]. In contrast, a slow start polymerization technique initiated relatively few foci and hence generated a more linear structure exhibiting a reduced generation of contraction stress [Oberholzer et al., 2003; Petrovic & Atanackovic, 2008]. However, curing techniques such as 'slow-start' or 'pulse-delay' which employ reduced irradiance to delay the onset of gelation, have been contraindicated due to an increased linear polymeric structure which has been identified to exhibit a higher propensity to softening and release of residual monomers [Asmussen & Peutzfeldt, 2001b].

## 1.4. Overcoming RBC Limitations

Despite the continuing development of RBCs and subsequent improvement of clinical longevity [Mjör et al., 1997], optimum mechano-physical properties of RBCs remain compromised by diverse factors including the generation of polymerization shrinkage stress [Davidson & Feilzer, 1997; Palin et al., 2005a], limited depth of cure [Jandt et al., 2000; Fleming et al., 2008], decreased monomer conversion [Ferracane et al., 1997; Palin et al., 2003a], insufficient wear resistance [Hu et al., 2002; Palin et al., 2005b], hydrolytic instability [Mohsen & Craig, 1995; Palin et al., 2005c] and technique sensitivity of application (Section 1.2.2.2) [Lucarotti et al., 2005; Opdam et al., 2004; 2007]. Of these limitations possibly the most detrimental is polymerization shrinkage and the subsequent generation of polymerization shrinkage stresses.

### 1.4.1 Polymerization shrinkage stress

Polymerization of RBC restorations is accompanied by volumetric shrinkage of 1.5-5% and the subsequent generation of internal stress as a rigid crosslinked structure is produced by conversion of carbon double bonds of the monomer to the physically shorter single bonds of the polymerized network [Sideridou et al., 2002; Ferracane, 2005]. Hydrostatic tensile stresses develop as covalent bonding produced during polymerization reduces the free volume. At the

onset of photoactivated polymerization the matrix is relatively plastic and stresses generated during crosslinking and subsequent shrinkage will be relieved due to viscous flow of the material. As the reaction proceeds and crosslink density increases the viscosity will become sufficiently high to impede flow, introducing hydrostatic tensile stresses to material and effectively placing the matrix in tension [Darvell, 2006]. Consequently, it is the post-gelation rigid contraction which generates polymerization shrinkage stresses that may compromise the marginal seal of restorations placed within confined cavities and result in microleakage and recurrent caries [Davidson & Feilzer, 1997; Whitters et al., 1997; Braga et al., 2005; Fleming et al., 2005; Palin et al., 2005a].

The ability of RBCs to compensate for polymerization shrinkage is also dependent upon the cavity configuration factor (C-factor). The C-factor has essentially been defined as the ratio of bonded to non-bonded surfaces, whereby a high ratio of bonded surfaces limits the materials ability to flow, which induces higher interfacial stresses [Feilzer et al., 1987]. Clinically, this influences the cavity design to minimize the number of restricting surfaces whilst maximizing free surfaces.

Light-activated polymerization has been suggested to restrict stress reduction by flow to a greater extent than the comparatively slower chemical curing polymerization reaction. Moreover, in clinical situations the surface exposed to the curing light is polymerized first which restricts flow and stress relief [Feilzer et al., 1990]. The addition of a low viscosity 'flowable' RBC with a low elastic modulus as a cavity liner (Section 1.3.2.3) relieves and distributes internal shrinkage stresses uniformly at the RBC/tooth interface, thereby reducing marginal debonding, gap formation, cracking and tooth deflection to relieve internal stress [Braga et al., 2005; Ferracane et al., 2005].

The incorporation of higher filler loadings in RBCs has sought to reduce volumetric shrinkage and minimize development of shrinkage stresses which has led to the introduction of universal (80wt%) and packable RBCs (86wt%) described in Sections 1.3.2.1 and 1.3.2.2, respectively. In essence the increased filler loading simply reduces the amount of resin, thereby reducing the component wholly responsible for shrinkage [Davidson & Feilzer, 1997; Ferracane, 2005]. However, factors such as the filler size and resin chemistry also influence the magnitude of shrinkage [Aw & Nicholls, 2001; Ernst et al., 2004]. Polymerization shrinkage may also be reduced by the use of alternative curing methods, such as a 'soft-start' technique. Here, a low

light intensity is initially employed to extend the pre-gel phase prior to curing at high intensity. By delaying the onset of gelation the increased ability of monomer to flow, reduces the occurrence of contraction stresses and may improve the restoration bond integrity [Watts et al., 1999; Braga et al., 2005]. However, as described previously (Section 1.3.4.1) Asmussen & Peutzfeldt (2001b) contraindicated techniques which employed an initially lower intensity cure due to the production of a more linear polymeric structure, decreased cross-linking and more susceptibility to solvent degradation.

The introduction of 'nanofilled' RBCs has also sought to reduce the occurrence of polymerization shrinkage, due to the small size of the 'nano' particulates, wide size distribution and subsequently increased filler load [Moszner & Salz, 2001; Lu et al., 2006]. Consequently, the polymerization shrinkage of nanofills was highlighted by Kleverlaan & Feilzer (2005) to be comparable with or significantly lower than conventional materials. In contrast, Ferracane (2005) speculated that the large surface-area-to-volume-ratio of nanofill particles (<100nm) and subsequent surface interactions with the polymerizing monomers may increase the shrinkage stress by restricting monomer flow. Alternatively, studies of non-bonded nanofiller particles, namely unsilanated particles, highlighted a reduction in polymerization stress of up to 31% [Condon & Ferracane, 2002], whilst unsilanated microfill particles produced 30% less contraction stress following photo-activation compared with silanated particles [Condon & Ferracane, 1998]. Thus it was suggested that the addition of 10 vol% non-bonded nanofill particles may provide the greatest level of stress relief in hybrid-type RBCs whilst maintaining adequate rheological properties [Condon & Ferracane, 2002]. However, unsilanated fillers fail to promote adhesion between the filler and resin matrix, which may compromise mechanical properties of the resulting material (Section 1.3.3.1).

#### 1.4.1.1 Modifying the resin matrix chemistry

A further approach to reduce the polymerization shrinkage of RBCs has been the introduction of materials possessing modified resin matrix chemistries, which are frequently based on derivatives of BisGMA [Moszner & Salz, 2001; Moszner & Klapdor, 2004; Weinmann et al., 2005; Perieira et al., 2007].

"Silorane"-containing resins were recently introduced by 3M ESPE as Filtek™ Silorane as an alternative low-shrinkage material. Silorane-based RBCs possess a modified resin

consisting of siloxane and oxirane (epoxy) functional groups. The cyclosiloxane imparts hydrophobicity [Eick et al., 2004; Palin et al., 2005c], whilst the cycloaliphatic oxirane monomer possesses a high reactivity and reduced shrinkage during polymerization compared with conventional methacrylate-based resins [Braga & Ferracane, 2004]. The subsequent polymerization shrinkage of silorane RBCs has been reported to be significantly less than that of conventional RBC materials [Braga & Ferracane, 2004; Ernst et al., 2004; Weinmann, 2005]. The cationic ring-opening reaction of silorane monomers has previously been described as 'living' polymerization as the free-radicals are not extinguished as rapidly as those in conventional RBCs [Millich et al., 1998; Tilbrook et al., 2000]. Subsequently, this reduces shrinkage stress as the monomer flow was not restricted and may be manifested as an increased stress relaxation of the polymerizing RBC and decreased cuspal flexure, thereby improving the marginal seal and limiting potential microleakage [Palin et al., 2005a]. Silorane-based RBCs have also been identified to possess an increased hydrolytic stability compared with conventional RBCs due to the presence of hydrophobic silorane-monomers which reduce water sorption, solubility and diffusion coefficient [Palin et al. 2005c].

Organically modified ceramics (Ormocers) are organic-inorganic hybrid materials composed of a methacrylate-functionalised organic phase and inorganic glasses or ceramics synthesised by sol-gel processing of organofunctional metal alkoxides, such as Ti, Al or Zr, to produce functionalised alkoxy silane. Subsequent hydrolysis and condensation produces a three-dimensionally branched oligomeric Si-O-Si network where the organic and inorganic components are combined at a nanoscopic or microscopic scale [Moszner & Salz, 2001; Moszner et al., 2007a; Sabbagh et al., 2004]. A number of commercial ormocers (Definite; Degussa AG, Hanau, Germany and Admira; Voco, Cuxhaven, Germany) have been produced based on a methacrylate-functionalised polysiloxane, such as urethane- or carboxy-functionalised methacrylate alkoxysilanes and a $SiO_2$ network, with the aim of reducing polymerization shrinkage and increasing biocompatibility [Manhart et al., 2000; Moszner & Salz, 2001; Janda et al., 2006]. However, the drawback remains that ormocer materials contain dimethacrylate monomers (BisGMA and TEGDMA) and consequently experience shrinkage and reduced biocompatibility due to monomer elution [Al-Hiyasat et al., 2005; Moszner et al., 2007a]. In an effort to reduce or eliminate these drawbacks a recent study conducted by Moszner et al. (2007a) reported reduced cytotoxicity, improved flexural strength and modulus of elasticity for ormocers

based on amine or amide dimethacrylate trialkoxysilanes and which also possessed a nanoparticulate fraction, namely $ZrO_2$ clusters or $SiO_2$ organosols [Moszner et al., 2007a].

Oligomeric thiol-ene monomers also offer an alternative as a novel low-shrinkage RBC material exhibiting as much as a 92% reduction in shrinkage stress compared with conventional-RBC resins [Carioscia et al., 2005]. The thiol-functionalised oligomers were produced by photopolymerization using monomers such as triallyl-1,3,5-triazine-2,4,6-trione (TATATO), pentaerythritol tetra(3-mercaptopropionate) (PETMP), trimethacrylolpropane tris(3-mercaptopropionate) (trithiol) and pentaerythritol tetracaptropropionate (tetrathiol) [Carioscia et al., 2005; Lu et al., 2005]. In contrast with the free-radical chain propagation mechanism of conventional methacrylate-based RBCs, thiol-ene polymerization occurs via a step-growth addition reaction initiated by a rapid free-radical transfer process. Consequently, the gel-point is not reached until a relatively high monomer conversion is achieved, which relieves contraction stresses [Cramer & Bowman, 2001]. In addition, Lu et al. (2005) reported that the increased monomer conversion of thiol-ene materials reduced monomer elution and also eliminated oxygen inhibition. However, the flexural strength of conventional BisGMA/TEGDMA RBCs was identified to be superior to those of thiol-ene materials [Lu et al., 2005].

The use of expanding monomers, known as spiro-orthocarbonates (SOCs) have been a further approach devised to reduce polymerization shrinkage stresses, which is reduced via cationic ring-opening polymerization which promotes a volumetric expansion [Sanda et al., 1992; Rokicki, 2000]. However, Chappelow et al. (1997) suggested the observed lower shrinkage compared with conventional RBCs was due to the lower monomer conversion of SOCs compared with higher monomer conversion of conventional RBC resins. A variety of further less developed approaches also exist to produce low-shrinkage materials, including bismethacrylates [Holter et al., 1997], liquid-crystal monomers [Rawls et al., 1997] and cyclopolymerizable di- and multi-functional acrylate resins [Stansbury et al., 1995].

#### 1.4.1.2 Depth of cure

Throughout cure of photoactivated RBCs light is absorbed and scattered by the inorganic filler particulates, which reduces irradiance through the RBC bulk. Therefore the degree of conversion (Section 1.3.4.1) is reduced as depth increases [Watts et al., 1984]. The depth of cure is dependant on filler type, size and load [DeWald & Ferracane, 1987], light irradiance

[Rueggeberg et al., 2000] and exposure time [Halvorson et al., 2002] (radiant exposure) and also resin composition and shade [Atmadja & Bryant, 1990; Tanoue et al., 2001]. The presence of unreacted monomer within the RBC bulk may also attenuate the irradiating light, preventing the formation of free-radicals and thus reducing the depth of cure [Rueggeberg et al., 1997]. The recommended maximum curing depth of the majority of RBCs is 2mm which has resulted in the necessity of incremental placement techniques when the cavity to be filled exceeds this depth. Incremental placement of RBC is itself 'technique sensitive' as a consequence of the need for attention to detail and the requirement to achieve adequate bonding between the previous increment and cavity wall [Liebenberg, 2000; Fleming et al., 2008]. Subsequently, improving the achievable depth of cure is vital to producing clinically successful materials, therefore recent developments in modern RBCs have included packable RBCs (Section 1.3.2.2) and clinical placement techniques which have sought to increase the depth of cure[Jackson & Morgan, 2000]. In addition, RBCs which possess an improved depth of cure, such as X-tra fil (Voco, Cruxhaven, Germany) which possess a 4mm depth of cure, have been developed [Fleming et al., 2008].

The depth of cure has also been identified to be limited where a refractive index mismatch between the monomer and filler exists [Söderholm et al., 1993]. Shortall et al. (2008) suggested that optimisation of the filler/resin refractive index mismatch may improve transmission of the irradiating light and provide an increased depth of cure, in addition to assisting shade matching as the opacity or translucency of RBCs is changed as a consequence of polymerization.

An alternative approach to improving the depth of cure and also reducing the curing time was the introduction of 'boosted' light curing units (LCUs) which emit a higher light intensity than conventional QTH-LCUs and improve the depth of light penetration, although as previously noted (Section 1.3.4.1) the generation of polymerization shrinkage stress may increase due to the rapid onset of gelation [Visvanathan et al., 2007].

#### 1.4.4.3 Technique sensitivity

The ease of manipulation and placement of amalgams compared with RBCs has been identified as one reason for the continued use of amalgam restorations [Fleming et al., 2001]. The technique sensitive application of RBCs is attributed to difficulties obtaining adequate contour and proximal contact as a consequence of the non-'packability' of RBCs compared with the condensability of amalgams [Cunningham et al., 1990; Tyas et al., 1998]. The development of

packable RBCs has sought to provide handling properties and ease of manipulation comparable with amalgam (Section 1.3.2.2).

The addition of an adhesive layer prior to placement of RBC restorations, which are not in themselves self-adhesive, may exhibit technique sensitivity where a uniform layer is not deposited. The development of acid-etching and simplified placement techniques has sought to limit technique sensitivity produced during the application of bonding agents, although glass-ionomer cements are considered the only true self-adhesive material [Yoshida et al., 2000; Peuman et al., 2005]. Furthermore the incremental placement of RBC restorations recommended due to limited depth of cure may also exhibit technique sensitivity due to lack of adhesion between the increments [Cobb et al., 2000; Jackson & Morgan, 2000].

#### 1.4.4.4 Toxicity concerns

Concerns regarding the cellular cytotoxicity and biocompatibility of methacrylate monomers used in RBCs have also arisen, specifically, the leaching of TEGDMA and HEMA (2-hydroxylethyl methacrylate) monomers into the oral environment and either subsequent local irritation and inflammation or systemic effects in patients [Geurtsen, 2000]. However, the potential toxicity is dependent upon monomer elution, diffusion through the dentine and subsequent accumulation in the pulpal tissue [Fleming et al., 2008]. Hume & Gerzina (1996) and Geurtsen (2000) reported a growing hypersensitivity and allergic dermatitis amongst dental personal as a result of reaction to one or more resin component. Of greater concern was the finding reported by Söderholm & Marriotti (1999) implicating leached impurities of BisGMA monomers as being potentially estrogenic. Despite these concerns the quantity of monomer leached from RBCs is extremely small and well below levels recorded to have a detrimental effect [Söderholm & Marriotti, 1999]

The development of new RBCs with reduced toxicity includes SOCs [Rokicki et al., 2000] and Ormocers, although the presence of BisGMA within Ormocer materials and subsequent potential monomer leaching continue to raise toxicity concerns [Başeren et al., 2004]. Low-cytoxic BisGMA analogues and monomer derivatives, such as a partially aromatic tetramethyl-*m*-xylylene UDMA (TMX-UDMA) have also been developed [Moszner et al., 2007b].

## 1.5 Summary

The introduction of innovative filled methacrylate resin composites revolutionised the field of dental restorative materials and has provided a clinically viable alternative to amalgam-based restorations. However, the mechano-physical properties and resultant clinical longevity of RBCs has been limited as a consequence of polymerization shrinkage stresses, technique sensitivity and the depth to which RBCs may be successfully cured. Subsequently, the continuing development and refinement of RBCs has sought to overcome these drawbacks through the modification of the filler size and morphology to improve filler loading and distribution. Also, the resin-matrix chemistry of recent materials, particularly siloranes, has been modified to reduce the occurrence of shrinkage. This has resulted in the introduction of new materials and proposed new material classifications, although the subtle and often incremental modification of filler or resin has often rendered classification difficult. The introduction of materials containing fillers purported to be in the nano-range (<100nm) would appear to be a continuation of the trend to decrease filler size and such materials have been described as 'nanofill' or 'nano-hybrid' RBCs. Manufacturers have suggested that 'nano'-sized particles provide improved mechano-physical properties, consequently considerable debate exists within the dental research community as to the efficacy and potential advantages of these so-called 'nano' materials.

# CHAPTER 2 FAILURE MECHANISMS OF RESIN-BASED COMPOSITES

## 2.1 Chemically Induced Degradation of RBCs

The median service-life of RBC restorations is approximately six years [Mjör et al., 1997] and is influenced by their susceptibility to chemically induced degradation, in addition to mechanistic aspects of wear and failure (Section 2.2). The extent and rate of chemical degradation following placement is influenced by the monomer constituents within the resin matrix [Munksgaard & Freund, 1990; Assmussen et al., 1998], degree of monomer conversion [Asmussen & Peutzfeldt, 2002; 2003a; 2003b], filler morphology [Schwartz et al., 2004; Bagheri et al., 2007] and silanization of the filler/matrix interface [Söderholm et al., 1983; 1984; Anagnostopoulos et al., 1993]. The degradation of RBC restorations occurs in-service due to the presence of moisture which produces hydrolytic degradation [Söderholm et al., 1984; Palin et al., 2005c; Ferracane, 2006], saliva which initiates enzymatic degradation [Freund & Munksgaard, 1990; Larsen & Munksgaard, 1991; Yap et al., 2000] and also solvent induced degradation instigated by routinely consumed foodstuffs [Ferracane & Marker, 1992; Yap et al., 2002; Schwartz et al., 2004].

### 2.1.1 Degradation of the resin matrix

The degradation of the methacrylate-based resin matrix monomers has been identified to be the most prevalent form of degradation in RBC materials [Eliades et al., 2003] and occurs either passively by hydrolysis or actively by enzymatic action to produce smaller molecules, specifically via chain scission and also oxidation or attack of functional groups [Göpferich, 1996; Ferracane, 2006]. Essentially, chain scission of polymeric structures involves cleavage of the highly crosslinked polymeric chains of the photo-polymerized matrix to shorter oligomeric structures and subsequently to monomeric chain fragments (Figure 2.1) [Göpferich, 1996].

The process of chain scission has been broadly divided into two types, namely single and multiple scission mechanisms. During single-scission only one bond is hydrolysed per chemical or enzymatic attack, whilst during multiple-scission the initial degradation is followed by further cleavage of polymer fragments produced during the initial scission [Tayal & Khan, 2000]. Tayal & Khan (2000) reported three modes of chain scission, namely random, central or Gaussian,

dependent upon the section of the polymeric chain undergoing scission. 'Random' scission was identified to occur at any point within the polymeric chain, whilst 'central' scission occurred at the midpoint of the polymeric chain and 'Gaussian' scission occurred non-randomly around the chain midpoint [Glynn et al., 1972; Tayal & Khan, 2000].

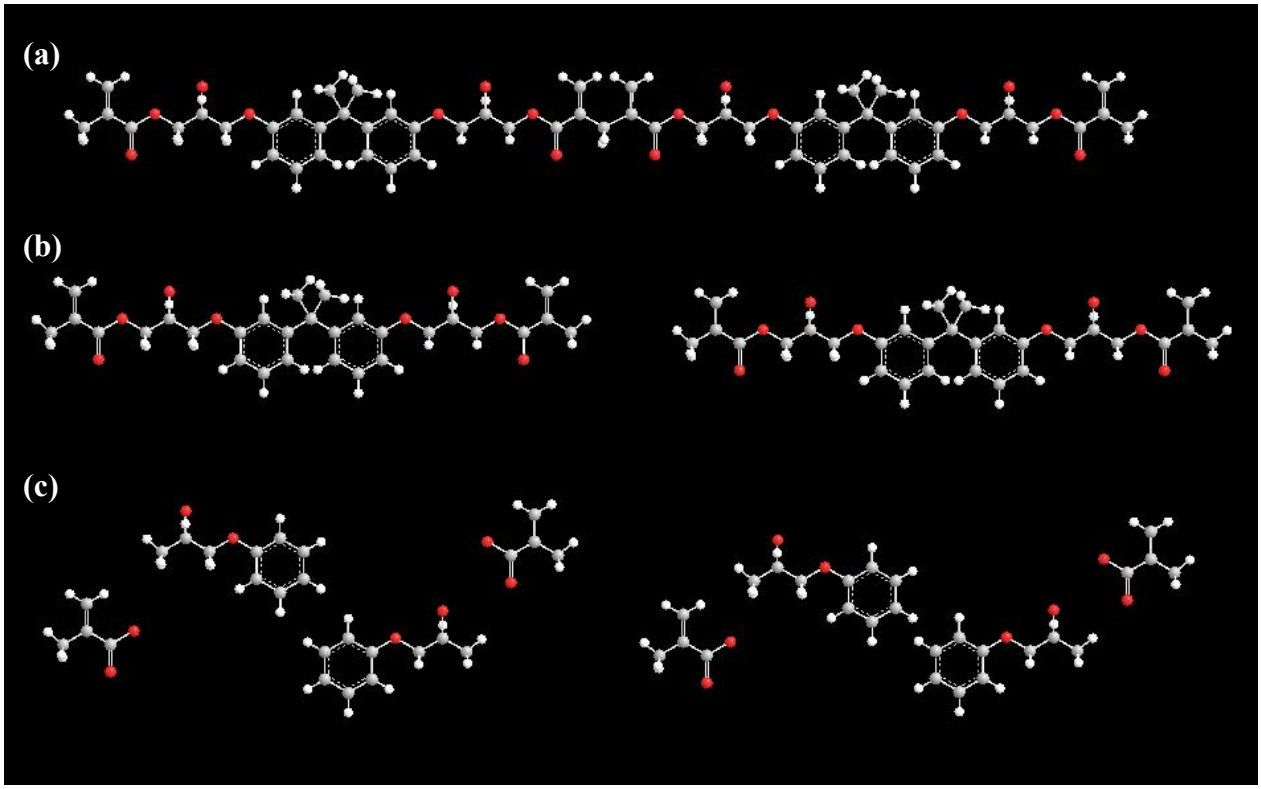


**Figure 2.1 Schematic diagram representing chain scission of (a) a polymeric BisGMA-based structure to (b) shorter oligomeric structures and finally to (c) monomeric chain fragments, the process is initiated by hydrolysis, chemical and enzymatic degradation of the RBC. Image produced using ChemDraw Ultra 11.0 (CambridgeSoft, UK).**

The occurrence of degradation and subsequent scission of the polymeric chain was identified to be influenced by the degree of conversion (DC) and hence extent of chain polymerization. The DC in the majority of RBCs ranges from 35-80% [Asmussen & Peutzfeldt, 2001a; 2002], whereby a high DC produces a highly crosslinked structure and improved mechanical properties (Section 1.3.4.1). Conversely, a low DC and increased quantities of residual monomer produce a structure more susceptible to hydrolytic and chemical degradation [Asmussen & Peutzfeldt, 2003a; 2003b].

#### 2.1.1.1 Water sorption

The presence of water is widely recognised to degrade the mechanical properties of RBC restorations during a time-dependent process proportional to the degree of water sorption into the material as determined by Fickian diffusion [Pearson et al., 1979, Bastoli et al., 1990; Asoaka et al., 2003; Göhring et al., 2005; Söderholm et al., 1984; 1996; Söderholm & Roberts, 1990; Turssi et al., 2005; Lohbauer et al., 2003b]. Hydrolytic degradation and erosion of RBCs has been identified to produce up to a 20% decrease in the fracture strength and elastic modulus following ninety days immersed in distilled water [Lohbauer et al., 2003b]. Likewise, Braem et al. (1995) highlighted that immersion in water caused a decrease in the Young's Modulus of 12 to 25%, whilst Palin et al. (2005c) identified a moderate decrease in the bi-axial flexure strength of Filtek™ Z100 (3M ESPE) of 133MPa to 123MPa following twenty-six weeks stored in water.

RBCs which possess resin monomers that exhibit a hydrophilic nature, such as TEGDMA (Section 1.3.4), exhibit an increased susceptibility to water sorption and subsequent hydrolytic degradation of the resin matrix [Musanje et al., 2001]. This occurs as polar hydrophilic monomers enable hydrogen-bonding with water molecules from the surrounding oral environment and subsequent uptake of water into the bulk of the resin matrix [Asmussen et al., 1984; Asumussen & Peutzfeldt, 2001; Floyd & Dickens, 2006]. Water sorption into the bulk of the RBC structure causes the material to become plasticized, inducing swelling, ductility, polymeric chain scission and the leaching of unreacted monomers [Ferracane et al., 1998; Martin et al., 2003; Ito et al., 2005]. In addition, phase-separation occurs as comparatively large water molecules diffuse into intermolecular spaces between the polymeric chains, thus increasing the distance between chains held together by comparatively weak van der Waals forces, particularly where a high DC was not obtained [Eliades et al., 2003; Wilson et al., 2005]. Consequently, the swelling and expansion of the resin matrix, in addition to degradation of the silane interface, may lead to phase-separation as filler particulates are eluted from the polymeric matrix [Eliades et al., 2003; Wilson et al., 2005].

The dental research literature appears curiously bereft of long-term *in vitro* studies, namely studies exceeding six months, into the influence of water sorption on clinical longevity of RBC restorations, especially considering the nature of the oral environment and the recognized detrimental influence of water sorption and subsequent hydrolytic degradation.

#### 2.1.1.2 Enzyme induced degradation

In addition to water, RBCs are subjected to enzymatic degradation due to saliva, however the extent of enzymatic degradation varies as the quantity of enzymes in saliva differs between individuals [Musanje et al., 2001; Martin et al., 2003]. Human saliva contains enzymes such as esterase (hydrolase), which have been identified to increase the wear rate of RBCs via softening of the methacrylate resin as a consequence of hydrolysis of ester bonds to methacrylic acid [Freund & Munksgaard, 1990; Larsen & Munksgaard, 1991; Yap et al., 2000]. Enzymatic catalysis of polymer resins has also been identified to be pH dependent, as scission of the polymeric chains is increased and may become autocatalytic when specific monomers, such as carboxylic acid are produced [Göpferich, 1996]. In addition, Munksgaard & Freund (1990) identified that TEGDMA was hydrolysed faster in esterase compared with BisGMA, highlighting that the specific monomer chemistry also influences the rate and extent of degradation.

Artificial saliva, such as that derived from porcine liver esterase, has been identified to produce softening equivalent to that of human saliva [Larsen & Munksgaard, 1991] and also leaching of monomers, which occurs at a greater rate in artificial saliva than in de-ionised water [Musanje & Darvell, 2003]. However, the type of artificial saliva employed in a specific study has been identified to have a distinct effect on the results obtained [Musanje et al., 2001; Martin et al., 2003]. Consequently, whilst *in vitro* studies should be conducted in medium that resembles the complex chemistry of natural saliva, in order to obtain clinically relevant results, the use of de-ionised water provides an easily reproducible reference solution, enabling comparisons between institutions and with published results [Martin et al., 2003].

RBCs are also subjected to degradation from chemical compounds within foodstuffs; consequently *in vivo* study of new and existing restorative materials is essential to predict probable failure rates. However, such studies are frequently time-consuming as degradation occurs at different rates, in some cases over a considerable period of time, whilst commercial considerations and time-constraints to introduce new materials may limit such testing [Sarkar, 2000]. Therefore, solvents and food simulating liquids, such as sodium hydroxide and ethanol, are employed during *in vitro* studies to accelerate the rate and extent of material degradation and also with the aim of mimicking conditions in the oral environment [Badra et al., 2005].

Sodium hydroxide has been identified to simulate *in vivo* degradation and to accelerate hydrolysis of the siloxane bridge bonds between filler and resin (Section 1.3.3.1) due to the high concentration of hydroxyl ions ($OH^-$), which are approximately one million times greater than in saliva (pH of ~13 compared with ~6.5, respectively) [Sarkar, 2000; Bagheri et al., 2007]. Bagheri et al. (2007) highlighted that sodium hydroxide induced cracking and surface peeling, identifying a depth of penetration into the bulk of the RBCs tested of up to 176.4±1.5μm, in comparison distilled water penetrated to a maximum depth of 61.6±0.5μm.

Ethanol is a common constituent of many alcoholic beverages and specifically degrades the resin matrix, as both BisGMA and ethanol possess a comparable solubility parameter, resulting in leaching of unreacted monomer molecules [Badra et al., 2005; Yap et al., 2005; Polydorou et al., 2007]. The infiltration of ethanol into the organic resin plasticizes the matrix, which initiates swelling as the diffusing molecules expand the inter-chain spacing, subsequently softening the resin matrix [Asmussen et al., 1984; Asmussen & Peutzfeldt, 2001a; Schwartz et al., 2004; Polydorou et al., 2007]. Schneider et al. (2008) highlighted that ethanol storage at concentrations of 75 and 100% resulted in an 11.8±3.9 and 8.8±3.9% decrease in Knoop surface hardness for Filtek™ Z100 (3M ESPE) and a decrease of 13.5±3.4 and 14.1±3.5% for Filtek™ Z250 (3M ESPE). The diametral tensile strength of Filtek™ Z250 specimens stored in ethanol was also identified by Aguiar et al. (2005) to be significantly decreased to 51.3±7.5MPa compared with 71.1±10.2MPa following storage in water.

### 2.1.2 Degradation of the silane coupling agent

As previously described the silane coupling agent promotes adhesion between the otherwise incompatible filler and matrix, in addition to improving particle dispersion and wetting, inhibiting crack propagation and absorbing masticatory loads. However, the silane interface represents a comparatively weak interface within the RBC, from which premature failure of the restoration may occur (Section 1.3.3.1). Hydrolytic or chemical degradation of the silane interface facilitates interfacial cracking and filler particle elution [Söderholm et al., 1983; 1984], thereby limiting the clinical longevity of the restoration. Following *in vivo* clinical service or *in vitro* solvent storage, hydrolytic degradation reduces the interfacial siloxane bridge bonds present at the filler/matrix interface to the original silanol groups, thus producing hydroxyl ions.

The production of hydroxyl ions during hydrolytic degradation of the siloxane bridge bonds cause the concentration of $OH^-$ ions at the interface to increase which further promotes the degradation of the interface and the reaction to become autocatalytic. Subsequently, degradation of the silane interface initiates particle debonding, leaching of inorganic ions and interfacial microcracking which reduces the mechanical properties and fatigue resistance of the RBC [Söderholm et al., 1983; 1984; Øysæd & Ruyter, 1986; Stokes et al., 1988; Ortengren et al., 2001; Takeshige et al., 2006]. Furthermore, hoop stresses exist around filler particles as a consequence of polymerization shrinkage, which increase the frictional forces between filler and resin matrix, limiting filler debonding. However exposure to water degrades the silane interface (Figure 2.2) reducing the tensile strength and causing the matrix to swell and plasticize thus reducing the hoop stresses, which increases the occurrence of particle debonding [Söderholm & Roberts, 1990].

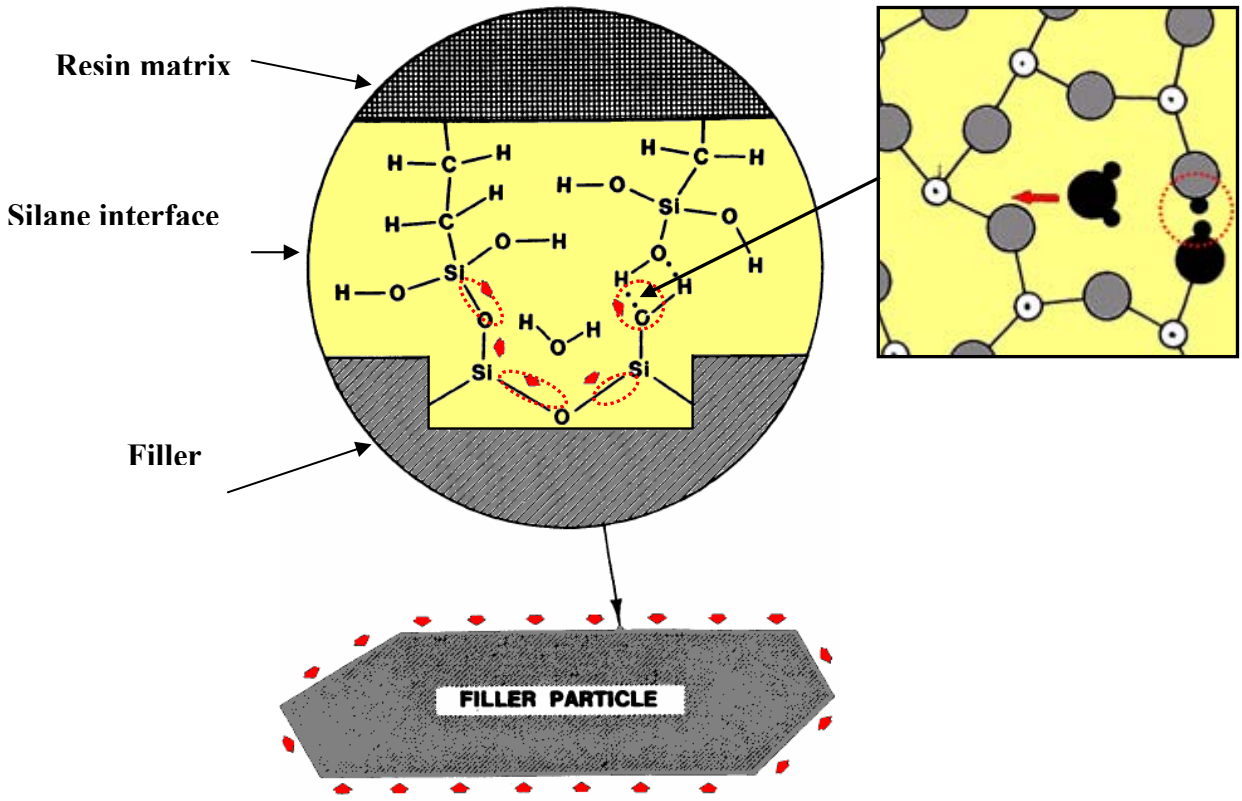


**Figure 2.2. Diagram representing filler particles surrounded by hoop stresses (red arrows) within the resin matrix. The insets represent the interfacial region and highlights (circled) interaction and subsequent hydrolytic degradation of siloxane bridge bonds by water. Diagram modified from Söderholm et al. (1983); Söderholm & Roberts (1990).**

Johannson et al. (1967) reported that the interfacial silane layer was previously and inaccurately described as possessing a uniform distribution and monolayer structure. However, multiple layers of silane molecules were later identified to be deposited on the filler particle surface during silanization [Johannson et al., 1967; Söderholm & Shang, 1993]. Subsequently, the interface exhibits a multilayered structure in which the silane molecules are randomly orientated in relation to the filler surface. The silane molecules at the interface are either chemicosorbed or physicosorbed. Silane molecules adjacent to the filler form siloxane bonds (Section 1.3.3.1), whilst concurrent condensation of the silanol groups within the deposited silane molecules produce a multilayered chemicosorbed layer. In contrast, the physicosorbed layers of deposited silane are easily degraded due to a lack of chemical bonding and subsequently lack structural coherence and organization [Söderholm & Shang, 1993]. Therefore, the thickness, disposition, concentration and coverage of the silane, in addition to the orientation of the silane molecules within the interfacial layer, influence the degree of physicosorption and subsequent degradation due to chemically active environments [Söderholm et al., 1984; Söderholm & Shang, 1993; Eliades, 2003].

### 2.1.3 Degradation of filler particles

The reinforcing inorganic filler particles comprise the majority of the RBC microstructure and influence the mechano-physical properties of the resulting material (Section 1.3). Söderholm, (1981) identified that the surface of filler particles in RBCs stored in water exhibited significant degradation, the extent of which was associated with the presence or absence of the silane interface. The occurrence of filler degradation was attributed to the presence of hydroxyl ions within the resin matrix, whilst silanization of the filler was identified to reduce the release rate of $OH^-$ ions [Söderholm, 1981].

Similar to the degradation of the siloxane bridge bonds by water (Section 2.1.2), the Si-O-Si network of the silica filler particles is also degraded by the ingress of water. The bonding within silica has been reported to be short-range, irregularly distributed and to possess strained bond angles due to the amorphous nature of silica [Söderholm, 1983]. Consequently, as water infiltrates the RBC, the resultant hygroscopic expansion of the resin matrix stresses the filler surface and deforms the Si-O-Si structure, which occurs concurrently with $OH^-$ ions to induce stress corrosion of the reinforcing filler particles [Söderholm, 1981; 1983]. As hydrolytic

degradation progresses, the production of $OH^-$ ions during the rupture of the Si-O-Si network of both silica and also the silane interface causes the reaction to become autocatalytic as the pH is increased, resulting in degradation of the filler surface and debonding [Bowen & Reed, 1976; Söderholm, 1981; Eliades et al., 2003].

#### 2.1.3.1 The elution of filler particles

Although filler elution is initiated by the mechanistic wear, hydrolytic degradation and subsequent production of $OH^-$ ions and stress corrosion of the filler particulates has been identified to initiate elution of filler elements dependent upon the filler constituents, such as Si, Ba or Sr, [Söderholm, 1983]. The occurrence of filler leaching was identified by Söderholm, (1981) to be retarded by effective silanization of the filler (Section 1.3.3.1), whilst leaching was accelerated due to the introduction of cyclic stresses. The occurrence of an ion exchange mechanism was also postulated by Söderholm et al. (1996) to occur at the filler interface and to drive filler leaching. During interaction with water the Si-O-Si network develops a negative charge which restricts cations from leaving the filler surface, however positive ions ($H^+$) diffusing through the matrix interact with the negatively charged silica and additional leaching occurs [Söderholm et al., 1996]. The leaching of filler from RBCs immersed in water [Söderholm et al., 1983; Söderholm & Roberts, 1990] has prompted a range of cytotoxicity studies, although no specific cytotoxic effects were identified for fillers whilst the leaching of monomeric components (Section 1.4.4.4) continues to cause concern [Lee et al., 1998; Bouillaguet et al., 2002; Al-Hiyasat et al., 2005].

## 2.2 Mechanistic Degradation of RBC Restorations

The clinical longevity of RBC restorations following placement in the oral environment is influenced by the occurrence of fatigue [Söderholm & Richards, 1998; Papadogoannis et al., 2006; Garoushi et al., 2007], environmentally assisted crack growth [Söderholm et al., 1984; Söderholm & Roberts, 1990] and wear resistance [Braem et al., 1986a; Bagheri et al., 2007], in addition to chemically induced degradation as previously described in this chapter. Subsequently, RBCs susceptible to such degradation mechanisms exhibit a propensity to premature failure at loads considerably lower than the determined mean strength values.

### 2.2.1 Crack propagation and fracture

The Griffith criterion describes the occurrence of fracture in terms of the potential energy of the propagating crack and the specific surface energy, which must be exceeded to initiate the propagation of cracks. The presence of surface defects, structural inclusions or water all reduce this critical energy value, enabling crack propagation at lower stresses [Griffith, 1920; Roesler et al., 1956]. In addition, the filler type and loading has been identified to influence crack propagation, specifically the incorporation of fillers with a spheroidal morphology improve the loading and packing efficiency, enabling an increase in volume fraction of the filler [Ferracane et al., 1998; Sabbagh et al., 2004]. The spherical morphology also enhances fracture strength as mechanical stresses concentrate around irregularities of the filler/matrix interface, such as angles and protuberances of the filler particles, particularly where fillers possess an irregular morphology [Suzuki et al., 1995; Sabbagh et al., 2004].

### 2.2.2 Static fatigue

The filler particles and resin matrix of RBCs are susceptible to static fatigue, also described as environmentally assisted crack growth, whereby water molecules act to propagate existing defects and reduce the critical energy at which crack propagation occurs. This occurs in combination with fatigue and sustained loading of the material which results in stress corrosion cracking of the material and significantly reduces the clinical longevity of the restoration [Wei & Simmons, 1981; Söderholm & Roberts, 1990; Takeshige et al., 2007]. Previous investigations have highlighted that the fatigue fracture resistance of RBCs stored in water was significantly decreased. This was attributable to a decrease in the Griffith's critical energy value (Section 2.2.1.), water absorption of the resin matrix (Section 2.1.1.1) and hydrolysis of the silane interface (Section 2.1.2). Takeshige et al. (2007) identified that the fatigue fracture resistance of RBCs stored in distilled water for up to three months was consecutively decreased. Likewise, Lohbauer et al. (2003b) identified that the flexure strength of an RBC stored in water for three months (73.9±6.7MPa) was significantly reduced compared with specimens of the same RBC stored for one day (102.3±6.9MPa).

Static fatigue and propagation of existing defects has been identified to occur from the surface of inorganic ceramic filler particles and also from the silane interface, both of which

possess Si-O-Si bonding [Söderholm et al., 1981; 1983; 1984]. During static fatigue water molecules are absorbed at the crack-tip, which strains the Si-O-Si bonds, resulting in transfer of protons and electrons between oxygen atoms within the water molecule and Si atoms within the silica structure. The hydrogen-bond is ruptured resulting in the formation of Si-OH groups and enabling crack propagation within the surface layer of the silica ceramic filler particles [Michalske & Freiman, 1982].

It is also interesting to note that Söderholm et al. (1984) identified that crack formation, at the filler surface and silane interface, also occurred due to osmotic pressure build-up at the matrix/filler interface due to hydrolytic degradation of the filler. This study also determined that microfill materials were the most stable in a wet environment compared with RBCs containing larger fillers, which Söderholm et al. (1984) attributed to filler composition, morphology and distribution within the resin matrix. In addition, crack growth was suggested to be retarded due to the pre-polymerized matrix surrounding the filler particles [Söderholm et al., 1984].

In contrast, Kawakami et al. (2007) identified that fatigue crack initiation in RBCs was retarded, whilst dental ceramics were more susceptible to crack propagation within aqueous environments, although no explanation was offered for this. Takeshige et al. (2007) also identified that the fatigue crack threshold was increased following storage in water which retarded crack propagation. This study attributed the apparent toughening of the RBC to 'plasticization' of the resin matrix and subsequent hygroscopic expansion following water sorption, resulting in blunting the tip of fatigue cracks with reduced stress concentration, release of internal stresses accumulated during polymerization shrinkage (Section 1.4.1) and also the generation of residual stresses at the crack-tip [Ferracane et al., 2006; Takeshige et al., 2007].

#### 2.2.2.1 Static testing

The generation of intra-oral stresses is a complex process, involving compressive, shear and tensile stress formation [Berenbaum & Brodie., 1959], consequently the production of reproducible *in vitro* stresses is both difficult and expensive and renders reliable comparison impossible between different laboratories and investigators [Langitan & Lawn, 1970; Dong & Darvell, 2003]. Subsequently, the testing methodologies employed by dental materials researchers have sought to improve the reliability and clinical relevance by adapting conventional mechanical testing techniques [Palin et al., 2003b]. The most routinely used mechanical tests are

diametral [Aguiar et al., 2005; Casselli et al., 2006], compressive [Brosch et al., 1999; Jandt et al., 2000] and flexural testing methodologies [Manhart et al., 2000; Palin et al., 2003b; 2005d; Junior et al., 2008].

**Diametral testing**

The diametral (or Brazilian) test provides a simple method of measuring the tensile strength of brittle materials by applying a compressive force to a cylindrical specimen across its diameter, thus establishing a uniform tensile stress across the diametral plane of the specimen [Earnshaw & Smith, 1966; Lloyd & Mitchell, 1984; Ban & Anusavice, 1990]. Diametral tensile testing has been reported to produce tensile stresses in the diametral plane where shear forces were initiated at the point of contact (Figure 2.3) [Palin et al., 2003b].

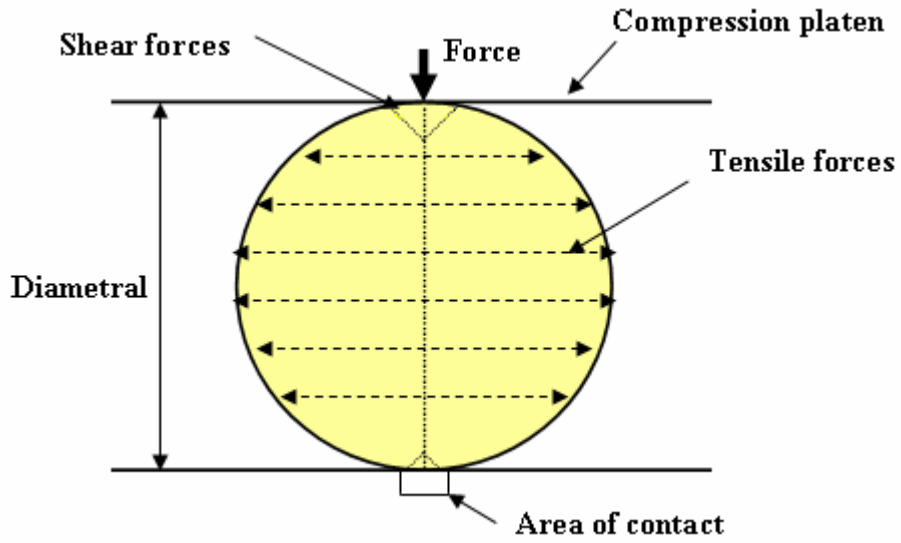


**Figure 2.3. Diagram representing diametral testing of a disc-shaped specimen compressed diametrally between compression platens at an 'area of contact'. Compressive forces are resolved into shear forces along a cone-shaped area at either end, subsequently generating tensile stresses within the central portion of the cylinder.**

Diametral testing eliminated the difficultly of fabricating dumb-bell shaped specimens, required by some tensile strength tests and the subsequent surface defect dependency [Bowen et al., 1962b]. However, the complexity of the stress distribution developed as a result of diametral loading can result in inconsistent modes of fracture [Ban & Anusavice, 1990]. The existence of a compressive stress along the loaded diameter was identified to hinder the propagation of the tensile crack [Kendall, 1978], while the occurrence of large shear stresses in the contact area,

may induce shear failure mechanisms [Lloyd & Mitchell, 1984]. However, where specimens are less brittle, deformation increases the area of contact as the specimen exhibits 'barrelling', which generates complex shear stress patterns (Section 2.3) which are difficult to interpret and may result in erroneous data [Darvell, 1990; van Noort, 2007].

**Compressive testing**

RBC restorations are subjected to compressive loading during the masticatory cycle, however the formation of complex shear and tensile stress during longitudinal compression testing of cylindrical specimens (Figure 2.4) [Berenbaum & Brodie, 1959] renders the reliability of compressive testing open to discussion [Ban & Anusavice, 1990]. Brosh et al. (1999) determined that compressive strength testing was limited as the failure of brittle materials occurs in tension. Furthermore, the cylindrical test specimens may not be representative of the clinical situation as light-activated RBC specimens require irradiation from both surfaces to ensure complete polymerization as the depth of cure in most RBCs is limited to 2-4mm (Section 1.4.2) whilst cylindrical compressive test specimens possess a height of 6mm. Consequently, it has been suggested that the middle portion of specimens may be incompletely cured, producing variations in the compressive strength results obtained [Palin et al., 2003b].

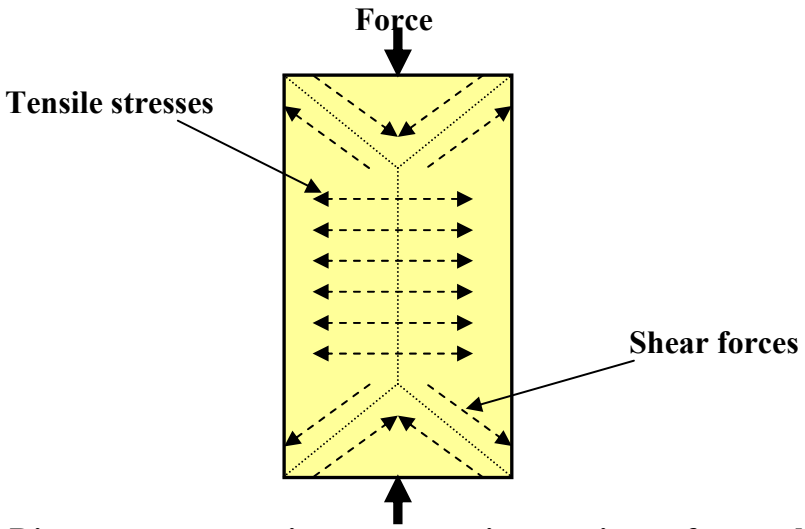


**Figure 2.4. Diagram representing compressive testing of a cylindrical specimen, compression generated shear stresses at both ends of the specimen and tensile stresses within the central portion of the cylinder. The stresses induced in cylindrical specimens are no different from those induced during diametral testing, except that the pattern is radially symmetrical.**

**Flexural testing**

The International Standard Organization (ISO) stipulates the use of a three-point flexure method to determine the flexure strength of RBCs as the simple shapes of test specimens, such as bars and rods, ensure the reproducibility of the results [ISO 4049]. Furthermore, the method does not require special grips which have previously been identified by photoelastic studies to result in inconsistent failure results [Bowen et al., 1962b; Ritter et al., 1995a; 1995b]. However, three-point and four-point flexure testing has been identified to produce a non-uniform stress distribution throughout the bulk of the specimen undergoing testing [Williams & Smith, 1971]. The stress varies from zero at the neutral layer to a maximum at the outer surfaces, where tensile stresses were generated on the lower surface of the specimen (Figure 2.5), accentuating the influence of the surface condition [Rudnick, 1963] and has been identified to produce strength values in excess of the true tensile strength [Wright, 1955; Rudnick 1963; Earnshaw & Smith 1966].

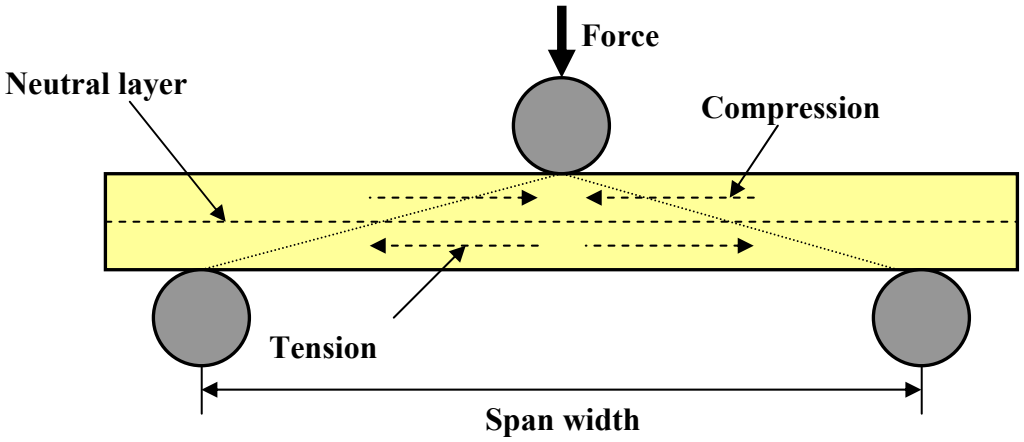


**Figure 2.5. Diagram representing the three-point flexure test and highlighting the presence of compressive and tensile stresses above and below the neutral axis, which were resolved within the cone-shaped area generated between the loading crosshead and the roller-supports.**

Unless a bespoke curing-tip is used which irradiates the bar-specimen (25mm length) in 'one-shot', the production of specimens for both three- and four-point flexure testing requires an overlapping curing regime. Palin et al., (2005d) suggested that an overlapping curing regime of bar-specimens result in an inhomogeneous cure, which produced residual stresses across the bar and decreased the reliability of the strength data. Furthermore, three-point flexure tests were

originally designed for relatively large engineering specimens, which Ban & Anusavice (1990) suggested was not completely relevant to the smaller dental materials test specimens.

**Bi-axial flexure testing**

Bi-axial flexure strength testing is a well established technique, albeit for the study of ceramics [Ban et al., 1992; Cattel et al., 1997], although bi-axial flexure testing of RBCs is gaining greater acceptance [Palin et al., 2005b; 2005c; 2005d; Fleming et al., 2008]. The bi-axial flexure strength test is employed to assess tensile stresses and is considered to be more reliable than the other tensile testing techniques available, such as uni-axial flexure, diametral tensile testing and three- and four-point flexure tests [Ban & Anusavice, 1990]. The central loading of the disc-shaped specimens used by bi-axial testing produces the maximum tensile stress at the centre of the specimen [Ban et al., 1992]. The tensile stress decreases rapidly with increasing radial distance from the centre of the disc, thereby eliminating the occurrence of spurious edge failures associated with three-point flexure tests. The results obtained from bi-axial flexure testing are also independent of defect direction [Shetty, 1980; Piddock, 1987; Ban & Anusavice, 1990; 1992]. The disc-shaped specimens used were also a closer representation of clinical material geometry compared with bar-shaped specimens, although specimen geometry does not mimic that of clinical restorations. Furthermore, the specimen geometry enables a single reproducible curing regime, eliminating the requirement of three-point flexure testing of overlapping curing regimes and subsequently providing an improved reliability of the disc-shaped specimens [Palin et al., 2005d]. Also, irradiation of specimens from a single surface is more clinically realistic than curing methods specifying irradiation of both upper and lower surfaces prior to testing [Palin et al., 2005d].

**Weibull modulus**

The evaluation of mean flexural strength data and associated standard deviations may be misleading, as the generation of a mean strength value for any material assumes that the material possesses a ‘normal’ defect distribution that is duplicated within all such materials and that the mean value is therefore representative. However, the defect population frequently lacks this level of homogeneity resulting in failure at lower strengths and premature clinical failure where a higher defect distribution exists [McCabe & Carrick, 1986]. Therefore, statistical analysis, such

as Weibull modulus and survival probability distribution, is vital to provide a meaningful interpretation of the flexural strength, determine the reliability of the data and predict the probability of failure of brittle materials [Weibull, 1951; McCabe & Carrick, 1986]. The Weibull modulus of a group of specimens, provided that the group size is equal to or exceeds twenty specimens, provides an indication of the defect distribution. A high Weibull modulus is indicative of a narrow distribution of defects and increased reliability of the strength data of that particular material. The presence of a single defect population is indicated by an $R^2$-value greater than 0.95, whilst a value of 1 would represent a perfect distribution and a value of less than 0.95 was attributable to a multi-modal distribution which distorts the flexural strength data away from the straight line [Fleming et al., 1999a; 1999b; 2000; Bhamra et al., 2002]. Subsequently, the Weibull modulus enables the failure probability of a material to be predicted at any level of stress and indicates the reliability of that material during the life-time of the restoration [McCabe & Carrick, 1986].

The use of Weibull statistics has allowed comparisons of flexural strengths determined using different test methodologies to be produced [Junior et al., 2008]. Palin et al. (2003b) compared the strength data of bi-axial and three-point flexure test methods using Weibull statistics and determined that the former exhibited a significantly more reliable data set. This was proposed since the variability introduced during the overlapping curing regimes required to polymerize bar-specimens was eliminated by the single-hit cure of the disc-shaped specimens [Palin et al., 2003b].

### 2.2.3 Fatigue induced degradation

Fatigue induced degradation occurs when one surface slides over or impacts a second surface, generating a zone of compressive stress ahead of the sliding surface whilst tensile stress and plastic deformation is generated behind the sliding surface. Garoushi et al. (2007) reported that the intraoral stress received by dental restorations during mastication is repeated in excess of three-hundred thousand times per year, at loads of 100 to 200N for anterior restorations [Helkimo, 1978], whilst posterior restorations may be loaded to 800N [Graf, 1969]. However, masticatory loading forces generated whilst chewing foodstuffs were identified to be considerably lower at approximately 10 to 20N [Anderson, 1956].

The cyclic masticatory stress, whilst lower than the stresses required to initiate catastrophic failure, generate subsurface crack propagation and the accumulation of fatigue stresses which result in the eventual displacement and loss of material from the restoration [Söderholm et al., 1984; Söderholm & Roberts, 1990; Mair, 1996; Sarkar et al., 2000]. Fatigue stresses include masticatory loads which may result in premature failure at stresses considerably below the reported mean strength of the material due to stress accumulation, such as sub-critical crack growth and slow crack propagation, localised around the point of contact [Söderholm & Richards, 1998; Papadogoannis et al., 2006]. Generally, the occurrence of catastrophic failure following flexure testing and stress accumulation within modern microhybrid and nanofill RBCs has also been attributed to surface defects such as scratches, voids, inclusions or non-uniform phase distribution of the resin and filler [Lohbauer et al., 2003a; 2003b; Papadogiannis et al., 2006; Takeshige et al., 2007; Junior et al., 2008]. The degradation of the silane interface due to propagating stresses induced by loading, or chemical degradation (Section 2.1.2), also induces defects and microcracks in the material which initiate premature failure of the restoration [Söderholm et al., 1981; 1982; 1984; Takeshige et al., 2007].

As a result, defects whether induced by stress accumulation due to repeated loading of the RBC or degradation of the silane interface, initiate cracking from the point of contact where tensile and compressive stresses were greatest and propagate from the surface, through the resin matrix and silanated filler/matrix interface (Figure 2.6a). Alternatively, cyclic loading may generate a network of subsurface laminated cracks below the point of contact, which, as loading continues, propagate resulting in delamination and loss of a layer of material (Figure 2.6b) [Mair, 1994; Lohbauer et al., 2006].

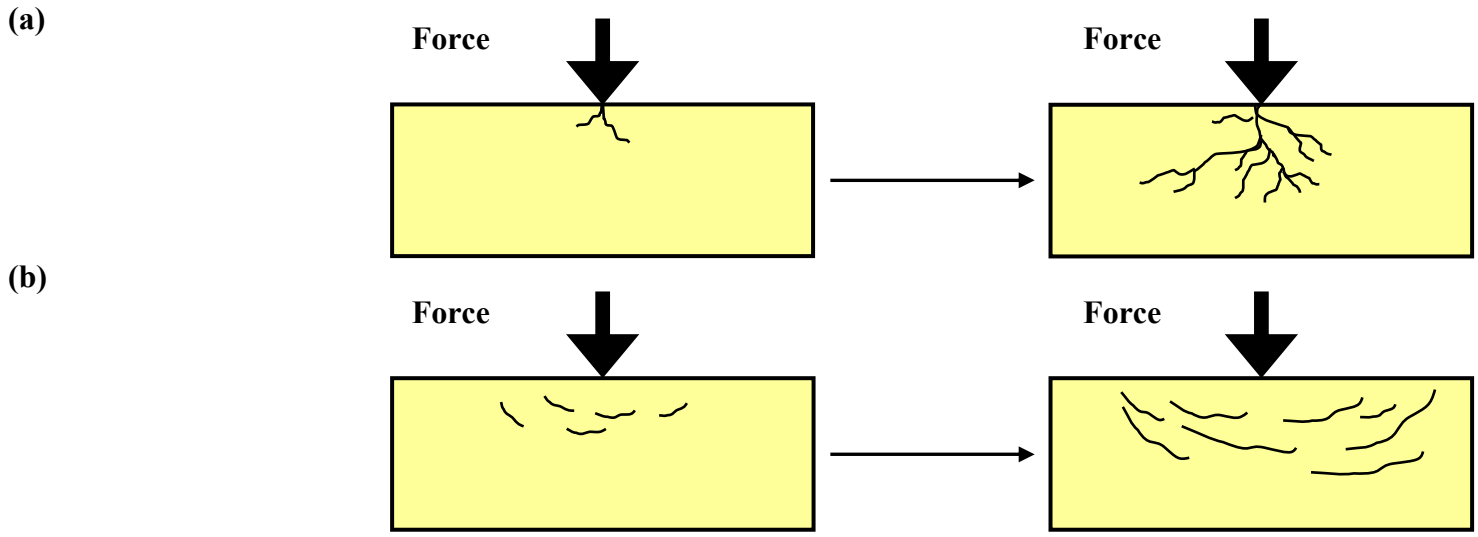


**Figure 2.6 Diagram representing (a) propagation of cracks from surface defects which pass through the resin matrix and silane interface and are the dominant fracture mechanism of RBCs, and (b) the nucleation of subsurface cracks which eventually result in delamination of the material surface.**

An *in vivo* evaluation of posterior RBCs conducted by Braem et al. (1986a) identified that intermittent sliding-loading during mastication introduced fatigue and subsurface microcracking which propagated through the RBC bulk and reached the surface to induce severe pitting. Furthermore, whilst microfill RBCs (Section 1.3.1.3) exhibit good wear resistance [Lambrachts et al., 1987], clinical observations have identified that such materials exhibit pronounced chipping in stress-bearing situations, such as occlusal or incisal contact. This produces fatigue and subsequent pitting caused by failure of the silane interface and debonding of the resin matrix and pre-polymerized filler particles [Lambrachts et al., 1982; Okamoto et al., 1993]. The repeated cyclic loading of RBCs further introduce fatigue stresses which initiate the breakdown of the silanated filler/matrix interface, introducing progressive crack growth and voids within the RBC structure where particles are lost, resulting in substantial weakening of the restoration [Condon & Ferracane, 1996; Drummond et al., 2005]. This highlights the importance of *in vitro* cyclic testing of existing and novel RBCs to predict *in vivo* behaviour and the potential subsequent occurrence of premature failure of the restoration during masticatory loading.

#### 2.2.3.1 Fatigue testing

RBCs are subjected to multiple stressing mechanisms in the oral environment, including static, dynamic and cyclic fatigue. Subsequently, the rate and extent of degradation has been identified to be a material dependent process influenced by both filler and resin chemistry [Braem et al., 1995]. Dynamic and cyclic fatigue (mastication) involves repeated loading of the restoration or tooth structure which induces cyclic stresses and the presence of surface or bulk defects [McCabe et al., 1990b].

Cyclic loading regimes have been used to simulate masticatory loading. Hu et al. (1999) sought to simulate masticatory loading of RBCs using a sine cam mechanism to produce sine curve loading on the wear surface and introduce variable loading patterns associated with mastication. Alternatively, a well established approach to simulate cyclic loading and determine fatigue resistance is known as the ‘staircase’ method. In essence, this method involves alternating the applied stress between 1MPa and a predetermined maximum, the tests were conducted sequentially with the maximum stress being increased or decreased dependent upon whether the specimen survived the previous test. If the specimen survives the preceding test the stress level

was increased by 4%, if failure occurs the stress level is decreased until a mean value is obtained [Braem et al., 1995; Lohbauer et al., 2003a; 2005; Turssi et al., 2006; Garoushi et al., 2007].

## 2.3 Wear of RBC restorations

Following placement RBC restorations are subjected to tribological wear, such as attrition, abrasion, erosion and parafunctional habits, in addition to masticatory fatigue (Section 2.2.3), which act either independently or in combination to produce loss of anatomical form and bulk fracture [Mair, 1996; Söderholm & Richards, 1998]. The occurrence of abrasion is the most common type of tribological wear of posterior RBC restorations and occurs as two or more substances, whether foreign particle, enamel or dentine, come into direct physical contact [Mair, 1996]. Abrasion is divided into two categories, namely two- or three- body wear, although clinically a combination of two- and three-body wear mechanisms often occur to degrade the tooth or RBC [Mair et al., 1996; Söderholm & Richards, 1998].

Two-body wear occurs when two occluding or proximal surfaces come into direct physical contact with opposing or adjacent tooth surfaces whilst undergoing loading [Mair, 1996]. The subsequent compression or sliding of these surfaces generates surface and subsurface damage, whilst plastic shear deformation induces high tensile stresses and cracking (Figure 2.7a) [Mair, 1994]. Three-body wear occurs when hard foreign particles present in the food bolus or toothpaste, are compressed and slide against occluding structures during mastication. These particulates effectively act as ‘milling grist’ and abrade the occluding surface where the tooth or restoration is softer than the particle (Figure 2.7b) [Söderholm & Richards, 1998].

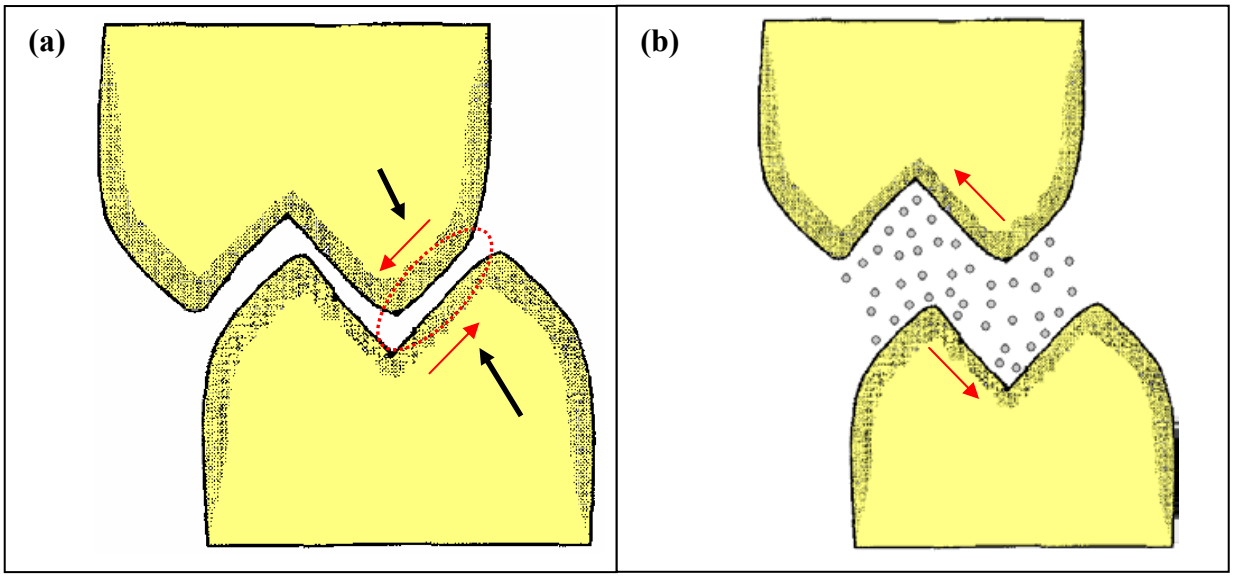


**Figure 2.7 Diagram representing (a) two- and (b) three-body wear, highlighting occlusal contact (black arrows and circled) and direction of tooth movement during mastication (red arrows).**

Hu et al. (2002) identified that two- and three-body wear mechanisms induced two distinct mechanisms of wear, namely deformation and delamination. Areas of deformation were identified to be initiated as specimen surfaces moving against a counter-surface caused the resin to be plastically deformed and generated subsurface microcracking. Subsequently, delamination mechanisms occur as these microcracks coalesce resulting in cracking parallel to the specimen surface. In contrast to the deformed regions, delamination produces rougher surfaces possessing observable filler particles which may be dislodged from the resin to produce a 'pitted' surface [Hu et al., 2002].

Adhesive wear occurs when two apparently flat surfaces are forced together, introducing a highly localised load to a comparatively small area of tooth structure which effectively 'cold welds' the asperities of the two surfaces. Subsequent movement, described as 'sliding', initiates transfer of material between surfaces and crack propagation through the bulk of the weaker material as the 'welds' are torn apart [Mair, 1996; Söderholm & Richards, 1998].

The occurrence of *in vivo* wear and the wear resistance of RBCs have been identified to be influenced by the filler size, morphology and distribution [Leinfelder, 1987; Schwartz et al., 2004]. Following the loss of the resin matrix at the surface of RBC restorations protruding filler particles remain. Subsequently, the rate of wear was initially slow as the protruding filler acts as a

'protective shoulder' to the remaining resin matrix, whilst continued loss of the resin causes filler 'plucking' and surface void formation [Hu et al., 2002]. The presence of larger fillers, such as those in traditional RBCs (Section 1.3.1.1), exhibit stress-induced 'tilting' and subsequent removal of protruding particles, resulting in increased surface roughness due to large pores and defects.

Jørgensen et al. (1979) determined that decreased interparticle spacing improved the clinical wear resistance, suggesting that shorter interparticle spacing of smaller fillers provided increased matrix protection. Likewise, the addition of colloidal silica particles with a mean size of 0.04μm to a BisGMA/TEGDMA resin was identified by Pallav et al. (1989) to increase wear resistance compared with an identical resin matrix reinforced with inorganic quartz fillers with a mean size of 3μm. A further wear study comparing filler sizes highlighted that resins reinforced with fillers that possessed a mean size of 1.5μm exhibited a wear value of $0.393\pm0.076mm^2$, whilst fillers with a mean size of 3.0 and 10.0μm exhibited successively increased mean wear values of $0.441\pm0.080$ and $0.528\pm0.094mm^2$ [Schwartz et al., 2004]. Schwartz et al. (2004) hypothesised that in addition to the matrix protection provided by shorter interparticle spacing suggested by Jørgensen et al. (1979), that the shorter interparticle spacing and high surface area of the smaller fillers reduced the diffusion rate of plasticizing agents, such as water or ethanol, thereby increasing the wear resistance. Consequently, the development of smaller particles, such as submicron and nanofills in modern RBCs, has sought to further reduce the interparticle spacing and thereby increase wear resistance [Mair, 1994; Söderholm & Richards, 1998].

### 2.3.1 The influence of 'nano' particles on tribology

The introduction of RBCs with an inorganic phase consisting of nano-sized filler particles (Section 1.3.2.4) has also sought to provide increased wear and fatigue resistance compared with pre-existing restoratives [Mitra et al., 2003; Turssi et al., 2005; 2006]. Despite this stated intention, a wear and fatigue study of several commercially available 'nanofills' highlighted no significant differences between two of the nanofills (Filtek™ Supreme; 3M ESPE and Grandio; Voco) compared with a microfill control (Heliomolar; Ivoclar vivadent), whilst the two other nanofills studied (Ceram-X; Dentsply and Premise; Kerr USA) possessed a lower fatigue strength [Turssi et al., 2006]. This disparity between the theoretical advantages of 'nanofills' and the apparent reality, was explained by Turssi et al. (2006) who noted that the size of discrete 'nano'

and ‘micro’ particles is approximately the same. Interestingly, the study suggested that the presence of pre-polymerized particles (Heliomolar and Premise) or ‘nanoclusters’ (Supreme) reduced the amount of wear due to the smaller particle size and the suggested improved interfacial bonding of Supreme and Premise, whilst Heliomolar exhibited interfacial failure, although the filler size and volume limited the occurrence of wear [Turssi et al., 2006].

Therefore, whilst the influence of nano-sized fillers on tribological wear in dental restorative materials remains debatable [Başeren et al., 2004; Lohbauer et al., 2006; Turssi et al., 2006; Bagheri et al., 2007; Beun et al., 2007; Masouras et al., 2007; Junior et al., 2008; Watanabe et al., 2008], the introduction of nanosized particulates to filled composite systems outside of the field of dental materials research has highlighted distinct improvements. The addition of 40nm alumina nanofillers at 20wt% to polytetrafluorethylene (PTFE) with a solid lubricant application was identified to significantly increase the wear resistance (x600) compared with unfilled PTFE [Sawyer et al., 2003]. Likewise, the addition of 1-10wt% 38nm alumina nanoparticles to semi-crystalline poly(ethylene) terephyhalate (PET) increased the wear resistance (x2) and decreased the mean coefficient of friction (10%), which was attributed to the formation of a more coherent and adherent transfer film [Bhimaraj et al., 2005].

### 2.3.2 Wear tests

The wear of RBC restorations has been identified to be a multi-factorial process involving mechanistic wear due to particles either from food or dislodged inorganic fillers which abrade the surface of RBC restorations [Schwartz et al., 2004], fatigue induced stress accumulation (Section 2.2.3), chemical and enzymatic wear (Section 2.1). Consequently, the wear of RBCs following placement in the oral cavity is difficult to accurately reproduce *in vitro*, although a variety of wear testing methodologies and machines have been developed.

Wear testing methodologies have included ‘pin-on-disc’ tests to determine movement between an abrasive and the specimen undergoing testing [Luo et al., 1998] and also ‘scratch’ tests where microscopy was employed to evaluate the depth and mechanism of wear [Jardret et al., 1998]. A further approach is the Academisch Centrum Trandheelkunde Amsterdam (ACTA) wear testing machine as described by Gee & Pallov (1994), which simulates *in vivo* wear at a predetermined force and rotational speed to mimic chewing frequency in abrasive slurry. The wear and surface hardness of the RBCs were subsequently determined.

A more advanced approach to *in vitro* determination of masticatory induced loading and fatigue has been the introduction of 'oral wear simulators' [Condon & Ferracane, 1996] and 'artificial mouths' [DeLong & Douglas, 1991] which sought to mimic abrasion and attrition mechanisms or to reproduce loads and movements of the masticatory cycle. The Oregon Health Sciences University (OSHU) 'oral wear simulator' described by Condon & Ferracane (1996) sought to mimic three-body wear of an enamel cusp acting as the antagonist in a food-like slurry against the RBC surface, profilometry and microscopy was than used to determine the extent of wear [Condon & Ferracane, 1996]. The 'artificial mouth' sought to mimic *in vivo* masticatory loading utilising two servo-hydraulic actuators to produce horizontal and vertical 'chewing' motions at a frequency of 4Hz within an environmental chamber which contained natural or artificial saliva. The study concluded that a high correlation existed between wear produced in the artificial mouth and corresponding clinical wear [DeLong & Douglas, 1991].

## 2.4 Summary

The degradation and subsequent failure of RBC restorations is a complex and multi-factorial process involving aspects of both physical and chemical wear. The fatigue of RBC materials introduces sub-critical cracking, the accumulation of which may result in premature failure of the restoration at loads considerably below the predicted mean strength of that material. The occurrence of fatigue induced damage, whether mechanistic or chemical in nature, degrades the resin matrix, interfacial silane coupling agent, the filler particle or a combination of these. Consequently, *in vitro* characterization of RBCs aims to mimic the occurrence of *in vivo* degradation, although the complex nature of wear mechanisms renders such investigations difficult. Thus a multi-disciplinary approach is required to yield data that may be combined to produce an overall indication of the degradation and subsequent mechanical and physical properties of modern RBCs and in particular the properties of so-called 'nanofills' reinforced with individually dispersed nano-sized filler particles and also 'nanocluster' particles.

## 2.5 Aims of Current Investigation

The mechanical and physical properties of the RBCs used in posterior and anterior restorations are influenced by the resin matrix chemistry, the silane interface and the size, morphology, distribution and loading of inorganic filler particles. Whilst the resin chemistry has, until recently, remained unchanged, the size of the filler particles has generally decreased to improve loading, aesthetics and the resulting mechanical properties of the RBC. The introduction of materials containing nano-sized particles and marketed as 'nanofill' and 'nano-hybrid' RBCs has resulted in speculation as to whether these so-called 'nano' materials exhibit improved mechano-physical properties compared with existing conventional RBCs.

**Null Hypothesis**

The 'nanocluster' particulate complex will not exhibit a significantly different fracture mechanism compared with representative spheroidal or irregular particles. Furthermore, the presence of nano-sized filler particles and 'nanoclusters' will not significantly influence the mechanical properties compared with existing conventional modern RBC materials.

1. In order to elucidate the reinforcement provided by the 'nanocluster' particles compared with inorganic filler particulates possessing conventional morphologies, namely spheroidal or irregular, the mechanical properties of discrete particles and agglomerates will be investigated. The efficacy of a novel micromanipulation technique to test the micromechanical properties of the filler particulates will also be investigated and developed.

2. The reinforcement provided by 'nanocluster' particles to the resin matrix, compared with conventional fillers, will be further investigated to determine the mechanical properties of these RBCs following cyclic pre-loading of disc-shaped specimens. The bi-axial flexure strength (BFS) data will also be assessed for reliability using the associated Weibull modulus. Furthermore, the influence of water storage on the resultant mechanical properties of the RBC specimens following pre-loading will be investigated.

3. The short-, medium- and long-term storage of RBC specimens in distilled water will be undertaken to determine the mechanical properties of the 'nanocluster' reinforced RBC compared with nano-hybrid and conventional RBCs. The water sorption will be examined using a near-infrared spectroscopy (NIRS) technique to determine the presence of water prior to and following storage. The filler morphology and the potential hydrolysis of the interfacial layer will also be examined using scanning electron microscopy (SEM).

4. The mechanical properties of the 'nanocluster', nano-hybrid and conventional RBCs will also be determined following storage in solvents known to initiate degradation of the interfacial silane coupling agent (sodium hydroxide) and the polymeric resin matrix (ethanol) in order to further characterize the reinforcement provided by the filler particulates. The extent of degradation of the resin matrix will be further characterized by determining the surface hardness (VHN) following solvent storage. Fourier transform infrared (FTIR) spectroscopy in the mid-range, in addition to SEM, will be used to assess the integrity of the interfacial silane layer following solvent storage.

5. Furthermore, whilst many manufacturers widely bandy terms such as 'nanofill', 'nano-hybrid' and 'nano-composite' these are not official classifications according to the accepted nomenclature established by Lutz & Philips (1983) and Willems et al. (1992). This system requires that filler morphology, size and loading provide distinct mechano-physical properties to the subsequent material. Consequently, the current study also aims to determine whether so-called 'nano' RBCs necessitate a classification according to this system.

# CHAPTER 3 EXPERIMENTAL PROCEDURE

## 3.1 Materials

The mechanical and physical properties of two commercially available 'nanofilled' resin-based composite (RBC) restorative materials, namely Filtek™ Supreme Body (FSB; batches: 6GY, 5CT, 6EE, 5BC and 5BB; shade A3) and Filtek™ Supreme Translucent (FST; batches: 7CT, 5BX, 5BT and 6CL; shade YT) (3M ESPE Dental Products, St Paul, MN, US) were evaluated and compared with two 'nano-hybrid' RBCs, namely Grandio (GR; batch: 671469; shade A3) and Grandio Flow (GF; batches: 671609 and 701238; shade A3) (VOCO, Cuxhaven, Germany). Two established RBCs, namely the microhybrid Filtek™ Z250 (FZ; batches: 6CR, 5UC, 6FC, 6EC, 6CR, 6FC, 6WU, 5TF and 7HY; shade A3) and the microhybrid Filtek™ Z100 (Z100; batches; 5UR, 7YG, 6YF and 7ET; shade A3) supplied by 3M ESPE were also investigated and compared. An additional microfill RBC Heliomolar (Ivoclar Vivadent, Schaan, Liechtenstein) was also investigated (HM; batch G05532; shade A3).

### 3.1.1 Resin matrix chemistry

The dimethacrylate-based resin matrix of FSB, FST, FZ, GR, GF, Z100 and HM, consisted of a photoactive monomer blend of 2,2-bis[4-(2-hydroxy-3-methacryloxypropoxy)phenyl]propane (bisphenol-A diglycidyl ether dimethacrylate; BisGMA) and the diluent triethylene glycol dimethyacrylate (TEGDMA). In addition, FSB, FST and FZ contained monomers of 2,2-bis[4-(2-methacrlyloxyethoxy)phenyl]propane (bisphenol-A hexaethoxylated dimethacrylate; $BisEMA_6$) and 1,6-bis(methacryloxy-2-ethoxycarbonylamino)-2,4,4-trimethylhexane (urethane dimethacrylate; UDMA). GF also contained 5-ethyl-1,3-dioxane-5-yl(methyl methacrylate) (hydroethyl dimethacrylate; HEDMA), whilst HM also contained dicandiol dimethacrylate ($D_3MA$) (Figure 3.1; Table 3.1).

**(a) BisGMA**

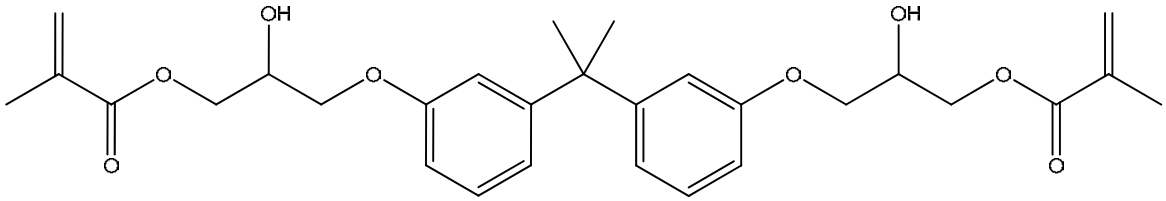

**(b) TEGDMA**

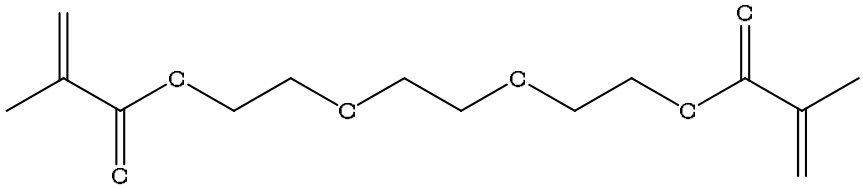

**(c) BisEMA**

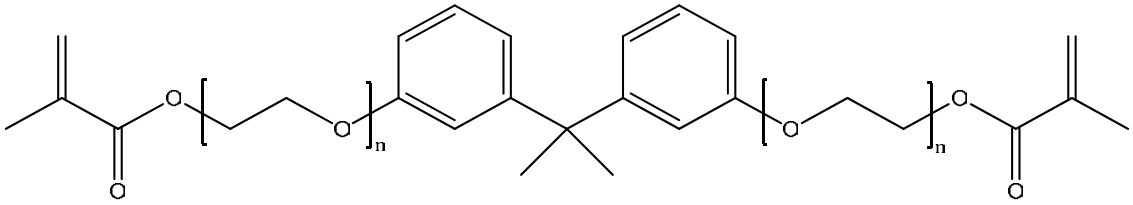

**(d) UDMA**

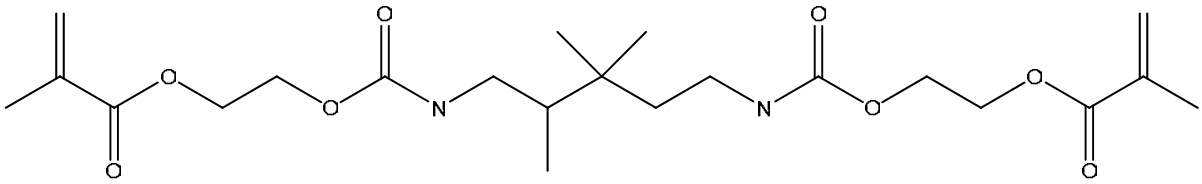

**(e) HEDMA**

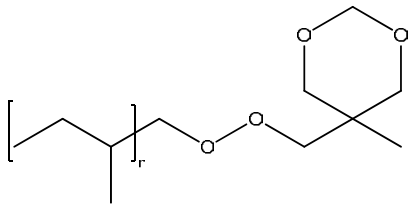

**Figure 3.1. The chemical structure of (a) bisphenol A glycol dimethacrylate (BisGMA), (b) triethyleneglycol dimethacrylate (TEGDMA), (c) bisphenol A hexaethoxylated dimethacrylate ($BisEMA_6$), (d) urethane dimethacrylate (UDMA) and (e) hydroethyl dimethacrylate (HEDMA).**

Light-activated polymerization of all RBCs was achieved by the admixture of initiator and co-initiating compounds. According to Shintani et al. (1985) and Alvin et al. (2007) dl-2,3-diketo-1,7,7-trimethylnorcamphane (camphorquinone; CQ) was a commonly used initiator, whilst Ferracane, (1995) and Chen et al. (2006) identified the routine use of the co-initiators dimethylaminoethylmethacrylate (DMAEMA) and an iodonium salt, such as (4-octylphenyl)phenyliodonium hexafluoroantimonate (OPIA), which act as electron donors. Alvin et al. (2007) identified 0.059, 0.082 and 0.054wt% CQ in FSB, FST and FZ respectively, whilst to the author's knowledge the photo-initiator content within GR, GF, Z100 and HM has not been reported. Furthermore, whilst the manufacturers were also not forthcoming regarding the specific inhibitors present within the resin matrix it is likely that hydroquinone was employed in a few parts per million [Combe & Burke, 2000]. An unspecified low molecular weight UV stabiliser/absorber was also added to limit degradation of the organic polymer by ultra-violet light [Lee et al., 1998].

### 3.1.2 Particulate filler morphology

The dimethacrylate monomer resin matrix of FSB and FST are reinforced with 'nanocluster' particulate complexes with a reported size distribution of 0.6-1.4μm and loaded to 71 and 30wt% respectively. The 'nanocluster' is an agglomeration of either nanosized (0.002-0.02μm; 2-20nm) colloidal silica and zirconyl salt to form Zr-$SiO_2$ particles (FSB), or nanosized (0.075μm; 75nm) silica, $SiO_2$, particles (FST) produced by a proprietary sol-gel technique from aqueous colloidal silica sols (Section 1.3.3) [Mitra et al., 2003]. The 'nanoclusters' are then partially calcined and silanated first with a silane coupling agent (γ-MPS) (Section 1.3.3.1) diluted with an unspecified solvent and water to ensure infiltration of the silane into the interstices of the clustered particle [Private communication; S. Mitra, 3M ESPE]. The 'nanocluster' particle was subsequently admixed with an undilute silane coupling agent (γ-MPS) prior to incorporation into the resin matrix [Mitra et al., 2003; Filtek™ Supreme Product Report 2003]. The resin matrix of FSB and FST were also loaded with dispersed nanosized silica, so-called 'nanomers', to 8 and 40wt% with a mean size of 0.005-0.02μm (5-20nm) and 0.075μm (75nm), respectively, produced by a proprietary sol-gel technique (Section 1.3.3). The filler particles were coated with a functionalized silane coupling agent (γ-MPS) (Section 1.3.3.1) prior to incorporation into the matrix. The total filler loading of FSB and FST was 79.0wt%

(59.5vol%) and 70.0wt% (57.5vol%), respectively [Mitra et al., 2003; Filtek™ Supreme Product Report 2003] (Table 3.1).

The resin matrix of the nano-hybrid materials GR and GF were loaded with two distinct filler size distributions to 87wt% (71.4vol%) and 80.2wt% (65.6vol%), respectively. Barium-alumina borosilicate ($BaAl_2O_3$-$BSiO_2$) was milled (Section 1.3.3) to produce particles with a mean size distribution of 0.1-2.5μm and possessed an irregular morphology. The resin loading was maximised by the addition of nanosized silica particles produced by a proprietary sol-gel method which possessed a mean size of 0.02-0.06μm (20-60nm) and a spherical morphology. The irregular and spherical fillers were also silanated (γ-MPS) [Grandio/Grandio Flow Scientific Documentation, 2006] (Table 3.1).

The microhybrid and microfill materials FZ and Z100 were both loaded to 84.5wt% (60 and 66vol%, respectively) with fused spheroidal silica-zirconia particles which possessed a size distribution of 0.01-3.5μm and a mean size of 0.6μm, produced by a sol-gel technique and admixed with a silane (γ-MPS) [Filtek™ Z100 Product Report, 1996; Filtek™ Z250 Product Report, 1998]. The microfill HM was loaded to 66.7wt% (46vol%) with pre-polymerized silica particles (Section 1.3.1.3) in addition to spherical ytterbium trifluoride filler, also produced by a proprietary sol-gel technique, which possessed a size distribution of 40-200nm (Table 3.1).

**BisGMA** bis-phenol A diglycidy ether dimethacrylate; **TEGDMA** triethyleneglycol dimethacrylate; **BisEMA$_6$** bis-phenol A polyethylene glycol diether dimethacrylate; **UDMA** urethane dimethacrylate; **HEDMA** hydroethyl dimethacrylate; **D$_3$MA** dicandiol dimethacrylate.

| | Classification | Resin | Filler | Total filler content | |
|---|---|---|---|---|---|
| Filtek Supreme Body (FSB) | Nanofill | BisGMA<br>UDMA<br>BisEMA$_6$<br>TEGDMA | Silica; 5-20nm nanoparticle (8.0wt%)<br>Zirconia/silica; 0.6-1.4μm nanocluster (71.0wt%) | 79.0wt% | 59.5vol% |
| Filtek Supreme Translucent (FST) | Nanofill | BisGMA<br>UDMA<br>BisEMA$_6$<br>TEGDMA | Silica; 75nm nanoparticle (40.0wt%)<br>Silica; 0.6-1.4μm nanocluster (30.0wt%) | 70.0wt% | 57.5vol% |
| Grandio (GR) | Nanohybrid | BisGMA<br>TEGDMA | Silica; 20-60nm<br>Barium-alumia borosilicate; 0.1-2.5μm | 87.0wt% | 71.4vol% |
| Grandio Flow (GF) | Nanohybrid | BisGMA<br>TEGDMA<br>HEDMA | Silica; 20-60nm<br>Barium-alumia borosilicate; 0.1-2.5μm | 80.2wt% | 65.6vol% |
| Filtek Z250 (FZ) | Microhybrid | BisGMA<br>UDMA<br>BisEMA$_6$<br>TEGDMA | Zirconia/silica; 0.01-3.5μm | 84.5wt% | 60.0vol% |
| Filtek Z100 (Z100) | Microhybrid | BisGMA<br>TEGDMA | Zirconia/silica; 0.01-3.5μm | 84.5wt% | 66.0vol% |
| Heliomolar (HM) | Microfill | BisGMA<br>UDMA<br>D$_3$MA | Pre-polymer (containing silica)<br>Ytterbium trifluoride; 40-200nm | 66.7wt% | 46.0vol% |

**Table 3.1. Summary of the resin matrix constituents, filler and loading in the nanofill (FSB and FST), nano-hybrid (GR and GF), microhybrid (FZ and Z100) and microfill (HM) materials studied in the current investigation. The main photoinitiator was camphoroquinone, with co-initiators DMAEMA and an iodonium salt.**

## 3.2 Mechanical Properties of Nanofilled RBCs

### 3.2.1 Characterising discrete filler particles and agglomerates

A micromanipulation technique was employed to assess the mechanical properties of discrete inorganic filler particulates with various morphologies, namely 'nanocluster', spheroidal or irregular, representative of filler types routinely employed in modern RBCs. The micromanipulation technique is essentially a compression test, whereby an individual particle is loaded to catastrophic failure between a micron diameter glass probe and a parallel glass slide [Zhang et al., 1992]. The subsequent force at fracture is measured and pseudo-modulus of stress deteremined [Zhang et al., 1991]. Furthermore, as micromanipulation has not previously been employed in the field of dental materials research the validity and efficacy of the technique was also investigated.

#### 3.2.1.1 Discrete filler particles

The micromanipulation technique required filler particles discrete from the resin matrix. The manufacturers supplied unsilanated 'nanocluster' (3M ESPE) and irregular (Voco) filler particles, whilst spheroidal zirconia-silica fillers were obtained by separation from the unpolymerized monomer paste of FZ using a chemical dissolution technique. Preliminary studies identified no significant differences in mechanical properties identified using the micromanipulation technique between particles supplied by the manufacturers compared with those separated from commercial RBC pastes using the dissolution technique. In addition, comparison of unsilanated and silanated irregular filler particles supplied by the manufacturer identified no significant difference between the subsequent mechanical properties (Appendix 1).

**Dissolution technique**

The dissolution technique required a consistent resin composite mass (0.5±0.01g) to be dissolved in 4ml of undilute acetone (laboratory reagent grade, Fisher Scientific Ltd., Loughborough, UK) and centrifuged for 2mins at 1000rpm (IEC Centra-3, Damon, Bedfordshire, UK). The excess liquid was removed using a pipette and the centrifugation technique was repeated twice with fresh acetone each time. The remaining mass was dissolved in 4ml of undilute chloroform (laboratory reagent grade, Fisher Scientific Ltd., Loughborough, UK) and

centrifuged a further three times for 2mins at 1000rpm [Beun et al., 2006]. The filler particles were dried for 1h in an oven at 90±5°C (LTE Scientific Ltd., Oldham, UK).

#### 3.2.1.2 Micromanipulation technique

A probe was produced from a borosilicate glass capillary tube (GC100-15, 1.0mm diameter; MicroInstruments Ltd., UK) using a glass puller (PE-21; Narishinge, Japan) and microforge (MF900; Narishinge, Japan) to draw the glass tube to a tip with a diameter of 40µm. The probe-tip was subsequently ground and polished using a graduated grinding regime; 320, 800 and 1200 grit silicon carbide (Strueres Ltd., UK), in a micropipette grinder (Narishinge, Japan) for 120mins to produce a theoretically perfectly flat and infinite surface [Zhang et al., 1992; Shiu et al., 1999; Blewett et al., 2000].

The filler particles were dispersed in a suspension of distilled water on a glass microscope slide and placed on the micromanipulation rig. The suspension was allowed to dry and isolated individual particles were identified using an inverted and side-angle light-microscope (LWD MPlan APO; Meiji Techno, Mitutoyo, Japan) and camera (Chou, High Performance CCD Camera) mounted on a UniSlide platform (LG Motion Ltd., Basingstoke, UK) at magnification of x1000. The two microscopes enable the slide to be viewed from below and the side, facilitating identification of single particles, which was a potentially extremely time consuming process due to the small particle size, even when magnified. Particles were positioned centrally under the probe. It was essential to ensure that the particles loaded were discrete from adjacent particles within a radius of 40µm (the diameter of the probe) to prevent multiple particles undergoing loading and potentially generating spurious results. The diameter of the particle was measured (µm) prior to loading using a graticule, where 1mm on the light microscope screen was known to be equal to 1µm [Private communication, K. Liu, University of Birmingham School of Chemical Engineering]. Irregular particles were measured at the widest point. The probe was connected to a force transducer (Model 406A, Cambridge Technology, Watertown, USA) using paraffin wax, and possessed a response sensitivity of 486µN/V at a resolution of 0.01µN. The probe was driven by a micromanipulator (MicroInstruments Ltd, Oxford, UK) compressing the filler particle at a constant velocity of 2.0±0.2µm/s. The force imposed on the particle during loading was measured by the transducer and the voltage output (magnitude of force) was recorded on a PC-30D data acquisition card (Amplicon Live-line, Brighton, UK) (Figure 3.2).

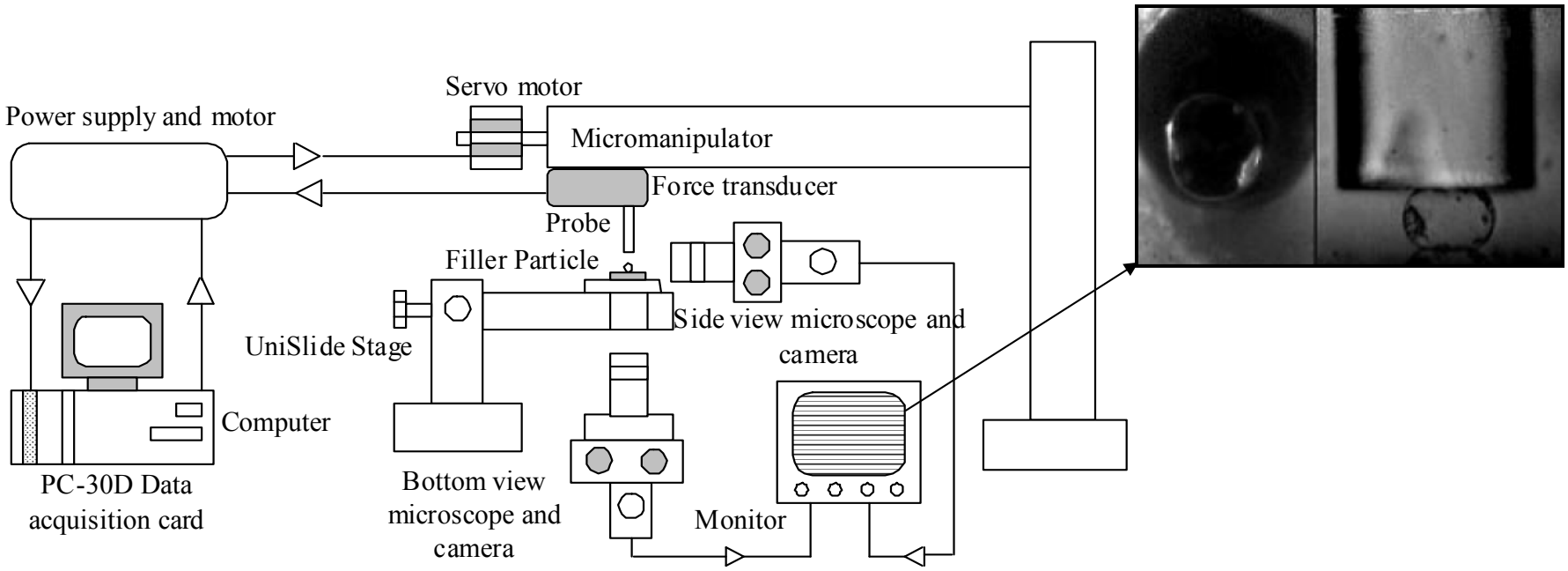


**Figure 3.2. Schematic diagram representing the micromanipulation apparatus. (Reproduced with the kind permission of Prof. Z. Zhang, School of Chemical Engineering; University of Birmingham). Insert represents view of particle (left: inverted-view microscope camera, right: side-view microscope camera) undergoing compression. It is important to note that due to the set-up of the micromanipulation rig used by the author that capturing images of the particles under compression was unfortunately not possible. The image seen here is that of a cell and is modified from Blewett et al. (2000), the diameter of the cell is 35-85µm, which is markedly greater than that of the particulates (2-12µm) which underwent micromanipulation in the current study.**

**Compliance**

The compliance of the micromanipulation probe was calculated prior to particle loading to determine accurate displacement and deformation curves following micromanipulation. Compliance, C (μm/μN) was determined by compressing the probe directly against a glass slide and calculated according to Equation 3.1,

$$C = \frac{\alpha v}{r\omega} \qquad \text{Equation 3.1}$$

where α was the acquisition time between collection of data points (0.01872s), v the probe velocity (2.0±0.2μm/s), r the mean gradient of the regression line on the load-deformation graph and ω the transducer sensitivity (486μN/V).

**Force/displacement**

The force, f, imposed during compression and the force at fracture (μN) of the selected filler particles was calculated as in Equation 3.2,

$$f = V\omega \qquad \text{Equation 3.2}$$

where V was the voltage of the descending probe recorded during testing. The displacement, d (μm) of the filler particles during compression was calculated in accordance with Equation 3.3,

$$d = (V\alpha) - (fC) \qquad \text{Equation 3.3}$$

Force and displacement were plotted and the occurrence of particle fracture recorded. The force prior to fracture and the related particle displacement were measured from the graph.

**Stress/deformation**

The pseudo-stress (MPa) of the filler particles during loading and at fracture was calculated using Equation 3.4 [Chung et al., 2005; Müller et al., 2005],

$$\sigma = \frac{4f}{\pi ø^2}$$ Equation 3.4

where ø was the diameter of the filler particle (μm) measured prior to micromanipulation. The 'pseudo-stress' describes the ratio of applied force divided by the original cross-sectional area of each particle prior to deformation. The term 'pseudo' was used, as to calculate the 'real' stress the contact area between the particle and probe must be known. However, since the contact area varies with deformation and as particles were extremely small it was not possible to accurately measure the contact area. Therefore, a 'pseudo' stress is calculated which provides an approximation of the 'real' stress. The percentage deformation of the filler particles during compression was calculated according to Equation 3.5,

$$def(\%) = d/ø$$ Equation 3.5

The pseudo-modulus of stress was determined by superimposing a regression line through the linear section of stress-deformation graphs.

**3.2.1.3 Filler morphology**

The filler morphology and size of discrete particles was examined using a scanning electron microscope (SEM; JSM 5300 LV, Jeol Ltd., Akishima Tokoyo, Japan). The SEM operates by producing a beam of electrons from a tungsten filament gun focused onto the surface of the sample within an SEM chamber maintained under vacuum. Condenser lenses focus the electron beam between 5nm to 1μm, operating at a current of $10^{-6}$ to $10^{-12}$ amps with an accelerating voltage of between 1 and 30kV, depending on the image quality to magnification required by the operator. The resultant electron beam scans the specimen surface to produce low energy secondary electrons which pass into a cathode ray tube to form an image that can be displayed. The resolution of the image was modified by adjustment and refinement of the parameters at which the electron gun operated, specifically the spot size, current, voltage, detector efficiency and also the working distance between filament and specimen surface; namely

distance the electron beam travels. Adjusting the strength at which the condenser lenses operate produced high magnification and sharp images of specimen surfaces.

Prior to SEM analysis individual filler particles were deposited on an aluminium specimen SEM stub (Agar Scientific Ltd., Essex, UK) using adhesive carbon conducting tags (Agar Scientific Ltd.). Particles were sputter coated to deposit a 2±0.2μm layer of gold from a TK8842 gold target (Emitech Ltd., Ashford, Kent, UK) using an Emitech K550X sputter coater (Emitech Ltd.) with a runtime of 2mins and a voltage of 25mA. Sputter coating creates a conductive surface across the specimen and reduces the occurrence of electron charging, which would reduce the image quality attainable. The sample was carefully handled throughout the procedure using tweezers and cotton gloves to prevent damage which may dislodge particles following sputter coating and create artefacts which subsequently reduce the image quality and attainable magnification.

The filament gun conditions were maintained throughout the procedure by controlling the spot size and operating current and maintaining the accelerating voltage at 20kV. Images were captured using Semaphore computer software (Digital slow scan image recording system, Version 4.01, LEAD Technologies, Jeol, Sundbyberg, Sweden).

**Cryo-SEM Procedure**

A cryo-SEM technique (Jeol JSM 7000F; Jeol Ltd, Akishima Tokyo, Japan) was also employed to produce a cross-sectional fracture surface through the bulk of the RBC to further examine the particle size, morphology and filler distribution. The cryo-SEM technique was employed to ensure fast and homogeneous freezing of the specimen structure and used a plunge freezing technique whereby specimens were manually plunged into liquid nitrogen. Specimens were then transferred into the cyro-preparation unit, maintained at ˉ170°C under vacuum. An accessory tool enabled brittle fracture of the frozen specimen to expose the internal structure, the specimen was then sputter coated with a uniform 2±0.2μm layer of gold to reduce the occurrence of electron charging. The prepared specimen was transferred to the cryo-stage in the SEM chamber, also maintained at ˉ170°C. The fracture surface was subsequently examined in the BEI mode with an operating voltage of 5kV.

### 3.2.2 The impact of cyclic loading on nanofill RBCs

The seven commercially available RBCs; FSB, FST, GR, GF, FZ, Z100 and HM (Section 3.1), underwent a series of pre-loading regimes to simulate masticatory loading forces of 10-20N typically generated whilst chewing foodstuffs [Anderson, 1956] and also loads of up to 100N [Helkimo, 1978] (Section 2.2.3). The specific aim of pre-loading was to determine the influence of nano-sized filler particles and 'nanoclusters' in RBCs on the mechanical properties following cyclic pre-loading and subsequent 'dry' or 'wet' storage.

#### 3.2.2.1 Specimen preparation

Eight groups of each RBC were produced consisting of twenty nominally identical disc-shaped specimens (12mm diameter, 1mm thickness) using a black nylon ring-mould. A preliminary study identified that 0.235±0.003g of RBC paste measured using a Mettler AE 163 analytical balance (Mettler-Toledo Ltd., Leicester, UK) accurate to $1x10^{-4}$g was sufficient to slightly overfill the ring-mould. The measured quantity of RBC paste was packed into the nylon mould with the upper and lower surfaces covered with acetate strips (approximately 0.1mm thick) to limit surface oxygen inhibition on the outer layers of the specimen. A 1kg weight was applied to the specimen surface for 20s to ensure homogeneous distribution of the RBC paste within the disc-shaped mould. The filled mould was placed within a black nylon curing light guide (24mm diameter, 6mm height and 30mm diameter, 18mm height, respectively) to ensure concentric placement of the curing-tip for each successive specimen irradiation [Harrington & Wilson, 1993]. This was placed on a stainless steel platen and irradiated from one side for 20s at an ambient temperature of 23±2°C, in accordance with the manufacturer's instructions. A quartz-tungsten halogen (QTH) light-curing unit (LCU; Optilux 501; Kerr, Orange, USA) with a curing-tip exit window diameter of 12mm was used to irradiate all disc-shaped specimens (Figure 3.3).

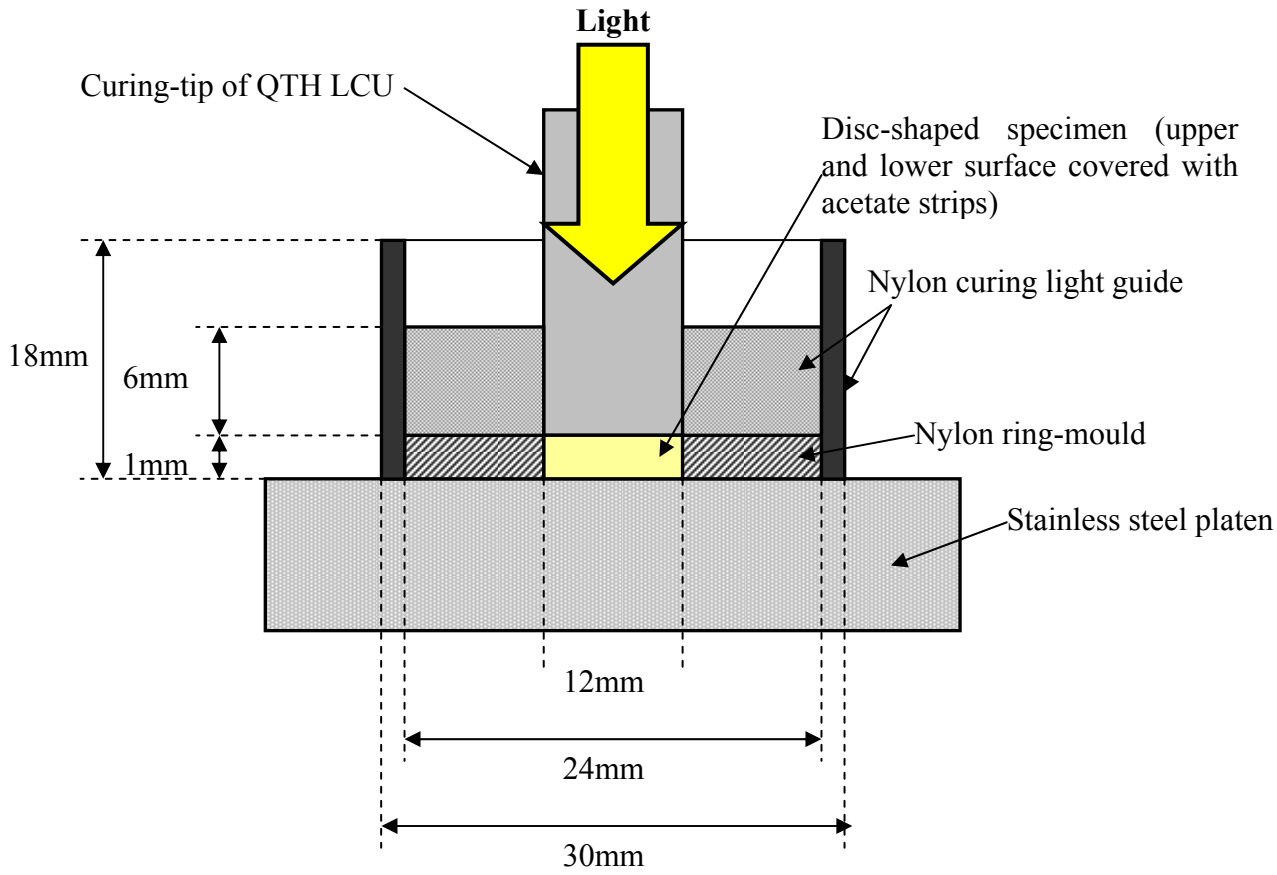


**Figure 3.3. Diagram representing the placement of the disc-shaped RBC specimen (12mm diameter and 1mm thickness), nylon ring-mould, curing guide, curing-tip of the QTH LCU and stainless steel platen during light-activated polymerization.**

Since a large number of specimens were fabricated the light intensity of the LCU was measured at regular intervals to ensure consistent irradiation, the maximum output at the outset of this research measured at full aperture (Model 100, Demetron Research Corp., Danbury, CT, US) was 690±20mWcm$^{-2}$. When the intensity decreased to below 650±20mWcm$^{-2}$ the halogen bulb was replaced and the irradiance remeasured to be 690±20mWcm$^{-2}$. Following irradiation of each specimen the cellulose acetate strip was discarded and flash cut away using a sharp blade. Each disc-shaped specimen was examined for obvious surface or bulk defects using a light-box, discarded if necessary and sample numbers replenished as required. One group of each material was stored 'dry' in a lightproof container or 'wet' in a lightproof water-bath at 37±1°C for 24h.

### 3.2.2.2 Pre-loading regimes

The remaining six groups of each RBC material were subjected to pre-loading of 20, 50 or 100N for 2000 cycles using a universal tensile machine (UTM) (Model 5544, Instron Ltd.,

Buckinghamshire, UK). Each specimen was placed within a bespoke stainless steel alignment jig (12.2mm diameter and 5.0mm depth cavity) to fit the UTM and allow for stable positioning of each disc-shaped specimen. Specimens were centrally loaded with a stainless steel ball-indenter (3mm diameter) either 'dry' or 'wet' in distilled water at 37±1°C. Cyclic testing was performed using a sinusoidal waveform at a crosshead speed of 8mm $min^{-1}$ (1.67Hz). Following pre-loading, specimens were stored either in a lightproof container or a lightproof waterbath maintained at 37±1°C for 24h dependent on test condition, prior to bi-axial flexure strength testing.

#### 3.2.2.3 Bi-axial flexure strength testing

The bi-axial flexure strength (BFS) was determined by centrally loading each specimen using a 3mm diameter ball-indenter at a crosshead speed of 1mm $min^{-1}$, with the cured side in tension on a UTM (Model 5544) with a 2kN load cell. The specimens were positioned on a 10mm knife-edge support with a thin sheet of rubber placed between the specimen and the support to ensure uniform loading and to accommodate variations in the peripheral thickness or distortions of the specimen surface. The load (N) and extension (mm) at failure of each specimen was recorded and the specimen thickness at the point of fracture was measured (mm) using a screw-gauge micrometer (Moore & Wright, Sheffield, UK) read to an accuracy of 10µm (Figure 3.4).

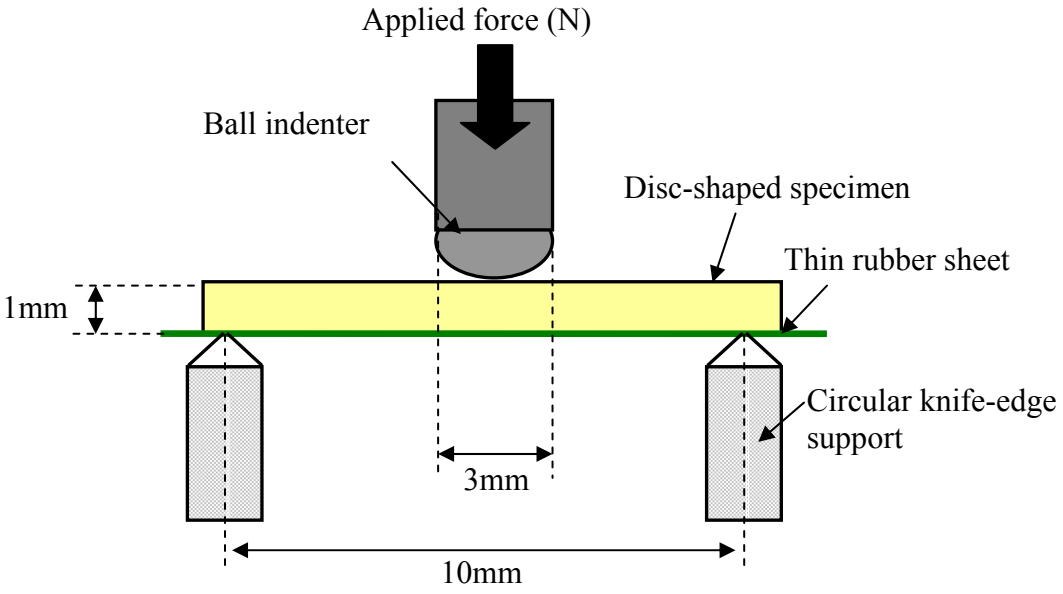


**Figure 3.4. Schematic representing bi-axial flexure testing of a disc-shaped RBC specimen (12mm diameter and 1mm thickness) on a knife-edge support with the cured side placed in tension. A UTM with a 3mm ball indenter was used at a crosshead speed of 1mm $min^{-1}$.**

The BFS of the RBC specimens was then calculated according to Equation 3.6 [Timoshenko et al., 1959]

$$\sigma_{max} = \frac{P}{h^2}\left\{(1+v)[0.485\ln\left(\frac{a}{h}\right)+0.52]+0.48\right\} \qquad \text{Equation 3.6}$$

where $\sigma_{max}$ was the maximum tensile stress (MPa), P was the measured load at fracture (N), a was the radius of the knife-edge support (mm), h was the specimen thickness at the point of fracture (mm) and υ the Poisson's ratio for the composite investigated. The Poisson's ratio of a material was defined by Kingery (1976) as the lateral contraction per unit breadth divided by the longitudinal extension per unit length. A value of 0.225 was substituted for the RBC systems used in the current investigation [Ban & Anusavice, 1990].

**3.2.2.4 Flexural modulus**

Two groups of each RBC consisting of five nominally identical beam-shaped specimens (2mm width, 25mm length and 2mm thickness) were produced. A predetermined quantity of monomer paste, 0.260±0.005g, was employed to slightly overfill the rectangular beam-shaped black Nylotron split mould. A split mould was employed to enable specimen removal without the introduction of excessive bending stresses which may influence the resultant flexure strength. Cellulose acetate strips were placed over the upper and lower surfaces to reduce oxygen inhibition on the outer layers of the specimen. A 1kg weight was applied to the specimen surface for 20s to ensure homogeneous distribution of the RBC paste within the beam-shaped mould. To provide a 'one-hit' cure and to prevent inhomogeneous cure associated with overlapping irradiation techniques [Palin et al., 2005b] the mould and monomer paste were irradiated in a light-curing oven (Visio-Beta Vario, 3M ESPE), for 14min. The irradiance of the oven-LCU was not quoted by the manufacturer, however a previous investigation with the same oven calculated the irradiance using the output from a light-dependent resistor (LDR) to determine an irradiance of 67.6±3.1mW/cm$^2$ [Palin et al., 2005b]. For the current investigation preliminary data suggested a curing time of 14mins for the oven-LCU to provide an equivalent radiant exposure

and curing extent as the handheld-LCU (Appendix 2). The specimen was carefully removed from the split-mould following irradiation and excess flash was cut away using a sharp blade. Specimens were examined for surface or bulk defects using a light-box and discarded and replaced as required. The specimens were subsequently stored either 'dry' in a lightproof container or 'wet' in a lightproof waterbath maintained at 37±1°C for 24h prior to three-point flexure testing.

The flexural strength was determined in accordance with the International Standard for Dental Polymer-Based Filling, Restorative and Luting Materials (ISO 4049 3rd Edition, 2000), although as previously described in Section 2.2.2.1 the overlapping curing method was replaced with a 'one-hit' cure in an oven-LCU. The beam-shaped specimens were placed across a support span of 20mm with the surface directly facing the curing bulb within the oven-LCU in tension. Specimens were centrally loaded using a roller indenter with a 3mm width, on a UTM at a crosshead speed of 1mm $min^{-1}$. The load (N) and deflection (mm) of the beam at failure was recorded, the width and thickness of the specimen at the point of fracture (mm) was measured using the screw-gauge micrometer. The flexure strength of the beam-shaped specimens, σ (MPa), was determined in accordance with Equation 3.7

$$\sigma = \frac{3Fl}{2bh^2} \qquad \text{Equation 3.7}$$

where F was the applied load at fracture (N), l is the span length (20mm), b is the width of the test specimen (mm) and h is the thickness of the test specimen (mm). The flexural modulus E (GPa) of the six RBCs studied in the current investigation was then calculated according to Equation 3.8,

$$E = \frac{Fl^3}{4bh^3d} \qquad \text{Equation 3.8}$$

where d was the deflection of the specimen corresponding to load at F where failure occurred (mm).

## 3.3 Degradation of Nanofilled RBCs

### 3.3.1 Water storage

The aim was to determine the influence of short-, medium- and long-term immersion on the water uptake and mechanical properties of 'nanofill' compared with conventional RBC materials. Disc-shaped RBC specimens (12 diameter, 1mm thickness) prepared as described in Section 3.2.2.1 were stored in high purity double distilled de-ionised water (Fistreem Cyclon, Sanyo Gallenkamp, Leicester, UK) to provide a reproducible reference solution [Martin et al., 2003] (Section 2.1.1.2).

Specimens stored in the waterbath were first placed within a polypropylene (PP) container (90mm diameter and 35mm depth), to allow maximum water exposure to surrounding solute the specimens were supported at the diametral axis using a small quantity of dental wax [Palin et al., 2005c]. To further ensure maximum water exposure to the disc-shaped specimens the PP container was prepared by adding a total of approximately thirty holes (6mm diameter) prior to submerging both container and specimens in the waterbath (Figure 3.5).

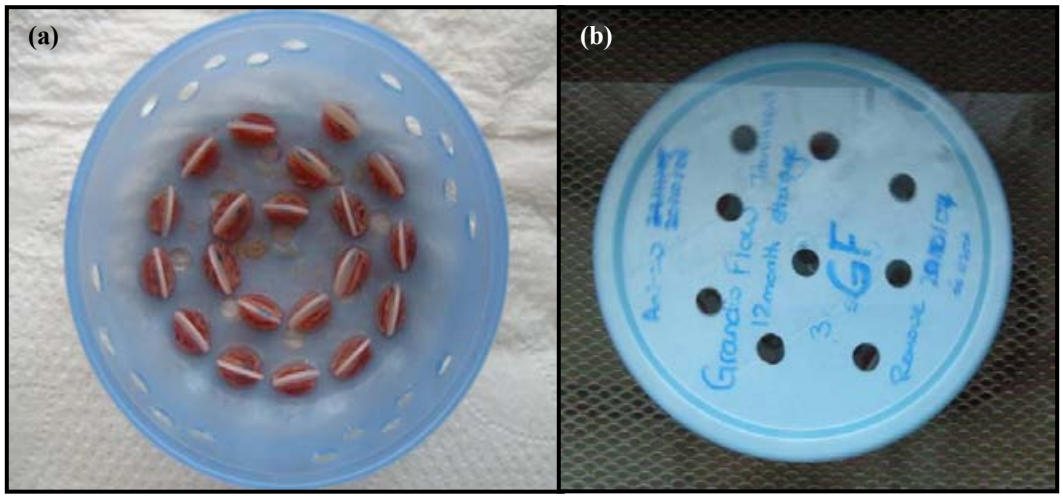


**Figure 3.5. (a) Image of disc-shaped specimens supported at the diametral axis placed within the PP container (without lid) and (b) image of the container (with lid attached) submerged in the waterbath.**

One group (n=20) of disc-shaped specimens of each material; FSB, FST, GR, GF, FZ, Z100 and HM, were produced according to the method previously described (Section 3.2.2.1) and stored 'wet' in a lightproof waterbath (Type JB2, Grant Instruments, Cambridge, UK) at 37±1°C for 24h to represent short-term storage and also as the control group. To avoid the potential accumulation of leached RBC components in the waterbath, 1L of distilled water was removed and replaced with freshly distilled water on a weekly basis. The specimens were subsequently loaded to failure under bi-axial flexure (Section 3.2.2.3).

Four groups (n=20) of disc-shaped FSB, FST and FZ specimens were produced (Section 3.2.2.1) and underwent medium-term storage for 1, 4, 13 or 26 weeks in a waterbath maintained at 37±1°C prior to BFS testing (Section 3.2.2.3). In addition, two groups of GR and GF specimens were also produced and stored in the waterbath for 13 and 26 weeks prior to testing.

A further two groups of FSB, FST and FZ specimens (n=20) were produced (Section 3.2.2.1) and underwent long-term storage for 52 and 78 weeks, whilst an additional group of disc-shaped GR and GF specimens underwent storage for 52 weeks, prior to bi-axial flexure testing (Section 3.2.2.3). The apparent discrepancy between FSB, FST and FZ and GR and GF specimen storage (Table 3.2) occurred as the reinforcement of the so-called 'nanoclusters' and 'nanomers' (FSB and FST) compared with micro-sized particles (FZ) within an identical resin matrix was studied. Furthermore, the reinforcement of differing inorganic filler types within the varied organic matrices was also studied, although material and time limitations constrained this.

| | 24h | 1wk | 4wks | 13wks | 26wks | 52wks | 78wks |
|---|---|---|---|---|---|---|---|
| **FSB** | ✓ | ✓ | ✓ | ✓ | ✓ | ✓ | ✓ |
| **FST** | ✓ | ✓ | ✓ | ✓ | ✓ | ✓ | ✓ |
| **FZ** | ✓ | ✓ | ✓ | ✓ | ✓ | ✓ | ✓ |
| **GR** | ✓ | | | ✓ | ✓ | ✓ | |
| **GF** | ✓ | | | ✓ | ✓ | ✓ | |

**Table 3.2. Table highlighting the short-, medium- and long-term storage of the nanofill (FSB and FST), microfill (FZ) and nano-hybrid (GR and GF) specimens.**

For comparative purposes additional specimen groups (n=20) of FSB, FST, GR, GF, FZ, Z100 and HM were produced and stored 'dry' in a lightproof container maintained at 37±1°C for 24h.

### 3.3.1.1 Near-infrared spectroscopy

Fourier transform infra-red (FTIR) spectroscopy in the near-infra-red (NIR) range (4000-12000cm$^{-1}$) was used to determine the extent of water uptake following short-, medium- and long-term storage in the waterbath, the water content of specimens stored 'dry' for 24h was also determined. An additional five disc-shaped specimens of FSB, FST, FZ, GR and GF were produced (Section 3.2.2.1) and dehydrated in accordance with the process stipulated by ISO4049. Specimens undergoing dehydration were weighed prior to transfer to a light-proof desiccator containing dehydrated silica gel (Fischer Scientific, Leicester, UK) maintained at 37±1°C for 22h, followed by 2h at 23±1°C. The specimens were then reweighed and the conditioning cycle repeated until the mass loss of each specimen was not more than 1x10$^{-3}$g. Following the conditioning cycle the NIR technique was used to determine presence or absence of water.

Five specimens of each RBC were examined following the requisite storage or conditioning regimes using a Matrix-F spectrophotometer (Bruker, WI, USA) to determine water content from the absorbance band centred around 5200cm$^{-1}$, associated with symmetric stretch and bend of the O-H bond of water [Keyworth, 1961; Venz & Dickens, 1991; Diaz-Arnold & Williams, 1992]. Specimens stored 'wet' were dried using absorbent paper and allowed to further dry in air for 60s at an ambient temperature of 23±1°C.

Prior to testing a background air spectra was produced and subtracted from proceeding spectra. The specimen was placed on a stainless steel platen at an ambient temperature of 23±1°C and an absorbance spectrum was collected by averaging 62 scans over the spectral region of 11000 to 4000cm$^{-1}$ with a resolution of 4cm$^{-1}$ and a base-line correction was conducted. A spectral manipulation program (Opus 5.5, Bruker, WI, US) was used to process the spectra and calculate the area under the water absorbance band. An integration method available in the spectral manipulation program calculated the square root of the sum of squares of the spectral intensities over the frequency range of 4875-5350cm$^{-1}$. The absorbance units of water content were then calculated from a logarithm of each spectral point.

### 3.3.1.3 Fracture morphology

A cross-sectional fracture surface through the bulk of specimens following BFS testing was produced using the cryo-SEM technique (Section 3.2.1.3) to examine the particle size, morphology and filler distribution in specimens stored 'dry' for 24h and 'wet' for 26 weeks.

### 3.3.2 Accelerated degradation of RBCs

Six groups of nominally identical disc-shaped specimens (n=5) of FSB, FST, GR, GF, FZ and Z100 were prepared in accordance with the method outlined in Section 3.2.2.1 and stored in either sodium hydroxide (NaOH) or ethanol (EtOH) to examine the degradation of the silane coupling agent and the resin matrix (Section 2.1.1.2). Three groups of each material were stored in 0.1M NaOH solution (laboratory reagent grade, Fisher Scientific Ltd., Loughborough, UK), whilst the remaining three groups were stored in 75% absolute EtOH (Fisher Scientific Ltd., Loughborough, UK). The specimens and solvent solution were placed in glass beakers (150ml, Fisherbrand, Fisher Scientific Ltd., Loughborough, UK), in a lightproof waterbath maintained at 37±1°C for 24h, 1 and 2 weeks. Following storage specimens were loaded to failure using the bi-axial flexure test (Section 3.2.2.3) and the BFS was calculated.

#### 3.3.2.1 Surface Hardness Testing

The surface hardness of the RBCs following storage in EtOH and also following storage 'dry' and 'wet' for 24h (Section 3.3.1) was assessed using a Duramin-1 Vickers hardness tester (Struers, Glasgow, UK). The hardness of a material is not an absolute value as no universal hardness scale has been established. Instead hardness relates to the force applied and is a function of the test method employed, such as Knoop, Wallace or Vickers [Darvell, 2006]. The Vickers indentation test employed in the current study provided a hardness value as a Vickers Hardness Number (VHN).

Following bi-axial flexure testing five specimen fragments were selected at random and the upper surface was indented within 2mm of where the centre of the complete disc-shaped specimen had been to ensure a uniform degree of polymerization [Palin et al., 2008]. Specimens were indented at a load of 9.8N using a Vickers hardness tester (Struers) with a diamond pyramid head for a constant dwell time of 15s to produce the characteristic diamond-shaped indent (Figure 3.6).

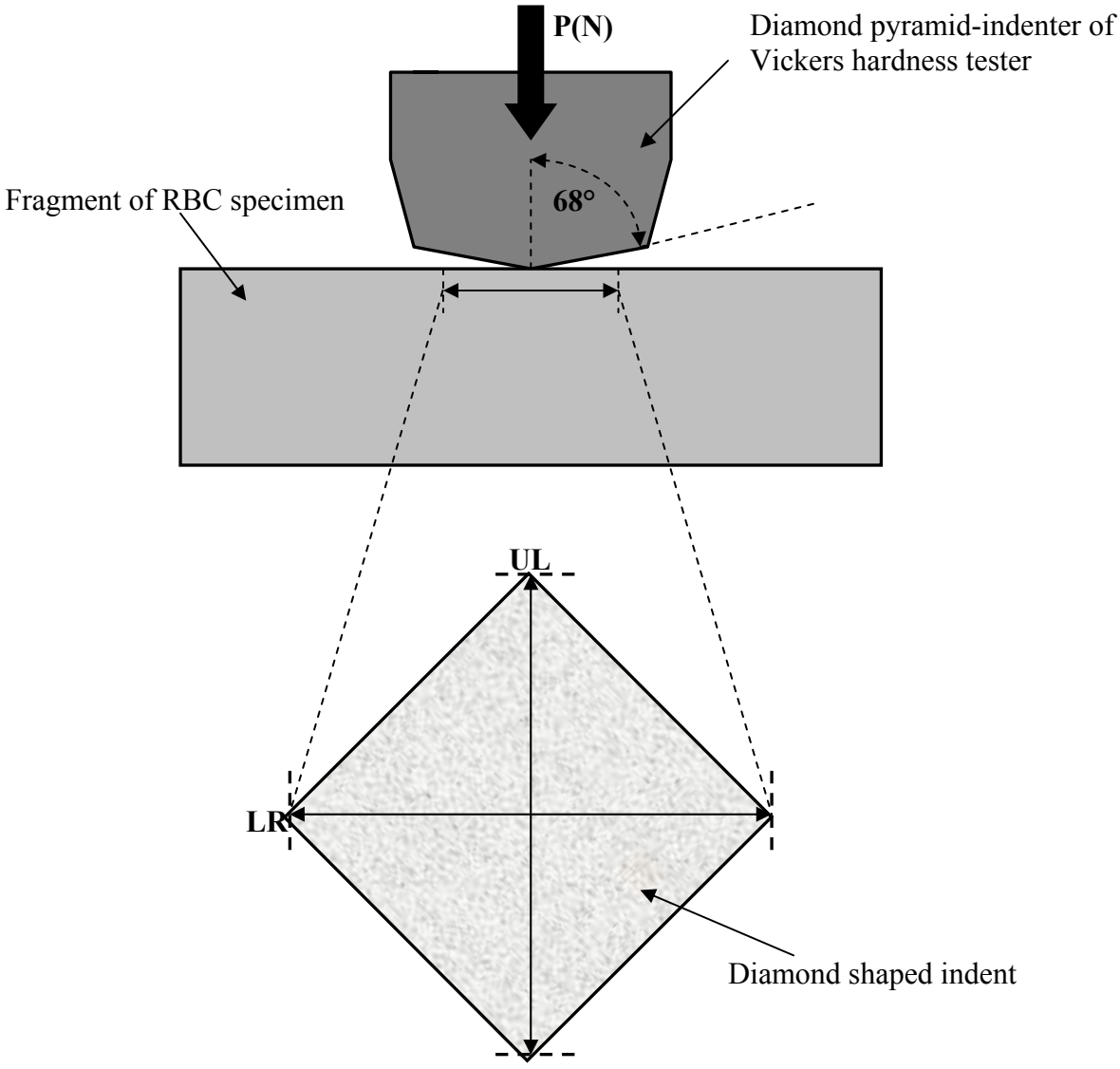


**Figure 3.6. A schematic diagram of Vickers indentation technique; the diamond crosshead indenter with a 68° angle of indentation was applied at a pre-determined load of 9.8N (P). The average upper-lower (UL) and left-right (LR) diagonal distance of the diamond-shaped indent was measured and the VHN calculated.**

Each specimen was indented five times and a mean VHN calculated. The dimensions of the indent were measured using a calibrated graticle, which had been 'zeroed' prior to testing, situated within the light microscope attachment of the hardness indenter to obtain a mean diagonal distance (μm) of the left-right and upper-lower points of the indent. The VHN was then obtained by calculating the surface area of the indent in accordance with Equation 3.9,

$$VHN = \left(\frac{2P}{D^2}\right)\sin\left(68^o\right) = \left(\frac{1.854P}{D^2}\right) \qquad \text{Equation 3.9}$$

P was the predetermined load applied in Newtons (N), D the average diagonal distance (μm) and 68° was the angle of indentation of the diamond pyramid head indenter of the Vickers hardness tester. A large diamond-shaped indent was indicative of reduced surface hardness, resulting in an increase in the measured diagonal distance [McColm, 1990].

### 3.3.2.2 Mid-range FTIR spectroscopy

FTIR spectroscopy in the mid-infra-red range (700-4000cm$^{-1}$) was used to qualifiedly determine the silica and silane content and degradation of the silane coupling agent (from vibration of the Si-O bond) present in the RBCs prior to and following solvent storage for 24h, 1 and 2 weeks.

An FTIR spectrometer (Nicolet Magna-IR 860; Thermo-Nicolet Instrument Corp., Madison, WI, US) in Transmission ESP (enhanced synchronisation protocol) with a Golden Gate MkII attenuated total reflectance (ATR) accessory (Thermo-Nicolet) was employed. Spectra were produced at 4000-750cm$^{-1}$ at an ambient temperature of 23±1°C. An air spectrum was produced prior to specimen analysis and subtracted from proceeding spectra to eliminate contamination by background environmental conditions.

Following bi-axial flexure testing five specimen fragments were selected at random and placed on the ATR accessory base-plate, which consisted of a diamond top-plate and zinc selenide (ZnSe) lenses, the accessory head was tightened firmly against the specimen fragment. The specimen was scanned using an IR beam produced by an Everglo™ mid-IR source (Thermo Fisher Scientific, Hemel Hempstead, UK) with an aperture size of 100μm x 100μm and which operated at approximately 1200°C. Spectra were produced from 100 scans at a velocity of 5.7μm/s, with a resolution of 4cm$^{-1}$ and data spacing of 1.9cm$^{-1}$. The FTIR spectrophotometer possessed a proprietary XT-KBr™ beamsplitter (Thermo-Nicolet) and a MCT-A (Thermo-Nicolet) detector to record spectra. Omnic software (version 7.3; Thermo Fisher Scientific Inc., Loughborough, UK) was subsequently used to examine FTIR spectra.

#### 3.3.2.3 Fracture morphology

SEM was used to examine either the cured surface or the fractured surface of randomly selected fragments of specimens following storage in NaOH and EtOH and subsequent bi-axial flexure testing. Where the cured surface was examined the specimen fragment was placed on an adhesive carbon conducting tag (Agar Scientific Ltd.) on an aluminium SEM stub (Agar Scientific Ltd.). Specimens were sputter coated to deposit a conductive 2±0.2μm layer of gold (Emitech Ltd.) with a runtime of 2mins and a 25mA voltage, as previously described (Section 3.2.1.3), prior to placement in the SEM chamber.

The specimen fragments (n=5) used to examine the cross-sectional fracture surface through the bulk of RBC specimen were placed on their diametral edge on the adhesive tag and SEM stub. To ensure the specimen fragment remained in this position a small amount of a putty-like pressure sensitive adhesive was moulded around the base of the fragment. This was coated with adhesion electrodag (Ag in methyl-isobutyl ketone; Agar Scientific Ltd.) to ensure a uniform conductive surface. The specimens were subsequently sputter coated and examined (Section 3.2.1.3). The depth of penetration of solvent into the bulk of the RBC was quantified using ImageJ software (version 1.38x; Wayne Rasband, NIH, US). Three representative SEM images of each RBC fragment were produced which highlighted the depth of solvent penetration as a distinct structural change and/or delamination layer following 2 weeks storage, which was measured at three characteristic points and a mean value calculated.

## 3.4 Statistical Analysis

### 3.4.1 Analysis of Variance

Multiple comparisons were conducted as appropriate on the combined BFS data using a general linear model (GLM) analysis of variance (ANOVA) following pre-loading, where the load (4 levels), the storage condition (2 levels) and also the material type (7 levels) were the independent variables. Post-hoc Sidak test Comparions (P=0.05) were also conducted. Two-way analysis of variance was performed on complete data sets for each RBC following the water storage and solvent degradation regimes with the material groups and storage conditions as the independent variables. The BFS data was checked for normality using a Kolmogorov-Smirnov test at a critical level set at P=0.05 and compared with Holm-Sidak comparison tests performed at

a significance level of P=0.05 (Sigmastat 9v3.5; Sigma Plot for Windows, Systat Software Inc., US). Box and whisker plots were produced to highlight the mean, median and inter-quartile ranges of the BFS and NIR data (Minitab Release 14.02; Minitab Ltd., Coventry, UK). The fracture strength and pseudo-modulus of stress data produced by micromanipulation was tested for normality using the Anderson-Darling and Kruskal-Wallis & Mann Whitney U tests to determine significance (P=0.05) (Minitab). Supplementary one-way ANOVAs with post-hoc Tukey multiple comparison tests were performed, also at a significance level of P=0.05, to highlight differences between the group mean BFS values following pre-loading and storage (SPSS® for Windows®, Version 12.0.1, SPSS Inc, Chicago, Illinois, US).

### 3.4.2 Pearson correlation

A Pearson correlation was applied to the pseudo-modulus of stress and particle size data at a significance level of P=0.05, to provide a measure of the linear relation between these two variables. The Pearson correlation provides a range of values from ¯1 to +1, whereby a value of 0 is indicative of no linear relationship between the variables, whilst a correlation of ¯1 indicates a perfect negative linear relationship and +1 indicates a perfect positive linear relationship. The Pearson correlation was calculated using Excel (Microsoft® Office Professional Edition Excel 2003 SP1, Microsoft Corporation, US). The basic formula of the Pearson correlation was;

$$r = \frac{\sum\left(x - \bar{x}\right)\left(y - \bar{y}\right)}{\sqrt{\sum\left(x - \bar{x}\right)^2 \sum\left(y - \bar{y}\right)^2}} \qquad \text{Equation 3.10}$$

where x and y were the mean pseudo modulus of stress and the particle size.

### 3.4.3 Weibull distribution

A Weibull statistical analysis was employed to assess the reliability of the bi-axial flexure data and to provide a Weibull modulus for each group of BFS data (Section 2.2.2.1). The Weibull modulus was derived by Weibull (1951) to define the strength distribution and brittleness of a material and the probability of failure at an applied load. The Weibull distribution operates on the

weakest-link principle, whereby failure occurs at the weakest point within the structure before propagating to catastrophic failure. The occurrence of failure is determined by the distribution of stress, the location, size, shape and orientation of flaws inherent to the material or generated as a result of manufacturing and processing techniques [Trustrum & Jayatilaka, 1979; Robin et al., 2002].

To determine the Weibull modulus of a given specimen group the BFS data for each specimen was first ranked in ascending order. A Weibull analysis was then performed on the resultant data to establish the reliability of the disc-shaped specimens by determining the probability of failure as a function of the applied stress. The basic form of the Weibull distribution was then calculated in accordance with Equation 3.11

$$P_f = 1 - \exp\left[ -V\left( \frac{\sigma - \sigma_u}{\sigma_0} \right)^m \right] \qquad \text{Equation 3.11}$$

where $P_f$ was the probability of failure, V was the specimen volume, $\sigma$ was the applied stress at failure (MPa) and $\sigma_u$, $\sigma_o$ and *m* were constants. *m* was the Weibull modulus which was defined by Trustrum & Jayatilaka (1979) as characterising the 'brittleness' of a material. *m* describes the flaw size and the distribution of the defect population within a material and therefore the resultant scatter and associated reliability of the flexural strength data. A high value of *m* was perceived to be desirable, being indicative of a material with a predictable rate of failure and reliable flexure strength. $\sigma_o$ is normally referred to as the normalising or scaling constant, $\sigma_u$ was the stress at which the failure probability approaches zero and is known as the threshold stress (MPa). $P_f$ was the probability of failure, which varies from zero to one and is calculated using Equation 3.12

$$P_f = \left( \frac{n}{N^* + 1} \right) \qquad \text{Equation 3.12}$$

where N* was the total number of specimens (n=20) and n is the ranked specimen number when the flexural strength is ranked in ascending order. The volume term, V, was disregarded as previous studies have reported that $\sigma_u$ equal to zero can be assumed a safe stress level for brittle

materials since there is always a finite probability that a critical flaw may be present in the material prior to stressing [Davies, 1973; Stanley et al., 1973]. Therefore, Equation 3.11 may be reduced to the form of Equation 3.13

$$1 - P_f = 1 - \left\{ 1 - \exp\left[ -\left( \frac{\sigma}{\sigma_0} \right) \right]^m \right\} \qquad \text{Equation 3.13}$$

Equation 3.12 may be further simplified using logarithms to the equation of a straight line y=mx+c to allow the flexure strength data and resultant Weibull analysis to be presented in a graphical form (Equation 3.14)

$$\ln\ln\left( \frac{1}{P_s} \right) = m\ln(\sigma) - m\ln(\sigma_0) \qquad \text{Equation 3.14}$$

$P_s$ was the probability of survival ($P_s$ is equal to 1-$P_f$) the x-axis and y-axis intercepted the axis at -mln($\sigma_0$), the gradient of the graph was *m* signifying the reliability of the specimen group to have undergone testing. The Weibull analysis was performed on the flexural strength data by plotting lnln($1/P_s$) against ln$\sigma$. The gradient of the strength distribution data (*m*) was determined by superimposing a regression line along the data points to calculate the Weibull modulus for each specimen group. A high *m* indicates an increased homogeneity in flaw population and a more predictable rate of failure observed as a steep slope with a reduced scatter of data. Conversely, a shallow slope with a wide distribution of data and a low *m* is indicative of the presence of inhomogeneities within the flaw population resulting in less predictable failure and reduced reliability.

Trustram et al. (1979) established that the number of specimens used to determine the Weibull constants (*m* and $\sigma_0$) for brittle materials influences the accuracy of the results obtained. A minimum sample size of twenty specimens was recommended to reduce the occurrence of standard error and produce accurate results [Trustram et al., 1979]. Consequently, a specimen group size of 20 was employed throughout the current investigation where a Weibull modulus was calculated.

The standard deviation of the Weibull modulus (*m*) was calculated in relation to the sample size (N) in accordance with Equation 3.15

$$\text{Standard deviation (m)} = \frac{\text{m}}{\sqrt{\text{N}}} \qquad \text{Equation 3.15}$$

A survival probability distribution of flexure strength was produced by plotting the probability of survival (ranging from zero to one) against the BFS data ranked in ascending order. The survival probability distribution was then assessed to further examine the occurrence of mono-, bi- and multi-modal distributions of failure and hence determine the nature of the defect population.

### 3.4.4 Regression analysis

The confidence intervals for the specimen groups were calculated to determine statistically significant differences between the Weibull modulus of the flexure strength data of each group of specimens. The confidence intervals were calculated using regression analysis of the flexure strength data at a 95% significance level using statistical analysis software (Excel 2003, Microsoft Corporation, US). The 95% confidence intervals were considered to be significant when the range of values between groups did not overlap [Thoman et al., 1969]. The $R^2$-values were also calculated from a regression analysis of the flexure strength data where the $R^2$-values represented the scatter of flexure strength data along the regression line, or line of 'best fit', where the $R^2$-value corresponded with the data correlation coefficient determined following a least square analysis on the plots of $\ln\ln(1/P_s)$ against the $\ln\sigma$. The $R^2$-value was indicative of the grouping of the BFS data of the disc-shaped specimens, where a value of 1 represents a perfect alignment of data along the line of best fit. A high $R^2$-value is considered to be desirable indicating a high reliability of the BFS data, whilst a lower value indicates a bi- or multi-modal distribution of data.

### 3.4.5 Non-parametric statistical analysis

Non-parametric statistical analysis was performed were data did not possess a normal distribution, unlike the preceding methods described which were performed where the data

exhibited a normal distribution as determined by either Kolmogorov-Smirnov or Anderson-Darling tests set at a significance of P=0.05 (Section 3.4.1). Subsequently, where data did not fit the normal distribution alternative non-parametric analytical techniques were employed. Z-tests were employed at a significance level of P=0.05 to determine the significance of the number of particle fractures identified using micromanipulation. The z-test specifically determined if the difference between a sample mean and the population mean was large enough to be significant, calculated in accordance with Equation 3.16,

$$z = \frac{x - \mu}{\left(\sigma / \sqrt{n}\right)} \qquad \text{Equation 3.16}$$

where x was the mean of the sample, μ was the mean value, σ was the standard deviation and n was the sample size, calculated using Sigmastat (v3.5; Systat Software Inc., Dundas Software Ltd., Germany).

# CHAPTER 4 RESULTS & DISCUSSION: MODIFIED FAILURE MECHANISMS

## 4.1 RESULTS: The Mechanical Properties of 'Nanofilled' RBCs: Micromanipulation

A micromanipulation technique was employed to assess the mechanical properties of discrete spheroidal, irregular and agglomerated 'nanocluster' particles representative of fillers present in modern RBCs.

### 4.1.1 Mechanisms of particle fracture

The filler types possessed varying fracture mechanisms and a differing number of particle fractures (Figure 4.1). The stress-deformation curves of the spheroidal (FZ) and irregular (GR) particles exhibited either no distinct fracture (Figure 4.2a) as the load applied was insufficient to initiate particle fracture or a single distinct fracture (Figure 4.2b). In contrast, the 'nanocluster' (FSB) particles underwent up to four multiple distinct fracture events (Figure 4.2c), although some 'nanoclusters' fractured only once and some did not fail (Figure 4.1). Z-tests identified no significant difference ($P>0.05$) between the spheroidal (FZ) and irregular (GR) particles in respect to fracture events, whilst the 'nanoclusters' were unique in that on 24 out of 30 occasions they fractured, in some cases multiple times. Therefore, the resultant frequency of first fracture of FZ and GR was significantly lower ($P<0.001$ and $P<0.002$, respectively) compared with the 'nanoclusters' ($P=0.8$).

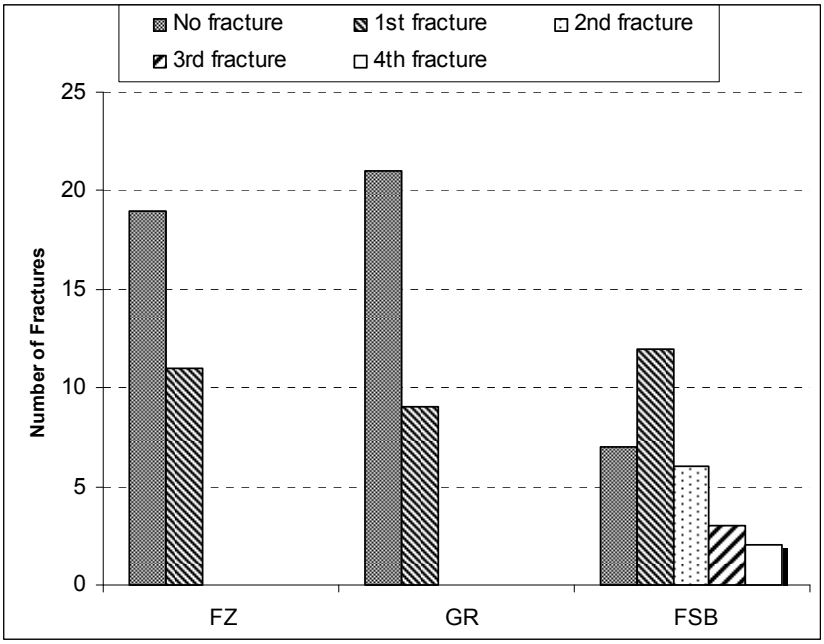


**Figure 4.1. Histogram of the distinct fracture events exhibited by the three filler-types.**

(a)

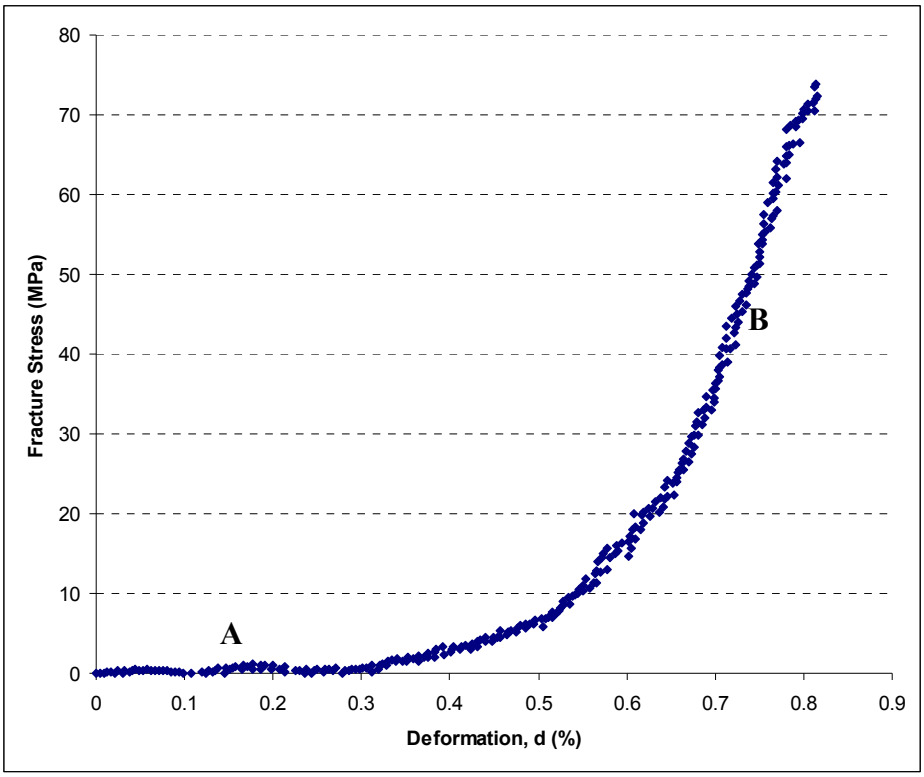


(b)

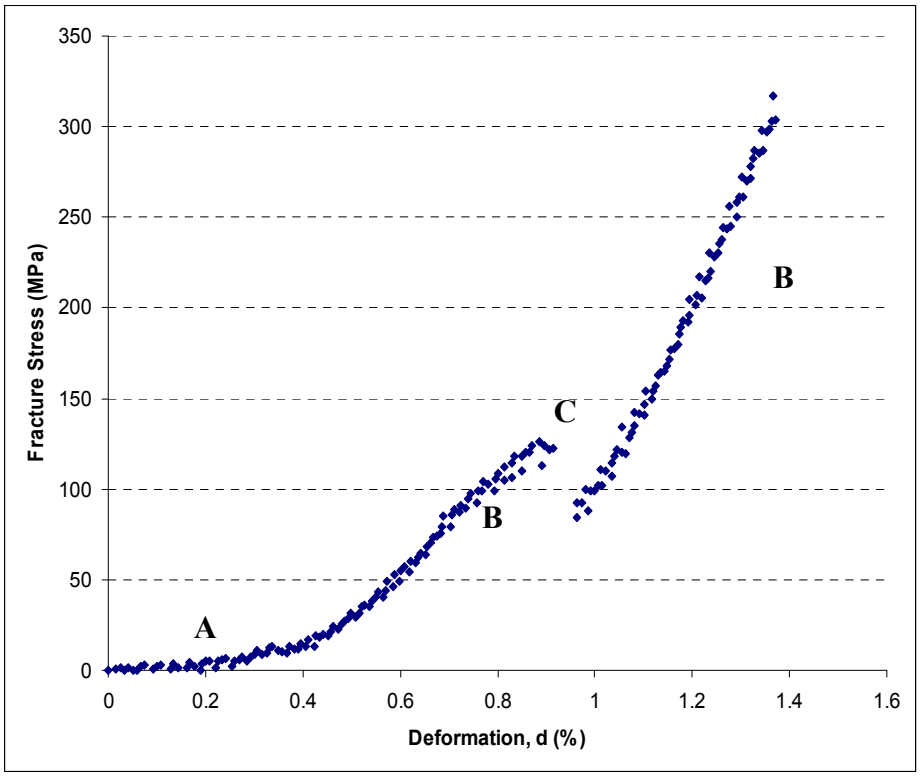


**Figure 4.2. Representative micromanipulation plots highlighting the occurrence of (a) no distinct fracture and (b) single distinct fracture of FZ, GR and FSB particles. Curve region 'A' corresponds with probe movement and particle alignment prior to initiation of compression, 'B' particle loading and 'C' particle fracture.**

**(c)**

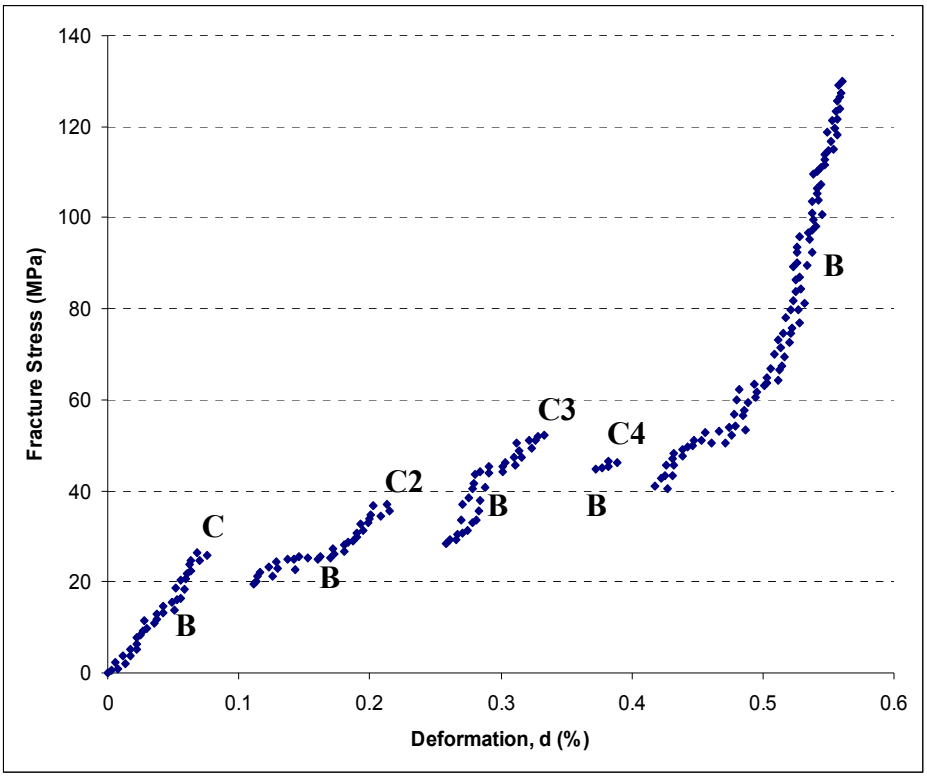


**Figure 4.2(continued). Representative micromanipulation plot highlighting the occurrence of (c) multiple distinct fractures of the agglomerated 'nanocluster' particle. Curve region 'A' corresponds with probe movement and particle alignment prior to initiation of compression and 'B' particle loading. 'C' was attributed to particle fracture, whilst 'C2-4' related to multiple distinct fracture events.**

### 4.1.2 Force at fracture

Loading to failure of 30 spheroidal and irregular particles using the micromanipulation technique resulted in failure loads of 1389±1342 and 1356±1093µN, respectively. In contrast loading of the 'nanoclusters' highlighted up to four distinct fractures with an initial mean force at fracture of 1702±909µN, which increased following additional fractures to mean loads of 1958±1132 and 2674±1485µN, whilst the final mean fracture was 1661±158µN (Table 4.1). Kruskal-Wallis & Mann Whitney U tests highlighted that for those particles which fractured there was no significant difference in fracture strength ($P>0.05$) due to the high standard deviation. Likewise, z-tests failed to highlight a significant difference between the occurrences of multiple fractures ($P=0.76$).

| | Force at Fracture (f) (μN) | | | |
|---|---|---|---|---|
| | 1st fracture | 2nd fracture | 3rd fracture | 4th fracture |
| **FZ** | 1389±1342(0.28±0.14) | - | - | - |
| **GR** | 1356±1093(0.38±0.17) | - | - | - |
| **FSB** | 1702±909(0.46±0.67) | 1968±1132(1.31±1.15) | 2674±1486(0.61±0.61) | 1661±158(0.43±0.06) |

**Table 4.1. The mean force at fracture (μN) and associated deformation (%) of spheroidal, irregular and 'nanocluster' filler particles discrete from the resin matrix of FZ, GR and FSB following compression to failure using the micromanipulation technique.**

### 4.1.3 Pseudo-modulus of stress

The mean pseudo-modulus of stress of the spheroidal or irregular particles prior to first fracture was 587±439 and 570±243MPa respectively, whilst the 'nanocluster' possessed a markedly higher pseudo-modulus of stress prior to first fracture of 797±555MPa. Following subsequent single fracture of the spheroidal or irregular particles the mean pseudo-modulus of stress at fracture increased to 819±859 and 617±298MPa, respectively. In comparison, following multiple fracture of 'nanoclusters' the subsequent mean pseudo-modulus of stress decreased to 704±590, 465±403, 247±200 and 304±84MPa (Table 4.2). Statistical analysis highlighted no significant difference in the pseudo-modulus data ($P>0.05$) due to the high scatter and relatively small sample size.

| | Pseudo-Modulus of Stress (σ) (MPa) | | | | |
|---|---|---|---|---|---|
| | No fracture | 1st fracture | 2nd fracture | 3rd fracture | 4th fracture |
| **FZ** | 587±439 | 819±859 | - | - | - |
| **GR** | 570±243 | 617±298 | - | - | - |
| **FSB** | 797±555 | 704±590 | 465±403 | 247±200 | 304±84 |

**Table 4.2. The pseudo-modulus of stress (MPa) of spheroidal, irregular and 'nanocluster' particles separated from the resin matrix and compressed to failure using the micromanipulation technique.**

A Pearson correlation identified a negative linear relationship between the pseudo-modulus of stress and particle size for FZ ($r^2$= ¯0.70 and ¯0.78) and GR ($r^2$= ¯0.59 and ¯0.79) prior to and following particle fracture, respectively ($P<0.001$). In contrast, FSB exhibited no correlation between pseudo-modulus of stress and particle size prior to first and subsequent particle fractures ($r^2$ = ¯0.38, ¯0.33, ¯0.28, ¯0.08; $P>0.05$) (Figure 4.3).

**(a)**

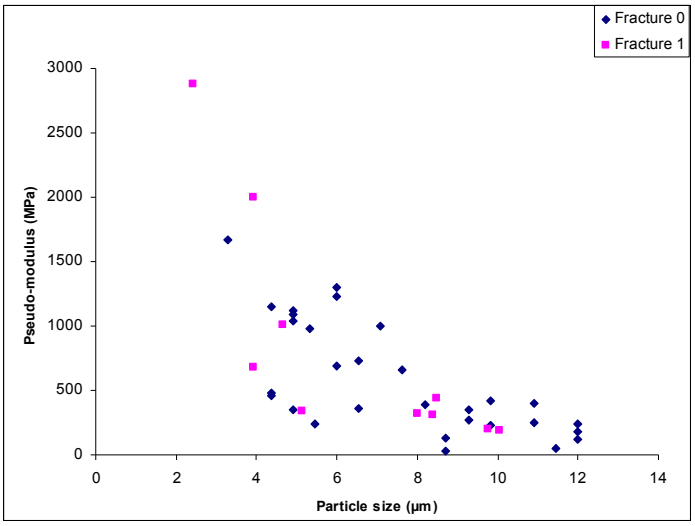


**(b)**

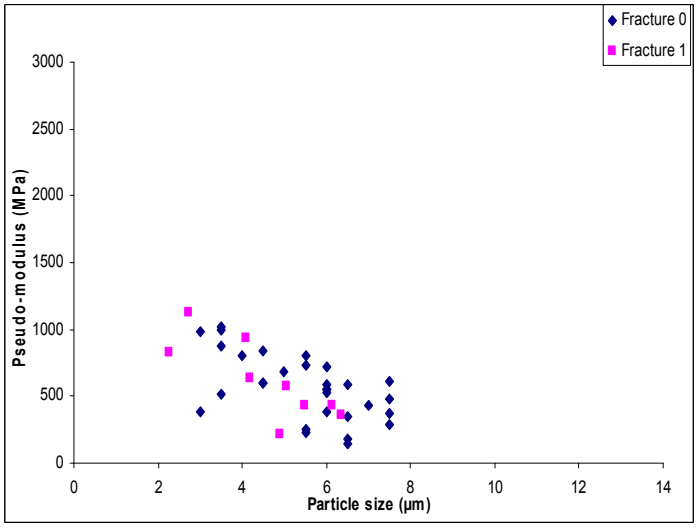


**(c)**

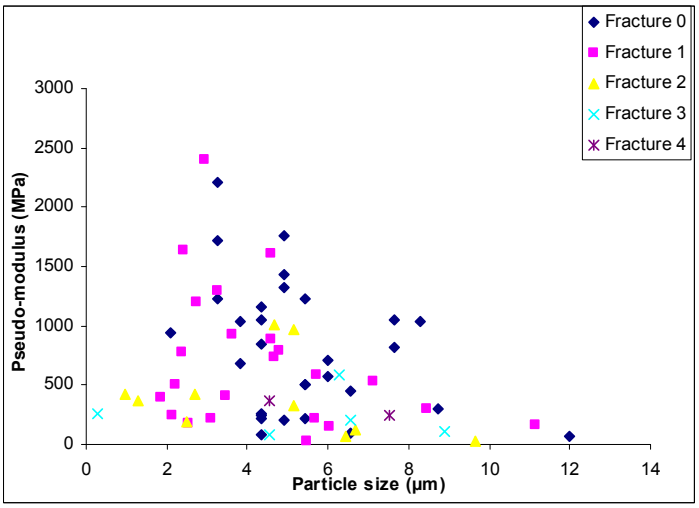


**Figure 4.3. Pseudo-modulus of stress scatter plots following micromanipulation of (a) FZ, (b) GR and (c) FSB. Pearson coefficient identified that the 'nanocluster' particles exhibited a higher level of variability between particle size and stress, whilst the spheroidal and irregular particles demonstrated a higher level of consistency.**

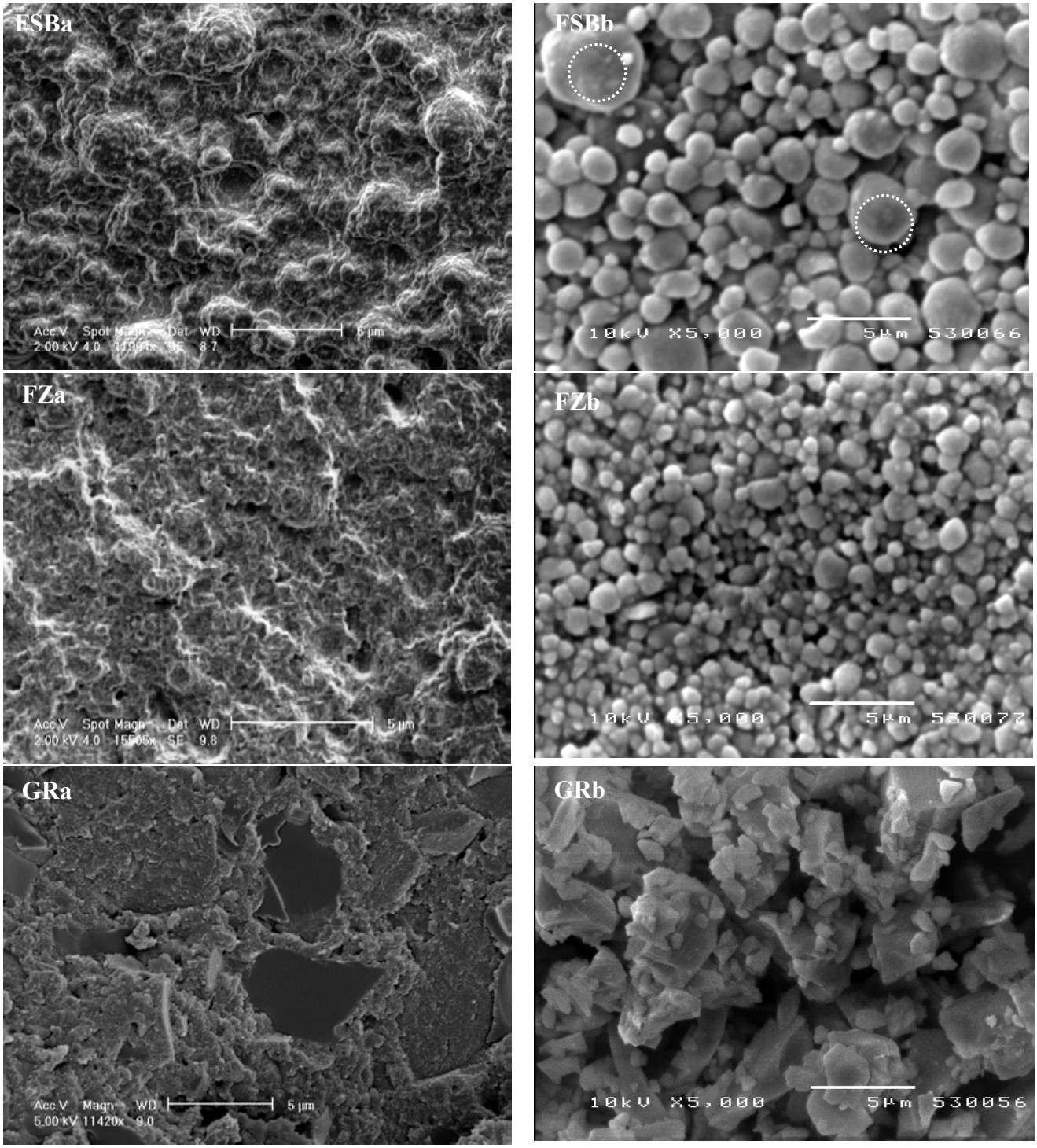


**Figure 4.4. (a) Cryo-SEM images of cross-sectional fracture surfaces, highlighting the size and morphology of filler particles embedded in the resin matrix of the complete composite system. (b) Size and morphology of filler particles separated from the resin matrix. The 'nanoclusters' exhibited a wide size distribution, distinct topographical variation and apparent random distribution of nanoparticles within the agglomerated particle (circled). The spheroidal fillers demonstrated a comparably uniform distribution, whilst the irregular borosiliciate GR fillers also highlighted a wide range of particle sizes.**

## 4.2 RESULTS: The Mechanical Properties of 'Nanofilled' RBCs: Pre-loading

Specimens were pre-loaded to simulate masticatory loading and induce sub-critical damage to determine the reinforcement provided by the filler particle on the subsequent mechanical properties of the RBCs.

GLM-ANOVA of the combined BFS data of the seven RBCs following pre-loading and storage in either 'dry' or 'wet' conditions highlighted an overall general decrease in measured BFS as a consequence of increasing levels of pre-loading (Figure 4.5). However, individual RBCs, in particular the 'nanocluster' reinforced system (FSB and FST), differed from the general trend by exhibiting either an increased or comparable BFS and Weibull modulus following pre-loading, particularly 20 and 50N, compared with unloaded specimens and the other RBCs tested in either 'dry' or 'wet' conditions (Figure 4.5).

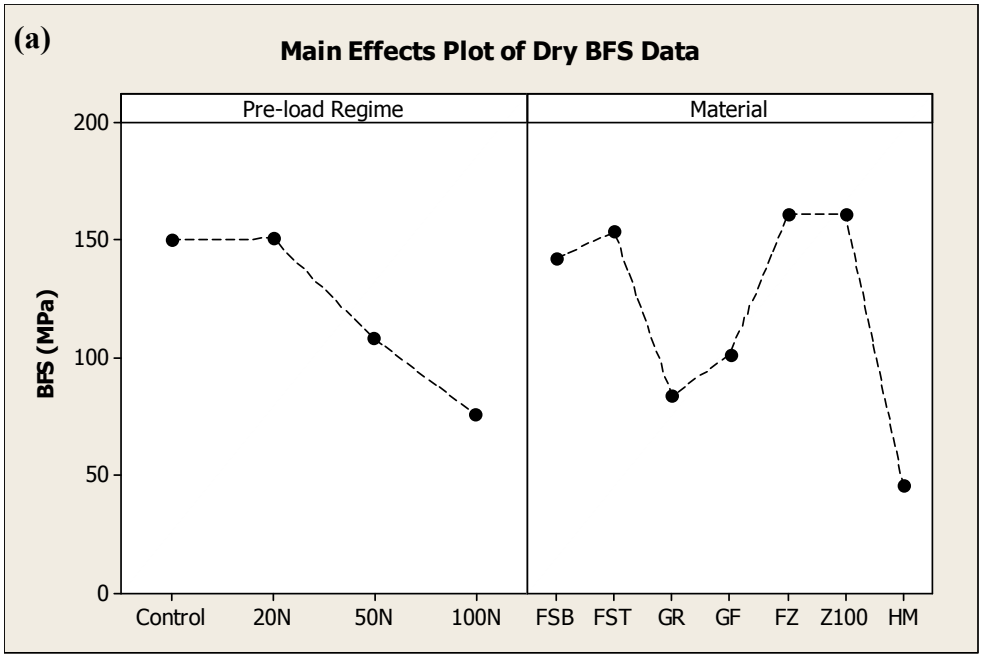


**Figure. 4.5. GLM-ANOVA Main Effects plots of the data means following 'dry' storage conditions, the plot highlights the downward trend in mean BFS data as a consequence of increasing pre-loading regimes.**

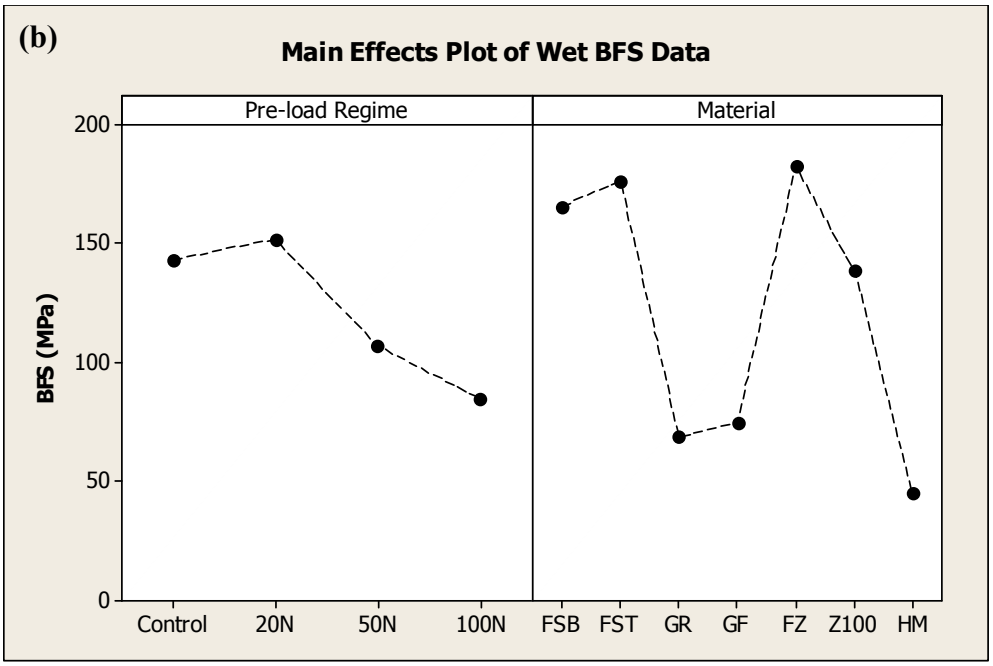


**Figure. 4.5(continued). GLM-ANOVA Main Effects plots of the data means following 'wet' storage conditions, the plot highlights the downward trend in the mean BFS data as a consequence of increasing pre-loading regimes and also the influence on the mean BFS of the RBCs following 'wet' storage compared with 'dry' (Figure 4.5a) conditions.**

### 4.2.1 BFS and associated reliability (*m*)

One-way ANOVA highlighted that the BFS of 'dry' FSB pre-loaded to 20N and 50N was not significant compared with unloaded specimens (137±15MPa and 146±12MPa; P=0.403 and P=0.999, respectively), although a significant decrease occurred following 100N (127±25MPa; P=0.002). Following pre-loading to 20, 50 and 100N for 2000 cycles and subsequent 'wet' storage the BFS was either maintained or significantly increased compared with unloaded specimens (179±19, 183±19 and 145±34MPa; P=0.179, P=0.021 and P>0.05, respectively). Likewise, the 10% failure probability increased up to 100N. The Weibull modulus of FSB was increased or maintained following pre-loads of 20 and 50N and storage 'dry' (9.49±2.12 and 11.82±2.64) or 'wet' (8.53±1.91 and 10.23±2.29) (Table 4.3a).

The BFS of FST following pre-loading and 'dry' storage was not significantly decreased compared with unloaded specimens (165±19, 148±15 and 141±21MPa; P>0.05, P>0.05 and P=0.758, respectively). Likewise, following pre-loading and 'wet' storage the BFS (182±12, 171±17 and 175±21MPa) was also not significantly different compared with the control (177±22MPa; P>0.05). However, the 10% failure probability of BFS progressively decreased as a

consequence of both ‘dry’ and ‘wet’ pre-loading regimes. The Weibull modulus exhibiting either a significantly increased or maintained reliability up to and including 100N pre-loads following ‘dry’ (8.54±1.91, 10.71±2.39 and 6.04±1.35) and ‘wet’ (16.89±3.78, 10.91±2.45 and 8.03±1.79) storage compared with the control (Table 4.3b).

The mean BFS and Weibull modulus of GR specimens following pre-loads of 20N ‘dry’ was 171±22MPa ($P>0.05$) and 7.25±1.62, whilst following pre-loading and ‘wet’ storage the BFS was 151±7MPa ($P=0.06$) and 10.64±2.38, neither of which were significantly different from their respective controls. Total failure of GR specimens to complete 50 and 100N pre-loads rendered further statistical analysis meaningless (Table 4.4a).

GF specimens were not significantly influenced by pre-loads of 20 or 50N either ‘dry’ (119±17 and 122±22MPa; $P>0.05$) or ‘wet’ (90±14 and 73±24MPa; $P>0.05$ and $P=0.998$). The Weibull modulus of ‘dry’ specimens was significantly decreased (6.70±1.49 and 4.77±1.07), whilst following 50N pre-loads ‘wet’ the *m* was also significantly decreased (2.48±0.62) compared with the unloaded controls. Failure of approximately half of GF specimens to survive 100N pre-loads prevented further meaningful analysis (Table 4.4b; Figure 4.6 page 100).

| | Dry | | | | Wet | | | |
|---|---|---|---|---|---|---|---|---|
| | **Control** | **20N** | **50N** | **100N** | **Control** | **20N** | **50N** | **100N** |
| **(a)** | **Nanocluster RBC (FSB)** | | | | | | | |
| **BFS (MPa)** | 125-205 | 101-161 | 112-168 | 87-172 | 102-198 | 138-203 | 139-206 | 68-202 |
| **Mean BFS (MPa)** | $159(20)^{A,B,C}{}_{1}$ | $137(15)^{C,D}{}_{3}$ | $146(12)^{C,D}{}_{2}$ | $127(25)^{D}{}_{1}$ | $155(27)^{B,C}{}_{2}$ | $179(19)^{A,B}{}_{1,2}$ | $183(18)^{A}{}_{1}$ | $145(34)^{C,D}{}_{2,3}$ |
| **10% FP (MPa)** | 128 | 114 | 132 | 88 | 115 | 141 | 157 | 96 |
| **Weibull modulus (*m*)** | 8.07 (1.80) | 9.49 (2.12) | 11.82 (2.64) | 5.29 (1.18) | 5.98 (1.34) | 8.53 (1.91) | 10.23 (2.29) | 4.02 (0.90) |
| **95% CI** | 6.99-9.15 | 8.55-10.45 | 9.99-13.66 | 4.79-5.80 | 5.66-6.30 | 7.62-9.09 | 9.46-11.39 | 3.61-4.42 |
| **$R^2$-value** | 0.93 | 0.96 | 0.91 | 0.96 | 0.99 | 0.97 | 0.97 | 0.96 |
| **Specimens survived (%)** | 100 | 100 | 100 | 100 | 100 | 100 | 100 | 100 |
| **(b)** | **Nanocluster RBC (FST)** | | | | | | | |
| **BFS (MPa)** | 109-218 | 113-196 | 116-172 | 87-168 | 126-205 | 159-204 | 141-198 | 120-196 |
| **Mean BFS (MPa)** | $160(27)^{A,B,C,D}{}_{1}$ | $165(19)^{A,B,C}{}_{2}$ | $148(15)^{B,C,D}{}_{2,3}$ | $141(21)^{C,D}{}_{1}$ | $177(22)^{A}{}_{1,2}$ | $182(12)^{A}{}_{1,2}$ | $171(17)^{A,B}{}_{1,2}$ | $175(21)^{A}{}_{1}$ |
| **10% FP (MPa)** | 123 | 139 | 131 | 103 | 135 | 167 | 148 | 135 |
| **Weibull modulus (*m*)** | 6.23 (1.39) | 8.54 (1.91) | 10.71 (2.39) | 6.04 (1.35) | 7.99 (1.78) | 16.89 (3.78) | 10.91 (2.45) | 8.03 (1.79) |
| **95% CI** | 5.69-6.76 | 7.41-9.67 | 9.52-11.89 | 5.09-6.99 | 7.21-8.79 | 15.15-18.60 | 9.98-11.88 | 6.79-9.25 |
| **$R^2$-value** | 0.97 | 0.93 | 0.95 | 0.91 | 0.96 | 0.96 | 0.97 | 0.91 |
| **Specimens survived (%)** | 100 | 100 | 100 | 100 | 100 | 100 | 100 | 100 |

Mean values within rows and columns (including Tables 4.4, 4.5 and 4.6) exhibiting different letters (in superscript) and numbers (in subscript) respectively, were significantly different ($P<0.05$).

**Table 4.3. The range, mean and 10% failure probability (FP) of bi-axial flexure strengths (BFS), Weibull modulus (*m*), 95% associated confidence intervals (CI), $R^2$-value and percentage of specimens to survive pre-loading of the 'nanocluster' reinforced RBCs (a) FSB and (b) FST to 20, 50 or 100N for 2000 cycles and storage for either 24h 'dry' or in a waterbath maintained at 37 ± 1°C.**

| | Dry | | | | Wet | | | |
|---|---|---|---|---|---|---|---|---|
| | **Control** | **20N** | **50N** | **100N** | **Control** | **20N** | **50N** | **100N** |
| **(a)** | **Nano-hybrid RBC (GR)** | | | | | | | |
| **BFS (MPa)** | 115-195 | 109-198 | - | - | 107-1424 | 121-187 | - | - |
| **Mean BFS (MPa)** | $165(18)^{A}{}_{1}$ | $171(22)^{A}{}_{1,2}$ | - | - | $125(11)^{B}{}_{2}$ | $151(7)^{A,B}{}_{3}$ | - | - |
| **10% FP (MPa)** | 145 | 130 | - | - | 108 | 129 | - | - |
| **Weibull modulus (*m*)** | 9.03 (2.02) | 7.25 (1.62) | - | - | 12.11 (2.71) | 10.64 (2.38) | - | - |
| **95% CI** | 7.83-10.22 | 6.06-8.43 | - | - | 10.80-13.42 | 9.17-12.12 | - | - |
| **$R^2$-value** | 0.93 | 0.90 | - | - | 0.95 | 0.93 | - | - |
| **Specimens survived (%)** | 100 | 100 | 0 | 0 | 100 | 100 | 0 | 0 |
| **(b)** | **Nano-hybrid RBC (GF)** | | | | | | | |
| **BFS (MPa)** | 93-141 | 76-142 | 58-155 | 34-130 | 53-117 | 59-110 | 27-106 | 57-120 |
| **Mean BFS (MPa)** | $125(13)^{A}{}_{2}$ | $119(18)^{A,B}{}_{3,4}$ | $122(22)^{A,B}{}_{3}$ | $79(34)^{B,C,D}{}_{2}$ | $87(17)^{B,C,D}{}_{4}$ | $90(14)^{B,C,D}{}_{4}$ | $73(24)^{B,C,D}$ | $91(17)^{B,C,D}{}_{4}$ |
| **10% FP (MPa)** | 98 | 91 | 97 | 34 | 63 | 60 | 38 | 84 |
| **Weibull modulus (*m*)** | 9.54 (2.13) | 6.70 (1.49) | 4.77 (1.07) | 2.09 (0.66)* | 5.11 (1.14) | 6.29 (1.41) | 2.78 (0.62) | 4.63 (1.39)* |
| **95% CI** | 8.36-10.71 | 5.69-7.44 | 3.81-5.72 | 1.67-2.50 | 4.82-5.39 | 5.44-7.15 | 2.50-3.05 | 2.89-6.37 |
| **$R^2$-value** | 0.94 | 0.95 | 0.86 | 0.94 | 0.99 | 0.93 | 0.96 | 0.80 |
| **Specimens survived (%)** | 100 | 100 | 100 | 50 | 100 | 100 | 100 | 55 |

Mean values within rows and columns (including Tables 4.3, 4.5 and 4.6) exhibiting different letters (in superscript) and numbers (in subscript) respectively, were significantly different ($P<0.05$).
**Weibull values determined with a decreased sample size (n<20)*

**Table 4.4. The range, mean and 10% failure probability (FP) of bi-axial flexure strengths (BFS), Weibull modulus (*m*), 95% associated confidence intervals (CI), $R^2$-value and percentage of specimens to survive pre-loading of the nano-hybrid RBCs (a) GR and (b) GF to 20, 50 or 100N for 2000 cycles and storage for either 24h 'dry' or in a waterbath maintained at 37±1°C.**

Following pre-loading of FZ specimens for 2000 cycles to 20 and 50N and storage 'dry' the BFS was not significantly different compared with unloaded specimens (171±16 and 155±20MPa; P>0.05 and P=0.0536, respectively), whilst a significant decrease occurred following 100N (142±32MPa; P=0.001). Furthermore, pre-loading of FZ up to 100N followed by storage 'wet' did not significantly modify the BFS compared with unloaded specimens (198±22MPa, 170±24 and 171±31MPa; P>0.05, P=0.416 and P=0.494, respectively). In contrast, the 10% failure probability was progressively decreased following 'dry' and 'wet' pre-loads. The Weibull modulus was also significantly reduced following 50 and 100N pre-loads and subsequent 'dry' (8.10±1.81 and 4.29±0.96) or 'wet' (7.22±1.61 and 5.66±1.27) storage compared with the control (Table 4.5a).

The mean BFS of 'dry' pre-loaded Z100 following 20 (194±20MPa; P=0.996) and 50N (188±18MPa; P>0.05) was not significantly different, whilst following 50N pre-loads 'wet' the BFS decreased significantly (152±23MPa; P=0.021) compared with the respective controls. The Weibull modulus of 'dry' Z100 increased significantly to 9.96±2.23 and 10.78±2.41 following pre-loads of 20 and 50N compared with the control, whilst *m* of Z100 'wet' significantly decreased to 6.60±1.48 and 6.56±1.47 following 20 and 50N compared with unloaded specimens. Failure of approximately half of Z100 specimens to complete 100N pre-loading prevented further meaningful analysis (Table 4.5b).

HM specimens stored either 'dry' or 'wet' following 20N pre-loads possessed a mean BFS of 96±13 and 93±22MPa, neither was significant compared with the control (P>0.05). The *m* 'wet' was significantly decreased (5.10±1.1) compared with unloaded HM. Pre-loading of specimens to 50 and 100N caused failure of all specimens rendering further analysis unfeasible (Table 4.6; Figure 4.6).

| | Dry | | | | Wet | | | |
|---|---|---|---|---|---|---|---|---|
| | **Control** | **20N** | **50N** | **100N** | **Control** | **20N** | **50N** | **100N** |
| **(a)** | **Mircohybrid RBC (FZ)** | | | | | | | |
| **BFS (MPa)** | 150-201 | 145-2035 | 126-206 | 79-191 | 142-241 | 135-235 | 120-204 | 109-216 |
| **Mean BFS (MPa)** | $176(16)^{A,B,C}{}_{1}$ | $171(16)^{A,B,C,D}{}_{1,2}$ | $155(20)^{C,D,E}{}_{2}$ | $142(32)^{E}{}_{1}$ | $192(23)^{A,B}{}_{1}$ | $198(22)^{A}{}_{1}$ | $170(24)^{B,C}{}_{1,2}$ | $171(31)^{B,C}{}_{1,2}$ |
| **10% FP (MPa)** | 150 | 148 | 126 | 82 | 162 | 177 | 127 | 131 |
| **Weibull modulus (*m*)** | 11.23 (2.51) | 11.51 (2.57) | 8.10 (1.81) | 4.29 (0.96) | 8.71 (1.95) | 8.65 (1.93) | 7.22 (1.61) | 5.66 (1.27) |
| **95% CI** | 9.73-12.73 | 10.29-12.79 | 7.03-9.17 | 3.91-4.67 | 7.87-9.56 | 7.23-10.07 | 6.69-7.74 | 5.28-6.04 |
| **$R^2$-value** | 0.93 | 0.95 | 0.93 | 0.97 | 0.96 | 0.90 | 0.98 | 0.98 |
| **Specimens survived (%)** | 100 | 100 | 100 | 100 | 100 | 100 | 100 | 100 |
| **(b)** | **Mircohybrid RBC (Z100)** | | | | | | | |
| **BFS (MPa)** | 108-225 | 151-223 | 141-214 | 75-190 | 137-224 | 114-226 | 96-196 | 81-148 |
| **Mean BFS (MPa)** | $180(31)^{A,B}{}_{1}$ | $194(20)^{A}{}_{1}$ | $188(18)^{A}{}_{1}$ | $149(38)^{B,C,D}{}_{1}$ | $180(23)^{A}{}_{1,2}$ | $169(27)^{A,B,C}{}_{2,3}$ | $152(23)^{C,D}{}_{2}$ | $119(27)^{D}{}_{3,4}$ |
| **10% FP (MPa)** | 133 | 152 | 162 | 93 | 145 | 131 | 122 | 96 |
| **Weibull modulus (*m*)** | 5.70 (1.27) | 9.96 (2.23) | 10.78 (2.41) | 3.27 (0.73)* | 8.07 (1.81) | 6.60 (1.48) | 6.56 (1.47) | 4.06 (0.91)* |
| **95% CI** | 5.29-6.12 | 8.58-11.33 | 9.87-11.69 | 2.61-3.93 | 7.42-8.72 | 5.99-7.21 | 5.49-7.63 | 2.78-5.34 |
| **$R^2$-value** | 0.98 | 0.93 | 0.97 | 0.93 | 0.97 | 0.97 | 0.90 | 0.89 |
| **Specimens survived (%)** | 100 | 100 | 100 | 55 | 100 | 100 | 100 | 55 |

Mean values within rows and columns (including Tables 4.3, 4.4 and 4.6) exhibiting different letters (in superscript) and numbers (in subscript) respectively, were significantly different ($P<0.05$).
**Weibull values determined with a decreased sample size (n<20)*

**Table 4.5. The range, mean and 10% failure probability (FP) of bi-axial flexure strengths (BFS), Weibull modulus (*m*), 95% associated confidence intervals (CI), $R^2$-value and percentage of specimens to survive pre-loading of the microhybrid RBCs (a) FZ and (b) Z100 to 20, 50 or 100N for 2000 cycles and storage for either 24h 'dry' or in a waterbath maintained at 37± 1°C.**

| | Dry | | | | Wet | | | |
|---|---|---|---|---|---|---|---|---|
| | **Control** | **20N** | **50N** | **100N** | **Control** | **20N** | **50N** | **100N** |
| | **Microfill RBC (HM)** | | | | | | | |
| **BFS (MPa)** | 71-100 | 72-116 | - | - | 58-103 | 57-124 | - | - |
| **Mean BFS (MPa)** | $87(8)^{A}{}_{3}$ | $96(13)^{A}{}_{4}$ | - | - | $88(12)^{A}{}_{4}$ | $93(22)^{A}{}_{4}$ | - | - |
| **10% FP (MPa)** | 72 | 78 | - | - | 64 | 59 | - | - |
| **Weibull modulus (*m*)** | 7.61 (1.7) | 6.53 (1.5) | - | - | 8.19 (1.8) | 5.10 (1.1) | - | - |
| **95% CI** | 6.78-8.45 | 5.99-7.06 | - | - | 7.56-8.83 | 4.65-5.55 | - | - |
| **$R^2$-value** | 0.95 | 0.97 | - | - | 0.98 | 0.97 | - | - |
| **Specimens survived (%)** | 100 | 100 | 0 | 0 | 100 | 100 | 0 | 0 |

Mean values within rows and columns (including Tables 4.3, 4.4 and 4.5) exhibiting different letters (in superscript) and numbers (in subscript) respectively, were significantly different ($P<0.05$).

**Table 4.6. The range, mean and 10% failure probability (FP) of bi-axial flexure strengths (BFS), Weibull modulus (*m*), 95% associated confidence intervals (CI), $R^2$-value and percentage of specimens to survive pre-loading of the microfill RBC HM to 20, 50 or 100N for 2000 cycles and storage for either 24h 'dry' or in a waterbath maintained at 37 ± 1°C.**

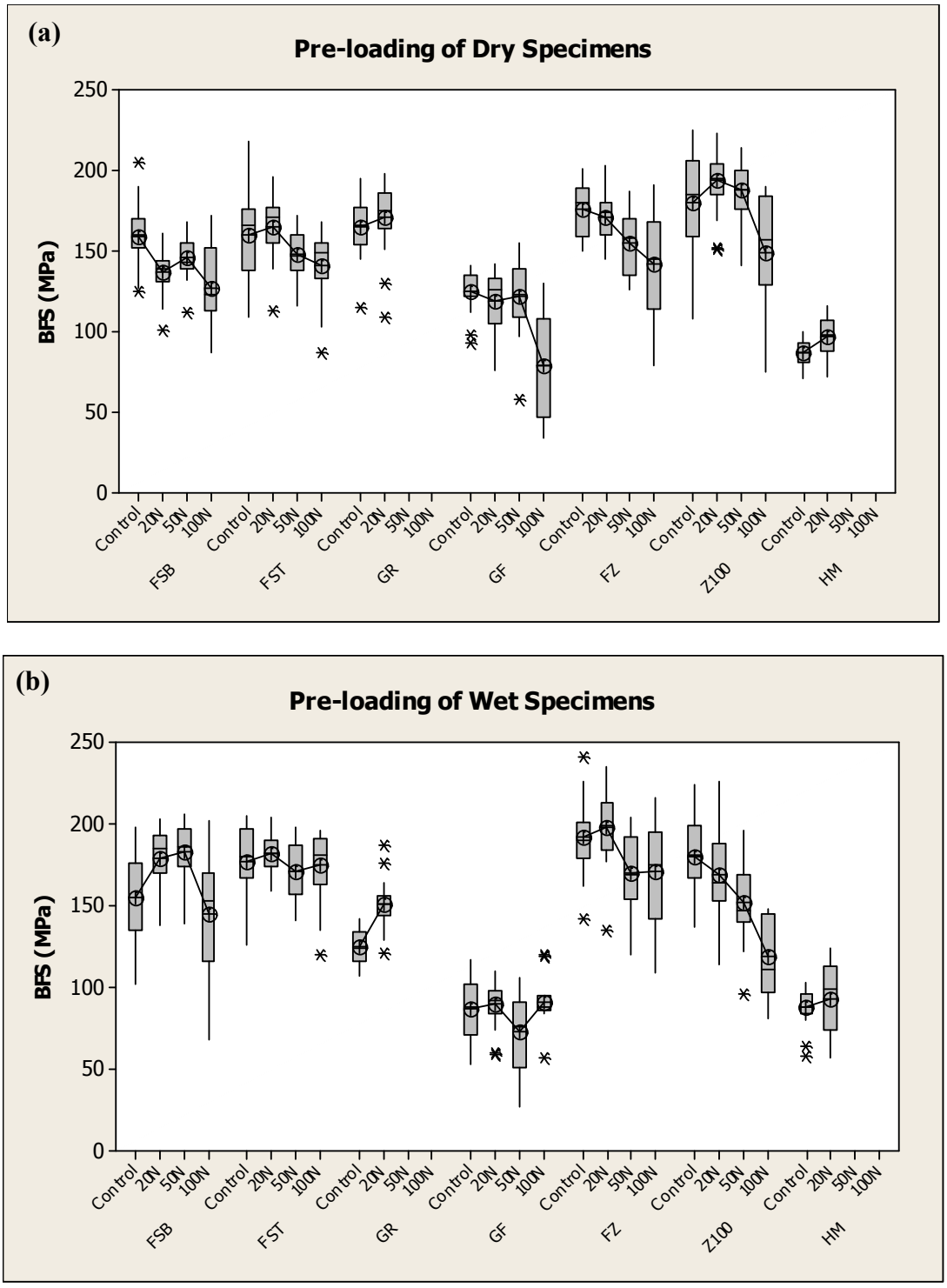


**Figure 4.6. Box and whisker plots of the BFS data of the seven RBCs following pre-loading regimes and (a) 'dry' or (b) 'wet' storage. The box represents the inter-quartile range containing 50% of the BFS data, the whiskers represent the highest and lowest data-points, the crosshair and line within boxes indicates the mean and median, whilst * represents outlaying data points.**

### 4.2.2 Survival probability distribution

The survival probability distributions for each RBC were plotted against the ranked BFS data for each specimen group following pre-loading and typically exhibited a normal distribution of data for unloaded specimens and following low pre-loads, suggesting that failure was related to a single defect type. The survival probability distribution plots highlighted a shift of the BFS data of FSB and FST into the higher strength range compared with the unloaded specimens. However, the distribution of FSB data exhibited a bi-modal distribution of data following 'dry' and 'wet' pre-loads of 100N, suggesting that pre-loading introduced a second defect population, interestingly this conflicted with the $R^2$-vaules (0.96 and 0.96, respectively) which indicate a monomodal defect distribution (Table 4.3, p97; Section 2.2.2.1, p49).

The survival probability distribution of 'dry' GR unloaded and 20N specimens was comparable, whilst following 'wet' storage the survival probability distribution of unloaded and 20N specimens was reduced (<150MPa) compared with the distribution of 'dry' data. Likewise, the distribution of GF stored 'wet' and pre-loaded was notably decreased (<100MPa) compared with 'dry' specimens. Furthermore, the distribution of GF data 'wet' following 50N pre-loads appeared bi-modal, however this was not consistent with the $R^2$-value (0.96), whilst that of GF 'dry' 50N was $R^2$=0.86 which is generally indicative of a multi-modal defect population which was not identified on the survival probably distribution plot (Figure 4.7). The distribution highlighted the damage induced following 100N pre-loads in those specimens that survived. 'Wet' storage of FZ increased the number of specimens exhibiting a higher survival distribution at >200MPa (unloaded and 20N pre-load) and >150MPa (50 and 100MPa pre-loads) compared with specimens stored 'dry'. 'Wet' pre-loading of Z100 to 50N produced a bi-modal distribution within the lower strength region ($R^2$=0.90). The distribution of HM BFS following 'wet' 20N pre-loads introduced a bi-modal data distribution, although this was inconsitent with the $R^2$-value (0.97) (Figure 4.7).

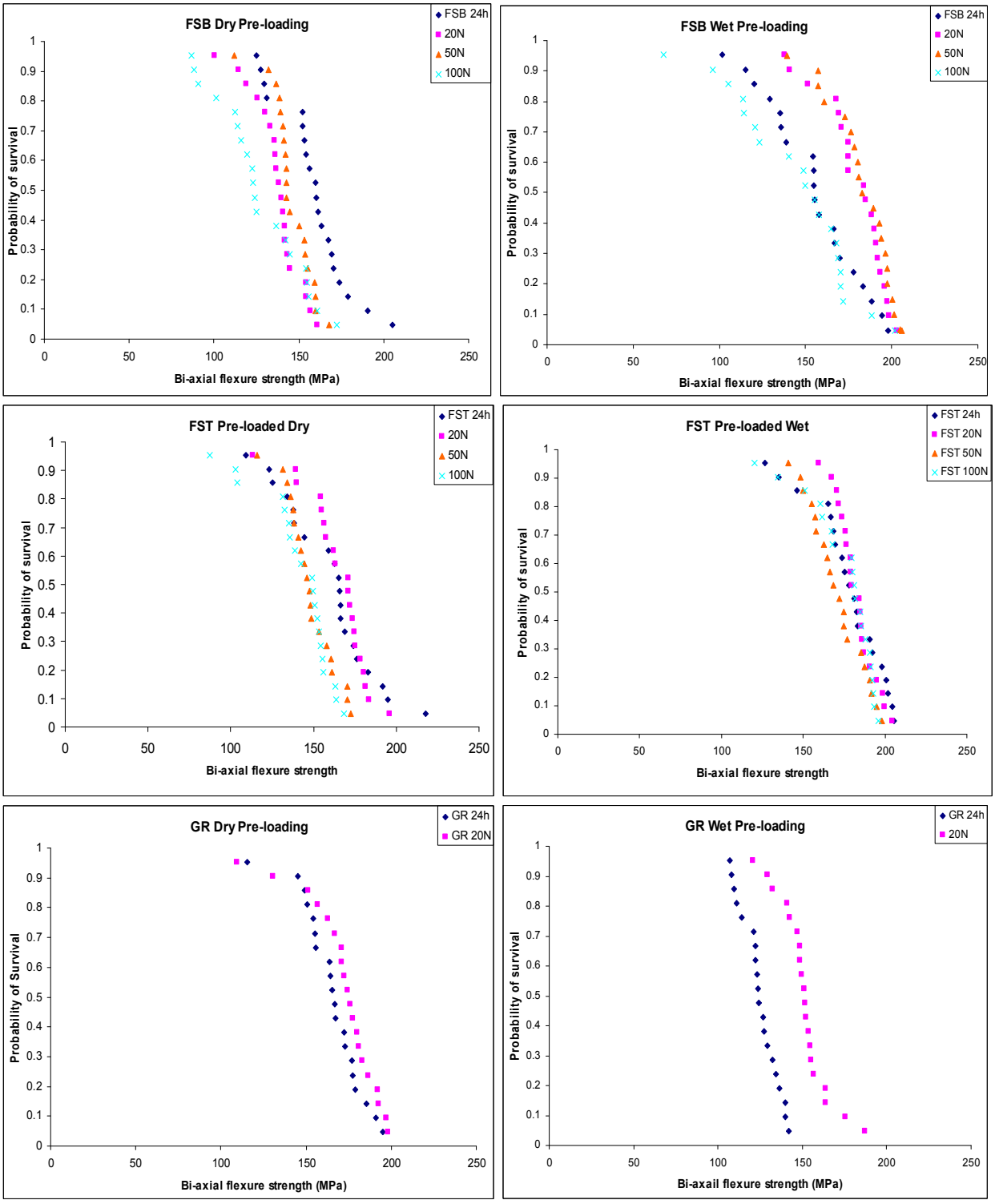


**Figure 4.7. The combined survival probability distribution plots of FSB, FST and GR following 24h storage and pre-loading at 20, 50 and 100N for 2000 cycles prior to bi-axial flexure testing.**

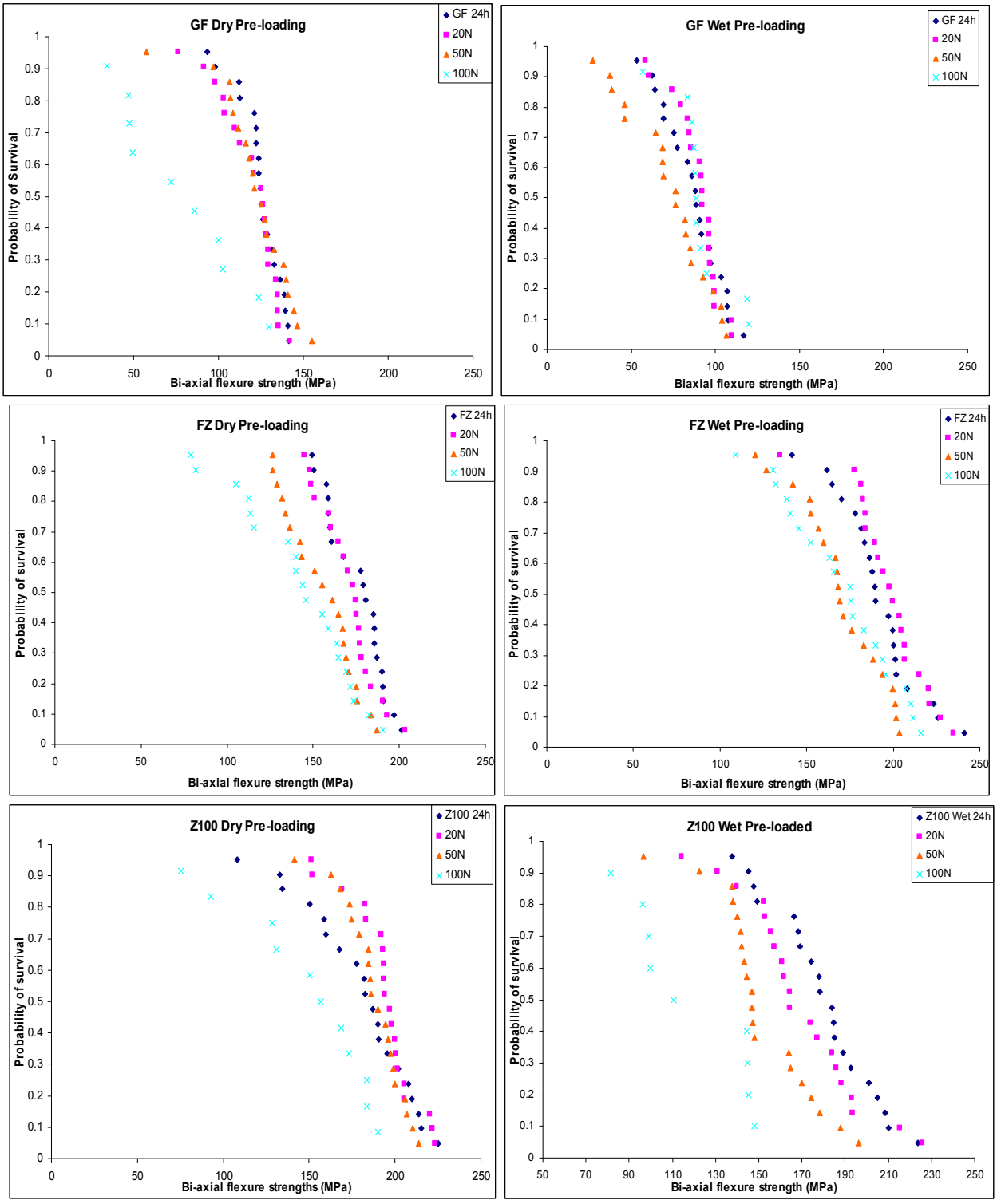


**Figure 4.7 (continued). The combined survival probability distribution plots of GF, FZ and Z100 following 24h storage and pre-loading to 20, 50 and 100N for 2000 cycles prior to bi-axial flexure testing.**

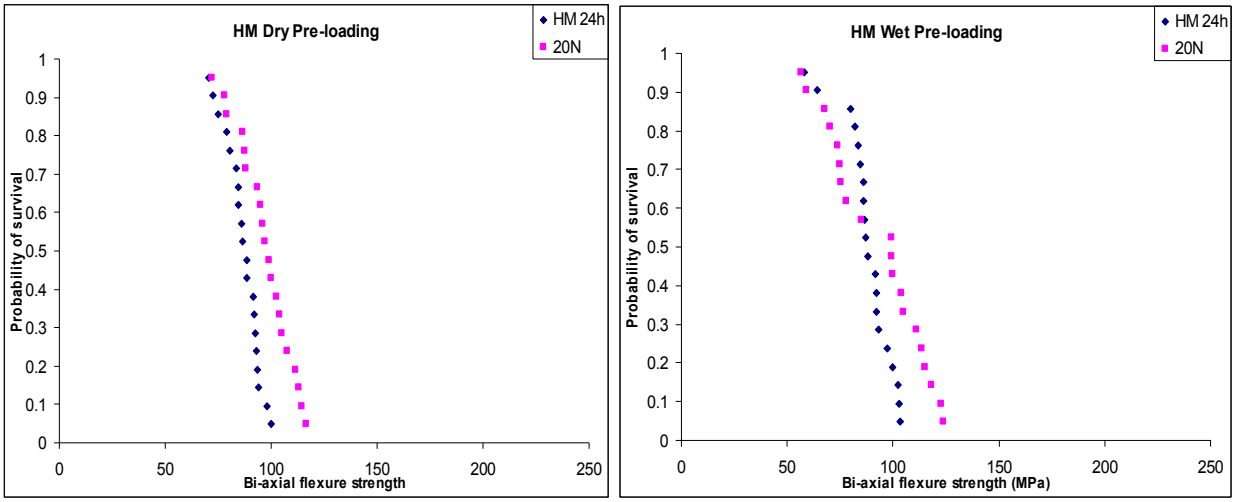


**Figure 4.7 (continued). The combined survival probability distribution plots of HM following 24h storage and pre-loading to 20, 50 and 100N for 2000 cycles prior to bi-axial flexure testing.**

### 4.2.3 Flexural modulus

Two-way ANOVA of specimens stored 'dry' or 'wet' for 24h following three-point flexure testing highlighted that the storage condition was significant (F=7.63; P=0.008) as was the material type (F=4.38; P=0.002), however no significant interaction was identified (F=0.53; P=0.750). Likewise, one-way ANOVA and paired Tukey test comparisons at the 95% significance level identified no significant difference between 'dry' and 'wet' storage of FSB (115±21; 129±13MPa; P=0.998), FST (129±26; 133±207MPa; P=0.758), FZ (121±27; 117±19MPa; P=0.938), Z100 (138±18; 129±18MPa; P=0.998), GR (134±10; 128±16MPa; P=0.790) and GF (107±17; 99±18MPa; P>0.05) (Table 4.4). The subsequent flexural modulus of 'dry' and 'wet' GR (13.4±1.1; 14.9±0.6) and Z100 (17.9±1.5; 16.0±1.6) was markedly greater than the generally comparable flexure modulus of the other materials also tested (Table 4.7).

| | FSB | FST | FZ | Z100 | GR | GF |
|---|---|---|---|---|---|---|
| | Dry | | | | | |
| **Flexural strength (MPa)** | 115 (21) | 129 (26) | 121 (27) | 138 (18) | 134 (10) | 107 (17) |
| **Young's Modulus (GPa)** | 8.5 (1.7) | 9.3 (0.8) | 10.6 (0.9) | 17.9 (1.5) | 13.4 (1.1) | 8.2 (0.6) |
| | Wet | | | | | |
| **Flexural strength (MPa)** | 129 (13) | 133 (20) | 117 (19) | 129 (18) | 128 (16) | 99 (18) |
| **Young's Modulus (GPa)** | 9.3 (0.6) | 8.5 (0.2) | 11.3 (0.5) | 16.0 (1.6) | 14.9 (0.6) | 8.9 (0.8) |

**Table 4.7. The flexure strength (MPa) and flexural modulus (GPa) of FSB, FST, FZ, Z100, GR and GF following 24h stored (a) 'dry' or (b) 'wet' at 37±1°C.**

## 4.3 DISCUSSION: The Mechanical Properties of 'Nanofilled' RBCs

The development and introduction of so-called 'nanofilled' RBCs to aesthetic restorative dentistry may be seen as a continuation of the trend for new RBCs to possess a reduced mean filler size, whilst also seeking to improve the filler loading and to optimise the subsequent physical properties and clinical performance [Ferracane, 1995; Mitra et al., 2003; Beun et al., 2007]. The development of 'nanofilled' RBCs for dentistry has not occurred in isolation; the introduction of 'nanocomposites' with a wide range of advanced materials and engineering applications, such as aerospace, electronics and biomaterials [Alexandre & Dubois, 2000; Abdalla et al., 2002; Dean et al., 2005; Thostenson, 2005] has occurred concurrently and utilise a diverse range of 'nano' filler-types [Tolle et al., 2002; McNally et al., 2005; McClory et al., 2007; Zhang et al., 2008] to significantly improve functional properties of the material.

'Nanofilled' RBCs routinely possess a bimodal filler distribution consisting of a distinct dispersion of spheroidal nano-sized silica particles and a phase of micro-sized particles to produce a hybrid-like structure [Lu et al., 2006; Turssi et al., 2006; Beun et al., 2007]. According to the manufacturer, the agglomerated 'nanocluster' filler offers an alternative approach to particle reinforcement of RBCs [Mitra et al., 2003], although considerable debate exists regarding the efficacy and clinical advantages associated with 'nanofilled' RBCs [CARE, 2003; Harris & Ure, 2006]. The term 'nanocluster' was coined by the manufacturer (3M ESPE) and may appear somewhat misleading as the mean cluster diameter was reported to be 0.6μm [Mitra et al., 2003]. Furthermore, SEM examination in the current study highlighted that the approximate mean cluster diameter in FSB was ~3.5μm (Figures 4.4, 5.12, 6.3 and 6.5), although the 'nanoclusters' in the translucent shade appeared to be generally smaller, ~0.2μm (Figures 4.4, 5.12 and 6.4). This may suggest that either the *in situ* 'nanoclusters' present in FSB were larger than the manufacturers reported [Mitra et al., 2003] or that the 'nanocluster' particles present in the polymerized resin matrix formed agglomerations of several 'nanoclusters'. Furthermore, the non-uniform distribution of constituent nano-sized particles within the structure of the 'nanocluster' and subsequent varied size and topographicical arrangement (Figures 4.4, 5.12 and 6.4), suggested that particle agglomeration during the production of the 'nanoclusters' occurred randomly. Despite the inhomogeneous filler structure and distribution of the 'nanoclusters' within the resin matrix and also the differing 'nanocluster' loading within FSB (79.0wt%;

59.5vol%) and FST (70.0wt%; 57.5vol%), the bi-axial flexure strength of control samples of FSB and FST (159 and 160MPa, respectively) was identified to be comparable with the conventionally filled FZ and Z100 (176 and 180MPa, respectively) and the nano-hybrid GR (165MPa) RBCs tested 'dry' (Tables 4.3-4.6). Likewise, published studies of the 'nanocluster' RBC have also identified equivalent, or improved, mechano-physical properties compared with conventionally filled RBCs [Mitra et al., 2003; Lohbauer et al., 2006; Turssi et al., 2006; Beun et al., 2007; Masouras et al., 2007; Junior et al., 2008; Watanabe et al., 2008].

### 4.3.1 Micromanipulation of discrete filler particles

The influence of common clinical scenarios on the mechanical (bulk and marginal fracture, strength degradation, cyclic fatigue, wear resistance) and physical (shrinkage, shrinkage stress/strain, colour stability) properties of filled dental resin matrices have been extensively studied, whilst the properties of individual filler particles are only inferred in relation to the complete RBC system [Yap et al., 2002; Adabo et al., 2003; Lohbauer et al., 2006; Lu et al., 2006]. An understanding of the mechanisms by which individual particles fail, the loads at which catastrophic failure of individual particles occur and their ability to deform and recover under load may therefore assist our understanding of the interaction of filler particles within the resin matrix and their influence on the overall mechano-physical properties of RBC materials.

The micromanipulation technique is a novel method enabling the characterization of the mechanical properties of discrete micro-sized particles and single cells. A form of micromanipulation was originally used to characterize the surface forces and mechanical properties of arbacia (sea urchin) eggs, although these were comparatively large and easy to handle considering that the subsequent development of the technique sought to characterize micro-sized particles [Cole, 1967]. Micromanipulation has since been used for both chemical engineering and biological applications to characterize the mechanical properties and investigate the relationship between composition and structure of micro-sized particles, such as microspheres, plant and animal cells, bacteria and microcapsules [Zhang et al., 1991; 1992; Mashmoushy et al., 1998; Shiu et al., 1999; Blewett et al., 2000; Sun & Zhang, 2002; Wang et al., 2004; Müller et al., 2005]. A further advantage of micromanipulation is the versatility and simplicity of use, although subsequent data analysis was time consuming [Shiu et al., 1999].

Following micromanipulation, the force at fracture of particles is determined and a 'pseudo-modulus' of stress is calculated [Zhang et al., 1991; 1992; Sun & Zhang, 2002]. The term 'pseudo-modulus' of stress is employed by studies using micromanipulation to describe the ratio of applied force divided by the original cross-sectional area of each particle prior to deformation [Bouwman et al., 2005; Chung et al., 2005; Müller et al., 2005]. Theoretically, in order to calculate the 'real' stress, the contact area between the particle and probe must be known. However, as the contact area varies with deformation and since particles are extremely small, it is often impossible to accurately measure the contact area. Therefore, a 'pseudo' stress is calculated which provides an approximation of the 'real' stress [Private communication with Prof. Z. Zhang].

#### 4.3.1.1 Fracture mechanisms of 'nanoclusters'

Micromanipulation of 'nanocluster', spheroidal and irregular particles produced a high scatter in the force at fracture (Table 4.1) and pseudo-modulus of stress (Table 4.2) data. This was consistent with data previously produced using micromanipulation which attributed a high data scatter to structural and morphological variation of the individual particle and highlighted that the trends identified were reproducible [Zhang et al., 1991; 1992]. The distinct structural and topographical variation of the 'nanocluster' particles (Figures 4.4, 5.12 and 6.4) may also be associated with the high data scatter identified in the current study.

Micromanipulation identified that the 'nanocluster' particles possessed significantly different fracture mechanisms compared with the spheroidal and irregular particles (Figure 4.1). The majority of spheroidal and irregular particles exhibited either no distinct fracture (Figure 4.2a), or a single distinct fracture (Figure 4.2b). In contrast, the 'nanocluster' filler complexes exhibited up to four distinct multiple fractures (Figures 4.1 and 4.2c) highlighting a unique mode of failure. Previous micromanipulation studies of microcapsules have highlighted similar occurrences where the incidence of multiple failures was attributed to the progressive break-up of particles [Sun & Zhang, 2002]. Therefore, the occurrence of multiple failures of the discrete 'nanocluster' particles is likely to be a consequence of the progressive break-up of the agglomerate following compressive loading. Two mechanisms of failure are proposed to describe the break-up of the 'nanocluster' particles identified following micromanipulation. Firstly, it is suggested that failure occurred along lines of internal porosity within the 'nanocluster' causing a

loss of cluster integrity, whereby the bifurcation of cracks either caused the cluster to fracture into several approximately equally sized fragments or to cause loss of smaller fragments of agglomerated particles (Figure 4.8a). Secondly, the 'nanocluster' may have been progressively deformed and subsequently collapsed into pre-existing interstitial cluster porosities to produce a denser compacted cluster thus acting to absorb or dissipate loading stresses (Figure 4.8b). The potential for denser and stronger clusters following loading was exhibited by the increased force at fracture of the 'nanocluster' (1702±909, 1968±1132, 2674±1486 and 1661±158μN) compared with the spheroidal (1389±1342μN) and irregular (1356±1093μN) particles (Table 4.1). Furthermore, propagation of micromanipulation loads and subsequent failure may be mitigated by the deposition and thickness of the silane coupling agent (Section 1.3.3.1) within the interstices of the agglomerated cluster. Essentially this may act as an elastic layer to absorb and dissipate loading stresses through the silane interface [Shirai et al., 2000].

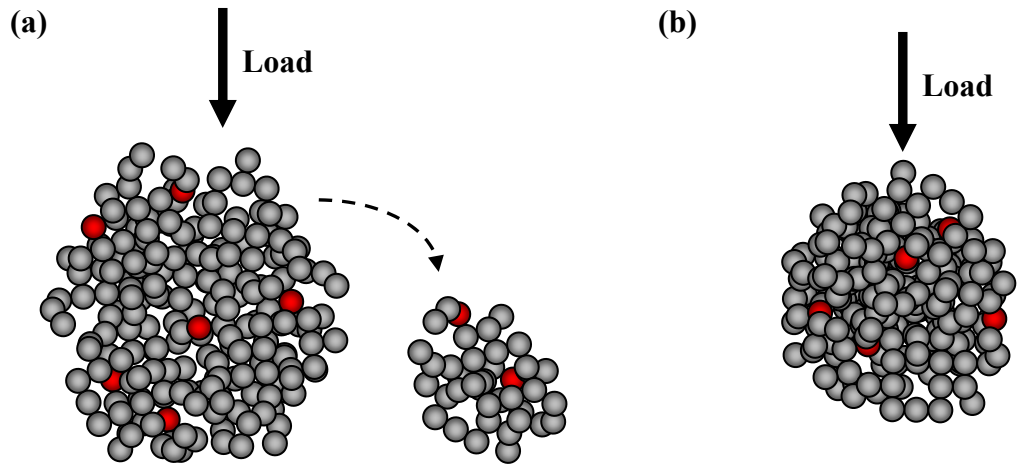


**Figure 4.8 Diagram representing the two fracture mechanisms proposed to explain the multiple fractures of 'nanocluster' particles, (a) bifurcation of cracks along lines of internal porosity resulting in fragmentation, (b) collapse of the 'nanocluster' into internal porosities to produce a denser particle complex.**

In contrast, micromanipulation of the spheroidal and irregular filler particulates produced either a single distinct fracture, in approximately a third of cases, whilst the remaining particles were not identified as failing (Figure 4.1). Ceramic structures, such as the silica-zirconia and barium-alumina borosilicate particles in the current study, have been identified to fracture within

the crystalline interfaces between the distinct crystalline phases [Brentel et al., 2007]. Furthermore, surface defects act as stress intensifiers and areas of local stress concentration to initiate failure [Lee et al., 2000; Junior et al., 2008]. This may suggest that failure of the fused spheroidal particles occurred by bifurcation of the fused zirconia-silica particles at the fused interface between the two phases as a consequence of the applied load (Figure 4.9a). Alternatively, single failure of the irregular barium-alumina borosilicate particles may be due to fracture of protuberances from the irregular particle or due to propagation of cracks from surface defects, potentially possessed by both the spheroidal and irregular particles, which were generated during particle production (Section 1.3.3) (Figure 4.9b).

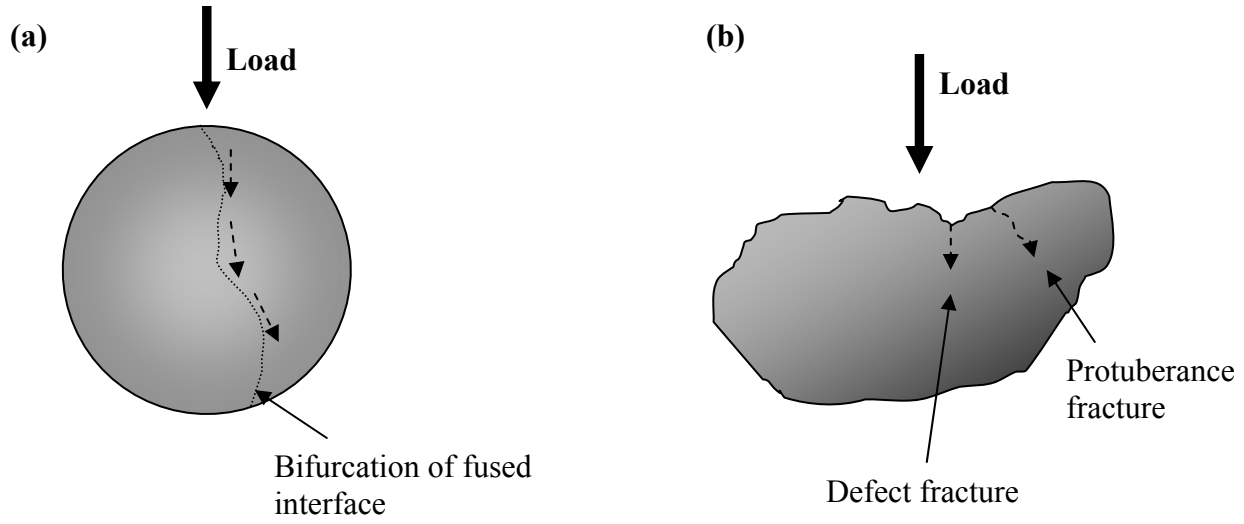


**Figure 4.9 Diagram representing of single failure of (a) spheroidal fused zirconia-silica particles at the fused interface and (b) fracture of protuberances or from surface defects generated by milling to produce irregular particles.**

The lack of failure exhibited by approximately two-thirds of spheroidal and irregular filler particles may be attributed to the orientation of the particle during loading, whereby the particle orientation effectively 'shielded' the surface defect, protuberance or fused crystalline interface between the crystalline phases, from which fracture occurred [Ritchie et al., 1988]. Interestingly, the pseudo-modulus of stress of the irregular and spheroidal particles was increased following fracture (Table 4.2), which may also suggest that the orientation of the particle fragments following fracture and lack of additional catastrophic defects prevented further failure.

It might be suggested that single or multiple particle failure occurred as aggregated or several distinct particles were loaded. However, the resolution of the light-microscope and camera set-up on the micromanipulator rig (Section 3.2.1.2) enabled identification of discrete particles prior to loading [Zhang et al., 1991; 1992], also the clear trends of none, single or multiple failure exhibited by the particle-types (Figure 4.1) refute this suggestion. To further clarify particle loading it may be suggested that future micromanipulation studies employ atomic force microscopy (AFM) to provide improved resolution and hence ease of individual particle identification and testing [Liu et al., 2005]. In addition, the efficacy of a nanomanipulation technique, which was a direct development of the micromanipulation technique, has recently been demonstrated by Lui et al. (2005) and may also enhance further study of particulate failure.

Deformation of 'nanocluster' particles which possess internal porosities due to the structural arrangement of the agglomerated nanoparticles may also modify crack propagation through the bulk of the particle. This was indicated by the increased associated percentage deformation exhibited by the 'nanoclusters' and subsequent cluster fragments (0.46±0.67, 1.31±1.15, 0.61±0.61 and 0.43±0.06%) compared with the spheroidal (0.28±0.14%) and irregular (0.38±0.17%) particles (Table 4.1). Consequently, blunting of the propagating crack-tip may occur, enhancing the dissipation of loading stresses and improving the ability of the 'nanocluster' complex to absorb compressive loads. The apparent influence of structural arrangement of nanoparticles within agglomerated fillers on the subsequent deformation and mechanical properties following micromanipulation is consistent with previous micromanipulation studies which also highlighted that deformation was influenced by particle microstructure in addition to water content and subsequent water loss. These studies identified an elastic recovery of 50-80% following deformation [Sun & Zhang, 2002; Chung et al., 2005], which may be attributed to the focus of the majority of previous micromanipulation studies on filled structures, such as cells and gel-filled microparticles which exhibited a degree of elastic recovery rather than the generally fused or monolithic structures employed in dental RBCs [Zhang et al., 1991; 1992; Anseth et al., 1996; Mashmoushy et al., 1998; Sun & Zhang, 2002; Wang et al., 2005; Ding et al., 2007; Lui & Webster, 2007].

Micromanipulation studies have previously identified that force and deformation at fracture increased proportionally with particle diameter [Zhang et al., 1992; Sun & Zhang, 2002]. In contrast, the current study identified a negative linear relationship between the particle size and

pseudo-modulus of stress of the spheroidal ($r^2$= ¯0.70 and ¯0.78) and irregular ($r^2$= ¯0.59 and ¯0.79) particles, suggesting instead that as particle size increases, pseudo-modulus of stress decreases. The focus of previous micromanipulation studies on filled structures, such as microgel particles, highlighted that deformation was related to release of the constituents from the particle [Sun & Zhang, 2002; Chung et al., 2005]. Consequently, since the spheroidal and irregular particles instead possessed fused and monolithic structures and did not exhibit significant deformation (Table 4.1) the previous correlation did not agree with the trends identified in the current study. Furthermore, despite the approximately equivalent sizes of the 'nanoclusters', spheroidal and irregular particles, the Pearson coefficient of 'nanoclusters' highlighted a comparatively higher level of inconsistency ($r^2$ closer to 0) between the size and pseudo-modulus of stress of the 'nanoclusters' ($r^2$=¯0.38, ¯0.33, ¯0.28, ¯0.08). This might suggest that the inhomogeneous distribution of nanoparticles within the agglomerated structure of the 'nanocluster', subsequent porosities and ability to deform influenced the force at fracture and pseudo-modulus of stress (Tables 4.1 and 4.2).

In conclusion, micromanipulation of the agglomerated 'nanocluster' particles identified distinctly different mechanical properties compared with particles possessing a spheroidal or irregular morphology. Therefore, incorporation of 'nanocluster' particles into a conventional resin matrix may modify the subsequent failure mechanisms and provide enhanced damage tolerance unique to 'nanocluster' reinforced RBCs.

### 4.3.2 Cyclic pre-loading of filled resin composite systems

Clinically, RBC restorations are subjected to multiple complex stressing mechanisms, due to masticatory loading and fatigue (Section 2.2.3), which induce surface and subsurface defects dependent upon the magnitude and duration of load [McCabe et al., 1990b]. This reduces the structural integrity of the RBC material and increases the likelihood of premature failure at stresses considerably below the reported mean strength values of those materials [Lohbauer et al., 2003a; 2003b; 2006; Papadogiannis et al., 2006]. Subsequently, the introduction of sub-critical stresses to an RBC restoration may significantly reduce clinical longevity. It is therefore highly pertinent to investigate *in vitro* cyclic pre-loading to characterise failure mechanisms of RBCs, which may assist in the prediction of *in vivo* behaviour and potential occurrence of premature failure due to masticatory loading of RBC restorations.

Generally, each of the seven materials tested following pre-loading highlighted a general decrease in the BFS and reliability of strength data, irrespective of storage conditions (Figure 4.5). This was consistent with previous studies which also reported that the fracture strength of pre-loaded materials was significantly reduced [Lohbauer et al., 2003a; 2003b; 2006; Papadogiannis et al., 2006]. Previous studies also identified that during pre-loading cracks were induced and propagated through the resin matrix and silane interface surrounding fillers. The occurrence of sub-critical crack growth was reported to be influenced by filler size, loading and interparticulate spacing and also in the specific case of microfill RBCs which possessed pre-polymerized fillers cracks were identified to propagate through the prepolymer particles themselves [Drummond, 1989; Htang et al., 1995].

The fracture strength and resistance to fatigue of dental RBCs is often related to the filler particle loading, whereby a higher filler loading produces improved mechano-physical properties [Ferracane, 1995; Cobb et al., 2000; Lu et al., 2006]. Therefore, the low unloaded fracture strength of the microfill RBC HM (87±8MPa) and failure to complete the pre-loading regimes (Table 4.6) was consistent with this and attributed to the limited filler loading of HM (66.7wt%; 46.0vol%). Consequently microfills have been contraindicated for posterior placement and areas of high stress [Lutz & Philips, 1983; Roulet, 1987; Lang et al., 1992], although HM is generally atypical of other microfills possessing a higher filler loading and fifteen years of proven clinical performance in posterior situations. However, the current study also revealed that the initial fracture strength and Weibull modulus of some RBCs material groups did not necessarily correspond with the fracture strength following pre-loading. This was particularly pronounced for GR and Z100, which despite a high filler loading (87.0wt%; 71.4vol% and 84.5wt%; 66.0vol%, respectively) and unloaded BFS of 165±18 and 180±31MPa, failed to respectively complete the 50 and 100N or 100N pre-loading regimes (Table 4.4a and 4.5a). In contrast, despite FSB and FST possessing a lower filler loading (79.0wt%; 59.5vol% and 70.0wt%; 57.5vol%, respectively) and also exhibiting a lower unloaded BFS (159±21 and 160±27MPa, respectively) compared with GR and Z100, one hundred percent of FSB and FST specimens survived pre-loading regimes up to and including 100N and also exhibited improved strengths and significantly increased Weibull moduli (Table 4.3). Likewise, Lohbauer et al. (2003a; 2003b; 2006) also identified that the fatigue resistance of ‘flowable’, microhybrid and nano-hybrid RBCs, which exhibited an initially

high flexure strength, did not necessarily result in a correspondingly high resistance to clinical fatigue.

Since all GR and HM specimens failed to survive pre-loading to 50 and 100N and approximately half of GF and Z100 specimens failed to survive pre-loads of 100N, the limited stress bearing capability of these materials may be of clinical concern as these materials have been indicated by their manufacturers for both anterior and posterior placement. The premature failure of GR and Z100 may be attributable to the significantly higher flexural modulus (13.4±1.1 and 17.9±1.5GPa, respectively) compared with the other RBCs tested (Table 4.7). A high flexural modulus has been identified to inhibit the ability of a material to resist deformation due to loading and the accumulation of surface and bulk defects resulting in premature failure [Emami et al., 2003; Lohbauer et al., 2003a; 2003b; 2006; Sabbagh et al., 2004; Calheiros et al., 2006]. However, significantly lower flexural moduli of approximately 6GPa [Calheiros et al., 2006] and 8.2±0.6GPa were identified for HM and GF respectively, which where comparable with the remaining RBCs (Table 4.7). Here, the low filler loading and subsequently lower BFS of the microfill HM may have resulted in the failure of all specimens prior to completion of the 50 and 100N pre-loading regime. Alternatively, the apparent intrinsic weakness of HM may also be attributed to the presence of pre-polymerized filler particles which act as defect centres [Drummond, 1989; Htang et al., 1995]. Microfills have been identified to routinely possess an inhomogeneous microstructure due to inhomogeneity of filler size and distribution derived from the high density of nano-sized fillers within the pre-polymerized particle, which may ultimately lead to reduced strength and a greater tendency for strength degradation due to fatigue and cyclic pre-loading [Ferracane et al., 1995]. Subsequently, the use of microfill RBCs in areas of high stress and high contact was contraindicated [Lang et al., 1992]. The production of RBCs has sought to limit in situ particle agglomeration which produce an inhomogeneous filler distribution and subsequent ‘filler rich’ regions which act as weak inclusions within the resin matrix [Willems et al., 1992; Gladys et al., 1997; Chou & Ren, 2000; Sawyer et al., 2003].

The resin matrix of GF has a decreased filler particle load and an irregular particle morphology. Irregular shaped particles have been associated with a high stress concentration due to the sharp edges and protuberances that may fail to dissipate loading stresses and subsequently enhance crack propagation [Sabbagh et al., 2004]. This strongly suggested that GF was an intrinsically weaker material since approximately half the specimens failed at a cyclic pre-load of

100N. However, 'flowable' RBCs have been developed to meet specific clinical needs, such as liners in deep cavities, repair of marginal defects, pit and fissure sealants and to act as stress absorbing layers in large RBC restorations (as a consequence of low elastic modulus). Subsequently their clinical placement does not routinely include high stress bearing locations [Combe & Burke, 2000; Sabbagh et al., 2004].

#### 4.3.2.1 Differential reinforcement provided by 'nanocluster' particles

The 'nanocluster' reinforced RBCs (FSB and FST) were identified to possess statistically similar or significantly increased BFS and associated Weibull moduli at cyclic pre-loads that initiated catastrophic failure of the other RBC materials tested in the current study (Table 4.3). In particular, the BFS of FSB pre-loaded to 20 and 50N both 'dry' (137±15 and 146±12MPa) and 'wet' (179±19 and 183±18MPa) was maintained or increased. Similarly, the BFS of FST was also improved or maintained following pre-loading up to and including 100N (Table 4.3a&b). Conversely, at 50 or 100N the BFS of the other RBCs tested were significantly decreased compared with the unloaded control groups (Tables 4.4, 4.5 and 4.6).

A Weibull analysis was subsequently applied to the mean BFS data since a potentially inhomogeneous defect distribution within specimens will render mean values inconclusive and potentially misleading, suitable only for comparative purposes [McCabe & Carrick, 1986]. Mean strength data assumes that the defect population possesses a 'normal' distribution, whilst in reality the defect population frequently lacks this level of homogeneity where a higher defect distribution exists. Therefore, to determine the reliability of the data and predict the probability of failure of brittle materials a suitable statistical function, such as Weibull modulus (Section 2.2.2.1) and associated survival probability distributions is vital to provide a meaningful interpretation of the flexural strength within a specimen group ($n \geq 20$), [Weibull, 1951; McCabe & Carrick, 1986]. Whereby a high Weibull modulus is indicative of a narrow distribution of defects and increased reliability of the strength data of that particular material. Weibull analysis identified that in addition to the increased BFS data of the 'nanocluster' RBC compared with conventionally filled RBCs, the Weibull modulus ($m$) was also identified to be significantly increased or maintained at pre-loads of 50 and 100N. In contrast, all other RBC materials investigated in the current study exhibited a significantly decreased Weibull modulus following

50 and 100N pre-loading compared with unloaded specimen groups since the 95% confidence intervals failed to overlap (Tables 4.3, 4.4, 4.5 and 4.6).

A significant increase was also identified between the Weibull modulus of 'nanocluster' RBC specimens stored 'dry' or 'wet' for 24h, which was consistent with the increase in BFS also identified. In particular, *m* of FST pre-loaded to 20N 'wet' (16.89±3.78) was identified to be significantly higher than 'dry' (8.54±1.91) as the 95% confidence intervals failed to overlap (15.15-18.60 and 7.41-9.67, respectively). In addition, the $R^2$-value also highlighted a reduction in the scatter of data exhibited by the 'nanocluster' RBCs due to pre-loading to 20 and 50N and subsequent storage in water, such as FSB 'wet' (0.97 and 0.97) compared with 'dry' (0.96 and 0.91) and also FST 'wet' (0.96 and 0.97) compared with 'dry' (0.93 and 0.95) (Table 4.3). The Weibull modulus has previously been identified to be valid when the BFS data approximates a straight line on the Weibull plot ($R^2$=1), whilst a value exceeding 0.95 constitutes a single defect population. Conversely, a deviation from the straight-line distribution of the Weibull plot and an $R^2$-value of less than 0.95 was indicative of a multi-modal defect distribution present within the specimen undergoing testing [Fleming et al., 1999a; 1999b; 2000; Bhamra et al., 2002]. The improved BFS and reliability of the 'nanocluster' RBCs stored 'wet' following pre-loading to 20 and 50N was also suggested by the survival probability distributions. FSB exhibited a distinct shift in the data distribution into the higher strength range (>150MPa) following 'wet' compared with 'dry' storage. Furthermore, FST specimens stored 'wet' following pre-loading to 20 and 50N highlighted a reduction in the asymmetry within the 'tail-end' of the data distribution and also that the homogeneity of the distribution of BFS data was markedly improved (Figure 4.7).

It was interesting to note that throughout the pre-loading study (and also the subsequent water storage study reported in Chapter 5) the defect population indicated by the survival probably distribution plot did not necessarily correspond with that suggested by the $R^2$-values (Section 4.2.2). The correlation coefficient ($R^2$-value) was calculated by a least square analysis of the plots of $\ln\ln(1/Ps)$ against $\ln\sigma$ and were indicative of how well the experimental data fits the Weibull distribution [McCabe & Carrick, 1986] and varied from 0.89-0.99, suggesting significant differences in the defect populations [Fleming et al., 1999a; 1999b; 2000; Bhamra et al., 2002]. It is therefore worth reiterating that direct comparison of $R^2$-values determined from the Weibull distribution with the survival probability plots may be misleading and also that the $R^2$-value is an indication [McCabe & Carrick, 1986] of the defect population and not definitive. However, the

inconsistancies between the suggested defect distribution and that highlighted by the survival probability distribution highlight that conclusions construed from the $R^2$-values alone (or any other source of data in isolation) is limited and that multiple sources of data are required to ensure the accuracy of conclusions.

The significantly different response to fatigue loading of the 'nanocluster' RBCs compared with the other RBCs tested was attributed to the reinforcement provided by the 'nanocluster' particles. Particularly as even FZ, which is known to possess an identical resin matrix to FSB and FST and also to possess a filler size comparable with the observed size of the 'nanoclusters' (Figures 4.4, 5.12 and 6.4) [Junior et al., 2008], exhibited a decreased fracture strength and reliability following the 50N cyclic pre-loading regime (Tables 4.3 and 4.5a). The fracture of dental RBCs is routinely related to failure of the interfacial layer between the inorganic fillers and the resin matrix, which subsequently acted as defect centres, promoting failure [Söderholm et al., 1983; 1984; Øysæd & Ruyter, 1986]. The significant increase in Weibull modulus of the 'nanocluster' RBCs following pre-loading (Tables 4.3) implied a differential impact on the 'nanocluster' particles compared with the spheroidal or irregular particles, which limited their function as defect centres. This suggests that pre-loading of FSB and FST modified the 'nanoclusters' to produce a more damage tolerant system. As discussed in Section 4.3.1, the micromanipulation of the 'nanocluster' particles produced a unique fracture mechanism compared with spheroidal and irregular particles. This may be a consequence of crack bifurcation and the ability of the 'nanocluster' to absorb and dissipate crack stresses by collapsing into pre-existing cluster porosities or due to the loss of fragments from the main clustered structure. The suggested ability of discrete 'nanoclusters' to deform and dissipate the accumulated fatigue loading stresses may enhance the fracture strength and resistance to premature fracture within the resin composite system.

The morphology of filler particles has also been identified to influence the subsequent reinforcement and resistance of RBCs to fracture [Lohbauer et al., 2003a; 2003b; 2006; Papadogiannis et al., 2006], therefore the 'nanocluster' morphology may also partially influence the response of the 'nanocluster' RBCs to pre-loading. Both the 'nanocluster' (FSB and FST) and microhybrid (FZ) RBCs contain fillers which possess a nominally spheroidal morphology (Figures 4.4, 5.12, 6.4). A spheroidal morphology has been associated with reduced stress concentration and dissipation of loading stresses compared with the sharp edges and

protuberances of irregular particles which may promote stress concentration and subsequent crack growth resulting in catastrophic failure [Sabbagh et al., 2004]. The non-uniform surface topography of the 'nanocluster' particles, due to the apparently random distribution of individual particles within the agglomerated complex, may enhance interfacial adhesion due to the higher surface area available for silanization, and also due to mechanical interlocking with the surrounding resin [Li et al., 2007].

The storage condition highlighted a significant difference between the 'dry' and 'wet' bi-axial flexure strength of the 'nanocluster' RBC, whereby specimens stored 'wet' exhibited a significantly increased bi-axial flexure strength (Table 4.3). The BFS of FST following 20, 50 and 100N 'wet' (182±12, 171±17 and 175±21MPa) was markedly higher than similar specimens pre-loaded prior to storage of the specimens 'dry' (165±19, 148±15 and 141±21MPa). This suggested that water induced hydrolysis and polymerization of the interfacial silane layer of the 'nanocluster' reinforced RBCs modified stress transfer both to and within the 'nanocluster' particles, producing an enhanced capacity to tolerate local stress and cluster deformation. In addition, 'wet' storage of the microhybrid FZ also improved the BFS, although not to the same extent as the 'nanocluster' materials as the fracture strength of FZ was reduced following pre-loading to 50N. It is suggested that since the resin matrix chemistry of FSB, FST and FZ was nominally identical and since NIRS identified that following immersion the subsequent uptake of water into the hydrophilic resin matrix was rapid even following 24h (Section 5.1), that hygroscopic expansion of the resin may have occurred. Hygroscopic expansion occurs as water molecules infiltrate porosities, vacancies and free volume between polymeric chains within the resin matrix, causing swelling which may impede defects and propagating cracks [Martin et al., 1998; Sideridou et al., 2003; Tay et al., 2002]. Therefore, a combination of water induced modification of the silane interface and hygroscopic expansion of the resin matrix may have occurred concurrently within the 'nanocluster' reinforced RBC to promote the observed increase or maintenance of BFS following pre-loads of 50 and 100N and wet storage. Conditions which were extremely detrimental to the other RBCs tested.

#### 4.3.2.2 Interpenetrating phase composite structure of 'nanoclusters'

The 'nanoclusters' undergo a dual silanization process with a dilute silane coupling agent to infiltrate the cluster interstices, whilst the surface of the 'nanocluster' is subsequently coated

with an undiluted silane to promote interfacial adhesion with the resin matrix [Private communication, S. Mitra, 3M ESPE at IADR 2007 New Orleans, US]. This produces an agglomerated particle consisting of a random interconnected network of silica-zirconia or silica nano-particles. If the interstices and internal porosities of the 'nanocluster' are fully infiltrated by the silane coupling agent, it might be assumed that an interpenetrating phase composite (IPC) structure will be generated. Essentially, IPC materials possess an interconnected three dimensionally continuous phase where the degree of crosslinking between the three constituent phases determines the ability to resist deformation [Clarke et al., 1992; Wegner & Gibson, 2001]. The presence of a fully infiltrated porous IPC structure is known to provide increased mechanical properties compared with a similar non-infiltrated porous particulate structure [Yang et al., 2003]. The interconnectivity of the distinct phases enables each structural phase of the IPC to contribute its most desirable properties, such as plastic deformation of a metal phase and high stiffness of a ceramic phase in metal/ceramic IPCs, thereby optimising the mechanical properties of the subsequent material [Wegner & Gibson, 2001; Zeschley et al., 2005]. For example, IPC structures have been identified to increase the compressive strength and Young's modulus by up to fifty percent compared with materials not possessing an IPC structure [Zeschley et al., 2005].

The 'nanocluster' particle possesses a high internal porosity infiltrated by a relatively weak second phase and would be expected to be inherently weaker than a 'dense' silica particle of the same size. However, the interpenetrating phase 'nanocluster' appears highly effective as a reinforcing filler within the polymeric matrix due to the statistically similar or significantly increased BFS and associated Weibull modulus, particularly following pre-loads and 'wet' storage, whilst the nano-hybrid and conventionally filled RBCs exhibited significantly reduced mechanical properties at 50 and 100N cyclic pre-loading regimes. In 'dry' environments the interfacial silane phase will be relatively stable, however the transmission of loading induced stresses through the silane layer may deform the 'nanocluster' creating defects in and around clusters. Silanated structures may also be modified by moisture which affects monomer polymerization, the interfacial silane layer and resin matrix bonds. The presence of water in the matrix could induce hydrolysis and polymerization of the interfacial silane layer, which modified stress transfer and inhibits crack propagation, blunting the crack-tip and thus reducing the stress concentration [Takashige et al., 2007].

The micromanipulation and pre-loading results suggested that the ability of ‘nanoclusters’ to undergo multiple fractures and the proposed IPC-like structure enhanced the damage tolerance and reliability of the material. This was exacerbated within an aqueous environment where the failure strength and Weibull modulus were significantly increased or maintained whilst that of conventionally filled RBCs decreased. However, as the current pre-loading study was limited to 24h, increasing the period of immersion in an aqueous environment may critically compromise the hydrolytic stability of the material.

# CHAPTER 5 RESULTS AND DISCUSSION: WATER STORAGE

## 5.1 RESULTS: Degradation of Nanofilled RBCs: Water Storage

The water storage regimes aimed to determine the influence of short- (24h), medium- (1, 4, 13 and 26 weeks) and long-term (52 and 78 weeks) immersion and water sorption on the subsequent mechanical properties of 'nanocluster', nano-hybrid and conventional RBCs.

### 5.1.1 Near-IR spectroscopy

FTIR spectroscopy in the near infrared range was employed to semi-quantify the water content and water sorption of the disc-shaped RBC specimens following storage.

**Water sorption of FSB, FST and FZ**

The water content of FSB and FZ was identified from the area under the absorbance band centred around 5200cm$^{-1}$ to increase up to between 1 and 13 weeks prior to equilibration, whilst the water content of FST increased concomitantly throughout the study (Figure 5.1).

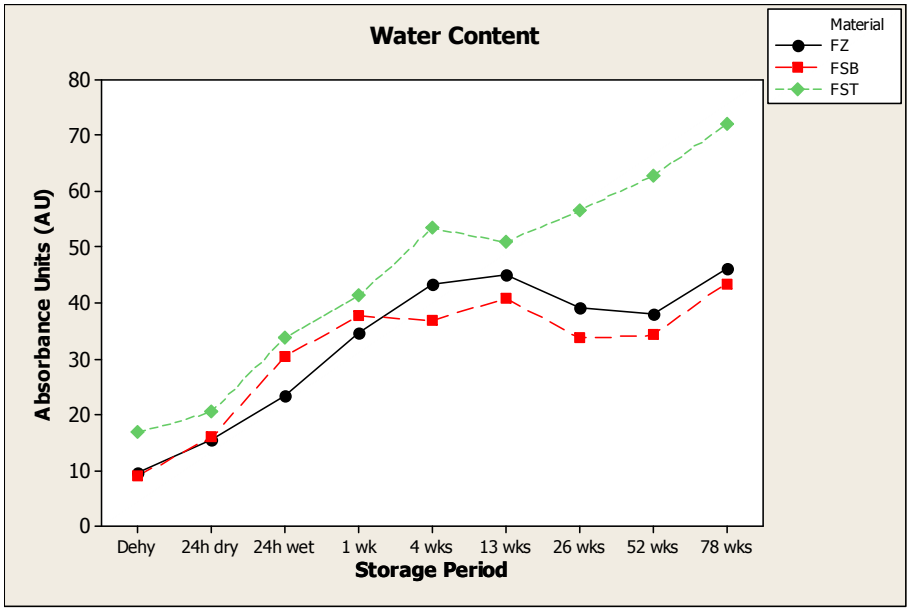


**Figure 5.1. Plot highlighting the mean water content of FSB, FST and FZ specimens (n=5) following specimen dehydration according to ISO 4049, 24h 'dry' storage and 24h, 1, 4, 13, 26, 52 and 78 weeks stored in a waterbath. Water content was calculated with a spectral manipulation program and integration method to determine the mean area under the absorbance band centred around 5200cm$^{-1}$.**

Following dehydration according to ISO 4049 a residual quantity of water was identified in FSB, FST and FZ (9.00±2.72, 16.85±1.66 and 9.50±3.00AU, respectively). In addition, 'dry' storage for 24h produced a mean absorbance of 15.97±2.97, 20.47±0.63 and 15.46±1.87AU respectively (Table 5.1).

The water content of FSB following 24h and 1 week stored in a waterbath was markedly increased (30.47±5.49, 37.72±1.79AU, respectively), whilst subsequent immersion for 4, 13, 26, 52 and 78 weeks highlighted apparent equilibration of the water content of FSB (36.81±2.23, 40.85±11.80, 33.68±7.36, 34.24±8.51 and 43.52±6.61AU, respectively) (Table 5.1; Figure 5.2a). Conversely, the water content of FST was identified to increase following consecutive immersion periods without apparent equilibration (33.79±5.9, 41.18±5.29, 53.38±2.26, 50.89±5.65, 56.57±5.78, 62.74±5.91 and 72.04±16.89AU, respectively) (Table 5.1; Figure 5.2b). The water content of FZ exhibited a comparable trend with FSB, increasing following 24h, 1 and 4 weeks immersion (23.46±2.3, 34.60±2.69 and 43.33±4.02AU, respectively), prior to apparent equilibration (45.12±4.28, 39.18±4.09, 37.93±3.79 and 46.33±4.07AU, respectively) (Table 5.1; Figure 5.2c).

| | **5200 $cm^{-1}$ (NIR absorbance)** | | |
|---|---|---|---|
| | **FSB** | **FST** | **FZ** |
| **Dehydrated** | 9.00 (2.72) | 16.85 (1.66) | 9.50 (3.00) |
| **24h Dry** | 15.97 (2.45) | 20.47 (0.63) | 15.46 (1.87) |
| **24h Wet** | 30.47 (5.49) | 33.79 (5.95) | 23.46 (2.37) |
| **1 week** | 37.72 (1.79) | 41.18 (5.29) | 34.60 (2.69) |
| **4 weeks** | 36.81 (2.23) | 53.38 (2.26) | 43.33 (4.02) |
| **13 weeks** | 40.86 (11.50) | 50.89 (5.65) | 45.12 (4.28) |
| **26 weeks** | 33.68 (7.36) | 56.57 (5.78) | 39.18 (4.09) |
| **52 weeks** | 34.24 (8.51) | 62.74 (5.91) | 37.93 (3.79) |
| **78 weeks** | 43.52 (6.61) | 72.04 (16.89) | 46.33 (4.07) |

**Table 5.1. NIR spectroscopy highlighting the water content of FSB, FST and FZ specimens following dehydration of specimens according to ISO specification 4049, 24h stored 'dry' and 24h, 1, 4, 13, 26, 52 and 78 weeks stored in a waterbath.**

**(a)**

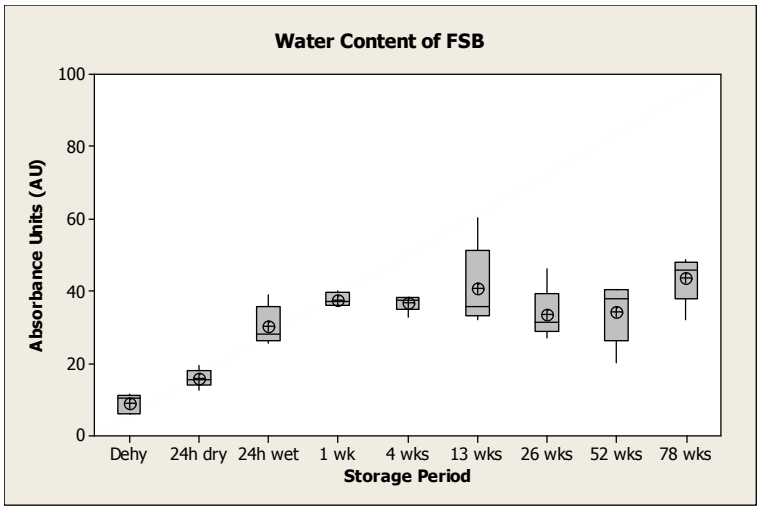


**(b)**

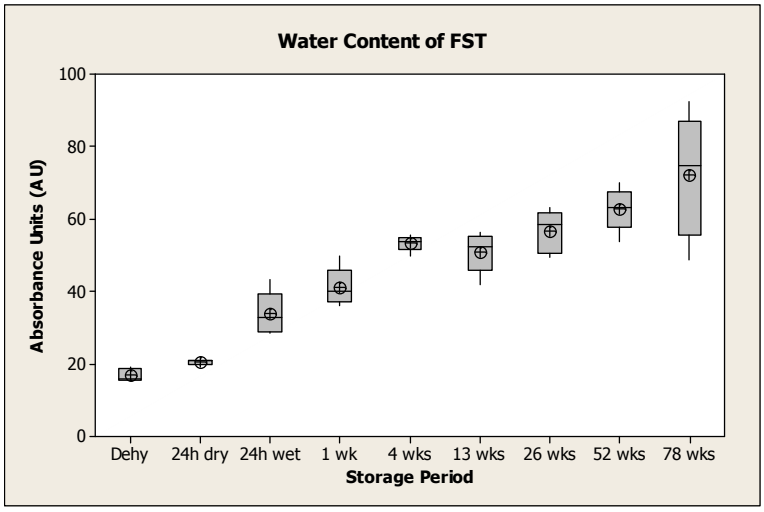


**(c)**

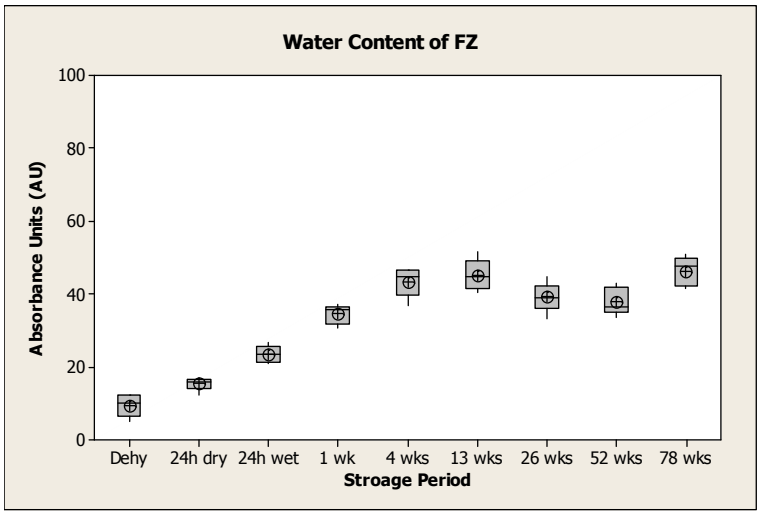


**Figure 5.2. Box and whisker plots highlighting mean, median and interquartile range of water content and water sorption of (a) FSB, (b) FST and (c) FZ following dehydration, 24h stored 'dry' and 24h, 1, 4, 13, 26, 52 and 78 weeks stored 'wet'. The plots highlight non-equilibration of FST, whilst FSB and FZ equilibrate following between 1 and 13 weeks.**

**Water sorption of GR and GF**

NIR spectroscopic analysis of the nano-hybrid materials GR and GF also highlighted increased water content as a consequence of the water storage periods employed in the investigation (Figure 5.3), although this was markedly lower than FSB, FST and FZ. The mean absorbance value of GR following 24h 'dry' was 5.57±0.96AU and increased comcomitently following 24h, 13, 26 and 52 weeks (9.12±0.79, 12.38±0.80, 14.93±1.72 and 18.39±2.13AU, respectively) (Table 5.2). The water content of GF was 4.51±0.56AU following 24h stored in 'dry' conditions and increased following storage until apparent equilibration following 13 weeks (14.45±2.79, 17.80±2.19, 18.71±5.47 and 16.09±2.84AU, respectively) (Table 5.2; Figures 5.2 and 5.3).

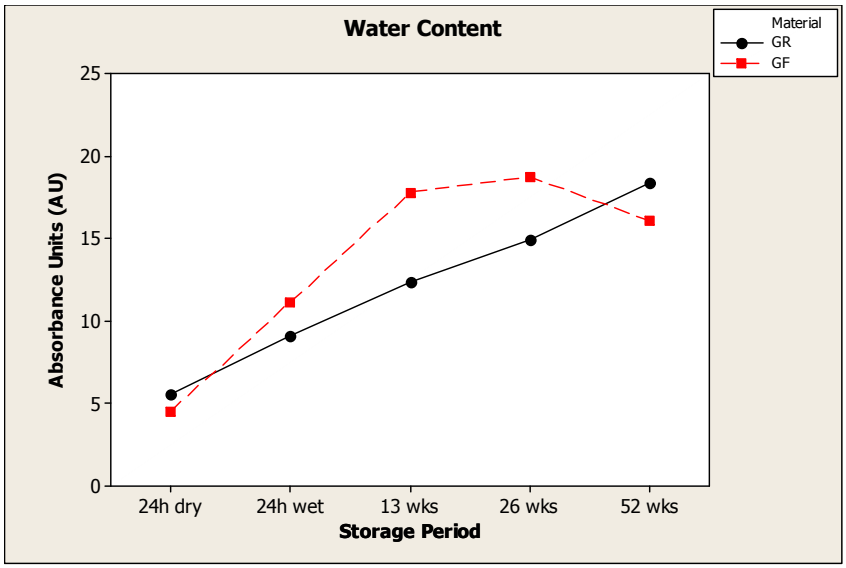


**Figure 5.3. Plot highlighting the mean water content of GR and GF specimens following 24h 'dry' storage and 24h, 13, 26 and 52 weeks stored in a waterbath; highlighting non-equilibration of GR and apparent equilibration of GF following 13 weeks.**

| | 5200 $cm^{-1}$ (NIR absorbance) | |
|---|---|---|
| | **GR** | **GF** |
| **24h Dry** | 5.57 (0.96) | 4.51 (0.56) |
| **24h Wet** | 9.12 (0.79) | 11.15 (1.15) |
| **13 weeks** | 12.38 (0.80) | 17.80 (2.19) |
| **26 weeks** | 14.93 (1.72) | 18.71 (5.47) |
| **52 weeks** | 18.39 (2.13) | 16.09 (2.84) |

**Table 5.2. NIR highlighting water content of GR and GF specimens following 24h stored 'dry' and 24h, 1, 13, 26 and 52 weeks 'wet'.**

**(a)**

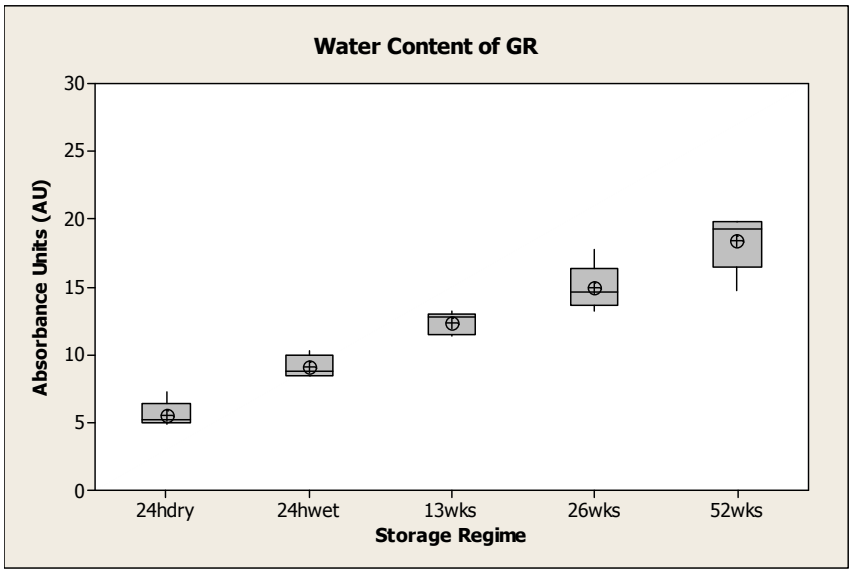


**(b)**

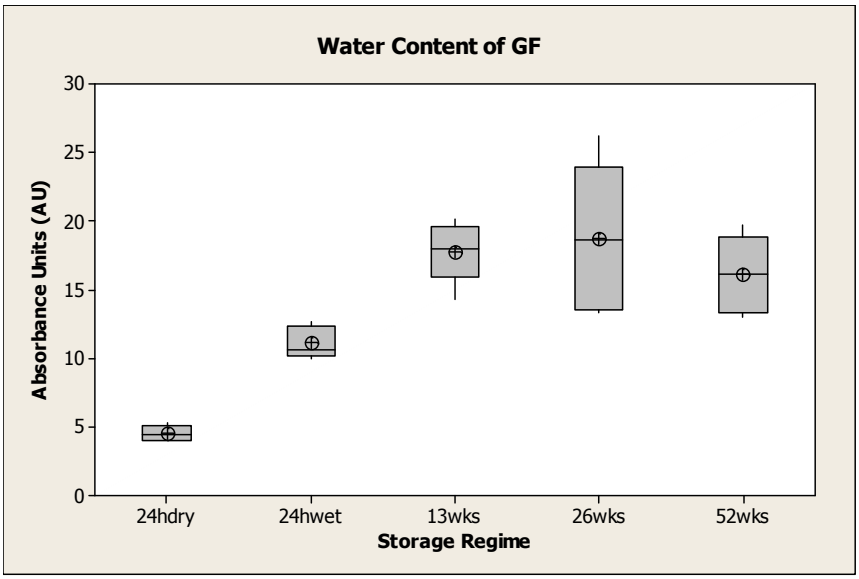


**Figure 5.4. Box and whisker plots highlighting the mean, median and inter-quartile range of the water content and water sorption determined using NIR spectroscopy of (a) GR and (b) GF specimens following 24h stored 'dry' and 24h, 13 26 and 52 weeks stored in a waterbath maintained at 37±1°C.**

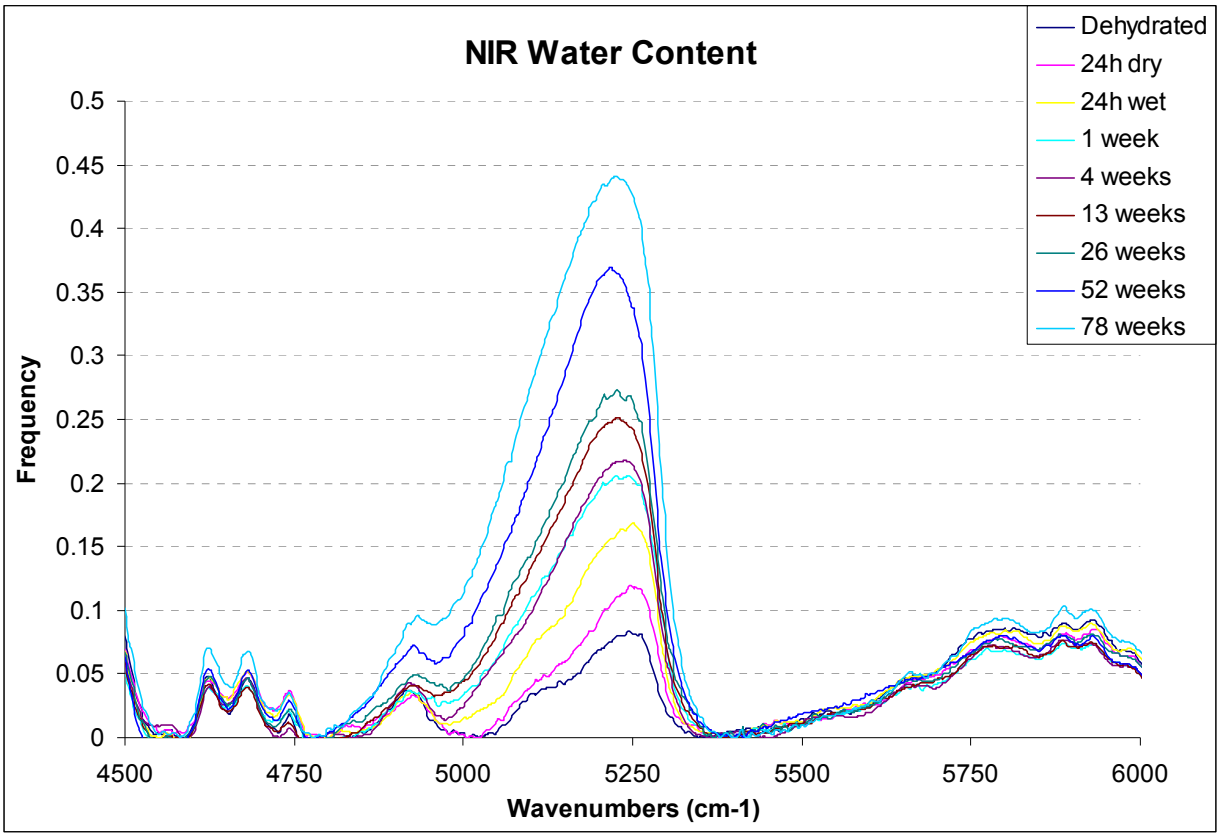


**Figure 5.5. Representative spectra (FST) in the NIR region of the Fourier transform infrared spectrum highlighting the progressively increased height and area of the absorbance band attributed to water centred around 5200cm$^{-1}$.**

### 5.1.2 Bi-axial flexure strength and Weibull modulus of FSB, FST and FZ

Two-way ANOVA of FSB, FST and FZ following 24h 'dry' and 'wet' and for 1, 4, 13, 26, 52 and 78 weeks stored in a waterbath maintained at 37±1˚C highlighted that the BFS of the RBCs was significantly reduced under 'wet' storage conditions (F=4.80; P<0.001) (Figure 5.5).

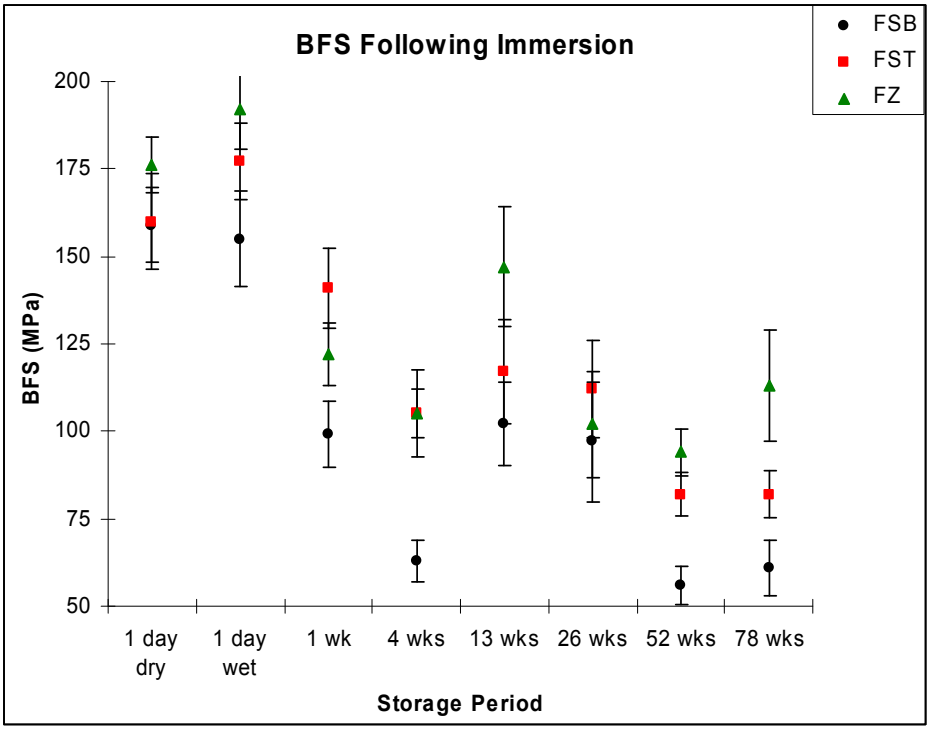


**Figure 5.6. Plot of the mean BFS exhibited by FSB, FST and FZ groups following the increasing immersion periods and demonstrating a general decrease in the BFS as a consequence of the water storage regimes.**

Supplementary one-way ANOVA and paired Tukey test comparisons at the 95% significance level highlighted no significant difference between the 'dry' and 'wet' BFS of FSB (159±21 and 155±27MPa; P>0.05). However, a significant concomitant reduction in BFS occurred following 1 (99±19MPa; P<0.001) and 4 (63±12MPa; P<0.001) weeks, whilst a significant increase was identified following 13 weeks (102±24MPa; P<0.001) and a further significant concomitant decrease was identified following 52 weeks (56±11MPa; P<0.001) (Table 5.3; Figure 5.7a). The Weibull modulus (*m*) was calculated and identified to be significant where the 95% confidence intervals failed to overlap. The *m* of FSB was significantly decreased following 24h stored 'wet' (5.98±1.34) compared with 'dry' (8.07±1.80) as the respective 95%

confidence intervals fail to overlap (6.99 to 9.15 and 5.66 to 6.30). A further significant decrease in the Weibull modulus was identified following 26 weeks (2.64±0.59), whilst *m* again significantly increased following 52 weeks (5.66±1.27) (Table 5.3).

The BFS of FST following 24h stored 'dry' or 'wet' was not significantly different (160±27 and 177±22MPa; P=0.907), whilst a significant concomitant decrease occurred following 1 week (141±23MPa; P<0.01). A further decrease occurred following 4 weeks (105±25MPa; P<0.001) and also following 52 weeks (82±12MPa; P<0.001) compared with the preceding storage regime (Table 5.3; Figure 5.7b). The associated Weibull modulus was significantly increased following 24h stored 'wet' (7.99±1.78) compared with 'dry' (6.23±1.39) as indicated by the failure of the 95% confidence intervals to overlap (7.21 to 8.79 and 5.69 to 6.76). A significant decrease occurred following 1 (6.15±1.38; 5.69 to 6.60) and 4 (4.39±0.98; 3.99 to 4.79) weeks, whilst overlap of the 95% confidence intervals following 4, 13 and 26 weeks highlighted that the *m* was not significantly modified. A concomitant significant increase in the Weibull modulus was identified to occur following 52 weeks (6.98±1.56) (Table 5.3).

The BFS of FZ following 'dry' compared with 'wet' storage for 24h was not statistically significant (176±16 and 192±23MPa; P=0.958), although a significant reduction in BFS was identified following 1 week (122±23MPa; P<0.001) compared with specimens stored 'wet' for 24h. A concomitant significant increase in BFS was identified following 13 weeks (147±34MPa; P<0.001) and a further significant decrease occurred following 26 weeks (105±14MPa; P<0.001). Succeeding data was not significantly different (Table 5.4; Figure 5.7c). The Weibull modulus of FZ was significantly reduced as a consequence of 'wet' (8.71±1.95; 7.87 to 9.56) compared with 'dry' (11.23±2.51; 9.73 to 12.73) storage, the *m* was further significantly decreased between 4 (7.92±1.77; 7.42 to 8.43) and 13 (3.91±0.87; 3.38 to 4.43) weeks, whilst following 52 weeks the reliability was increased (7.39±1.65; 5.59 to 9.19) although a subsequent decrease occurred following 78 weeks (3.87±0.86; 2.97 to 4.76) (Table 5.4).

| | Filtek Supreme (FSB) | | | | | | | |
|---|---|---|---|---|---|---|---|---|
| | **24h dry** | **24h wet** | **1wk wet** | **4wks wet** | **13wks wet** | **26wks wet** | **52 wks wet** | **78wks wet** |
| **Fracture strengths (MPa)** | 125-205 | 102-198 | 58-130 | 48-84 | 68-157 | 42-155 | 39-82 | 34-102 |
| **Mean BFS (MPa)** | $159\ (21)^{A}{}_{1}$ | $155\ (27)^{A}{}_{2}$ | $99\ (19)^{B}{}_{2}$ | $63\ (12)^{C}{}_{2}$ | $102\ (24)^{B}{}_{2}$ | $97\ (34)^{B}{}_{2}$ | $56\ (11)^{C}{}_{3}$ | $61\ (16)^{C}{}_{2}$ |
| **10% Failure Probability (MPa)** | 128 | 115 | 72 | 50 | 71 | 43 | 41 | 44 |
| **Weibull modulus** | 8.07 (1.80) | 5.98 (1.34) | 5.09 (1.14) | 5.29 (1.18) | 4.47 (0.99) | 2.64 (0.59) | 5.66 (1.27) | 4.22 (0.94) |
| **95% Confidence Intervals** | 6.99-9.15 | 5.66-6.30 | 4.47-5.73 | 4.26-6.31 | 3.86-5.08 | 2.37-2.91 | 4.79-6.54 | 3.69-4.76 |
| **$R^2$-value** | 0.93 | 0.99 | 0.94 | 0.87 | 0.93 | 0.96 | 0.91 | 0.94 |
| | **Filtek Supreme Translucent (FST)** | | | | | | | |
| | **24h dry** | **24h wet** | **1wk wet** | **4wks wet** | **13wks wet** | **26wks wet** | **52 wks wet** | **78wks wet** |
| **Fracture strengths (MPa)** | 109-218 | 126-205 | 92-184 | 67-155 | 51-172 | 70-166 | 58-101 | 48-103 |
| **Mean BFS (MPa)** | $160(27)^{A,B}{}_{1}$ | $177(22)^{A}{}_{1,2}$ | $141(23)^{B,C}{}_{1}$ | $105(25)^{D,E}{}_{1}$ | $117(30)^{C,D}{}_{2}$ | $112\ (28)^{D}{}_{2}$ | $82(12)^{E}{}_{2,3}$ | $82\ (13)^{E}{}_{2}$ |
| **10% Failure Probability (MPa)** | 123 | 135 | 101 | 67 | 75 | 78 | 61 | 63 |
| **Weibull modulus** | 6.23 (1.39) | 7.99 (1.78) | 6.15 (1.38) | 4.39 (0.98) | 3.73 (0.83) | 4.04 (0.90) | 6.98 (1.56) | 6.10 (1.36) |
| **95% Confidence Intervals** | 5.69-6.76 | 7.21-8.79 | 5.69-6.60 | 3.99-4.79 | 3.42-4.03 | 3.42-4.65 | 6.52-7.43 | 5.36-6.85 |
| **$R^2$-value** | 0.97 | 0.96 | 0.98 | 0.97 | 0.97 | 0.91 | 0.98 | 0.94 |

Mean values within rows and columns (including Tables 5.4 and 5.5) exhibiting different letters (in superscript) and numbers (in subscript) respectively, were significantly different ($P<0.05$).

**Table 5.3. The range, mean and 10% failure probability of the BFS (MPa), Weibull modulus, 95% associated confidence intervals and $R^2$-values of the 'nanocluster' reinforced RBCs (FSB and FST) following storage 'dry' and 'wet' for 24h, and for 1, 4, 13, 26, 52 and 78 weeks in a waterbath maintained at 37±1°C.**

| | Filtek Z250 (FZ) | | | | | | | |
|---|---|---|---|---|---|---|---|---|
| | **24h dry** | **24h wet** | **1wk wet** | **4wks wet** | **13wks wet** | **26wks wet** | **52 wks wet** | **78wks wet** |
| **Fracture strengths (MPa)** | 150-201 | 142-241 | 97-157 | 78-126 | 70-201 | 52-157 | 77-138 | 77-203 |
| **Mean BFS (MPa)** | $176\ (16)^{A}{}_{1}$ | $192\ (23)^{A}{}_{1}$ | $122(18)^{B,C}{}_{1,2}$ | $105(14)^{C,D}{}_{1}$ | $147\ (34)^{B}{}_{1}$ | $102(30)^{C,D}{}_{2}$ | $94\ (13)^{D}{}_{2}$ | $113(32)^{C,D}{}_{1}$ |
| **10% Failure Probability (MPa)** | 150 | 162 | 100 | 84 | 79 | 75 | 80 | 80 |
| **Weibull modulus** | 11.23(2.51) | 8.71 (1.95) | 7.17 (1.60) | 7.92 (1.77) | 3.91 (0.87) | 3.58 (0.80) | 7.39 (1.65) | 3.87 (0.86) |
| **95% Confidence Intervals** | 9.73-12.73 | 7.87-9.56 | 6.07-8.26 | 7.42-8.43 | 3.38-4.43 | 3.01-4.15 | 5.59-9.19 | 2.97-4.76 |
| **$R^2$-value** | 0.93 | 0.96 | 0.91 | 0.98 | 0.93 | 0.91 | 0.81 | 0.82 |

Mean values within rows and columns (including Tables 5.3 and 5.5) exhibiting different letters (in superscript) and numbers (in subscript) respectively, were significantly different ($P<0.05$).

**Table 5.4. The range, mean and 10% failure probability of the BFS (MPa), Weibull modulus, 95% associated confidence intervals, $R^2$-values of the microhybrid RBC (FZ) following storage 'dry' and 'wet' for 24h, and for 1, 4, 13, 26, 52 and 78 weeks in a waterbath maintained at 37±1°C.**

**(a)**

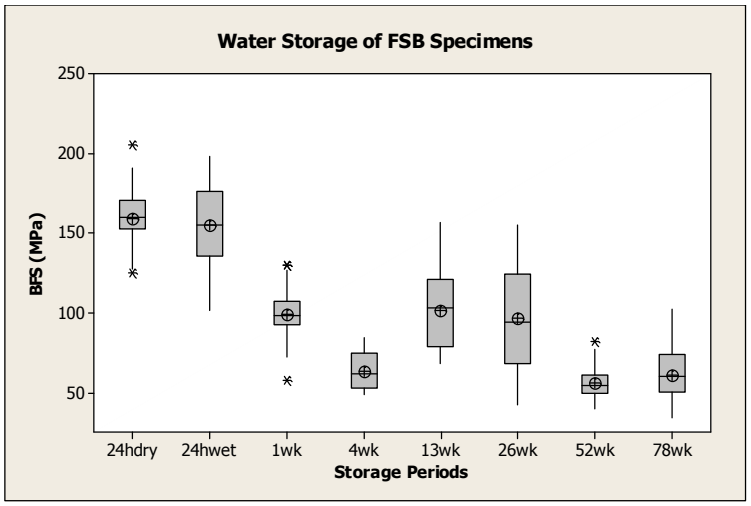


**(b)**

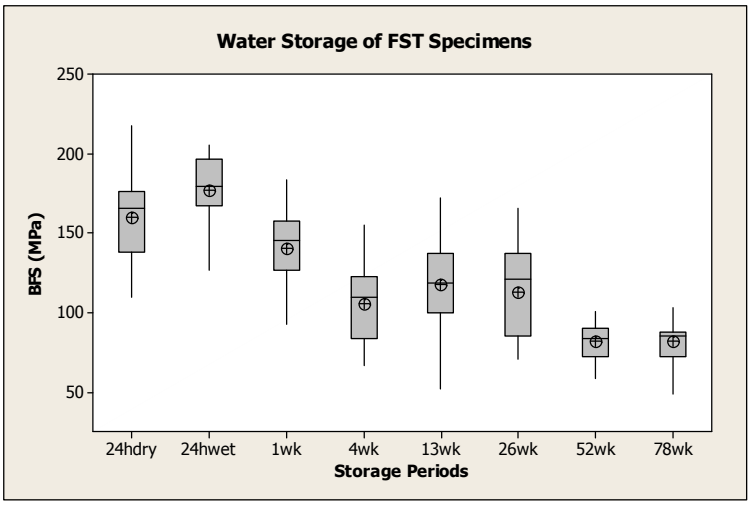


**(c)**

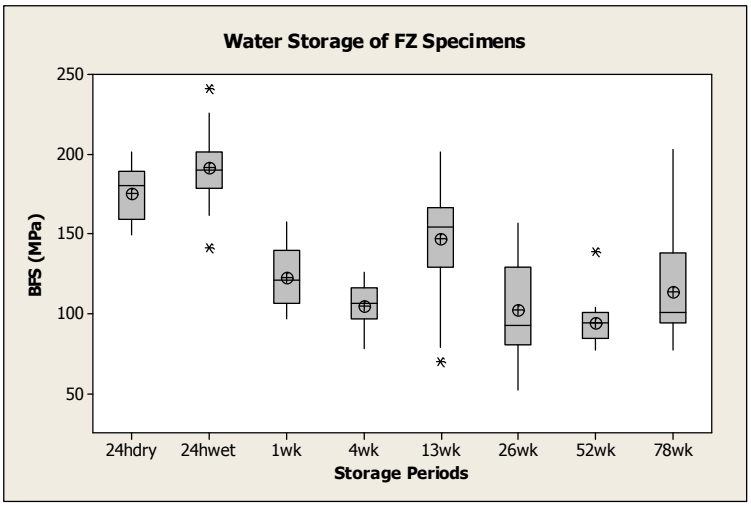


**Figure 5.7. Box and whisker plots highlighting the mean, median, inter-quartile range and outlaying data-points (*) of the BFS of (a) FSB, (b) FST and (c) FZ following 24h stored 'dry' and 'wet' and for 1, 4, 13, 26, 52 and 78 weeks in a waterbath.**

**Survival probability distribution**

The survival probability distribution of all the materials tested (FSB, FST and FZ) exhibited an asymmetric bi-modal distribution of data manifested as an apparent discontinuity in the lower range of bi-axial flexure strengths following 24h stored either 'dry' or 'wet', although this was inconsistent with the $R^2$-values, which generally exceeded 0.95, suggesting a mono-modal defect distribution. The survival probability distribution of FSB exhibited a bi-modal distribution suggesting the presence of two distinct defect populations, which following 4, 52 and 78 weeks was no longer present, implying the presence of a single defect population although specimen failure occurred at lower strengths (Figure 5.8a). However, this again conflicted with the $R^2$-values (Table 5.3, p130). The survival probability distribution of FST was also decreased following water storage, although the bi-modal distribution identified from the plot following 4, 13 and 26 weeks was eliminated following 52 and 78 weeks (however this did not concur with the $R^2$-values), suggesting that the lower strength defect population became dominant as a result of continued storage (Figure 5.8b). The survival probability distribution of FZ was reduced following storage, the distribution following 4, 26, 52 and 78 weeks was largely comparable, although an increased bi-modal distribution following 26 and 78 weeks, suggested the low strength defect population gained dominance as storage continued. Furthermore, the $R^2$-value of 52 weeks ($R^2$=0.81) also suggests a bi- or milti-modal defect distribution, although this was not observed on the plot (Figure 5.8c).

**(a)**

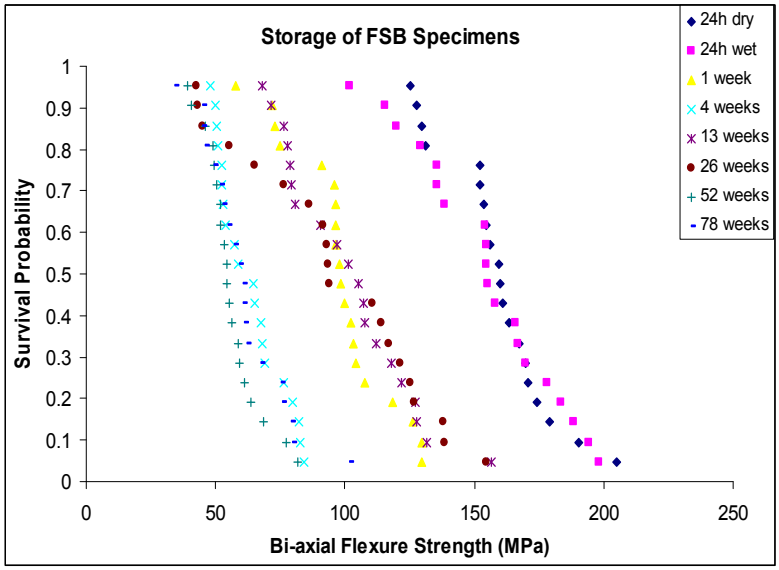


**Figure 5.8. The combined survival probability distribution plots of (a) FSB specimens stored 'dry' for 24h or in a water-bath at 37°C for 24h, 1, 4 13, 26, 52 and 78 weeks.**

**(b)**

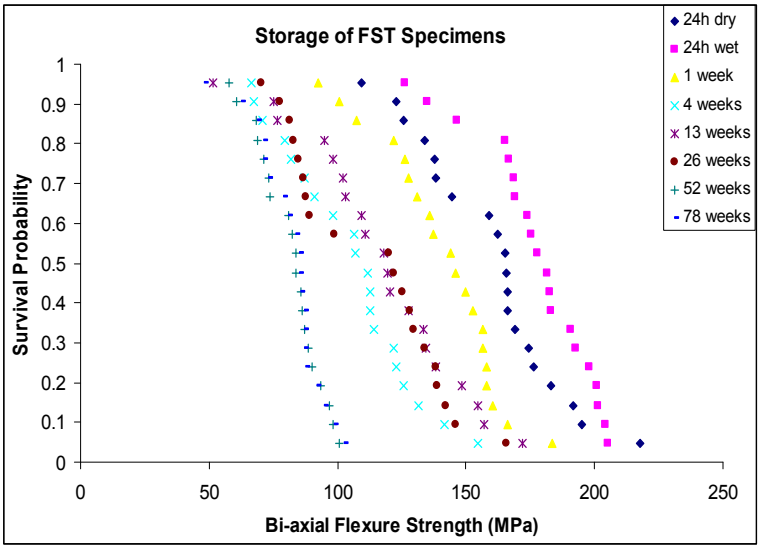


**(c)**

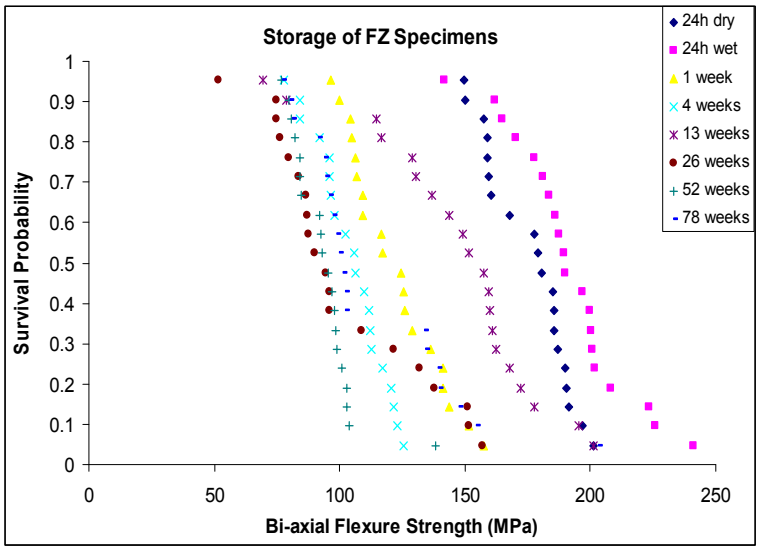


**Figure 5.8 (continued). The combined survival probability distribution plots of (b) FST and (c) FZ specimens stored 'dry' for 24h or in a water-bath maintained at 37°C for 24h, 1, 4 13, 26, 52 and 78 weeks.**

### 5.1.3. Bi-axial flexure strength and Weibull modulus of GR and GF

Two-way ANOVA of the nano-hybrid GR and GF specimens stored for 24h 'dry' and for 24h, 13, 26 and 52 weeks 'wet' highlighted an overall decrease in the BFS due to the interaction of storage condition and storage time ($F=7.57$; $P<0.001$) (Figure 5.9).

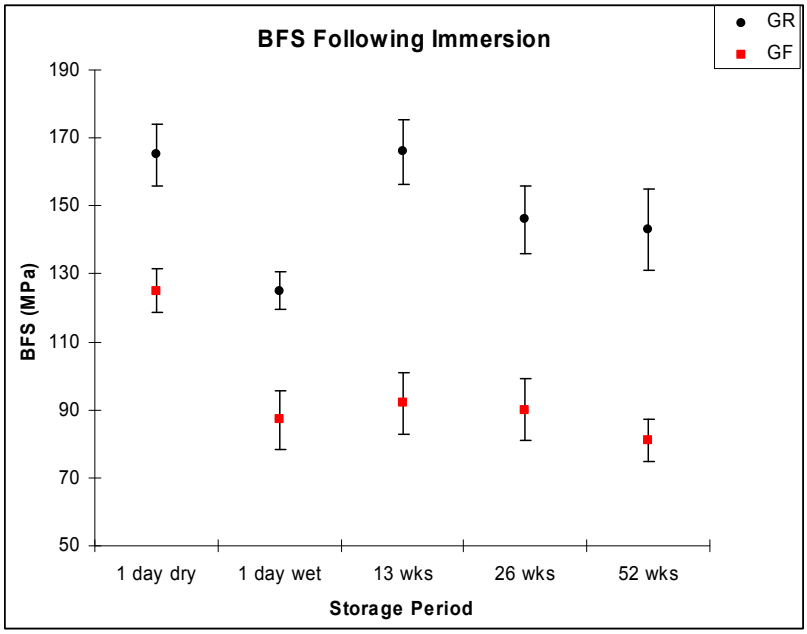


**Figure 5.9. Plot of the mean BFS exhibited by GR and GF groups following the storage regimes. The plot highlighted a general decrease in the BFS as a consequence of water storage regimes.**

One-way ANOVA of GR highlighted that the BFS following storage 'wet' for 24h was significantly reduced compared with 'dry' (125±11 and 165±18MPa; $P<0.001$). The BFS subsequently significantly increased following 13 weeks immersion compared with 24h 'wet' (166±19MPa; $P<0.001$), further storage for 26 weeks resulted in a significantly decreased BFS (146±20MPa; $P=0.004$) (Table 5.5; Figure 5.10a). The Weibull modulus of GR was initially increased following 'wet' (12.11±2.71; 10.80 to 13.42) compared with 'dry' (9.03±2.02; 7.83 to 10.22) storage, whilst the reliability following 13, 26 and 52 weeks was significantly reduced compared with the preceding storage regime (9.22±2.06, 7.69±1.72 and 5.93±1.33, respectively) (Table 5.5).

The BFS of GF was not significantly reduced following storage 'wet' for 24h compared with 'dry' (87±17MPa and 125±13; $P<0.001$), whilst further storage did not significantly influence the BFS (Table 5.5; Figure 5.10b). Likewise, the Weibull modulus was decreased following 'wet' compared with 'dry' storage for 24h (5.11±1.14; 9.54±2.13) as the 95% confidence intervals failed to overlap (4.82 to 5.39 and 8.36 to 10.71). Storage for 13 and 52 weeks resulted in an $m$ comparable with specimens stored 'wet' for 24h, whilst the reliability increased following 52 weeks immersion (7.18±1.61) (Table 5.5).

| | Grandio (GR) | | | | | Grandio Flow (GF) | | | | |
|---|---|---|---|---|---|---|---|---|---|---|
| | **24h dry** | **24h wet** | **13wks wet** | **26wks wet** | **52wks wet** | **24h dry** | **24h wet** | **13wks wet** | **26wks wet** | **52wks wet** |
| **Fracture strengths (MPa)** | 115-195 | 107-1424 | 138-211 | 109-186 | 87-212 | 93-141 | 53-117 | 57-134 | 56-123 | 57-112 |
| **Mean BFS (MPa)** | $165\ (18)^{A}{}_{1}$ | $125\ (11)^{B}{}_{3}$ | $166\ (19)^{A}{}_{1}$ | $146(20)^{A,B}{}_{1}$ | $143(24)^{A,B}{}_{1}$ | $125\ (13)^{A}{}_{2}$ | $87\ (17)^{B}{}_{4}$ | $92\ (18)^{B}{}_{2}$ | $90\ (18)^{B}{}_{2}$ | $81(12)^{B}{}_{2,3}$ |
| **10% Failure Probability (MPa)** | 145 | 108 | 142 | 120 | 117 | 98 | 63 | 61 | 66 | 67 |
| **Weibull modulus** | 9.03 (2.02) | 12.11 (2.71) | 9.22 (2.06) | 7.69 (1.72) | 5.93 (1.33) | 9.54 (2.13) | 5.11 (1.14) | 5.34 (1.19) | 5.15 (1.15) | 7.18 (1.61) |
| **95% Confidence Intervals** | 7.83-10.22 | 10.80-13.42 | 7.85-10.58 | 6.89-8.49 | 4.79-7.07 | 8.36-10.71 | 4.82-5.39 | 4.74-5.94 | 4.76-5.55 | 6.12-8.23 |
| **$R^2$-value** | 0.93 | 0.95 | 0.92 | 0.96 | 0.87 | 0.94 | 0.99 | 0.95 | 0.98 | 0.92 |

Mean values within rows and columns (including Tables 5.3 and 5.4) exhibiting different letters (in superscript) and numbers (in subscript) respectively, were significantly different ($P<0.05$).

**Table 5.5. The range, mean and 10% failure probability of the BFS (MPa), Weibull modulus, 95% associated confidence intervals and $R^2$-values of the nano-hybrid RBCs (GR and GF) following storage 'dry' or 'wet' for 24h and for 1, 4, 13, 26, 52 and 78 weeks in a waterbath maintained at 37±1°C.**

(a)

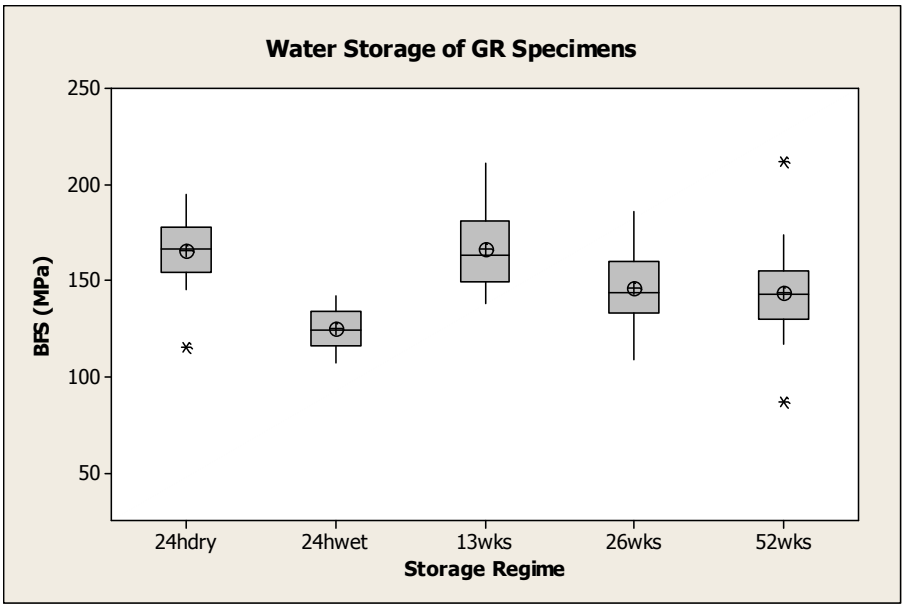


(b)

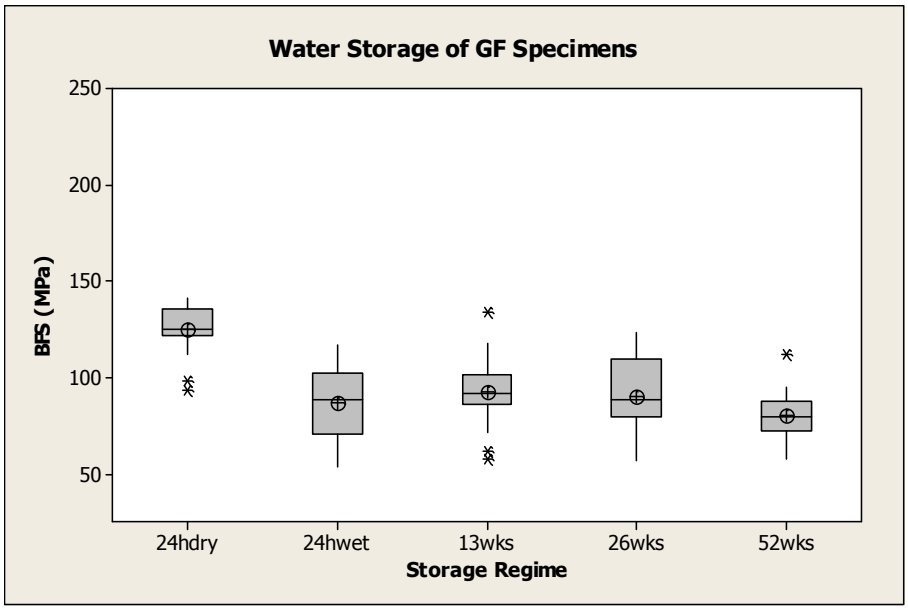


**Figure 5.10. Box and whisker plots highlighting the mean, median, inter-quartile range and outlaying data points (*) of the BFS of (a) GR and (b) GF specimens following 24h stored dry and storage in a waterbath maintained at 37±1°C for 24h, 13, 26 and 52 weeks.**

### Survival probability distribution

The survival probability distribution of the nano-hybrid GR highlighted a single defect population which was unaffected by water storage, although the BFS of specimens highlighted a decrease following storage, as previously remarked upon (Section 4.3.2.1) this did not necessarily

concur with the defect population distribution suggested by the $R^2$-values (Figure 5.11a). Conversely, a significant reduction in BFS was identified in the survival probability distribution of GF following storage, although the bi-modal distribution within the lower strength range identified from the distribution of 24h 'dry' ($R^2$=0.93) was progressively reduced as a consequence of immersion with the exception of the $R^2$-value following 52 weeks (Figure 5.11b).

**(a)**

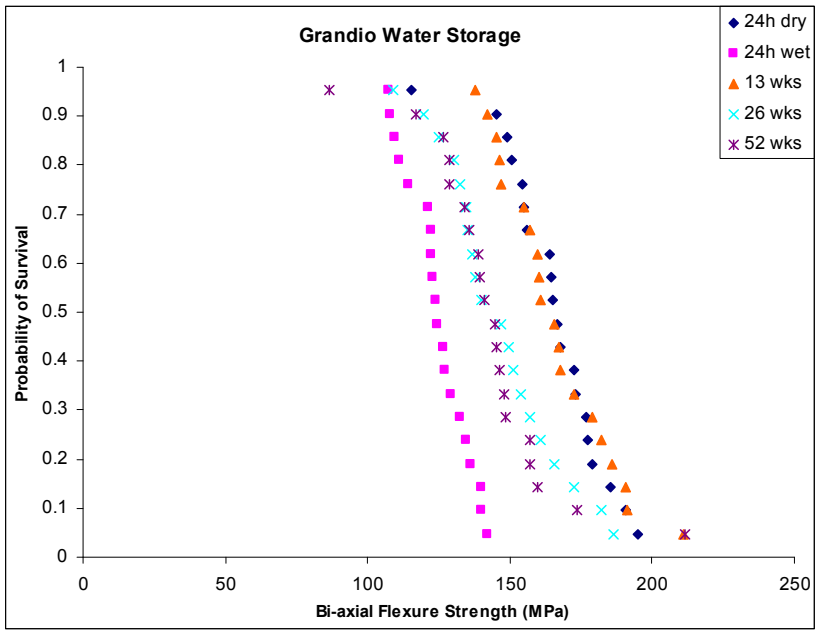


**(b)**

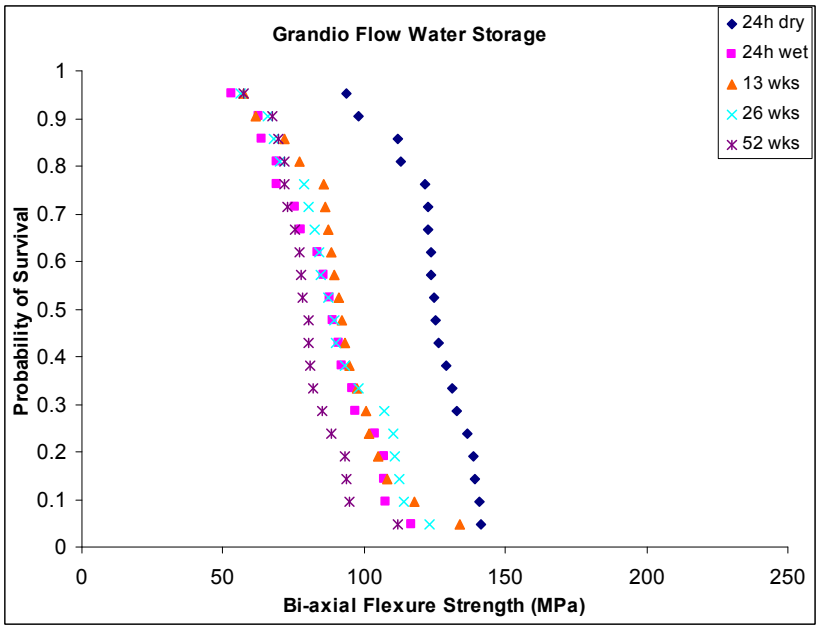


**Figure 5.11. The combined survival probability distribution plots of (a) GR and (b) GF specimens stored 'dry' for 24h or in a water-bath maintained at 37°C for 24h, 13, 26 and 52 weeks.**

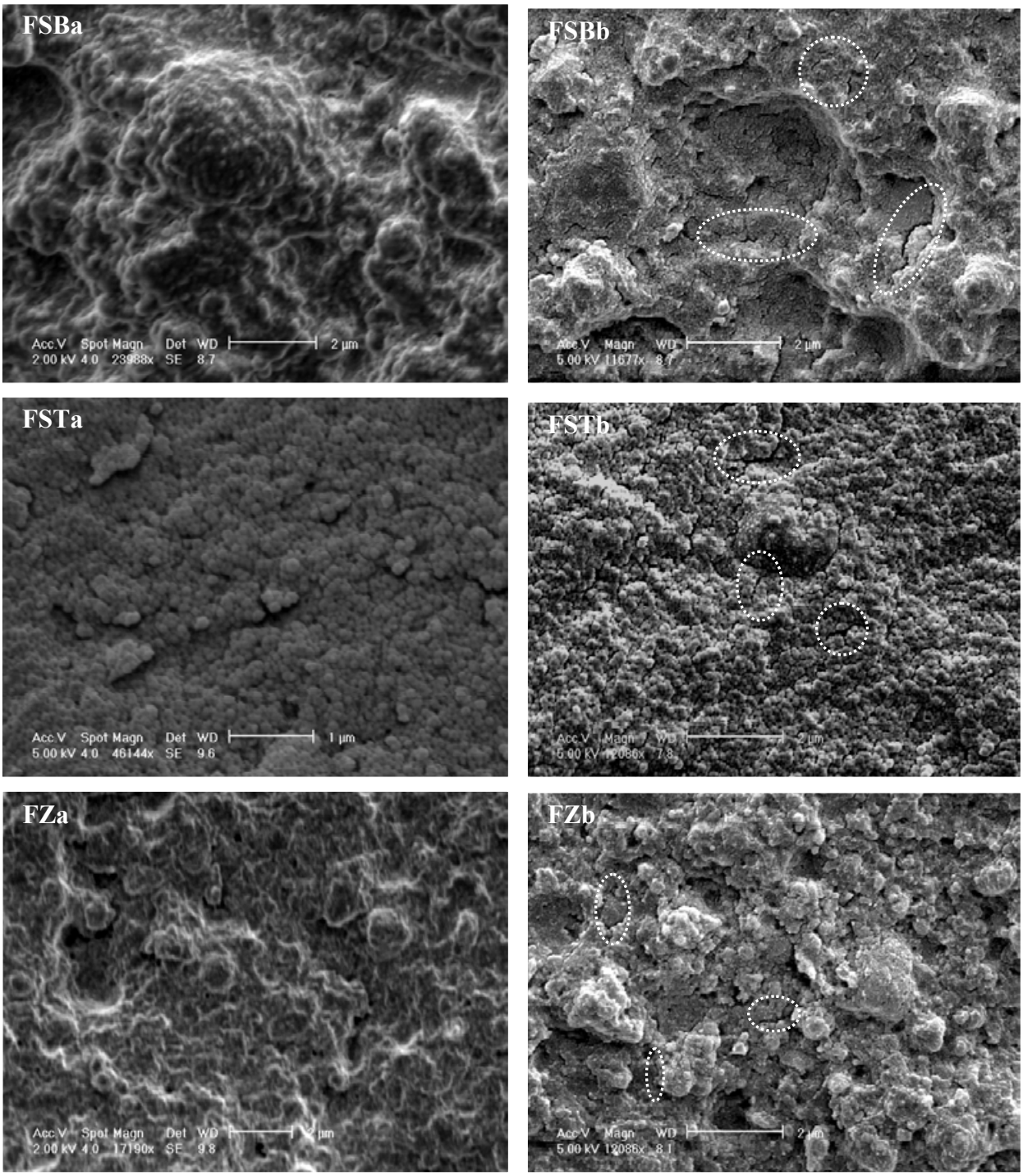


**Figure 5.12. SEM micrographs of a cross-sectional fracture surface through the bulk of RBC specimens, highlighting the size and distribution of filler particles following (a) 24h 'dry' and (b) interfacial cracking (circled) following 26 weeks immersed in a waterbath.**

## 5.2 DISCUSSION: The influence of water storage

The influence of *in vitro* water immersion and subsequent water sorption on the mechanical properties of RBCs and possible detrimental effect to *in vivo* restoration longevity has been widely acknowledged [Söderholm et al., 1984; Cesar et al., 2001; Ferracane, 2006; Bagheri et al., 2007]. Although many studies investigate the effect of short and medium-term immersion, namely up to six months [Pearson et al., 1979; Söderholm & Roberts, 1990; Bastoli et al., 1990; Palin et al., 2005c], few researchers have reported the long-term degradative effects of water uptake.

### 5.2.1 Near-infrared spectroscopic analysis of water sorption

The near-infrared spectroscopy (NIRS) technique employed in the current study highlighted similar patterns of water sorption compared with investigations using the gravimetric analysis technique stipulated by ISO 4049. Discrepancies in the reported water sorption values of FZ exist between laboratories using gravimetric analysis and although specific water sorption and solubility values may differ, the reported time to saturation is relatively common [Toledano et al., 2003; Palin et al., 2005c; Fleming at al., 2007]. This concurs with the present study, wherein FZ exhibited apparent saturation of the hydrophilic resin matrix and silane interface following 4 weeks immersion (Figure 5.1), thus highlighting comparable trends between NIRS and the gravimetric techniques for a specific material. Venz et al. (1991) suggested that a higher water sorption using an NIRS compared with a gravimetric technique for the same material was associated with dissolution of resin constituents. This is a recognised disadvantage of the gravimetric analysis method of water sorption [Diaz-Arnold & Williams., 1992; Mohsen & Craig, 1995], which assumes that weight gain proportionally represents water gain, whilst in reality it is the gain in water and also dissolution and elution of low molecular weight monomers from the resin matrix [Mohsen & Craig, 1995]. Therefore, although careful calibration of the NIRS absorptivity would be required for different monomer matrix chemistries [Venz & Dickens, 1991], the usefulness of the NIRS technique for assessing the influence of filler properties on water uptake was supported since the outcome is not influenced by the dissolution of polymeric components [Keyworth et al., 1961; Venz & Dickens, 1991; Diaz-Arnold & Williams, 1992].

For water sorption investigations, ISO 4049 stipulates that specimens should be equilibrated to a constant mass (within $1x10^{-3}$mg) by dehydration at 37±1°C. Consequently the

water content of RBCs following dehydration is considered to be effectively zero. In contrast, NIRS in the present study highlighted that all test materials contained an initial amount of water following dehydration and 'dry' storage for 24h. This is consistent with previous NIRS studies which reported that a small amount of residual water remained in the material following dehydration [Keyworth et al., 1961; Venz & Dickens, 1991; Diaz-Arnold & Williams, 1992]. The presence of water molecules in the resin matrix of equilibrated specimens may be generated as a by-product during the free-radical addition polymerization reaction, which occurs following photo-activation (Section 1.3.4.1) [Musanje et al., 2001]. Subsequently, the water molecules may be effectively bound within the resin matrix and were unable to be lost during the dehydration procedure. The presence of water molecules within the 'dry' RBC may also reflect the influence of ambient humidity during specimen production or at the source of manufacture of the monomer paste (Table 5.1; Figures 5.1 and 5.2). Alternatively, the 'residual water' content may be attributable to detection of the O-H bond of the $CH_3OH$ molecules produced as a by-product of the condensation reaction which occurred during silanization (Section 1.3.3.1). Therefore, the presence of water within dehydrated and 'dry' specimens identified by NIRS suggested that the standard gravimetric analysis technique stipulated by ISO 4049 may provide values of water content which were less than the true water content of the material.

Water sorption and water uptake in RBCs have previously been identified to be dependent on the constituents of the methacrylate resin matrix, morphology, filler dispersion and properties of the filler/resin interface [Pearson et al., 1979; Fan et al., 1985; Bastoli et al., 1990]. NIRS results in the current study highlighted that water sorption into all five RBCs (FSB, FST, FZ, GR and GF) was initially rapid, whilst the water content of FSB and FZ equilibrated due to apparent saturation of the hydrophilic resin matrix and interfacial silane layer following between one and thirteen weeks. In contrast, the water uptake in FST continued to increase markedly for each subsequent immersion period investigated, indicative of a non-equilibrated system (Table 5.1; Figure 5.1). This was attributable to the greater volume percentage of individually dispersed nanoparticles (Table 3.1) and comparatively smaller 'nanoclusters' than FSB (Figure 5.12), producing a greater surface area to volume ratio and hence a larger area of hydrophilic silane available for water sorption. Generally, the lower water content of GR and GF (Table 5.2; Figure 5.3 and 5.4) was attributable to the higher volume percent filler loading (Table 3.1) compared with FSB, FST and FZ and a less hydrophilic resin matrix, due to the absence of the $BisEMA_6$ monomer [Bagheri et al., 2007]. $BisEMA_6$ is generally considered to be a more hydrophobic

monomer than BisGMA or TEGDMA [Finer & Santerre, 2004; Palin et al., 2005c], although previous investigations conducted by Bagheri et al. (2007) and Ogliari et al. (2008), in addition to the current study, contradicated this highlighting that $BisEMA_6$ containing resins exhibited increased water sorption and hydrophilic tendencies. Ogliari et al. (2008) identified that water sorption into a BisEMA monomer increased proportionally with increase in ethylene oxide chain extenders, namely that water sorption into $BisEMA_{30}$ was significantly greater than $BisEMA_4$, due to increased interchain spacing between monomers available for water uptake. Furthermore, the admixture of BisGMA and $BisEMA_4$ doubled the water sorption, suggesting that the increased polarity of the BisGMA monomer increased water sorption [Ogliari et al., 2008]. Likewise, Bagheri et al. (2007) identified that the resin matrix of two nanofills, including Filtek Supreme™, which contained both TEGDMA and BisEMA exhibited significantly more degradation in solvent than monomers where BisEMA was absent, although no explanation was offered for this. Therefore, whilst a specific mechanism is not attributed to the increased water sorption of BisEMA monomers it highlights that the trend identified in the current study is consistent with the literature. This also concurs with the statement by Ogliari et al. (2008) which identified a lack of information in the current literature concerning BisEMA polymerization and the properties of the resultant monomer.

The more rapid increase in water content and subsequent saturation of GF was attributed to the lower filler loading compared with GR. The increased filler surface area available for silanization of the highly loaded GR, and subsequently for sorption of water, was suggested to be responsible for the concomitant increase in water content without apparent saturation throughout the period studied (Figure 5.4a).

### 5.2.2 The influence of water sorption on mechanical properties

The mechanical properties of RBC restorations are widely acknowledged to be detrimentally influenced as a consequence of water uptake which occurs as part of a time dependent process [Pearson et al., 1979, Bastoli et al., 1990; Söderholm et al., 1996; Ferracane et al., 1998; Catteni-Lorente et al., 1999; Martin et al., 2003; Asoaka et al., 2003; Ito et al., 2005]. The current study concurred with these previous investigations also highlighting that generally, the BFS of all five RBCs tested was significantly decreased as a consequence of water induced degradation following as little as 24h (GR and GF) or one week (FSB, FST and FZ) immersion (Tables 5.3; 5.4 and 5.5).

The observed degradation of RBCs in the current study due to water uptake can be considered by two mechanisms. Firstly the dimethacrylate resin matrix absorbs water, dependent upon the hydrophilic nature of the specific resin monomers, this initiates 'plasticization' which causes the matrix to become weak, ductile and swell, and also initiates chain scission and subsequent monomeric elution and leaching [Bastoli et al., 1990; Ferracane et al., 1998; Catteni-Lorente et al., 1999; Martin et al., 2003; Ito et al., 2005]. Secondly, hydrolysis of the siloxane bridge bonds of the filler/resin interface to the original silanol groups initiate debonding of the inorganic filler particles and a reduction in the mechanical properties of the material [Söderholm et al., 1984; 1996; Söderholm & Roberts, 1990; Stokes et al., 1988; Ortengren et al., 2001]. The formation of interfacial microcracks has been attributed to the degradation of the filler/resin interface [Calais & Söderholm, 1988; Ritter et al., 1996], which were identified from SEM images in the current study to occur as a consequence of water storage (Figure 5.12). Interfacial microcracking may act in terms of Griffith's Law, whereby the presence of any flaw or defect acts as a weak inclusion and hence as a critical defect accelerating failure and reducing the BFS of the material [Griffith, 1920]. However, Drummond & Saver (1993) and Ferracane et al. (1998) postulated that hydrolytic degradation of the filler interface did not generate a significantly increased concentration of defects within specimens undergoing long-term immersion. Conversely, other investigators have observed degradation of the interfacial silane layer, filler debonding and subsequent decrease in mechanical properties [Calais & Söderholm, 1988; Ritter et al., 1996]. The resin matrix chemistries of FSB, FST and FZ were known to be nominally identical (Table 3.1). Therefore, whilst the degradation of the matrix may in part be responsible for the loss of structural integrity of FSB, FST and FZ, the occurrence of microcracking at the silane interface suggested that a further mechanism may have occurred, generating additional defect centres and producing a more pronounced degradation of the 'nanocluster' reinforced RBCs.

The extent and rate of strength degradation exhibited by the nanofill, nano-hybrid and microhybrid materials following long-term storage highlighted distinct differences (Figures 5.6 and 5.9). The percentage decrease in BFS of FSB and FST following 78 weeks, compared with specimens stored 'dry' for 24h, was calculated to be 62 and 49% respectively, whilst the percentage reduction in BFS of FZ was 36% (Tables 5.3 and 5.4). Moreover, the percentage decrease of the nano-hybrid GR and GF following 52 weeks storage was 13 and 36%, compared with 65, 49 and 47% of FSB, FST and FZ respectively (Tables 5.3, 5.4 and 5.5). This highlighted

that the long-term hydrolytic stability of the 'nanocluster' reinforced RBC was more limited than the other RBCs tested. Since the key difference between FSB, FST and FZ was filler morphology, (the resin matrix being nominally identical and the size of 'nanoclusters' and microhybrid particles being approximately equivalent), it was proposed that the 'nanocluster' itself acted as the dominant defect centre. This may suggest that the long-term hydrolytic stability of the 'nanocluster' was limited due to hydrolytic degradation of the silane interface and also potential degradation of the silane bonds within the cluster itself which may subsequently produce a weakened particle. In addition to the differing BFS the decreased hydrolytic stability was also manifested by the survival probability distribution of FSB, which highlighted a greater loss of structural integrity due to long-term immersion as a pronounced shift into the lower strength region (less than 80MPa). Furthermore, the previous bi-modal distribution and asymmetry within the data distribution was eliminated following 52 and 78 weeks storage, suggesting that a single defect population, such as the weakened 'nanocluster', became the dominant defect centre (Figure 5.8).

Comparison of water sorption identified by NIRS (Figure 5.1) with the bi-axial flexure strength (Figure 5.6) did not identify a specific correlation between the extent of degradation and the water content. FSB and FZ exhibited comparable levels of water content following 78 weeks immersion, however the extent of degradation of FSB was greater than FZ (62 compared with 47% reduction compared with 'dry' specimens). This may suggest that degradation occurs irrespective of the actual water content and further suggested that the hydrolytic stability of the 'nanoclusters' was limited. Furthermore, FST exhibited a higher water content following 78 weeks compared with FSB although BFS of the former was significantly increased compared with the latter (82±13 and 61±16MPa; $P<0.001$), further highlighting the lack of a direct correlation between water content and flexure strength (Tables 5.1 and 5.3). The clinical implication of this may be that FST, which is indicated for anatomical build-up techniques to mimic enamel, will exhibit mechanical properties at least comparable with FSB increments to which it adheres, despite greater exposure to water sorption from the oral environment. The superior mechanical properties of FST compared with FSB despite their interaction with water, may be attributed to the filler loading of FST which contained a considerably lower content of 'nanoclusters' (30.0wt%) compared with FSB (71.0wt%), the 'nanoclusters' also being smaller (Figure 5.12), whilst the content of individually dispersed nanosized fillers was considerably higher in FST (40.0wt%) than FSB (8.0wt%). This may suggest either an improved filler packing

density due to the smaller particle sizes, or enhanced interfacial adhesion due to the higher content of individual nano-sized particles [Li et al., 2007]. In addition, since FST was identified by Alvin et al. (2007) to possess a higher concentration of photo-initiating CQ (0.082wt%), compared with a notably lower quantity within FSB (0.059wt%) and FZ (0.054wt%), the resin matrix may have possessed a higher degree of monomer conversion (Section 1.3.4.1) which may result in enhanced mechanical properties. The higher concentration of CQ, which will produce additional foci from which polymerization initiates [Asmussen & Peutzfeldt, 2001a], may produce a higher crosslink density between polymerized monomeric chains following light-activation [Ferracane et al., 1998; Peutzfeldt & Asmussen, 2000] and hence the improved resistance to fracture exhibited by FST. A previous study comparing the microhardness of various RBCs following curing highlighted that the surface hardness of FST was consistently superior to FSB. Furthermore, the hardness of the surface furthest from the curing light was identified to be markedly harder for FST compared with FSB [Price et al., 2006], suggesting an improved depth of cure which may be attributable to the increased content of photo-initiator and might also be due to the translucency of FST.

The investigation of nano-hybrid RBCs in the current study sought to highlight the influence of alternative filler types, morphologies and loadings and also differing resin matrix chemistries. Water storage of GR and GF significantly decreased the BFS following storage for up to 52 weeks (Table 5.5). The higher filler loading of GR (87.0wt%) compared with the flowable version (80.2wt%), provided improved mechanical properties. This concurred with a study by Ferracane et al. (1998) which concluded that increasing the mass fraction of reinforcing filler resulted in increased flexural strength, elastic modulus and fracture toughness of the subsequent RBC. As previously mentioned, GR exhibited a markedly lower percentage decrease in BFS following 52 weeks (13%) compared with the other RBCs tested (FSB, FST, FZ and GR). The high filler loading of GR reduced the resin content available for water uptake and subsequent mechanical degradation. In contrast, the higher resin content of GF suggested that the hydrolytic stability of the resin matrix chemistry was limited.

#### 5.2.2.1 Hygroscopic expansion

Generally, the five RBCs tested in the current study exhibited a decrease in bi-axial flexure strength as a consequence of storage in water ($F=4.80$; $P<0.001$). However, two sets of results conflicted with this overall trend. Firstly, following 13 weeks immersion the bi-axial

flexure strength of FSB and FZ were significantly increased compared with 4 weeks storage (63±12 to 102±24MPa and 105±14 to 147±34MPa, respectively $P<0.001$), whilst the BFS of FST was also increased, although this was not statistically significant (105±25 to 117±30MPa; $P>0.05$). Secondly, following 52 weeks the Weibull modulus of FSB, FST, FZ and GR was significantly increased compared with preceding storage for 26 weeks. This is indicative of a greater consistency in the distribution of data produced on specimen failure and a reduction in the defect population. The simplest explanation for these potentially spurious results was that of batch variation of the material used to produce the sample groups in question. However, since specimen groups for different material types were fabricated at different times and similar effects for different RBC brands following 13 weeks were observed, this suggested that a more complex explanation may be required. NIRS suggested that the resin matrix of FSB and FZ may be fully saturated following 13 weeks, exhibiting water content values comparable with FST (Figure 5.1; Table 5.1). Water sorption is known to result in hygroscopic expansion of the resin matrix as water molecules infiltrate porosities, vacancies and free volume between polymeric chains [Momoi & McCabe, 1994; Martin et al., 1998; Sideridou et al., 2003]. This generates a volumetric expansion of 0.02-1% during immersion, which has been identified to counteract polymerization shrinkage stresses generated at the restoration/tooth interface [Feilzer et al., 1990; Peutzfeldt, 1997; Vanlandingham et al., 1999; Cury et al., 2006]. Moreover, it might be suggested that hygroscopic expansion of the resin matrix may impede the propagating crack-tip and initiate closure of intrinsic bulk defects. Although this occurrence has not been directly related to water uptake of RBCs, previous studies conducted by Tay et al. (2002; 2003a) and Tay & Pashley (2003b) implicated closure of dendritic 'branches' related to the transport of water through a BisGMA-based resin. The volumetric expansion of the resin matrix and apparent closure of marginal gaps and channels may suggest that the same mechanism also restricts bulk defects, albeit temporarily. This potential modification of defect populations was suggested by an increase in $R^2$-values for FSB following 13 weeks (0.87 to 0.93), although the $R^2$-values of FSB, FZ and GF were inconclusive. Unlike FSB, FST, FZ and GF, GR did not exhibit an increased Weibull modulus following 52 weeks. Momoi & McCabe (1994) reported that a material possessing a high Young's Modulus, such as GR (13.4GPa; Table 4.7), exhibited reduced hygroscopic expansion, which may also be due to high filler loading and therefore a lower resin content reducing the potential for hygroscopic expansion. Despite the short-lived improvement to BFS and Weibull modulus observed for FSB, FST, FZ and GF, ultimately, the cumulative degradation

induced by the longest storage regimes resulted in significantly decreased mechanical properties of these materials (Tables 5.3, 5.4 and 5.5).

#### 5.2.2.2 Phase-separation

The increased use of nano-sized fillers in dental RBCs provide new opportunities to optimise the filler loading and packing within hybrid-like systems, however a higher degree of silanization will be required for RBCs with a high volume percentage of nanoparticles, subsequently the interfacial silane layer may influence the subsequent physico-chemical properties. High filler loadings with distinct nano-sized particles have been identified to result in an inhomogeneous filler distribution within the resin matrix, resulting in 'filler-rich' and 'resin-rich' regions which without adequate surface silanization resulted in detrimental physical phenomena, such as phase-separation during which nanofiller particles are 'plucked' from the resin [Wilson et al., 2005]. Phase separation may occur during polymerization to relieve thermodynamic instabilities generated due to the high molecular mass of mixed or blended polymer networks and between inhomogeneous regions of filler and resin distribution and subsequently causes filler particles to be effectively forced out of the polymer network [Wilson et al., 2005]. This occurs as phase separation degrades the adhesive interface, particularly where silanization is incomplete [Wilson et al., 2005] or degrades the adhesive hybrid-layer of bonded RBC restorations [Breschi et al., 2008]. Phase separation also compromises the stability of the resin-dentin bond due to infiltration of a solvent, such as water, into the adhesive layer between two distinct phases, particularly where one phase is hydrophilic and the other hydrophobic [Peumans et al., 2005; Cadenaro et al., 2008]. Although the current study was not able to identify the occurrence of phase-separation, or the loss of individual nano-sized particles, the increasing use of nano-sized filler in modern dental RBCs may cause such physical phenomena to become more prevalent and of greater clinical significance. Therefore, future research should be aimed at producing hydrophobic silane coupling agents, improved silane wetting of nanoparticles and subsequent silanization to ensure a homogeneous filler distribution to limit phase separation.

#### 5.2.2.3 'Nanocluster' modification

Following the micromanipulation and pre-loading studies (Chapter 4) the mechanical properties and damage tolerance of the 'nanocluster' reinforced RBCs appeared superior to the nano-hybrid and conventionally filled RBCs tested. In contrast, immersion for between 1 and 78

weeks highlighted that the hydrolytic stability of the 'nanocluster' RBC was limited to a greater extent than the conventional (FZ) and nano-hybrid materials (GR and GF), suggesting that the 'nanoclusters' may have acted as defect centres. These two distinct findings are apparently contradictory. Pre-loading is a dynamic testing technique which established improved mechanical properties and damage tolerance to the 'nanocluster' material in the current investigation. As a consequence repeated loading modified the IPC-like structure of the 'nanoclusters' to absorb and dissipate loading stresses more effectively. It may be speculated that the water storage regimes and subsequent static load to failure testing did not provide an opportunity for dynamic induced modification of the 'nanocluster', which may have otherwise demonstrated improved mechanical properties following immersion if repeated sub-critical loads were applied. This may suggest that repeated sub-critical loading prior to long-term immersion could provide the enhanced damage tolerance observed following the micromanipulation and pre-loading studies.

# CHAPTER 6 RESULTS & DISCUSSION: ACCELERATED DEGRADATION

## 6.1 RESULTS: Degradation of Nanofilled RBCs: Solvent Storage

The aim of the solvent storage regimes was to compare the mechanical properties of six RBC materials (FSB, FST, FZ, Z100, GR and GF) following accelerated degradation using sodium hydroxide and ethanol.

### 6.1.1 Storage in sodium Hydroxide

Specimens (n=5) of the RBCs studied were stored in sodium hydroxide for 24h, 1 and 2 weeks, prior to BFS testing.

#### 6.1.1.1 Bi-axial flexure strength

Two-way ANOVA highlighted a significant decrease in the mean BFS as a consequence of NaOH storage ($F=2.97$; $P=0.004$), the dependent variables of storage period ($F=68.21$; $P<0.001$) and material ($F=31.28$; $P<0.001$) were also identified to be significant (Figure 6.1).

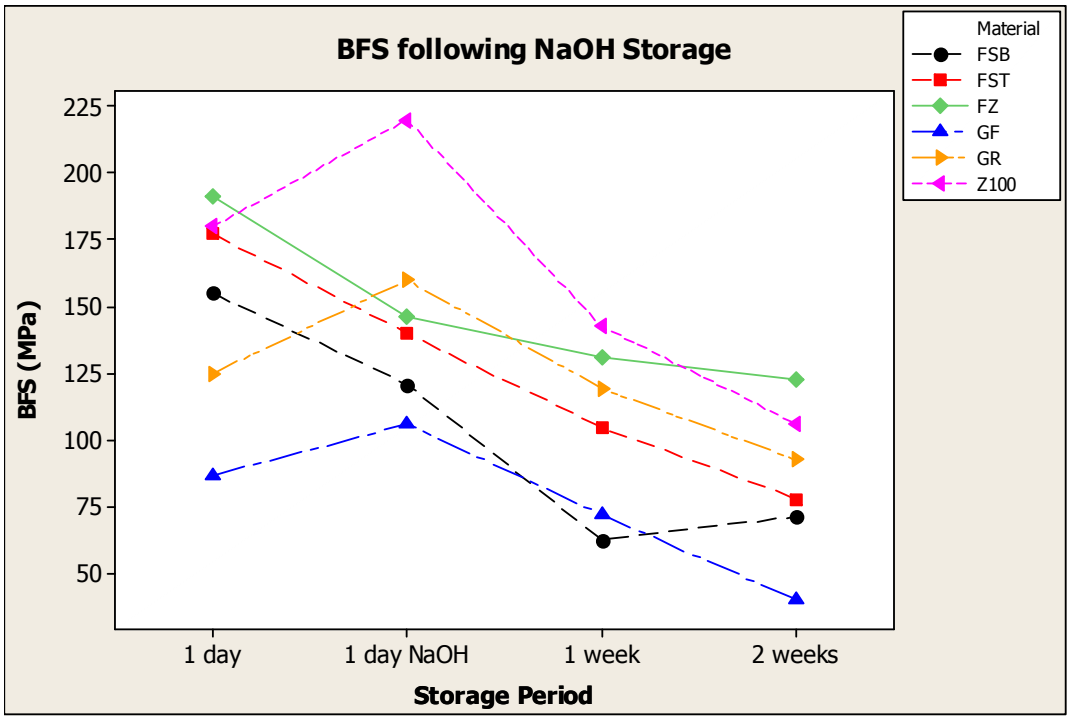


**Figure 6.1. Plot highlighting the mean BFS (MPa) of FSB, FST, FZ, Z100, GR and GF following 24h stored in a waterbath maintained at 37±1°C and 24h, 1 and 2 weeks in a 0.1M solution of NaOH also maintained at 37±1°C.**

The extent and rate of decrease was identified to differ significantly between the materials studied. One-way ANOVA identified a decrease in BFS of FSB following 24h stored in NaOH (121±51MPa; P=0.316) and a significant decrease following 1 week (63±15MPa; P=0.006), whilst a further increase in storage period to 2 weeks produced a mean BFS of 71±22MPa (P>0.05). The mean BFS of FST was continuously decreased to 140±10, 105±10 and 78±7MPa following 24h, 1 and 2 weeks respectively stored in NaOH, although this was not statistically significant when compared with the preceding BFS value (P=0.093; P=0.594; P=0.950). An initial significant decrease in the mean BFS of FZ to 146±26MPa was identified following 24h storage in 0.1M NaOH (P=0.007), whilst consecutive non-significant decreases in the BFS occurred following 1 (131±12MPa) and 2 (123±11MPa) weeks (P>0.05). The BFS of Z100 was significantly increased following 24h (220±18MPa; P=0.042), whilst a consecutive decrease occurred following 1 (143±25MPa; P<0.001) and 2 (106±47MPa; P=0.511) weeks. The mean BFS of GR was also significantly increased following 24h (160±10MPa; P=0.159), whilst the BFS was decreased to 119±3 and 93±6MPa following 1 and 2 weeks, respectively (P=0.304; P=0.950). The BFS of GF following 24h was also increased (106±16MPa; P=0.983), whilst consecutive reductions in BFS following 1 and 2 weeks to 72±14 (P=0.675) and 40±10MPa (P=0.760), were not significant (Table 6.1; Figure 6.2).

| (a) | FSB | | | | FST | | | |
|---|---|---|---|---|---|---|---|---|
| | Control | 24h | 1 week | 2 weeks | Control | 24h | 1 week | 2 weeks |
| Fracture strengths (MPa) | 102-198 | 78-182 | 45-81 | 53-109 | 126-205 | 126-153 | 92-118 | 69-87 |
| Mean BFS (MPa) | $155(27)^{A}{}_{2}$ | $121(51)^{A,B}{}_{2,3}$ | $63(15)^{C}{}_{3}$ | $71(22)^{B,C}{}_{2,3}$ | $177(22)^{A}{}_{1,2}$ | $140(10)^{A,B}{}_{2,3}$ | $105(10)^{B,C}{}_{1,2,3}$ | $78(7)^{C}{}_{1,2,3}$ |
| Percent difference (%) | - | -22 | -60 | -54 | - | -21 | -41 | -56 |

| (b) | FZ | | | | Z100 | | | |
|---|---|---|---|---|---|---|---|---|
| | Control | 24h | 1 week | 2 weeks | Control | 24h | 1 week | 2 weeks |
| Fracture strengths (MPa) | 142-241 | 106-170 | 120-150 | 111-138 | 137-224 | 190-235 | 98-163 | 50-169 |
| Mean BFS (MPa) | $192(23)^{A}{}_{1}$ | $146(26)^{B}{}_{2,3}$ | $131(12)^{B}{}_{1}$ | $123(11)^{B}{}_{1}$ | $180(23)^{B}{}_{1}$ | $220(18)^{B}{}_{1,2}$ | $143(25)^{B,C}{}_{1}$ | $106(47)^{C}{}_{1,2}$ |
| Percent difference (%) | - | -24 | -32 | -36 | - | +18 | -21 | -42 |

| (c) | GR | | | | GF | | | |
|---|---|---|---|---|---|---|---|---|
| | Control | 24h | 1 week | 2 weeks | Control | 24h | 1 week | 2 weeks |
| Fracture strengths (MPa) | 107-142 | 85-122 | 115-122 | 85-100 | 53-117 | 85-122 | 58-90 | 30-49 |
| Mean BFS (MPa) | $125(11)^{A,B}{}_{3}$ | $160(10)^{A}{}_{2}$ | $119(3)^{A,B}{}_{1,2}$ | $93(6)^{A}{}_{1,2}$ | $87(17)^{A}{}_{4}$ | $106(16)^{A}{}_{3}$ | $72(14)^{B,C}{}_{2,3}$ | $40(10)^{B}{}_{3}$ |
| Percent difference (%) | - | +22 | -5 | -26 | - | +18 | -17 | -54 |

Mean values within rows (for each material) and columns (for all materials) exhibiting different letters (in superscript) and numbers (in subscript) respectively, were significantly different ($P<0.05$).

**Table 6.1. The range, mean and percentage difference of the BFS (MPa) of (a) the nanocluster, (b) microhybrid and (c) nano-hybrid RBCs following 24h stored in a waterbath maintained at 37±1°C and following 24h, 1 and 2 weeks stored in 0.1M NaOH also in a waterbath at 37±1°C.**

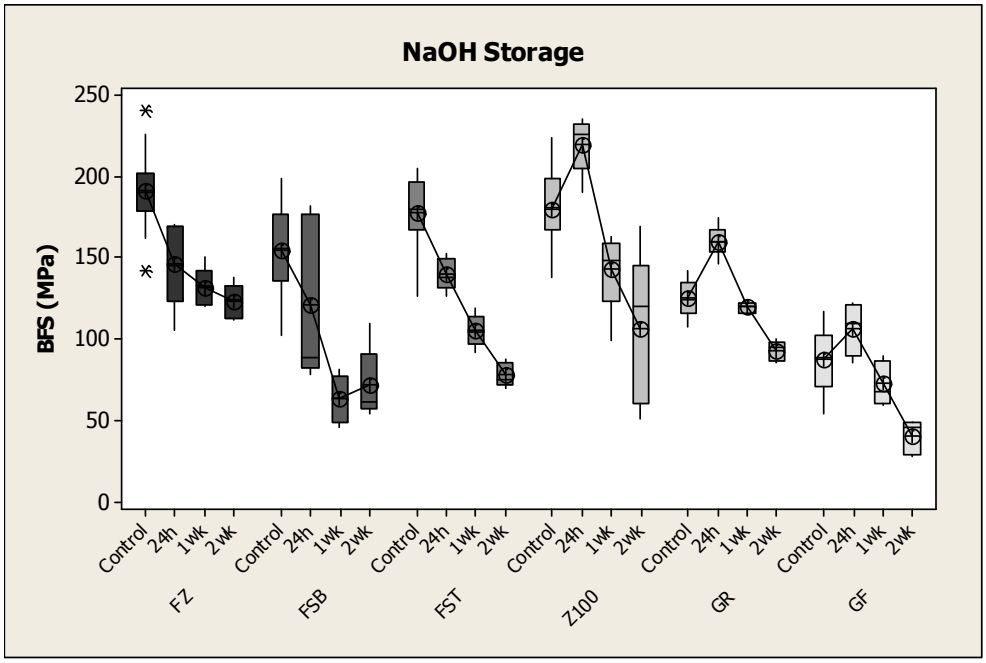


**Figure 6.2. Box and whisker plots highlighting the mean, median, inter-quartile range and outlaying data-points (*) of the BFS of FZ, FSB, FST, Z100, GR and GF following 24h storage in a waterbath and 24h, 1 and 2 weeks stored in 0.1M NaOH maintained at 37±1°C.**

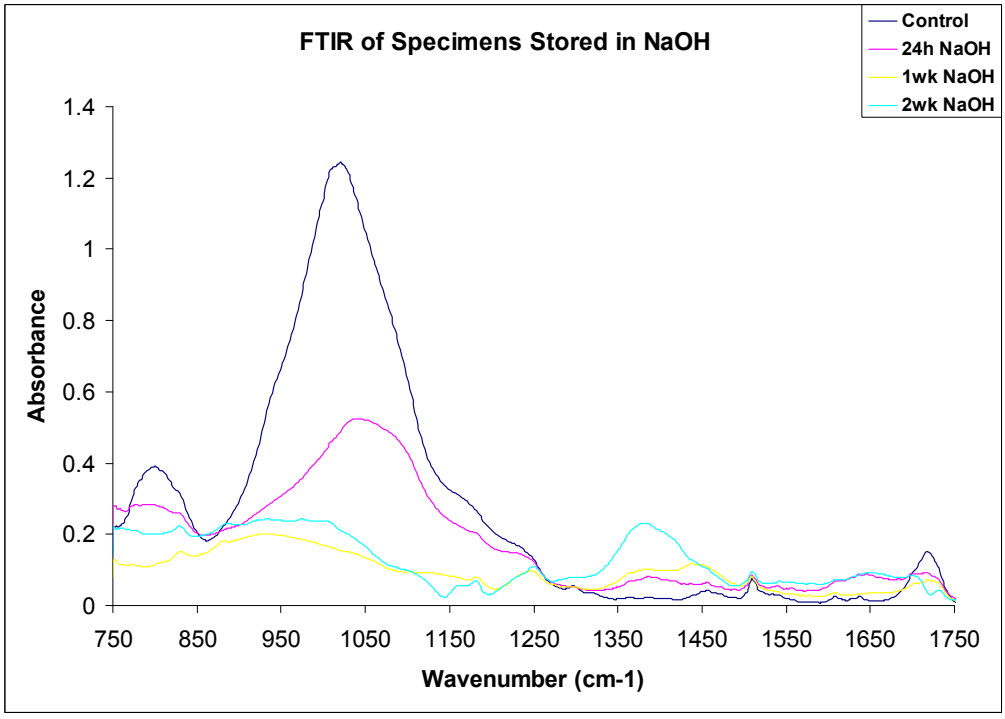


**Figure 6.3. Representative FTIR spectra of RBCs in the range of 750-1750cm$^{-1}$ following 24h 'wet' and 24h, 1 and 2weeks stored in 0.1M NaOH, highlighting a reduction in the peak centred around 1050cm$^{-1}$ and attributed to the Si-O bond present in the silane coupling agent and the silica filler particles.**

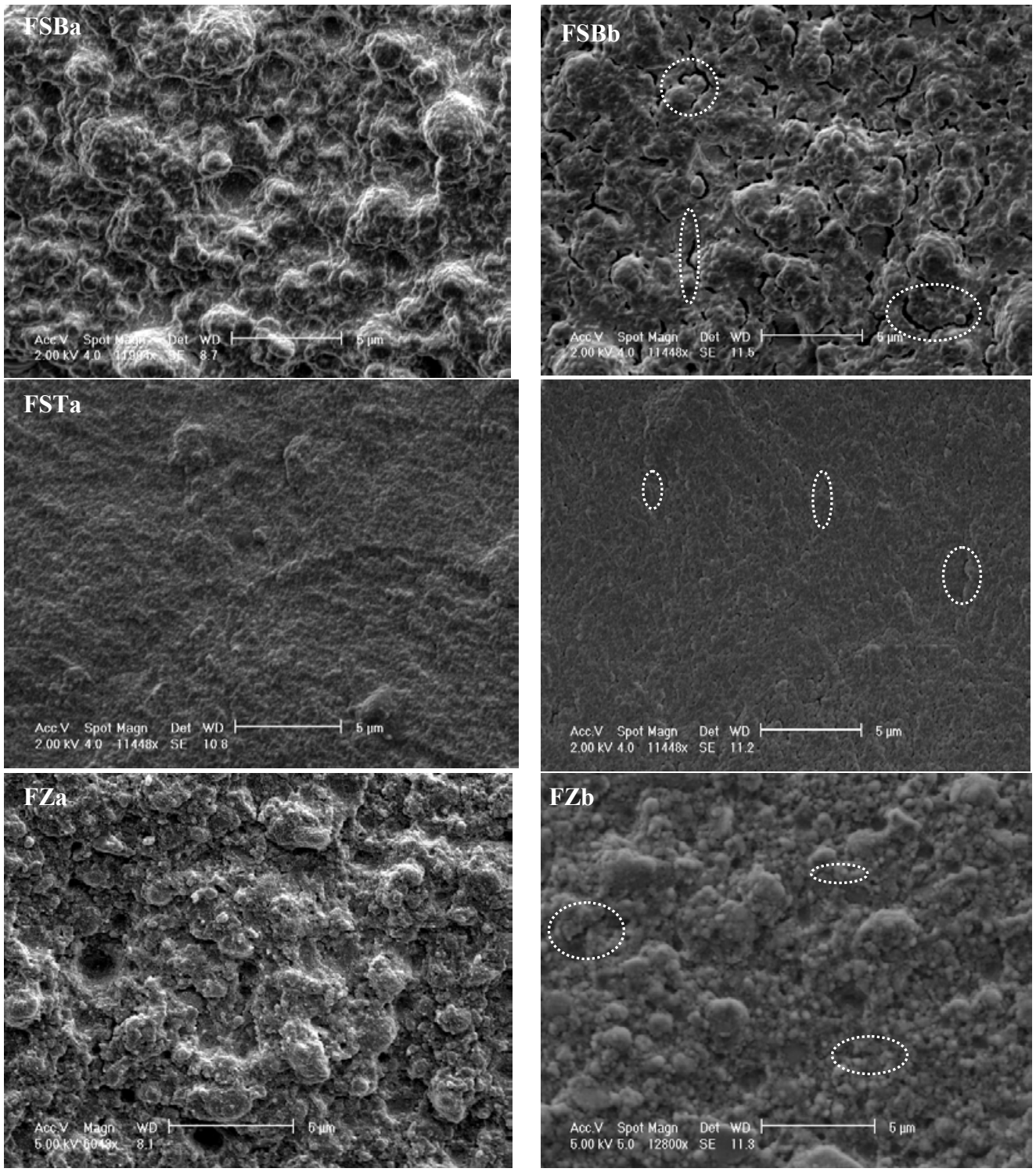


**Figure 6.4. Cryo-SEM images of fracture surfaces through the bulk of FSB, FST and FZ disc-shaped specimens (a) prior to and (b) following 2 weeks storage in 0.1M NaOH, highlighting degradation at the filler/silane/matrix interface (circled).**

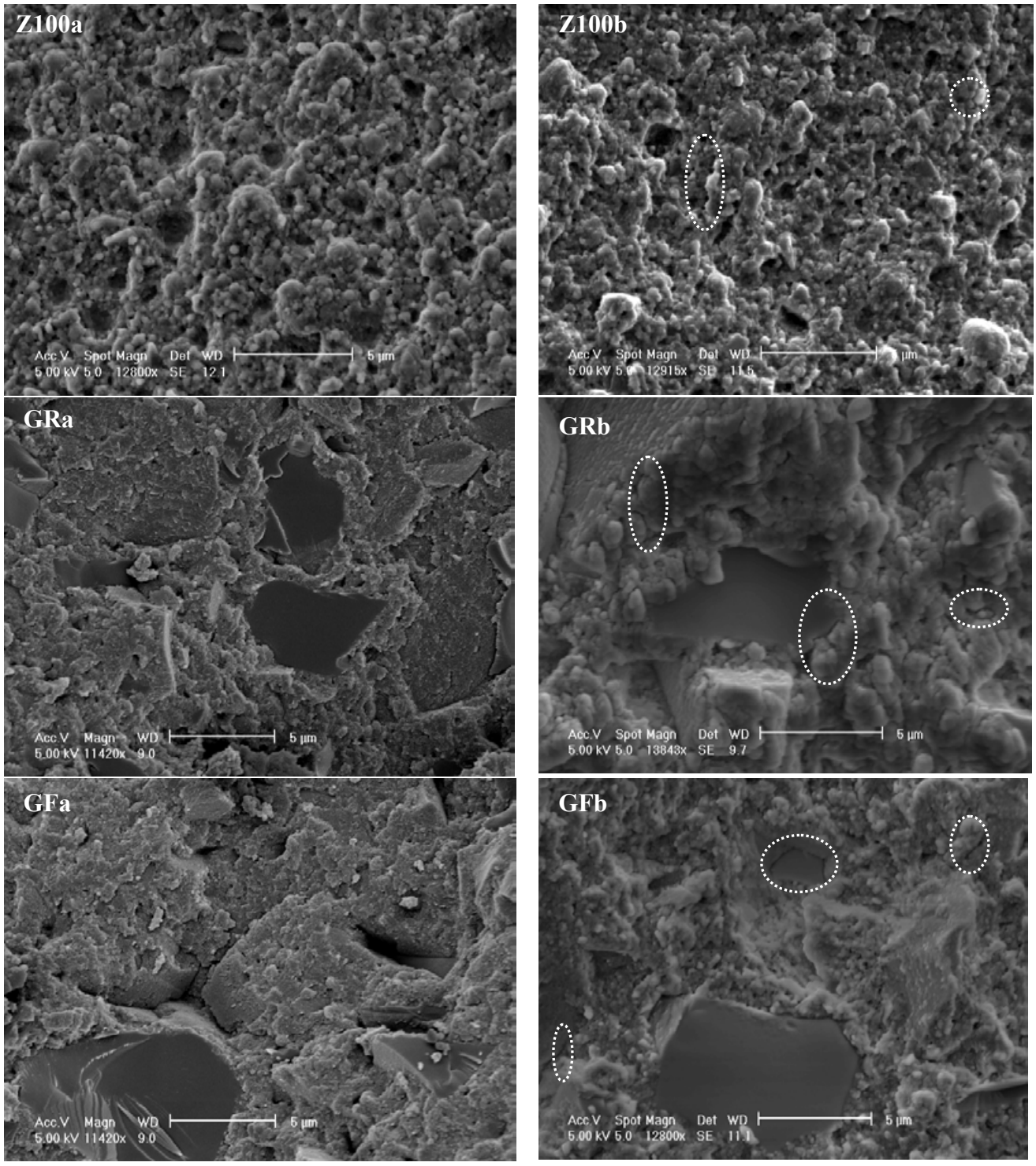


**Figure 6.4 (continued). Cryo-SEM images of fracture surfaces through the bulk of Z100, GR and GF disc-shaped specimens (a) prior to and (b) following 2 weeks storage in 0.1M NaOH, highlighting degradation at the filler/silane/matrix interface (circled).**

### 6.1.1.2 Depth of penetration

The depth of solvent penetration identified by a layer of degradation (Figure 6.5) highlighted a mean depth of between 61±15.7 and 197±69.9μm, dependent upon the material tested (Table 6.2).

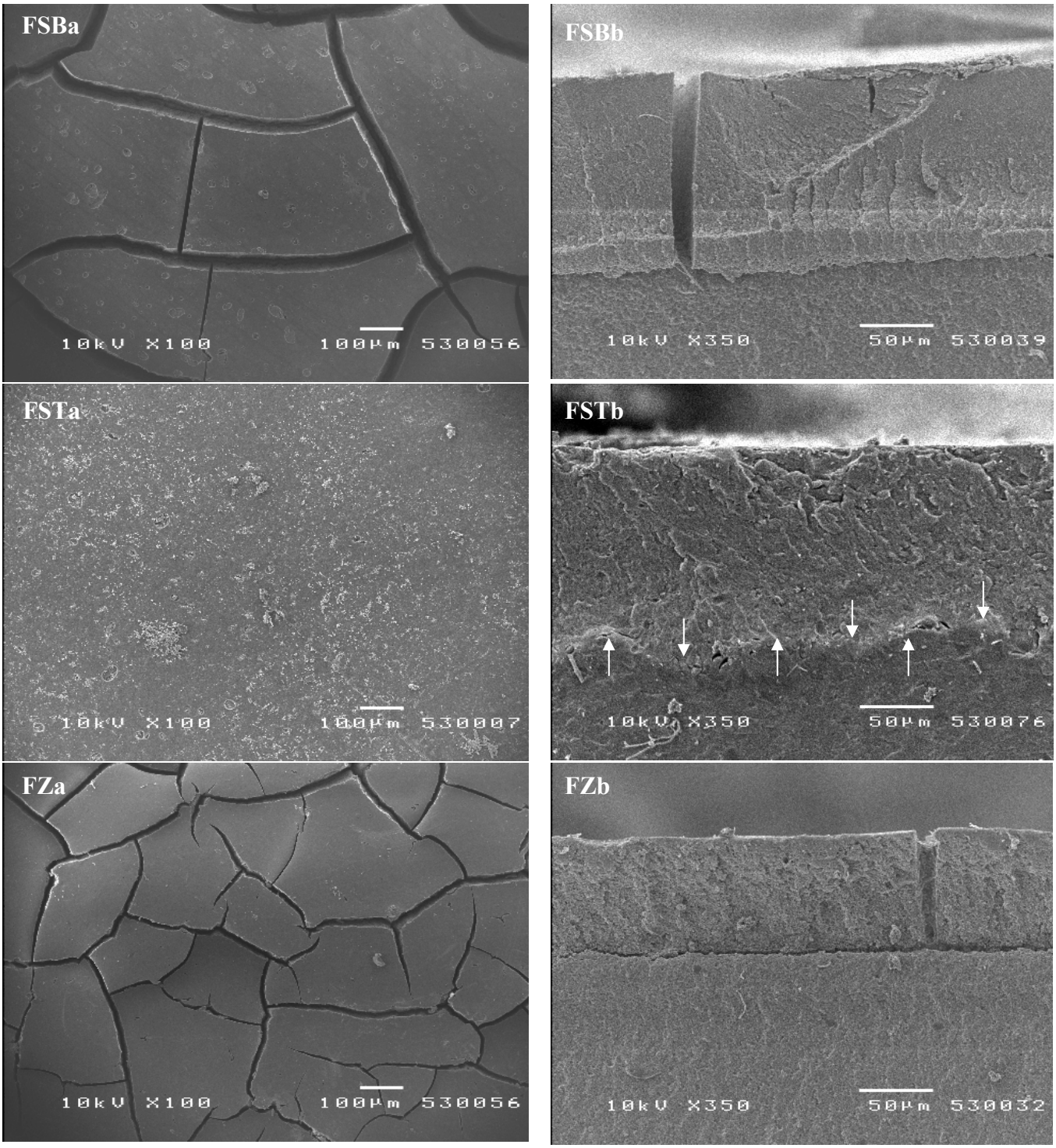


**Figure 6.5. SEM of the (a) surface and (b) fracture surface of FSB, FST and FZ specimens following storage in 0.1M NaOH for 2 weeks, highlighting surface cracking and subsurface cracking/delamination (indicated by arrows for FST).**

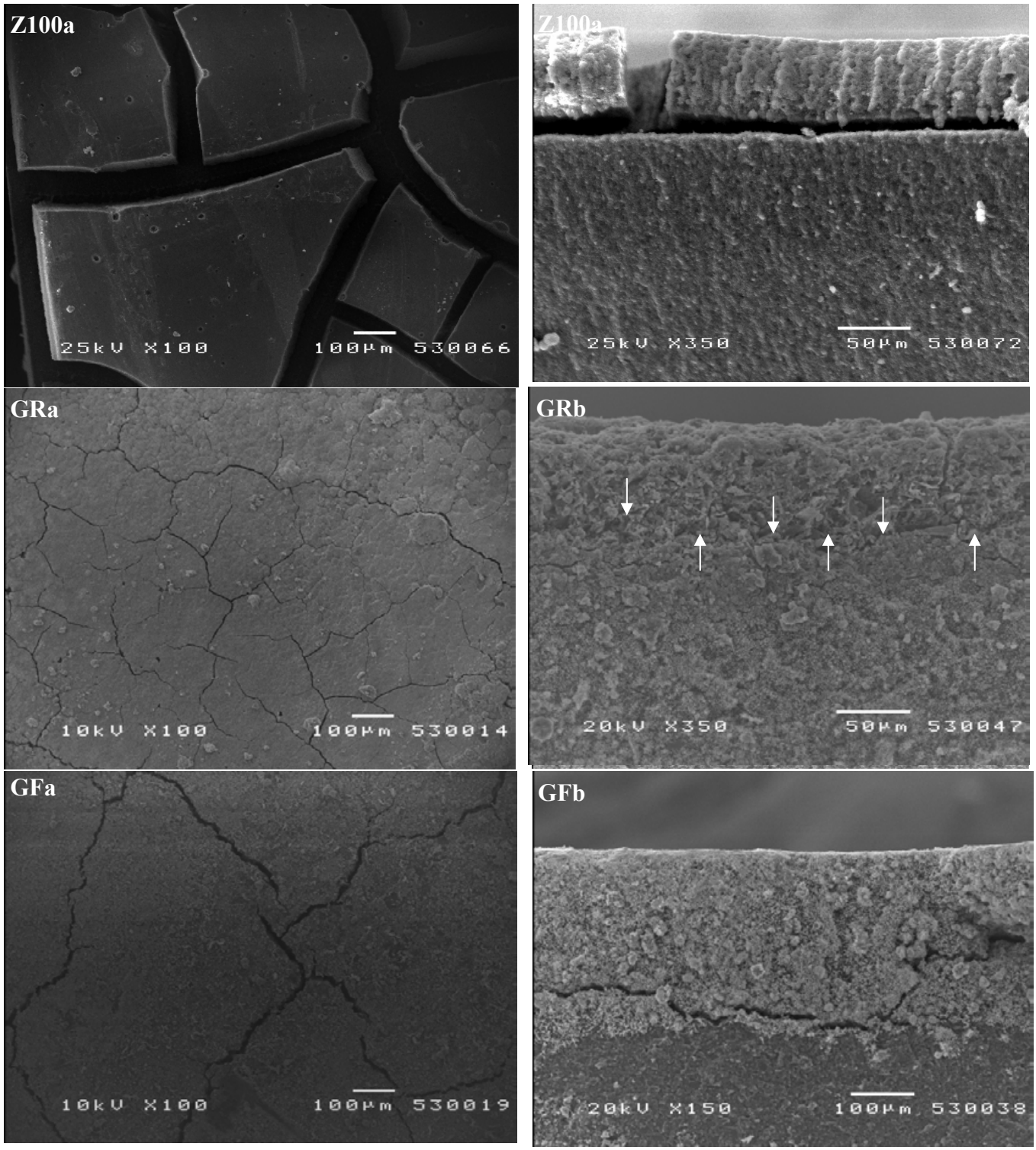


**Figure 6.5(continued). SEM of the (a) surface and (b) fracture surface of Z100, GR and GF specimens following storage in 0.1M NaOH for 2 weeks, highlighting surface cracking and subsurface cracking/delamination (indicated by arrows for GR). Note, due to the depth of solvent induced subsurface damage in GF the scale differs from other images.**

| | FSB | FST | FZ | Z100 | GR | GF |
|---|---|---|---|---|---|---|
| **Depth of penetration (µm)** | 91 (38.2) | 88 (28.5) | 69 (18.6) | 61 (15.7) | 91 (16.5) | 197 (69.9) |

**Table 6.2 Depth of solvent penetration (µm) identified by a layer of RBC degradation.**

### 6.1.2 Storage in ethanol

RBC specimens (n=5) were stored in EtOH for 24h, 1 and 2 weeks and the BFS and surface hardness subsequently determined.

#### 6.1.2.1 Bi-axial flexure strength

Two-way ANOVA of specimens stored in EtOH highlighted both storage ($F=55.72$; $P<0.001$) and material ($F=70.48$; $P<0.001$) to be significant, whilst their interaction significantly reduced the BFS ($F=9.39$; $P<0.001$) (Figure 6.6).

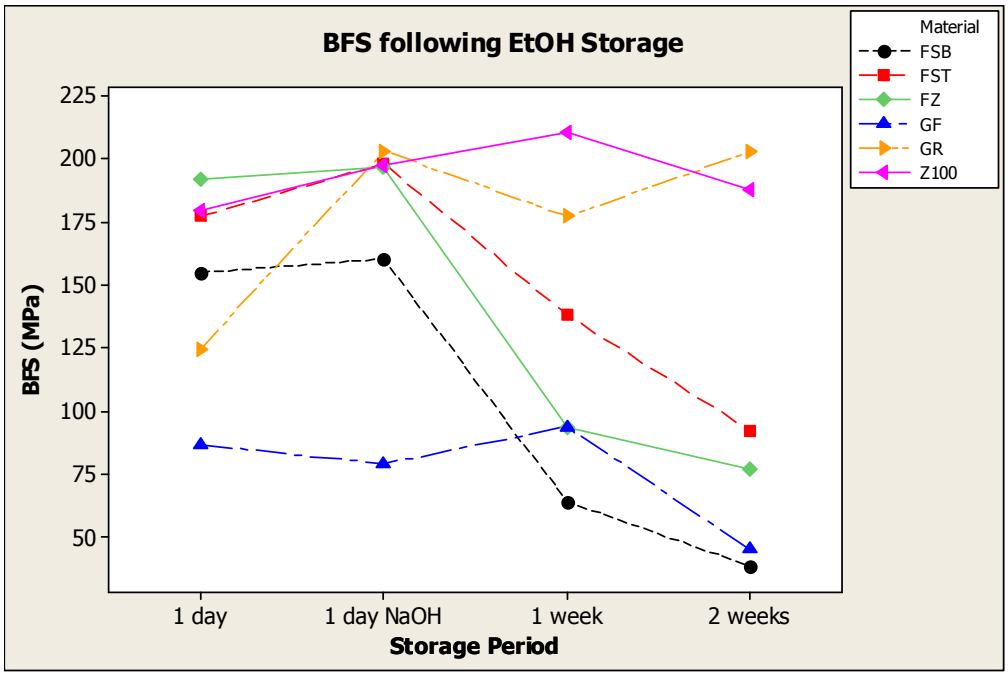


**Figure 6.6. Plot highlighting the mean BFS (MPa) of FSB, FST, FZ, Z100, GR and GF following 24h stored in a waterbath maintained at 37±1°C and 24h, 1 and 2 weeks in a 75% solution of EtOH also maintained at 37±1°C.**

One-way ANOVA identified that the BFS of FSB following 24h stored in EtOH was not significantly modified (160±30MPa; $P>0.05$), whilst a significant decrease in the BFS was

identified due to 1 week storage (64±15MPa; P<0.001), although the subsequent decrease following 2 weeks was not significant (39±4MPa; P=0.981). The mean BFS of FST was increased following 24h storage in EtOH, although this was not significant (198±35MPa; P=0.973), whilst following 1 week the BFS was significantly decreased (138±20MPa; P=0.008) and a further non-significant, decrease compared with the preceding BFS was identified following 2 weeks (92±9MPa; P=0.191). The BFS of FZ following 24h storage in EtOH was not significant (197±26MPa; P>0.05), although a significant decrease occurred following 1 week (93±5MPa; P<0.001) and a further non-significant decrease occurred following 2 weeks (77±4MPa; P>0.05). The mean BFS and standard deviation of Z100 following 24h, 1 and 2 weeks was 197±38, 210±23 and 188±36MPa respectively which was not significantly different compared with the control (P>0.05). The BFS of GR was significantly increased following 24h (203±28MPa; P>0.05) storage and the BFS after storage for 1 (177±36; P=0.978) and 2 (203±17MPa; P=0.980) weeks was not significantly affected. Likewise, the mean BFS of GF following 24h, 1 and 2 weeks (79±25, 94±5 and 45±28MPa) did not differ significantly compared with the 'wet' control (P>0.05) (Table 6.3; Figure 6.7).

#### 6.1.2.2 Surface hardness

The mean surface hardness of FSB and FZ was significantly decreased following EtOH storage for 24h, 1 and 2 weeks, whilst the VHN of FST was significantly decreased following 1 and 2 weeks compared with the control specimens (P<0.001). The VHN of Z100, GR and GF was only decreased following 2 weeks (P<0.05) (Table 6.3).

| (a) | FSB | | | | FST | | | |
|---|---|---|---|---|---|---|---|---|
| | Control | 24h | 1 week | 2 weeks | Control | 24h | 1 week | 2 weeks |
| **Fracture strengths (MPa)** | 102-198 | 128-192 | 54-90 | 33-42 | 126-205 | 146-233 | 114-164 | 84-105 |
| **Mean BFS (MPa)** | $155(27)^{A}{}_{2}$ | $160(30)^{A}{}_{1}$ | $64(15)^{B}{}_{4}$ | $39(4)^{B}{}_{3}$ | $177(22)^{A}{}_{1,2}$ | $198(35)^{A}{}_{1}$ | $138(20)^{B,C}{}_{2,3}$ | $92(9)^{C}{}_{2}$ |
| **Surface Hardness (VHN)** | 88(1.89) | 70 (4.84) | 60 (2.03) | 66 (5.02) | 84 (1.68) | 78 (2.39) | 65 (5.53) | 64 (3.53) |

| (b) | FZ | | | | Z100 | | | |
|---|---|---|---|---|---|---|---|---|
| | Control | 24h | 1 week | 2 weeks | Control | 24h | 1 week | 2 weeks |
| **Fracture strengths (MPa)** | 142-241 | 164-219 | 84-97 | 72-82 | 137-224 | 140-236 | 172-230 | 148-240 |
| **Mean BFS (MPa)** | $192(23)^{A}{}_{1}$ | $197(26)^{A}{}_{1}$ | $93(5)^{B}{}_{3,4}$ | $77(4)^{B}{}_{2,3}$ | $180(23)^{A}{}_{1}$ | $197(38)^{A}{}_{1}$ | $210(23)^{A}{}_{1}$ | $188(36)^{A}{}_{1}$ |
| **Surface Hardness (VHN)** | 93 (2.11) | 82 (3.94) | 69 (5.97) | 68 (4.65) | 120 (4.01) | 136 (5.43) | 129 (14.25) | 83 (6.79) |

| (c) | GR | | | | GF | | | |
|---|---|---|---|---|---|---|---|---|
| | Control | 24h | 1 week | 2 weeks | Control | 24h | 1 week | 2 weeks |
| **Fracture strengths (MPa)** | 107-142 | 169-231 | 128-215 | 178-221 | 53-117 | 49-109 | 88-99 | 24-84 |
| **Mean BFS (MPa)** | $125(11)^{B}{}_{3}$ | $203(28)^{A}{}_{1}$ | $177(36)^{A}{}_{1}$ | $203(17)^{A}{}_{1}$ | $87(17)^{A}{}_{4}$ | $79(25)^{A}{}_{3}$ | $94(5)^{A}{}_{3,4}$ | $45(28)^{A}{}_{2,3}$ |
| **Surface Hardness (VHN)** | 119 (13.43) | 136 (13) | 126 (4.94) | 86 (12.74) | 54 (5.88) | 60 (7.19) | 53 (3.16) | 37 (2.77) |

Mean values within rows (for each material) and columns (for all materials) exhibiting different letters (in superscript) and numbers (in subscript) respectively, were significantly different ($P<0.05$).

**Table 6.3. The range and mean bi-axial flexure strengths (MPa) and surface hardness (VHN) of (a) the 'nanocluster', (b) microhybrid and (c) nano-hybrid RBCs following 24h stored in a waterbath maintained at 37±1°C and following 24h, 1 and 2 weeks stored in 75% EtOH also in a waterbath at 37±1°C.**

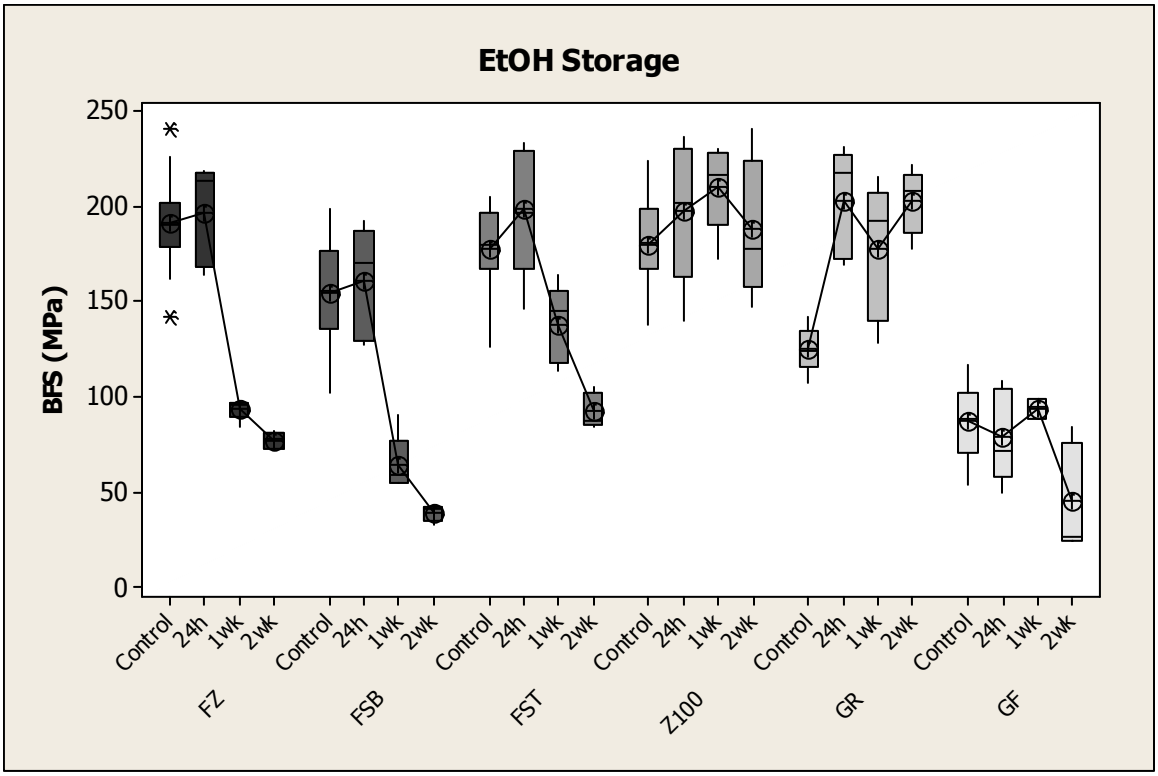


**Figure 6.7. Box and whisker plots highlighting the mean, median, inter-quartile range and outlaying data-points of the BFS (MPa) of FZ, FSB, FST, Z100, GR and GF stored 'wet' for 24h and in EtOH for 24h, 1 and 2 weeks.**

## 6.2 DISCUSSION: Accelerated degradation of nanofilled RBCs: Solvent Storage

The degradation of RBC restorations can be accelerated using solvents, such as sodium hydroxide (NaOH) and ethanol (EtOH) to simulate routine ingestion of foodstuffs [Sarkar, 2000]. The current study highlighted a significant reduction in the bi-axial flexure strength of the six RBCs tested following storage for up to two weeks in NaOH (Section 6.2.1) and of the BFS and surface hardness following storage in EtOH (Section 6.2.2).

### 6.2.1 Sodium hydroxide induced degradation

A greater extent of mechanical degradation was observed following storage of the RBCs for two weeks in NaOH compared with the storage of specimens in water (Chapter 5) or EtOH. The specific action of NaOH is to degrade the interfacial silane layer at the filler/resin interface, whereby hydroxyl ions provided by the solvent reduce the siloxane bridge bonds to the original silanol groups. This generates additional hydroxyl ions, raising the pH (~13) which enhances dissolution of both the silane interface and silica filler [Sarkar, 2000]. The reaction becomes autocatalytic; accelerating interfacial degradation as the concentration of hydroxyl ions is further increased [Ortengren et al., 2001; Bagheri et al., 2007]. The total concentration of hydroxyl ions generated by NaOH is significantly greater than water, EtOH or artificial saliva, being approximately one million times greater than saliva [Sarkar, 2000; Bagheri et al., 2007], subsequently degradation produced by NaOH is significantly greater than these alternative solutions.

Following two weeks immersion in NaOH the bi-axial flexure strength of FSB, FST, FZ, Z100, GR and GF (71±22, 78±7, 123±11, 106±47, 93±6 and 40±10MPa, respectively) was significantly reduced compared with the control specimens which were stored ‘wet’ for 24h (155±27, 177±22, 192±23, 180±23, 125±11 and 87±17MPa, respectively). The subsequent percentage decrease of FSB (54%), FST (56%), FZ (36%), Z100 (42%), GR (26%) and GF (54%) was calculated (Table 6.1), highlighting that although the pattern of decrease exhibited by the six RBCs was comparable (Figure 6.2) the ‘nanocluster’ reinforced RBCs (FSB and FST) and the ‘flowable’ RBC (GF) were most prone to degradation. In terms of the ‘nanocluster’ material this was consistent with the previous water storage studies which identified a decreased hydrolytic stability that became critical as a consequence of long-term storage (Section 5.1). The

similar, albeit off-set, pattern of decrease exhibited by GR and GF (Figure 6.2) highlighted the influence of decreased filler loading in the flowable material, which subsequently produced mechanical properties less than those obtained with a higher filler load in similar materials [Ferracane et al., 1998].

FTIR spectroscopy of all RBC specimens following immersion in NaOH highlighted a marked reduction in the absorbance peak at 1250-850cm$^{-1}$ (Figure 6.3). This broad band within the FTIR spectra is related to the symmetric stretching of bonds attributed to Si-O-Si of the inorganic silica filler particles [Anagnostopoulos et al., 1993; Aldrich, 1997; Bertelsen & Boerio., 2001]. This band also contains absorbance peaks attributed to the siloxane bonds and silanol groups associated with the silane interface [Ishida & Koenig, 1978; Antonucci et al., 2003], which includes stretch of Si-O-$CH_3$ at 1189cm$^{-1}$ associated with bonding of the silane coupling agent with the resin matrix [Anagnostopoulos et al., 1993]. In addition to also including the Si-O bond associated with formation of siloxane bridge bonds at 1090-1080cm$^{-1}$ and at 1000-900cm$^{-1}$, although these were generally masked by the silica absorbance peak which obscures this spectral region [Ishida & Koenig, 1978; Anagnostopoulos et al., 1993; Aldrich, 1997; Bertelsen & Boerio, 2001]. Furthermore, following hydrolysis of the siloxane groups FTIR has previously highlighted silanol groups generated at 915-905cm$^{-1}$ [Anagnostopoulos et al., 1993] and 930-840cm$^{-1}$ due to the Si-O stretching mode of the Si-OH groups [Ishida & Koenig, 1978]. Although peaks directly associated with the silane interface may be masked by the broad band associated with silica filler particles, the relative comparison of peak heights using FTIR spectroscopy in the current study was useful to corroborate with the observed decrease in mechanical properties of RBCs as a consequence of interfacial silane degradation (Figure 6.4).

#### 6.2.1.1 Surface and subsurface degradation

The surfaces of the RBC specimens were observed to be cracked and degraded following solvent storage (Figure 6.5), whilst a corresponding 'peel layer' was identified from bulk fracture analysis of the specimens (Figure 6.4). The peel layer was related to the depth of diffusion of NaOH into the specimen and whilst it may be assumed that the solvent diffused throughout the specimen, the peel layer was related to distinct structural modification of the RBC generated by the solvent [Mair, 1999; Hunter et al., 2003]. The depth of degradation in a given environment is dependent on the permeability of the RBC [Mair et al., 1989], which is determined by the physio-

chemical characteristics of the resin, filler and silane coupling agent such as the hydrophilicity of the resin and the hydrolytic stability of the fillers and silane coupling agent [Sarkar, 2000]. Surface cracking and peeling due to storage in NaOH was attributed to the specific degradation of the silane coupling agent and loss of filler particles, where unfilled resins exposed to NaOH did not exhibit subsurface damage or peel layers [Sarkar, 2000]. The structural integrity and subsequent depth of the subsurface damage layer was identified to vary between materials, highlighting that the greatest extent of degradation was associated with porous fillers, whilst compact adherent fillers exhibited the least degradation [Sarkar, 2000]. The current study highlighted two distinct forms of peel layer, whereby a sub-surface layer of each specimen of FSB, FZ, Z100 and GF appeared to be delaminated from the majority of the specimen bulk. Conversely, the diffusion layer in FST and GR was identifiable as a layer of subsurface cracking which remained connected to the specimen bulk (Figure 6.5).

A previous study highlighted that the depth of penetration of NaOH into the bulk of the RBCs tested (also manifested as surface cracking and subsurface peeling) ranged from 20.3±2.7 to 176.4±1.5µm, with FSB exhibiting a mean depth of penetration of 94.8±0.5µm [Bagheri et al., 2007]. Similarly, in the current study, FSB and FST possessed a mean depth of penetration of 91±38.2µm and 88±28.5µm, respectively (Table 6.1; Figure 6.4). The variance of the data reported by Bagheri, (2007) was markedly less than that reported in the current study. Following immersion in NaOH, Bagheri, (2007) placed the specimens in aqueous silver nitrate for 10 days at 60°C, which were subsequently soaked in a photo-developing solution exposed to fluorescent light for 8h, sectioned and ground prior to SEM examination to determine the depth of solvent degradation via depth of silver nitrate penetration. Conversely, following immersion in NaOH for two weeks the specimens in the current study were immediately dried and examined in SEM (Section 3.2.1.3). This suggests that the method employed by Bagheri, (2007) which possessed a greater sample size, was considerably more concise, although the similarity of the mean values of FSB highlights the efficacy of the method reported in the current study.

A markedly greater depth of solvent induced damage was identified for GF of 197±69.9µm (with a range of 105 to 275µm), whilst that of the remaining RBCs were broadly comparable, ranging from 61±15.7 to 91±38.2µm (Table 6.2). The markedly higher depth of solvent induced damage within GF was attributed to the intentionally lower filler loading of ‘flowable’ RBCs compared with conventional materials with higher filler loadings. Moreover, the

HEDMA monomer, which was incorporated to reduce the requisite activation energy of the resin matrix [Guzmán et al., 1997], has been reported to be extremely hydrophilic [Magni et al., 2007]. This was attributed to the presence of 1,3-dioxane rings as part of the monomeric structure of HEDMA, which whilst not initially hydrophilic were modified by hydrolysis to increase hydrophilicity [Guzmán et al., 1997]. This may suggest that the high concentration of hydroxyl ions generated by NaOH modified the 1,3-dioxane rings of HEDMA resulting in the high depth of solvent induced degradation observed in the current study.

### 6.2.2 Ethanol induced degradation

EtOH specifically degrades the resin matrix of RBCs since both BisGMA, the main constituent of the matrix, and EtOH possess a comparable solubility parameter [Badra et al., 2005; Yap et al., 2005; Polydorou et al., 2007]. EtOH specifically degrades the resin matrix due to chain scission which cleaves the polymeric chains to oligomers and individual monomers (Section 2.1.1) and also elution of unreacted monomers, swelling and concomitant softening due to expansion of the polymer chains as the solvent penetrates the polymeric structure [Asmussen et al., 1984; Asmussen & Peutzfeldt 2001; Polydorou et al., 2007]. Subsequently, degradation of the resin matrix reduces the crosslink density of the polymerized chain structure within the resin matrix which reduces the structural integrity and produces 'softening' of the material, indirectly quantifiable by assessing surface hardness and/or flexural modulus of the material [McKinney & Wu, 1985; Göpferich et al., 1996; Asmussen & Peutzfeldt, 2001].

The bi-axial flexure strength of the 'nanocluster' (FSB and FST) and the microhybrid (FZ) RBCs were significantly reduced following one week storage in EtOH (64±15, 138±20 and 93±5MPa, respectively) compared with the control groups. This decline in mechanical properties related to degradation of the polymerized structure and was further manifested as a reduction in surface hardness of FSB and FZ following 24h and one week storage in EtOH, whilst the VHN of FST was significantly reduced following one week (Table 6.3a). In contrast, the BFS of Z100 and GR was statistically similar or significantly increased following up to and including two weeks storage in EtOH, whilst the BFS of GF was significantly reduced following two weeks compared with the control. Furthermore, the surface hardness of Z100, GR and GF was only significantly decreased following two weeks storage in EtOH compared with the control (Table 6.3b&c). The extent and rate of degradation following storage in EtOH is attributable to the specific resin

matrix chemistry [Bastoli et al., 1990; Ferracane et al., 1998; Sarker, 2000; Göpferich et al., 1996]. Despite the significant influence the resin matrix chemistry imparts on the subsequent mechanical and rheological properties of RBCs, dental manufacturers seldom divulge the exact quantity or ratio of monomers reporting merely the generic resin chemistry to protect intellectual property and to prevent duplication by competitors. Thus, predicting the likely mechano-physical properties of RBCs is unreliable and potentially misleading without extensive *in vivo* and *in vitro* studies. Nevertheless, it has been reported that the diluent TEGDMA was virtually eliminated from the matrix of FSB, FST and FZ, compared with the earlier Z100, and replaced with UDMA and $BisEMA_6$. The replacement of TEGDMA with UDMA and $BisEMA_6$ has previously been identified to improve mechanical properties, such as tensile strength, elastic modulus and wear resistance of the resulting RBC [Indrani et al., 1995; Peutzfeldt, 1997]. The $BisEMA_6$ monomer is a lower viscosity analogue of BisGMA and has been identified to increase the degree of conversion and crosslink density to improve the flexural strength when admixed with BisGMA monomers [Ogliari et al., 2008]. In addition, $BisEMA_6$ is known to form weaker hydrogen bonds with water molecules than the hydroxyl groups of BisGMA and TEGDMA molecules, thereby reducing the hydrophilic nature of the constituent monomers and theoretically increasing the hydrolytic stability of the resin [Finer & Santerre, 2004; Palin et al., 2005c]. Despite this, Bagheri et al. (2007) identified that resins consisting of both TEGDMA and $BisEMA_6$, in particular FSB, exhibiting a higher susceptibility to solvent degradation than resins containing a higher quantity of BisGMA, although Bagheri et al. (2007) did not offer an explanation for this, suggesting that further work was required. In addition, Ogliari et al. (2008) identified that water sorption and solubility of resins consisting of BisEMA increased as the number of ethylene oxide groups increased. The current study concurred with Bagheri et al. (2007), highlighting a more significant extent of EtOH induced degradation of the RBCs possessing a resin matrix containing $BisEMA_6$ (FSB, FST and FZ). This may suggest that the presence of $BisEMA_6$ limited the hydrolytic stability of the material and initiated degradation of the of the resin matrix as highlighted by a pronounced strength reduction and surface softening. This may also partially explain the considerably higher percentage reduction in BFS identified following long-term water storage of FSB, FST and FZ compared with GR and GF identified following the water storage study reported in Chapter 5.

The enhanced fracture strength and surface hardness of Z100, GR and GF following storage in EtOH was also attributed to the resin matrix chemistry which consisted of BisGMA and TEGDMA (also HEDMA in the case of GF) (Table 3.1). Asmussen & Peutzfeldt (2001) reported polymerization and extent of crosslinking between the constituent monomer chains to be increased by a high proportion of TEGDMA in a mixture of BisGMA, manifested as an increased surface hardness. The TEGDMA monomer was originally incorporated as a diluent to decrease the viscosity of the BisGMA-based resin matrix due to the low molecular weight of TEGDMA (286 compared with 513g/mol [Ge et al., 2005]) and also the flexibility of the monomer as ether links present little steric hindrance to chain rotation [Ruyter & Svendsen, 1978]. TEGDMA monomers possess a high content of C=C linkages which provide many centres of polymer growth during polymerization, thus producing a highly crosslinked structure and high degree of conversion [Asmussen et al., 1982; Asmussen & Peutzfeldt, 2001; Feilzer & Dauvillier, 2003; Hunter et al., 2003]. As a consequence the mechanical properties of materials which contain a high quantity of TEGDMA are generally increased [Assmussen et al., 1998], this concurred with the current study where the three RBCs (Z100, GR and GF) which contained a high quantity of TEGDMA (and also an absence of $BisEMA_6$) possessed improved flexure strength and surface hardness values.

Despite its apparent beneficial influence the incorporation of TEGDMA into the resin matrix requires a degree of compromise since the high degree of conversion, in addition to providing improved mechanical properties [Asmussen et al., 1982; Asmussen & Peutzfeldt, 2001; Feilzer & Dauvillier, 2003; Hunter et al., 2003], also produces polymerization shrinkage, as the C=C bonds are converted to the physically shorter single bonds of the polymerized network [Sideridou et al., 2002; Ferracane, 2005]. This promotes marginal gap formation at the restoration/tooth interface and monomer elution [Asmussen et al., 1984; Asmussen & Peutzfeldt, 2001; Floyd & Dickens, 2006]. Furthermore, TEGDMA is a hydrophilic monomer, due to the ethylene-glycol groups and has been shown to be prone to degradation and erosion [Geurtsen & Leyhausen, 2001; Finer & Santerre, 2004], Kalachandra et al. (1987) highlighted that increasing the proportion of TEGDMA from 0 to 1.0wt% increased the water sorption. Therefore, the resin matrix chemistry may be modified to remove or reduce the quantity of TEGDMA present by the addition of an alternative monomer, such as UDMA and $BisEMA_6$ as in the case of FSB, FST and FZ. The UDMA and $BisEMA_6$ monomers possess a lower content of C=C bonds which

reduces polymerization shrinkage [Ellakwa et al., 2007], whilst also providing improved flexure strength [Assmussen et al., 1998]. Furthermore, compared with BisGMA-based RBCs the urethane linkage, decreased quantity of C=C bonds and therefore longer chain ends and increased molecular stability within UDMA monomers provides a lower viscosity and more flexible monomer, improving the tensile strength, elastic modulus and wear resistance [Peutzfeldt, 1997]. However, Ellakwa et al. (2007) identified that polymerization shrinkage increased again with an increased ratio of UDMA to BisGMA. This highlights the compromise between degree of conversion, mechanical properties and polymerization shrinkage which must be considered when selecting the specific resin matrix chemistry.

The increased BFS and surface hardness of Z100 and GR (Table 6.3) also suggested that post-cure polymerization of the resin occurred for up to seven days following irradiation. Post-curing occurs despite RBCs being described as so-called 'command cure' materials, whereby polymerization of the resin matrix is initiated by irradiation and continues following completion of the specified curing cycle. This is due to continued diffusion of free radicals resulting in an increased degree of conversion and subsequent reduction in pendent chain ends in the matrix [Yap, 1997; Tilbrook et al., 2000; Stansbury et al., 2001; Rueggeberg, 2002; Wilson et al., 2005]. Post-cure polymerization of resins may be promoted by heat treatment to reduce the viscosity of the resin enabling ease of free radical diffusion [Quance et al., 2001; Rueggeberg, 2002]. Therefore, it may be suggested that the presence of higher quantities of low viscosity monomers, such as TEGDMA in the current study of Z100 and GR, may also allow free radical diffusion to enhance the degree of conversion and subsequent mechanical properties.

# CHAPTER 7 EXECUTIVE SUMMARY

The ongoing development of RBCs has resulted in the introduction of so-called 'nanofills' which contain inorganic filler particles with a mean diameter of less than 100nm. Dental materials manufacturers have routinely adopted the approach of combining these nano-sized fillers with a dispersion of micron-sized particles to maximise the filler loading and produce a hybrid-type RBC [Kleverlaan & Feilzer, 2005; Lohbauer et al., 2006; Mui et al., 2006; Beun et al., 2007]. The introduction of 'nanocluster' fillers, which are essentially an agglomerated particle complex consisting of either silica-zirconia or silica particles, with a mean size of 5-20nm and 75nm respectively, was an alternative approach to the developing field of 'nanotechnology' in restorative dentistry [Mitra et al., 2003]. However, considerable debate amongst researchers [Harris & Ure, 2006] and manufacturers [CARE, 2003; Mitra et al., 2003] has been associated with the potential of these materials to provide improved mechano-physical properties and subsequently enhance the clinical longevity of modern RBCs.

## 7.1 The Mechanical Properties of 'Nanofilled' RBCs

The reinforcement provided by the 'nanoclusters' to the resin matrix was studied using a micromanipulation technique to determine the fracture strength, pseudo-modulus of stress and failure mechanisms of the particulates during compressive loading [Zhang et al., 1991; 1992]. Micromanipulation highlighted that the 'nanocluster' particles provided unique fracture mechanisms compared with the spheroidal and irregular particles, exhibiting multiple fracture events, which indicated that the progressive break-up of the 'nanoclusters' had the potential to absorb and dissipate loading stresses. A pre-loading technique was subsequently employed to induce sub-critical damage to the RBCs studied prior to loading to failure in bi-axial flexure to highlight the reinforcement provided by the inorganic fillers. The pre-loading results highlighted that the 'nanocluster' material exhibited increased resistance to fracture and improved reliability of the strength data following the pre-loading regimes, particularly following storage in water. In contrast, the RBCs reinforced either with irregular or spheroidal particles exhibited a predilection to premature specimen fracture prior to completion of the pre-loading regimes, due to high Young's modulus of the material or stress concentration around the fillers [Sabbagh et al., 2004].

Pre-loading also suggested that the 'nanoclusters' possessed an IPC-like structure produced by silane infiltration of the interstices and internal porosities to create an interconnected network of nanoparticles, which enhanced the resistance to deformation [Clarke et al., 1992; Wegner & Gibson, 2001]. Clinically the distinctive capacity of the 'nanocluster' to enhance the damage tolerance of the material due to crack bifurcation and the absorption and dissipation of crack stresses and accumulated fatigue by deformation of the 'nanocluster' may provide improved resistance to low stress failures and subsequently increase the clinical longevity of the restoration.

## 7.2 Water and solvent induced degradation of nanofilled RBCs

NIRS of the RBC specimens highlighted a residual quantity of water within the resin matrix, even following specimen dehydration. The identical resin matrices of FSB and FZ were saturated following 13 weeks immersion, whilst the continued increase in water content of FST identified throughout the study was attributed to the increased surface-area-to-volume ratio of the higher quantity of dispersed nano-sized silica available for wetting with the hydrophilic silane. Likewise, the increased water content of GR compared with GF was attributed to the higher filler loading and thus greater quantity of silane coupling agent.

The presence of water and subsequent hydrolytic degradation of the resin matrix [Bastoli et al., 1990; Ferracane et al., 1998; Catteni-Lorente et al., 1999] and interfacial siloxane bridge bonds [Söderholm et al., 1984; Söderholm & Roberts, 1990; Stokes et al., 1988] significantly degraded the mechanical properties of the RBCs in the current study. The nominally identical resin matrix chemistries of FSB, FST and FZ highlighted that the hydrolytic stability of the 'nanoclusters' was limited as the 'nanocluster' reinforced RBCs exhibited a greater reduction in BFS (62, 49 and 36% strength loss respectively following 78 weeks). This was further manifested as FSB, which contained a higher loading of 'nanoclusters' than FST exhibited a more pronounced loss of BFS. This suggested that following long-term immersion hydrolytic degradation of the silane interface with the surrounding resin and potentially also of the bonding between constituent nano-sized particles, caused the 'nanoclusters' to act as defect centres

Immersion of the RBC specimens (FSB, FST, FZ, Z100, GR and GF) in NaOH highlighted a significant reduction in the BFS, this was most pronounced for 'nanocluster' reinforced RBCs which further suggested that the hydrolytic stability of the 'nanoclusters' was

limited. FTIR spectroscopy and SEM identified this to be due to degradation of the silane layer at the filler/resin interface. Furthermore, SEM highlighted surface and subsurface microcracking related to the depth of diffusion of NaOH into the bulk of the RBC specimens [Mair, 1999; Hunter et al., 2003], which resulted in surface delamination of FSB, FZ, Z100 and GF specimens. In contrast, no delamination was identified for FST and GR specimens, in conjunction with the NIRS results which highlighted these two materials did not become saturated, this suggested an increased capacity to absorb solvent which limited the extent of degradation.

Following EtOH storage FSB, FST and FZ exhibited significant degradation due to the presence of $BisEMA_6$ in the resin matrix [Bagheri et al., 2007]. Conversely, the higher content of TEGDMA and corresponding absence of $BisEMA_6$ in the matrix of Z100, GR and GF appeared to promote additional crosslinking and post-cure polymerization [Asmussen & Peutzfeldt, 2001; Hunter et al., 2003; Holmes et al., 2007] which maintained or increased the mechanical properties of these materials.

## 7.3 The structure and classification of 'nanoclusters'

The modern 'nanocluster' particulate appears to exhibit a remarkable similarity with the 'agglomerated microfill complex' (AMC) particulates briefly utilised in certain RBCs during the late 1980s [Lutz & Philips, 1983; Roulet, 1987; Willems et al., 1992]. AMC fillers consisted of primary inorganic particles (1-100nm diameter) produced either by hydrolysis or precipitation and subsequent heat treatment at 600°C to agglomerate the primary particles to secondary particles possessing a size distribution of 0.5-50μm. The AMC particles were admixed with pyrolytic silica particles (0.05μm diameter) into an organic resin matrix. A number of commercial RBCs containing AMC particles were introduced in the 1980s, including Nimetic-Dispers (ESPE, Seefeld, West Germany) and Answer (Johnson & Johnson, East Windsor, NJ, US) with a filler loading of 39.8 and 39.1vol% and a mean sintered agglomerate particle size of 13.8 and 20.7μm, respectively [Willems et al., 1992]. However, comparative studies of Young's modulus highlighted that these products did not compare favourably with other commercially available restorative dental RBCs [Braem et al., 1986b; 1987]. The 'nanocluster' fillers studied possess a remarkable similarity with AMC fillers due to similar production techniques (Section 3.1.2) and microstructure (Figures 4.4, 5.12 and 6.4) to that described for the AMC, although the

'nanocluster' was markedly smaller (≤5.0μm). This may suggest that the 'nanocluster' is a development or refinement of this pre-existing technology, nevertheless studies of Filtek™ Supreme have highlighted that modern 'nanocluster' reinforcement produces mechano-physical properties at least comparable with conventionally filled materials [Kleverlaan & Feilzer, 2005; Lu et al., 2006; Beun et al., 2007; Turssi et al., 2007; Watanabe et al., 2008].

The classification of so-called 'nanofill' and 'nano-hybrid' RBCs remains an issue of considerable contention within the dental literature [CARE, 2003; Mitra et al., 2003; Harris & Ure, 2006; Junior et al., 2008]. Furthermore, these materials do not fit into the accepted classification scheme developed by Lutz & Philips (1983), whereby specific mechanical properties were attributed to specific filler loadings, size and morphology. This may suggest that more than twenty-five years since its introduction this scheme requires updating to remain relevant to modern dental restorative materials, such as 'packable' [Leinfelder et al., 1998; Combe & Burke, 2000], 'flowable' [Combe & Burke, 2000; Sabbagh et al., 2004], 'universal' [Cobb et al., 2000; Manhert et al., 2001] nanohybrid and 'nanofill' [Mitra et al., 2003; Beun et al., 2007] RBCs. The development of RBCs previously included distinct modification of the filler size and improved the filler distribution [Lutz & Philips, 1983; Roulet, 1987], whilst the subtle and often incremental modification of filler or resin during the development of modern materials (Section 1.3.2) has often rendered classification difficult.

The description of materials as 'nano' implies that these materials are an aspect of the field of nanotechnology and therefore will possess specific advantages due to features within the 'nano' range. Subsequently, there is considerable debate concerning the relevance of the 'nano' prefix to modern dental RBCs and the specific improvements provided by so-called nanoparticles compared with existing materials [CARE, 2003; Mitra et al., 2003; Harris & Ure, 2006]. 'Nanomaterials' are generally defined as possessing components and/or structural features with at least one dimension of <100nm and to subsequently demonstrate novel and distinct properties [Harris & Ure, 2006; Lui & Webster, 2007]. The discrete nano-sized (5-20 and 75nm) fillers comply with the first part of this definition, whilst the agglomerated 'nanoclusters' are markedly larger at 0.6-1.4μm according to the manufacturer or as identified in the current study up to approximately 5μm (Figures 4.4, 5.12 and 6.4). Despite this the 'nanoclusters' are agglomerates of constituent nanosized particles (5-20 and 75nm), suggesting compliance with the definition. To comply with the second part of the definition the material must possess novel and distinct

properties due to the presence of the feature described as being 'nano'. This is where considerable contention arises as some studies have suggested that 'nanoclusters' are simply a microhybrid-type particle under a different name, a name assumed due to marketing considerations rather than in relation to a specific technological advancement [CARE, 2003; Junior et al., 2008]. In contrast, previous studies of the 'nanocluster' reinforced RBC have highlighted that the mechano-physical properties were at least comparable, and on occasion superior, to the other RBCs investigated. Beun et al. (2007) identified that the elastic modulus, flexure strength and surface hardness of FSB, in addition to GR and GF, was superior to microfilled RBCs and comparable with the universal RBCs studied. Likewise, Mota et al. (2006) highlighted that of several commercial nanofills tested, FSB and GR exhibited superior mechanical properties when compared with 4 Seasons (Ivoclar Vivadent), Esthet-X Improved (Dentsply) and Palfique Estelite (Tokuyama Dental Corp.). The fracture toughness of FSB, and also FZ, was determined by Watanabe et al. (2008) to be superior to that of the microhybrid and microfills also studied. The polymerization shrinkage of FSB was identified by Kleverlaan & Feilzer (2005) to be 2.5vol%, which compared favourably with the other RBCs studied (2.0-5.6vol%). Likewise, Lu et al. (2006) identified that FSB exhibited the lowest polymerization shrinkage of the particular materials selected in that study. A study of the tensile, compressive and flexural strengths and also the fracture resistance conducted by Mitra et al. (2003) also identified that the 'nanocluster' reinforced RBC compared favourably with, or were superior to, the other commercially available RBCs studied, although this may not be surprising considering Mitra et al. (2003) developed the material. Furthermore, Turssi et al. (2007) highlighted that the wear and fatigue resistance of FSB, and also GR, was comparable with the microfill, although the other nanofills did not compare as favourably. Furthermore, the current study highlighted that the 'nanocluster' reinforced RBCs possessed unique failure mechanisms and enhanced damage tolerance due to absorption and dissipation of repeated stresses following pre-loading, which may suggest that the clinical occurrence of low stress failures may be reduced or eliminated. Consequently, when considering whether 'nanoclusters' fulfil the second caveat defining a 'nanomaterial', namely the provision of distinct properties due to the 'nano' feature, whilst it is difficult to provide a definitive answer the balance of probability seems to suggest this to be the case.

**Summary**

In summary, the unique fracture mechanisms exhibited by the 'nanocluster' particles and the IPC-like structure provided distinct improvements to the resistance to fracture and reliability, thus enhancing the damage tolerance and clinical longevity of the 'nanocluster' reinforced RBC. In contrast, the specific resin matrix chemistry and also the limited hydrolytic stability of the 'nanocluster' particles in solvents may reduce the fracture resistance and long-term efficacy of the 'nanocluster' reinforced RBC. Nevertheless, the ongoing development of hydrophobic resin matrix derivatives [Moszner et al., 2007b; Perieira et al., 2007] and alternative silane coupling agents [Debnath et al., 2004; Sabbagh et al., 2004; Torry et al., 2006] may enable the potential enhanced damage tolerance of 'nanocluster' reinforced RBCs to be realised.

# CHAPTER 8 CONCLUSIONS

The null hypothesis stated that the 'nanocluster' particle complex would not exhibit differing fracture mechanisms compared with conventional filler particles and also that 'nanocluster' reinforced RBCs would not exhibit significantly different mechanical properties compared with existing RBCs. This was rejected by the current study which identified that the 'nanoclusters' exhibited unique fracture mechanisms, improved fracture resistance and reliability following pre-loading, although the long-term hydrolytic stability of the 'nanocluster' RBC was identified to be limited.

In conclusion,

1. Micromanipulation of the agglomerated 'nanocluster' complexes highlighted a tendency to multiple fractures compared with conventional fillers. The fracture strength and pseudo-modulus of stress of the 'nanoclusters' was consistently higher than either the spheroidal or irregular particles. Furthermore, the efficacy of the micromanipulation technique was established.

2. Cyclic pre-loading of the 'nanocluster' RBCs generated statistically similar or significantly increased bi-axial flexure strengths and associated Weibull moduli at pre-loads (50 and 100N) that initiated catastrophic failure of the other RBCs tested. Furthermore, 'wet' storage of the 'nanocluster' RBC produced a significant increase in fracture strength and reliability compared with specimens stored 'dry'. Subsequently, the 'nanocluster' particle was identified to provide unique reinforcement to the resin matrix. The combination of unique reinforcement identified by micromanipulation and silane infiltration of structural porosities improved the damage tolerance of the 'nanocluster' material and may enhance the clinical longevity of restorations.

3. A residual quantity of water was identified by NIRS bound in the resin matrix following dehydration and 'dry' storage. Water content increased proportionally with time until the hydrophilic resin matrix and silane interface of FSB, FZ and GF became saturated

between one and thirteen weeks. Conversely, water sorption into FST and GR continued to increase throughout the study, due respectively to the higher content of non-aggregated nanofiller (FST) or high filler loading (GR) which provided an increased surface-area-to-volume ratio for silanization and thus available for water uptake.

4. Long-term storage of the 'nanocluster' RBCs in water reduced the mechanical properties to a significantly greater extent compared with the other materials tested, suggesting that the long-term hydrolytic stability of the 'nanoclusters' was limited and degradation of the silane interface caused the 'nanoclusters' to act as defect centres.

5. Storage in sodium hydroxide and ethanol accelerated degradation of the RBCs. FTIR and SEM following immersion in sodium hydroxide for two weeks highlighted degradation of the silane interface and subsequent microcracking. Ethanol storage highlighted that the resin matrix chemistry of FSB, FST and FZ, which was identical with the exception of the higher content of CQ in FST, limited the mechanical properties compared with the other RBCs tested. This was attributed to the $BisEMA_6$ monomer and absence of TEGDMA which enhanced the surface hardness of Z100, GR and GF.

In summary, whilst the long-term hydrolytic stability of the 'nanocluster' reinforced RBC was limited by the specific resin matrix chemistry and degradation of the interfacial silane layer, repeated sub-critical loading provided enhanced damage tolerance due to the ability of the 'nanocluster' to deform and absorb or dissipate crack stresses. This may provide improved resistance to low stress failures and subsequently increase the clinical longevity of 'nanocluster' reinforced RBC restorations.

# CHAPTER 9 RECOMMENDED FURTHER WORK

Interfacial failure of the siloxane bridge bonds produced by the silane coupling agent at the filler/resin interface occurred as a consequence of the storage regimes employed, which generated microcracks and limited the longevity of the RBCs. However, the extent of interfacial degradation was not quantifiable. It is therefore suggested that this should be characterized using an atomic force microscope (AFM) with nano-indentation attachment. In essence the nano-indentation technique will produce an array of indentations to determine the hardness of a specific area, enabling the hardness of the filler/silane/resin interface to be quantified and the extent of degradation to be determined.

The extensive degradation of the 'nanocluster' RBC due to water storage studies contradicted the enhanced damage tolerance suggested by micromanipulation and pre-loading results. Therefore a combination of pre-loading prior to long-term water storage may further elucidate the reinforcement provided by the 'nanoclusters', particularly if deformation of the 'nanoclusters' is required to provide the enhanced damage tolerance identified.

The NIR study of water sorption highlighted a discrepancy compared with results which may be obtained using the generally accepted gravimetric analysis technique, specifically NIR identified a quantity of water bound in the resin matrix even following dehydration whilst gravimetric analysis assumes water to have been eliminated. This suggests that additional study of a range of RBC materials should be conducted to compare the water content determined using NIR and gravimetric analysis to establish a 'true' value of water content for the materials.

The efficacy of employing the micromanipulation technique to characterize the mechanical properties of the micro-sized filler particles was determined. However, the micromanipulation rig was operating at the limit of what was achievable with the sensitivity of this technique. Therefore, to further characterize the properties of the 'nanoclusters', particularly smaller sub-micron clusters, and also the ubiquitous sub-micron silica fillers within many modern RBCs it is proposed that a nanomanipulation technique be employed. The nanomanipulation technique proposed [Liu et al., 2005; 2007] is a direct development of the micromanipulation

technique employed in the current study and essentially operates on the same principles whereby single nano-sized particles are compressed to failure. In this case loading occurs within an ESEM chamber to provide considerably higher image resolution and enable recording of the nanoparticles undergoing failure [Liu et al., 2005; 2007]. Furthermore, the nanomanipulation technique may be used to load and unload the 'nanoclusters' without inducing failure, or using a staircase-like fatigue technique (Section 2.2.3.1), thereby allowing study of the elastic recovery and damage tolerance of the 'nanocluster' particles.

The current study evaluated a commercial material to determine the mechanical and physical properties provided by a unique filler-type. Therefore, to further elucidate the effect of nanoscale particulates on deformation characteristics of resin-based composites, model systems may be investigated to determine the effect of various filler fraction proportions of agglomerated 'nanoclusters' to discrete nanoparticles on the long-term mechano-physical properties.

## REFERENCES


Abdalla MO, Dean D and Campbell S. Viscoelastic and mechanical properties of thermoset PMR-type polyimide-clay nanocomposites. Polymer, 2002; 43: 5887-5893.

Adabo GL, dos Santos Cruz CA, Fonseca RG and Vaz LG. The volumetric fraction of inorganic particles and flexural strength of composites for posterior teeth. Journal of Dentistry, 2003; 31: 353-359.

Aguiar FHB, Braceiro ATB, Ambrosano GMB and Lovadino JR. Hardness and diametral tensile strength of hybrid composite resin polymerised with different modes and immersed in ethanol or distilled water media. Dental Materials, 2005; 21; 1098-1103.

Aldrich Library of FTIR spectra. Aldrich, US; 1997 (2nd Edition): Vol.3 Spectra 4337-4439.

Alexandre M and Dubois P. Polymer-layered nanocomposites: preparation, properties and uses of a new class of materials. Materials Science and Engineering, 2000; 28: 1-63.

Al-Hiyasat AS, Darmani H and Milhem MM. Cytotoxicity evaluation of dental resin composites ad their flowable derivatives. Clinical Oral Investigations, 2005; 9: 21-25.

Alvin HH, Alecio AC, Vasconcellos WA, Furlan M, Oliverira JE and Saad JRC. Analysis of camphorquinone in composite resin as a function of shade. Dental Materials, 2007; 23: 1245-1249.

Anderson D. Measurement of stress in mastication. Journal of Dental Research, 1956; 35: 664-671.

Anagnostopoulos T, Eliades G and Palaghias G. Composition, reactivity and surface interactions of three dental silane primers. Dental Materials, 1993; 9: 182-190.

Anseth KS, Bowman CN and Brannon-Peppas L. Mechanical properties of hydrogels and their experimental determination: Review. Biomaterials, 1996; 17: 1647-1657.

Antonucci JM, Dickens S, Fowler BO, Hockin H, Xu K and McDonough WG. Chemistry of silanes: interfaces in dental polymers and composites. Transactions of the Academy of Dental Materials, 2003; 17: 81-109.

Asaoka K and Hirano S. Diffusion of water through dental composite resin. Biomaterials, 2003; 24: 975-979.

Asmussen E. Restorative resins: hardness and strength vs quantity of remaining double bonds. Scandanvian Journal of Dental Research, 1982; 90: 484-489.

Asmussen E. Softening of BisGMA-based polymers by ethanol and by organic acids of plaque. Scandinavian Journal of Dental Research, 1984; 92: 257-261.

Asmussen E and Peutzfeldt A. Influence of UEDMA, BisGMA and TEGDMA on selected mechanical properties of experimental resin composites. Dental Materials, 1998; 14: 44-50.

Asmussen E and Peutzfeldt A. Influence of selected components on crosslink density in polymer structures. European Journal of Oral Science, 2001a; 109: 282-285.

Asmussen E and Peutzfeldt A. Influence of pulse-delay curing on softening of polymer structures. Journal of Dental Research, 2001b; 80: 1573-1573.

Asmussen E and Peutzfeldt A. Influence of composition on rate of polymerisation contraction of light-curing resin composites. Acta Odontology Scandinavia, 2002; 60: 146-150.

Asmussen E and Peutzfeldt A. Two-step curing: influence on conversion and softening of a dental polymer. Dental Materials, 2003a; 19: 466-470.

Asmussen E and Peutzfeldt A. Polymer structure of a light-cured resin composite in relation to distance from the surface. European Journal of Oral Science, 2003b; 111: 277-279.

Atmadja G and Bryant RW. Some factors influencing the depth of cure of visible light activated composite resins. Australian Dental Journal, 1990; 35: 213-218.

Aw TC and Nicholls JI. Polymerisation shrinkage of densely-filled resin composites. Operative Dentistry, 2001; 26: 498-504.

Badra VV, Faraoni JJ, Ramos RP and Palma-Dibb. Influence of different beverages on the microhardness and surface roughness of resin composites. Operative Dentistry, 2005; 30: 213-219.

Bagheri R, Tyas, MJ and Burrow MF. Subsurface degradation of resin-based composites. Dental Materials, 2007; 23: 944-951.

Ban S and Anusavice KJ. Influence of the test method on failure stress of brittle dental materials. Journal of Dental Research, 1990; 69: 1791-1799.

Ban S, Hasegawa J and Anusavice KJ. Effect of loading conditions on bi-axial flexure strength of dental cements. Dental Materials, 1992; 8: 100-104.

Başeren M. Surface roughness of nanofill and nanohybrid composite resin and ormocer-based tooth coloured restorative materials after several finishing and polishing procedures. Journal of Biomaterials Applications, 2004; 19: 121-134.

Bastoli C, Romano G and Migliaresi C. Water sorption and mechanical properties of dental composites. Biomaterials, 1990; 11: 219-223.

Berenbaum B and Brodie I. Measurement of the tensile strength of brittle materials. British Journal of Applied Physics, 1959; 10: 281-287.

Bertelsen CM and Boerio FJ. Linking mechanical properties of silane to their chemical structure: an analytical study of γ-GPS solutions and films. Progress in Organic Coatings, 2001: 41; 239-246.

Beun S, Glorieux T, Devaux J, Vreven J and Leloup G. Characterization of nanofilled compared with universal and microfilled composites. Dental Materials, 2007; 23: 51-59.

Bhamra G, Palin WM and Fleming GJP. The effect of surface roughness on the flexure strength of an alumina reinforced all-ceramic crown material. Journal of Dentistry, 2002; 30: 153-160.

Bhimaraj P, Burris DL, Action J, Sawyer WG, Toney CG, Siegel RW and Schadler LS. Effect of matrix morphology on the wear and friction behaviour of alumina nanoparticles/poly(ethylene) terephthalate composites. Wear, 2005; 258: 1437-1443.

Black GV. Amalgam and amalgam fillings. British Journal of Dental Science, 1896; 39: 370-374.

Blewett J, Burrows K and Thomas C. A micromanipulation method to measure the mechanical properties of single tomato suspension cells. Biotechnology Letters, 2000; 22: 1877-1883.

Bogacki RE, Hunt RJ, Aguila M and Smith WR. Survival analysis of posterior restorations using an insurance claims database. Operative Dentistry, 2002; 27: 488-492.

Bouillaguent S, Shaw L, Gonzalez L, Wataha JC and Krejci I. Long-term cytotoxicity of resin-based dental restorative materials. Journal of Oral Rehabilitation, 2002; 29: 7-13,

Bouwman AM, Henstra MJ, Westerman D, Chung JT, Zhang Z, Ingram A, Seville JPK and Frijlink HW. The effect of the amount of binder liquid on the granulation mechanisms and structure of microcrystalline cellulose granules prepared by high shear greanulation International Journal of Pharmaceutics, 2005; 290: 129-136.

Bowen RL. Use of epoxy resins in restorative materials. Journal of Dental Research, 1956; 35: 360-369.

Bowen RL. Synthesis of a silica-resin direct filling material: progress report. Journal of Dental Research, 1958; 37: 90-91.

Bowen RL. Dental filling materials comprising of vinyl-silane fused silica and binder consisting of the reaction product of bispenol and glycidyl methacrylate. US Patent 3066112 (1962a).

Bowen, R.L and Rodriguez, M.S. Tensile strength and modulus of elasticity of tooth structure and several restorative materials. Journal of the American Dental Association, 1962b; 64: 378-387.

Bowen RL. Effect of particle shape and size distribution in a reinforced polymer. Journal of the American Dental Association, 1964; 66: 57-65.

Bowen RL and Reed LE. Semi-porous reinforcing fillers for composite resins: I. preparation of provisional glass formulations. Journal of Dental Research, 1976: 55: 738-747.

Braden M. Selection and properties of some new dental materials. Dental Update, 1974; 1: 489-501.

Braem M, Lambrechts P, Van Doren V and Vanherle G. *In vivo* evaluation of four posterior composites: quantitative wear measurements and clinical behaviour. Dental Materials, 1986; 2: 106-113.

Braem M, Lambrechts P, Van Doren V and Vamherle G. The impact of composite structure on its elastic response. Journal of Dental Research, 1986b; 64: 648-653.

Braem M, Van Doren VE, Lambrechts P, and Vanherle G. Determination of Young's modulus of dental composites: a phenomenological model. Journal of Materials Science, 1987; 22: 2037-2042.

Braem M, Lambrechts P, Gladys S and Vanherle G. *In vitro* fatigue behaviour of restorative composites and glass ionomers. Dental Materials, 1995; 11: 137-141.

Braga RR and Ferracane FL. Alternatives in polymerisation contraction stress management. Critical Review of Oral Biological Medicine, 2004; 15: 176-184.

Braga RR, Ballester RY and Ferracane JL. Factors involved in the development of polymerisation shrinkage stress in resin-composites: a systematic review. Dental Materials, 2005; 21: 962-970.

Bratel J, Haraldson T, Meding B, Yontchev E, Ohman SC and Ottosson JO. Potential side effects of dental amalgam restorations (I). An oral and medical investigation. European Journal of Oral Science, 1997a; 105: 234-243.

Bratel J, Haraldson T and Ottosson JO. Potential side effects of dental amalgam restorations (II). No relation between mercury levels in the body and mental disorders. European Journal of Oral Science, 1997b; 105: 244-250.

Brentel AS, Özcan M, Valandro LF, Alarca LG, Amaral R and Bottino MA. Microtensile bond strength of a resin cement to feldspathic ceramic after different etching and silanization regimes in dry and aged conditions. Dental Materials, 2007; 23: 1323-1331.

Breschi L, Mazzoni A, Ruggeri A, Cadenaro M, Lenarda RD and Dorigo EDS. Dental adhesion review: aging and stability of the bonded interface. Dental Materials, 2008; 24: 90-101.

Brosh T, Ganor Y, Belov I and Pilo R. Analysis of strength properties of light-cured resin composites. Dental Materials, 1999; 15: 174-179.

Buonocore MG. A simple method of increasing the adhesion of acrylic filling materials to enamel surfaces. Journal of Dental Research, 1955; 34:849-853.

Burke, FJT. Amalgam to tooth-coloured materials-implications for clinical practice and dental education: governmental restrictions and amalgam-usage survey results. Journal of Dentistry 2004; 32, 343-350.

Cadenaro M, Breschi L, Antoniolla F, Navarra CO, Mazzoni A, Tay FR, Di Lenarda R and Pashley DH. Degree of conversion of resin blends in relation t ethanol content and hydrophilicity. Dental Materials, 2008; In Print.

Calais JG and Söderholm 1988. Influence of filler type anmd water exposure on flexural strength of experimental composite resins. Journal of Dental Research, 1988; 67: 836-840.

Calheiros F, Kawano Y, Stansbury JW and Braga RR. Influence of radiant exposure on concentration stress, degree of conversion and mechanical properties of resin composites. Dental Materials, 2006; 22: 799-803.

Cannon MS, Kapes ED and Palkuti GA. Dr. Black and the amalgam question. Journal of the History of Medicine, 1985; 40: 309-326.

CARE group of professional services; Ivoclar Vivadent Inc. Nanofillers?: A microfill by any other name is still a microfill. Nanofillers, August 2003.

Carioscia JA, Lu H, Stansbury JW and Bowman CN. Thiol-ene oligomers as dental restorative materials. Dental Materials, 2005; 21: 1137-1143.

Casselli DSM, Worschech CC, Paulillo LAMS and Dias CTS. Diametral tensile strength of composite resins submitted to different activation techniques. Brazilian Oral Research, 2006; 20: 214-218.

Cattell MJ, Clarke RL and Lynch EJR. The biaxial flexural strength and reliability of four dental ceramics- Part II. Journal of Dentistry, 1997; 25: 409-414.

Catteni-Lorente MA, Dupuis V, Payan F, Moya F and Meyer JM. Effect of water on the physical properties of resin-modified glass ionomer cements. Dental Materials 1999; 15: 71-78.

Cesar PF, Júnior WGM and Braga RR. Influence of shade and storage time on the flexural strength, flexural modulus and hardness of composites used for indirect restorations. Journal of Prosthetic Dentistry, 2001; 86: 289-296.

Chapplelow CC, Pinzino CS, Power M and Eick JD. Photocured epoxy/SOC matrix resin systems for dental composites. Polymer Preprints 1997; 38: 90-91.

Chen MH, Chen CR, Hsu SH, Sun SP and Su WF. Low shrinkage light curable nanocomposites for dental restorative material. Dental Materials, 2006; 22: 138-145.

Chou K-S and Ren C-Y. Synthesis of nanosized silver particles by chemical reduction method. Materials, Chemistry and Physics, 2000; 64: 241-246.

Chung JT, Vlung-Wensink KDF, Hennink WE and Zhang Z. Effect of polymerisation conditions on the network properties of dex-HEMA microspheres and macro-hydrogels. International Journal of Pharmaceutics, 2005; 288: 51-61.

Clarke DR. Interpenetrating phase composites. Journal of the American Ceramics Societiy, 1992; 75: 739-759.

Cobb DS, MacGreggor KM, Vargas MA and Denehy GE. The physical properties of packable and conventional posterior resin-based composites: a comparison. Journal of the American Dental Association, 2000; 131: 1610-1615.

Cole KS. Surface forces of arbacia egg. Journal of Complete Cell Physiology, 1967; 1: 1-9.

Condon JR and Ferracane JL. Evaluation of composite wear with a new multi-mode oral wear simulator. Dental Materials, 1996; 12: 218-226.

Condon JR and Ferracane JL. Reduction of composite contraction stress through non-bonded microfiller particles. Dental Materials, 1998; 14: 256-260.

Condon JR and Ferracane JL. Reduced polymerization stress through non-bonded nanofiller particles. Biomaterials, 2002; 23: 3807-3815.

Combe EC and Burke FJT. Contemporary resin-based composite materials for direct placement restorations; packables, flowables and others. Dental Update, 2000; 27: 326-336.

Cook WD. Photopolymerization kinetics of dimethacrylates using the camphorquinone/amine initiation system. Polymer, 1992; 33: 600-609.

Cramer NB and Bowman CN. Kinetics of thiol-ene and thiol-acrylate photopolymerisations with real time Fourier transform infrared. Journal of Polymer Science; Part A: Polymer Chemistry, 2001; 39: 3311-3319.

Cunningham J, Mair LH, Foster MA and Ireland RS. Clinical evaluation of three posterior composites and two amalgam restorative materials: 3-year results. British Dental Journal, 1990; 130: 275-277.

Curtis AR, Shortall AC, Marquis PM and Palin WM. Water uptake and strength characteristics of a nanofilled resin-based composite. Journal of Dentistry, 2008: 36: 186-193.

Cury AH, Goracci C, Navarro MFL, Carvalho RM, Sadek FT, Tay FR and Ferrari M. Effect of hygroscopic expansion on the push-out resistance of glass ionomer-based cements used in luting of glass fiber posts. JOE 2006; 32: 537-540.

Daniels MW and Francis LF. Silane adsorption behaviour, microstructure and properties of glycidoxyopropyltrimethoxysilane-modified colloidal silica coatings. Journal of Colloid and Interface Science, 1998; 205: 191-200.

Darvel BW. Uni-axial compression tests and the validity of indirect tensile strength. Journal of Materials Science, 1990; 25: 757-780.

Darvell BW. Materials science for denistry. BW Darvell HK 2006; (8th Edition): Chapter 6.

Davidson CL and Feilzer AJ. Polymerisation shrinkage and polymerisation shrinkage stress in polymer-based restoratives. Journal of Dentistry, 1997; 25: 435-440.

Davies, DGS. The statistical approach to engineering design in ceramics. Proceedings of the British Ceramic Society, 1973; 22: 429-451.

Dean D, Walker R, Theodore M, Hampton E and Nyairo E. Chemorheology and properties of epoxy/layered silicate nanocomposites. Polymer, 2005; 46: 3014-3021.

Debnath S, Ranade R, Wunder SL, McCool J, Boberick K and Baran G. Dental Materials, 2004; 20: 677-686.

DeLong R and Douglas WH. An artificial oral environment for testing dental materials. IEEE Transactions on Biomedical Engineering, 1991; 38: 339-345.

DeWald JP and Ferracane JL. A comparison of four modes of evaluating depth of cure of light activated composites. Journal of Dental Research, 1987; 66: 727-730.

Diaz-Arnold AM and Williams VD. Measurement of water sorption by resin composites adhesives with near-infrared spectroscopy. Journal of Dental Research, 1992; 71: 438-442.

Ding P, Norton IT, Zhang A and Pacek AW. Mechanical properties of gelation-rich micro-particles. Journal of Food Engineering, 2008; 86: 307-314.

Dodes JE. The amalgam controversy. An evidence based analysis. Journal of the American Dental Association, 2001; 132: 348-356.

Dong XD and Darvell BW. Stress distribution and failure mode of dental ceramic structures under Hertzian indentation. Dental Materials, 2003; 19: 542-551.

Drummond JL. Cyclic fatigue of composite restorative materials. Journal of Oral Rehabilitation, 1989; 5: 509-520.

Drummond JJ and Savers EE. *In vitro* aging of a heat/pressure-cured composite. Dental Materials, 1993; 9: 214-216.

Drummond JL, Carlo FD and Super BJ. Three-dimensional tomography of composite fracture surfaces. Journal of Biomedical Materials Research, Part B: Applied Biomaterials, 2005; 74B: 669-675.

Earnshaw R and Smith DH. The tensile and compressive strength of plaster and stone. Australian Dental Journal, 1966: 415-422.

Eick JD, Smith RE, Yourtee D and Kostoryz EL. Comparative reactivities of aliphatic dioxaiane and silorane with water. Journal of Dental Research, 2004; 83 (SI-A) Abstract number 0250.

Eley BM. The future of dental amalgam: a review of the literature. Part 1: Dental amalgam structure and corrosion. British Dental Journal, 1997a; 182: 247-249.

Eliades G, Eliades T, Brantley WA and Watts DC. Dental materials *in vivo* aging and related phenomena. Quintessence Publishing Co. Inc., 2003 (1st Edition); Chap 7.

Elleka A, Cho N and Lee IB. The effect of resin matrix composition on the polymerization shrinkage and rheological properties of experimental dental composites. Dental Materials, 2007; 23: 1229-1235.

Emami N, Söderholm KJM and Berglund LA. Effect of light power density variations on bulk curing properties of dental composites. Journal of Dentistry, 2003; 31: 189-196.

Engelmeier RL. The history and development of posterior denture teeth- introduction. Part 1. Journal of Prosthodontics, 2003a; 12: 219-226.

Engelmeier RL. The history and development of posterior denture teeth- introduction. Part 2: artificial tooth development in America through the nineteenth century. Journal of Prosthodontics, 2003b; 12: 288-301.

Ernst CP, Meyer GR, Klocker K and Willerhausen B. Determination of polymerisation shrinkage stress by means of a photoelastic investigation. Dental Materials, 2004; 20: 313-321.

Fan PL, Edahl A, Leung RL and Stanford JW. Alternative interpretations of water sorption values of composite resins. Journal of Dental Research, 1985; 64: 78-80.

Feilzer AJ, Gee de AJ and Davidson CL. Setting stress in composite resin in relation to configuration of the restorations. Journal of Dental Research, 1987; 66: 1636-1639.

Feilzer AJ, Gee de AJ and Davidson CL. Quantitative determination of stress reduction by flow in composite restorations. Dental Materials, 1990; 6: 167-171.

Feilzer AJ and Dauvillier BS. Effect of TEGDMA/BisGMA ratio on stress development and viscoelastic properties of experimental two-paste composites. Journal of Dental Research, 2003; 82: 824-828.

Ferracane JL and Marker VA. Solvent degradation and reduced fracture toughness in aged composites. Journal of Dental Research, 1992; 71: 13-19.

Ferracane JL. Current trends in dental composites. Critical Review Oral Biological Medicine, 1995; 6: 302-318.

Ferracane JL, Mitchem JC, Condon JR and Todd R. Wear and marginal breakdown of composites with various degrees of cure. Journal of Dental Research, 1997; 76: 1508-1516.

Ferracane JL, Berge HX and Condon JR. *In vitro* aging of dental composites in water-effect of degree of conversion, filler volume and filler/matrix coupling. Journal of Biomedical Materials Research 1998; 42: 465-472.

Ferracane JL. Developing a more complete understanding of stresses produced in dental composites during polymerization. Dental Materials, 2005; 21: 36-42.

Ferracane JL. Hygroscopic and hydrolytic effects in dental polymer networks. Dental Materials, 2006; 22: 211-222.

Filtek™ Z100 Universal Restorative System; Technical Product Profile Filtek, Product Specification, 1993; 3M ESPE.

Filtek™ Z250 Universal Restorative System; Technical Product Profile Filtek, Product Specification, 1998; 3M ESPE.

Filtek™ Flow; Flowable Restorative, Technical Profile, 2000; 3M ESPE.

Filtek™ Supreme XT Universal Restorative System; Technical Product Profile Filtek, Product Specification, 2006; 3M ESPE.

Finer Y and Santerre JP. The influence of resin chemistry on a dental composite's biodegradation. Journal of Biomedical Materials Research, 2004; 69A: 233-246.

Fleming GJP, Shelton RM and Marquis PM. The influence of clinically induced variability on the bi-axial flexure strength of aluminous core porcelain discs. Journal of Dentistry, 1999a; 27: 587-594.

Fleming GJP, Shelton RM and Marquis PM. The influence of clinically induced variability on the biaxial fracture strength of cemented aluminous core porcelain discs. Dental Materials, 1999b; 15: 62-70.

Fleming GJP, Shaini FJ and Marquis PM. An assessment of the influence of mixing indiced variability on the bi-axial flexure strength of dentine porcelain discs and the implications for laboratory testing of porcelain specimens. Dental Materials, 2000; 16: 114-119.

Fleming GJP, Burke FJT, Watson DJ and Owen FJ. Materials for restoration of primary teeth: 1. conventional materials and early glass ionomers. Dental Update, 2001; 28: 486-491.

Fleming GJP, Hall D, Shortall ACC and Burke FJT. Cuspal movement and microleakage in premolar teeth restored with posterior filling materials of varying reported shrinkage values. Journal of Dentistry, 2005; 33: 139-146.

Fleming GJP, Awan M, Cooper PR and Sloan AJ. The potential of a resin-composite to be cured to a 4 mm depth. Dental Materials, 2008; 24: 522-529.

Floyd CJE and Dickens SH. Network structure of BisGMA and UDMA based resin systems. Dental Materials, 2006; 22: 1143-1149.

Freund M and Munksgaard EC. Enzymatic degradation of BisGMA/TEGDMA polymers causing decreased microhardness and greater wear *in vitro*. Scandinavian Journal of Dental Research, 1990; 98: 351-355.

Garoushi S, Vallittu PK and Lassila LVJ. Short glass fibre reinforced restorative composites resin with semi-inter penetrating polymer network matrix. Dental Materials, 2007; 23: 1356-1362.

Ge J, Trujillo M and Stansbury J. Synethesis and photopolymerization of low shrinkage methacrylate monomers containing bulky substituent groups. Dental Materials, 2005; 51: 1163-1169.

Gee de AJ and Pallav P. Occusal wear simulation with the ACTA wear machine. Journal of Dentistry Supplement, 1994; 22: S21-27.

Gelbier S. 125 years of developments in dentistry 1880-2005, Part 3: dental equipment and materials. British Dental Journal, 2005; 199: 536-539.

Geurtsen W. Biocompatibility of resin-modified filling materials. Critical Review of Oral Biological Medicine. 2000; 11: 333-355.

Geurtsen W and Leyhausen G. Chemical-biological interactions of the resin monomer triethyleneglycol-dimethacrylate (TEGDMA). Journal of Dental Research, 2001; 80: 2046-2050.

Gladys S, Van Meerbeek B, Braem M, Lambrechts P and Vanherle G. Comparative physico-mechanical characterization of new hybrid restorative materials with conventional glass ionomer and resin composite restorative materials. Journal of Dental Research, 1997; 76: 883-894.

Glynn PAR and Van der Hoff BME. A general model for the prediction of molecular weight distributions of degraded polymers. Development and comparison with ultrasonic degradation experiments. Journal of Macromolecular Science, Part A; 1972; 6: 1653-1664.

Göhring TN, Gallo L and Luthy H. Effect of water storage, thermocycling, the incorporation and site of placement of glass-fibers on the flexural strength and veneering composite. Dental Materials, 2005; 21: 761-772.

Göpferich A. Mechanisms of polymer degradation and erosion. Biomaterials, 1996; 17: 103-114.

Graf H. Bruxism. Dental Clinics of North America, 1969; 13: 659-668.

Grandio/Grandio Flow; Scientific Documentation, 2006; Voco.

Grant AA and Greener EH. Whisker reinforcement of polymethyl methacrylate denture base resins. Australian Dental Journal, 1967; 12: 29-33.

Griffith AA. The phenomena of rupture and flow in solids. Philosophical Transactions of the Royal Society, 1920; A221-222: 163-198.

Guzmán J, Iglesias MT and Riande E. Synthesis and kinetics of polymerisation of acrylic and methacrylic monomers containing 1,3-dioxane groups in their structure. Journal of Polymer Science A: Polymer Chemistry, 1996; 35: 1125-1132.

Halvorson RH, Erickson RL and Davidson CL. Energy dependent polymerisation of resin-based composites. Dental Materials, 2002; 18: 463-469.

Harrington E and Wilson HJ. Depth of cure of radiation-activated materials- effect of mould material and cavity. Journal of Dentistry, 1993; 21: 305-311.

Harris J and Ure D. Exploring whether ‘nano’ is always necessary. Nanotechnology Perceptions, 2006; 2: 1-15.

Helkimo E. Bite force and functional state of the masticatory system. Swedish Dental Journal, 1978; 2: 167-175.

Hillam C. The Roots of Dentistry. Lindsey Society for the History of Dentistry. British Dental Association. Willam Clowes Ltd., 1990; (1st Edition): Chapters 1 and 2.

Holmes RG, Rueggeberg FA, Callan RS, Caughman F, Chan DCN, Pashley DH and Looney SW. Effect of solvent type and content on monomer conversion of a model resin system as a thin film. Dental Materials, 2007; 23: 1506-1212.

Holter D, Frey H and Mulhaupt R. Branched bismethacrylates based on BisGMA- a synthetic route to low shrinkage composites. Polymer Preprints, 1997; 38: 84-85.

Hooshmand T, van Noort R and Keshvad A. Storage effect of a pre-activated silane on the resin to ceramic bond. Dental Materials, 2004; 20: 635-642.

Hörsted-Bindslev, P. Amalgam toxicity- environment and occupational hazards. Journal of Dentistry, 2004; 32: 359-365.

Hosoda H, Toshimoto Y and Shigeshisa I. SEM and elemental analysis of composite resins. Journal of Prosthetic Dentistry, 1990; 64: 669-676

Htang A, Ohsawa M and Matsumoto H. Fatigue resistance of composite restorations: effect of filler content. Dental Materials, 1995; 11: 7-13.

Hu X, Harrington E, Marquis PM and Shortall AC, The influence of cyclic loading on the wear of a dental composite. Biomaterials, 1999; 20: 907-912.

Hu X, Shortall AC and Marquis PM. Wear of three dental composites under different testing conditions. Journal of Oral Rehabilitation, 2002; 29: 756-764.

Hume WR and Gerzina TM. Bioavailability of components of resin-based materials which are applied to teeth. Critical Review of Oral Biological Medicine, 1996; 7: 172-179.

Hunter G, Lane DM, Scrimgeous SN, McDonald PJ and Lloyd CH. Measurement of the diffusion of liquids into dental restorative resins by stray-field nuclear magnetic resonance imagining (STRAFI). Dental Materials, 2003; 19: 632-638.

Hyson JM. Amalgam: its history and perils, review. Canadian Dental Association Journal, 2006; 34: 215-229.

Ikejima I, Nomoto R and McCabe JF. Shear punch strength and flexural strength of model composites with varying filler volume fraction, particle size and silanation. Dental Materials, 2003; 19: 206-211.

Indrani DJ, Cook WD, Televantos F, Tyas MJ and Harcourt JK. Fracture toughness of water-aged resin composite restorative materials. Dental Materials, 1995; 11: 201-207.

International Standards Organisation. Dentistry - Polymer-based filling restorative and luting materials. ISO 4049, 2000; (3rd Edition): 15-18.

Ishida H and Koenig JL. Fourier transform infrared spectroscopic study of the structure of silane coupling agent on e-glass fiber. Journal of Colloid and Interface Science, 1978; 64: 565-576.

Ito S, Masanori H, Wadgaonkar B. Svizero N, Carvalho M, Yiu C, Rueggebery FA, Foulger S, Saito T, Nishitani Y, Yoshiyama M, Tay FR and Pashley DH. Effects of resin hydrophilicity on water sorption and changes in modulus of elasticity. Biomaterials, 2005; 26: 6449-6459.

Jackson RD and Morgan M. The new posterior resins and a simplified placement technique. Journal of the American Dental Association, 2000; 131: 375-383.

Janda R, Roulet JF, Latta M and Rüttermann St. The effects of thermocycling on the flecural strength and flexural modulus of modern resin-based filling materials. Dental Materials, 2006; 22: 1103-1108.

Jandt KD, Mills RW, Blackwell GB and Ashworth SH. Depth of cure and compressive strength of dental composites cured with blue light emitting diodes (LEDs). Dental Materials, 2000; 16: 41-47.

Jardret V, Zahouani H, Loubet JL and Mathia TG. Understanding and quantification of elastic and plastic deformation during a scratch test. Wear, 1998; 218: 8-14.

Johannson OK, Stark FO, Vogel GE and Fleischmann RM. Evidence for chemical bond formation at silane coupling agent interfaces. Journal of Composite Materials, 1967; 1: 278-292.

Johnson LN, Asgar K and Peyton FA. Microanalysis of copper-tin phases in dental amalgam. Journal of Dental Research, 1969; 48: 872-878.

Jones DW. Has dental amalgam been torpedoed and sunk? Journal of Dental Research, 2008; 87: 101-102.

Jørgensen KD. Structure and corrosion of dental amalgams. Acta Odontology Scandinavia, 1970; 28: 129-142.

Jørgensen KD, Horsted P, Janum O, Krogh J and Schultz J. Abrasion of class 1 restorative resins. Scandinavian Journal of Dental Research, 1979; 87: 140-145.

Junior SAR, Ferracane JL and Bona AD. Flexural strength and Weibull analysis of a microhybrid and a nanofilled composite evaluated by 3- and 4-point bending tests. Dental Materials, 2008; 24; 426-431.

Kalachandra S. Influence of fillers on water sorption of composites. Dental Materials, 1989; 5: 283-288.

Kawakami Y, Takeshige F, Hayashi M and Ebisu S. Fatigue of tooth-coloured restoratives in an aqueous environment. Dental Materials Journal, 2007; 26: 1-6.

Kececi AD, Kaya U and Adanir N. Micro push-out bond strengths of four fiber-reinforced composite post systems and 2 luting materials. Oral Surgery, Oral Medical, Oral Pathology, Oral Radiology and Endodology, 2008; 105: 121-128.

Kendall, K. Complexities of compression failure. Proceedings of the Royal Society of London, 1978; A361: 245-249.

Keyworth DA. Determination of water by near-infrared spectrophotometry. Talanta, 1961; 8: 461-469.

Kleverlaan CJ and Feilzer AJ. Polymerisation shrinkage and contraction stress of dental resin composites. Dental Materials, 2005; 21: 1150-1157.

Khan AM, Suzuki H, Nomura Y, Taira M, Wakasa K, Shintani H and Yamaki M. Characterization of inorganic fillers in visible-light cured dental composites. Journal of Oral Rehabilitation, 1992; 19: 361-370.

Kim O and Shim WJ. Studies on the preparation and mechanical properties of esthetic polymeric dental restoratives using silane treated silica microfiller via freeze-drying. Polymer Composites, 2001; 22: 650-659.

Kingery WD, Bowen HK and Uhlmann DR. Microstructure of ceramics. Introduction to Ceramics. John Wiley and Sons, New York, 1976; (1st Edition): Chapter 15.1.

Lang BR, Jaarda M and Wang RF. Filler particle size and composite resin classification systems. Journal of Oral Rehabilitation, 1992; 19: 569-584.

Langitan FB and Lawn BR Effect of reactive environment on the Hertzian strength of brittle solids. Journal of Applied Physics, 1970; 41: 3357-3365.

Langworth S, Sällsten G, Barregård L, Cynkier I, Lind ML and Söderman E. Exposure to mercury vapor and impact on health in the dental profession in Sweden. Journal of Dental Research, 1997; 76: 1397-1404.

Larsen IB and Munksgaard EC. Effect of human saliva on surface degradation of composite resins. Scandinavian Journal of Dental Research, 1991; 99: 254-261.

Lee SY, Huang HM, Lin CY and Shih YH. Leached compoents from dental composites in oral simulating fluids and the resultant composite strengths. Journal of Oral Rehabilitation, 1998; 25: 575-588.

Lee SK, Tandon R, Ready MJ and Lawn BR. Scratch damage on zirconia ceramics. Journal of the American Ceramics Society, 2000; 83: 1428-1432.

Lee Y-K. Influence of scattering/absorption characteristics on the colour if resin composites. Dental Materials, 2007; 23: 124-131.

Leinfelder KF. Wear patterns and rates of posterior composite resins. International Dental Journal, 1987; 37: 152-157.

Leinfelder KF. Posterior composite resins: the materials fall short. Journal of the American Dental Association, 1995; 126: 663-676.

Leinfelder KF, Radz GM and Nash RW. A report on a new consdensable composite resin. Compendium of Continuing Education in Dentistry, 1998; 19: 230-237.

Leinfelder KF, Bayne SC and Swift EJ. Packable composites: overview and technical considerations. Journal of Esthetic Dentistry, 1999; 11: 234-249.

Li H, Khor KA and Cheang P. Adhesive and bending failure of thermal sprayed hydroapatite coatings:effect of nanostructures at interface ad crack propagation phenomenon during bending. Engineering Fracture Mechanics, 2007; 74: 1894-1903.

Liebenberg WH. Assuring restorative integrity in extensive posterior resin composite restorations: pushing the envelope. Quintessence International, 2000; 31: 153-162.

Liu T, Donald AM and Zhang Z. Novel micromanipulation in environmental scanning electron microscope for measuring mechanical properties of single nanoparticles. Materials Science and Technology, 2005; 21: 289-294.

Liu W, Aziz NA, Zhang Z and Fryer PJ. Quantification of cleaning of egg albumin deposits using micromanipulation and direct observation techniques. Journal of Food Engineering, 2007; 78: 217-224.

Lloyd CH and Mitchell L. The fracture toughness of tooth coloured restorative materials. Journal of Oral Rehabilitation, 1984; 11: 257-268.

Lohbauer U, Horst T, Frankenberger R, Kramer N and Petschelt A. Flexural fatigue behaviour of resin composite dental restoratives. Dental Materials, 2003a; 19: 435-440.

Lohbauer U, Frankenberger R, Kramer N and Petschelt A. Time-dependent strength and fatigue resistance of dental direct restorative materials. Journal of Materials Science: Materials in Medicine, 2003b; 14: 1047-1053.

Lohbauer U, Horst T, Frankenberger R, Kramer N and Petschelt A. Strength and fatigue performance versus filler fraction of different types of direct dental restoratives. Journal of Biomedical Materials Research, Part B: Applied Biomaterials, 2006; 76B, 114-120.

Loomans BAC, Opdam NJM, Roeters JFM, Bronkhorst EM and Plasschaert AJM. Influence of composite resin consistency and placement technique on proximal tightness of Class II restorations. Journal of Adhesive Dentistry, 2006; 8: 305-310.

Lu H, Carioscia JA, Stansbury JW and Bowman CN. Investigations of step-growth thiol-ene polymerizations for novel dental restoratives. Dental Materials, 2005; 21: 1129-1136.

Lu H, Lee YK, Oguri M and Powers JM. Properties of a dental resin composite with a spherical inorganic filler. Operative Dentistry, 2006; 31: 734-740.

Lucarotti PSK, Holder RL, Burke FJT. Outcome of direct restorations placed within the general dental services in England and Wales - (Part 1): Variation by type of restoration and re-intervention, Journal of Dentistry, 2005; 33: 805-815.

Lui H and Webster TJ. Nanomedicine for implants: a review of studies and necessary experimental tools. Biomaterials, 2007; 28: 354-369.

Luo J, Seghi R and Lannutti J. Effect of silane coupling agents on the wear resistance of polymer-nanoporous silica gel dental composites. Materials Science for Engineering C, 1997; 5: 15-22.

Luo J, Lannutti JJ and Seghi RR. Effect of filler porosity on the abrasion resistance of nanoporous silica gel/polymer composites. Dental Materials, 1998; 14: 29-36.

Lutz F and Philips RW. A classification and evaluation of composite resin systems. Journal of Prosthetic Dentistry, 1983; 50: 480-488.

Mackert JR and Berglund A. Mercury exposure from dental amalgam fillings: absorbed dose and the potential for adverse health effects: Review. Critical Review of Oral Biology and Medicine, 1997; 8: 410-436.

Magni E, Radovic I, ConiglioI, Papacchini F and Mazzitelli C. Bonding of self-etching adhesive/flowable composite combinations to enamel and dentin: a microtensile bond strength evaluation. Internal Dentistry SA Australian Edition, 2007; 4, 30-39.

Mahler DB. The high-copper dental amalgam alloys. Journal of Dental Research, 1997; 76: 537-541.

Mair LH. Surface permeability and degradation of dental composites resulting from oral temperature changes. Dental Materials, 1989; 5:247-255.

Mair LH. Subsurface compression fatigue in seven dental composites. Dental Materials, 1994; 10: 111-115.

Mair LH, Stolarski TA, Vowles RW and Lloyd CH. Wear: mechanisms, manifestations and measurement. Report of a workshop. Journal of Dentistry, 1996; 24:141.

Mair LH. The silver sorption layer in dental composites: three year results. Dental Materials, 1999; 15: 408-412.

Malhotra ML and Asgar K. Physical properties of dental silver-tin amalgam with high and low copper contents. Journal of the American Dental Association, 1978; 96: 444-450.

Manhart J, Kunzelmann KH, Chen HY and Hickel R. Mechanical properties and wear behaviour of light-cured packable composite resins. Dental Materials, 2000; 16: 33-40.

Manhart J, Chen HY and Hickel R. The suitability of packable resin-based composites for posterior restorations. Journal of the American Dental Association, 2001; 132: 630-645.

Manhard J, Chen H and Hamm G. Buonocore memorial lexture: review of the clinical survival or direct and indirect restorations in posterior teeth of the permanent dentation. Operative Dentistry, 2004; 29: 481-508.

Marshall GW, Marshall SJ and Bayne SC. Restorative dental materials: Scanning electron microscopy and x-ray microanalysis. Scanning microscopy, 1988; 2: 2007-2028.

Martin N, Jedynakiewicz NM and Fisher AC. Hygroscopic expansion and solubility of composite restoratives. Dental Materials, 2003; 19: 77-86.

Mashmoushy H, Zhang Z and Thomas CR. Micromanipulation measurement of the mechanical properties of baker's yeast cells. Biotechnology Techniques, 1998; 12: 925-959.

Masouras K, Silikas N and Watts DC. Correlation of filler content and elastic properties of resin-composites. Dental Materials, 2007; In Print.

Matinlinna JP, Lassila LVJ, Ozcan M, Yli-Urpo A and Vallittu PK. An introduction to silanes and their clinical applications in dentistry. International Journal of Prosthodontics, 2004; 17: 155-164.

Matinlinna JP, Lassila LVJ, Kangasniemi I and Vallittu PK. Isocyanato and methacryloxysilanes promote BisGMA adhesion to titanium. Journal of Dental Research, 2005; 84: 360-364.

Matinlinna JP, Lassila LVJ and Vallittu PK. The effect of three silane coupling agents and their blends with cross liner silane on bonding a bis-GMA resin to silicatized titanium (a novel silane system). Journal of Dentistry, 2006; 34: 436-443.

McCabe JF and Carrick TE. A statistical approach to the mechanical testing of dental materials. Dental Materials, 1986; 2: 139-142.

McCabe JF and Walls AWG. Applied dental materials. Blackwell Publishing, 1990a; ($8^{th}$ Edition): Chapters 1, 22, 24 and 25.

McCabe JF, Carrick TE, Chadwick RG and Walls AWG. Alternative approaches to evaluating the fatigue characteristics of materials. Dental Materials, 1990b; 6: 24-28.

McCabe JF. Resin-modified glass-ionomers. Biomaterials, 1998; 19: 521-527.

McClory C, McNally T, Brennan GP and Erskine J. Thermosetting polyurethane multi-walled carbon nanotube composites. Journal of Applied Polymer Sciences, 2007; 105: 1003-1011.

McColm IJ. Cracked indents-friend or foe? Their use in toughness and brittleness characterization. In: Ceramic Hardness, Plenum Press, 1990; New York.

McNally T, Potschke P, Halley P, Murphy M and Martin D, Bell SEJ, Brennan GP, Bein D, Lemoine P and Quin JP. Polyurethane multiwalled carbon nanotube composites. Polymer, 2005; 46: 8222-8232.

McKinney JE and Wu W. Chemical softening and wear of dental composites. Journal of Dental Research, 1985: 64; 1326-1331.

Meskin LH. Do no harm. Journal of the American Dental Association, 2001; 132; 1200-1201.

Mjör IA.The reasons for replacement and the age of failed restorations in general dental practice. Acta Odontology Scandinavia, 1997; 55: 58-63.

Mjör IA, Moorhead JE and Dahl JE. Selection of restorative materials in permanent teeth in general dental practice. Acta Odontology Scandinavia, 1999; 57: 257-262.

Michalske JJ and Freiman SW. A molecular interpretation of stress corrosion in silica. Nature, 1982; 295: 511-512.

Millich F, Jeang L, Eick JD, Chappelow CC and Pinzino CS. Elements of light-cured epoxy-based dental polymer systems. Journal of Dental Research, 1998; 77: 603-608.

Mitchell RJ and Okabe T. Setting reactions in dental amalgam, part 1, phases and microstructures between one hour and one week. Critical Review of Oral and Biological Medicine, 1996; 7: 12-22.

Mitchell RJ, Koike M and Okabe T. Posterior amalgam restorations- usage, regulation and longevity. The Dental Clinics of North America, 2007; 51: 573-589.

Mitra SB, Dong W and Holmes BN. An application of nanotechnology in advanced dental materials. Journal of the American Dental Association, 2003; 134: 1382-1390.

Mohsen NM and Craig RG. Hydrolytic stability of silanated zirconia-silica-urethane dimethacrylate composites. Journal of Oral Rehabilitation, 1995; 22: 213-220.

Momoi Y and McCabe JF. Hygroscopic expansion of resin based composites during 6 months of water storage. British Dental Journal, 1994; 176: 91-96.

Moszner N and Salz U. New developments of polymeric dental composites. Program of Polymer Science, 2001; 26: 535-576.

Moszner N and Klapdor S. Nanotechnology for dental composites. International Journal of Nanotechnology, 2004; 1: 130156.

Moszner N, Gianasmidis A, Klapdohr S, Fischer UK and Rheinberger V. Sol-gel materials 2. light-curing dental composites based on ormocers of crosslinking alkoxsilane methacrylates and further nano-components. Dental Materials, 2007a; In Print.

Moszner N, Fischer UK, Angermann J and Rheinberger V. A partially aromatic urethane dimethacrylate as a new substitute for BisGMA in restorative composites. Dental Materials, 2007b; 24: 694-699.

Mota EG, Oshima HMS, Burnett LH, Pires LAG and Rosa RS. Evaluation of diametral tensile strength and knoop microhardness of five nanofilled composites in dentine and enamel shades. Stomatologija, Baltic Dental and Maxillofacial Journal, 2006; 8: 67-69.

Müller E, Chung JT, Zhang Z and Sprauer A. Characterization of the mechanical properties of polymeric chromatographic particles by micromanipulation. Journal of Chromatography A, 2005; 1097: 116-123.

Mui SS, Sellinger A and Yap AUJ. Dental nanocomposites. Current Nanoscience, 2006; 2: 373-381.

Munksgaard EC and Freund M. Enzymatric hydrolysis of (di)methacrylates and their polymers. Scandinavian Journal of Dental Research, 1990; 98: 261-267.

Musanje L, Shu M and Darvell BW. Water sorption and mechanical behaviour of cosmetic direct restorative materials in artificial saliva. Dental Materials, 2001; 17: 394-401.

Musanje L and Darvell BW. Aspects of water sorption from air, water and artificial saliva in resin composite restorative materials. Dental Materials, 2003; 19: 414-422.

Nash RW, Lowe RA and Leinfelder K. Using packable composites for posterior restorations. Journal of the American Dental Association, 2001; 132: 1099-1104.

Nicholson JW. Chemistry of glass-ionomer cements: a review. Biomaterials, 1998; 19: 485-494.

Nishiyama N, Ishizaki T, Horie K, Tomari M and Someya M. Novel polyfunctional silanes for improving hydrolytic stability at the polymer-silica interface. Journal of Biomedical Materials Research, 1991; 25: 213-221.

Nishiyama N, Komatsu K, Fukai K, Nemoto K and Kumagi M. Influence of adsorption characteristics of silane on the hydrolytic stability of silane at the silica-matrix interface. Composite, 1995; 26: 309-313.

Oberholzer TG, Pameijer CH, Grobler SR and Rossouw RJ. The effect of different power densities and method of exposure on the marginal adaptation of four light-cured dental restorative materials. Biomaterials, 2003; 24: 3593-3998.

Ogliari FA, Ely C, Zanchi CH. Fortes CBB, Smuel SMW, Demarco FF, Petzhold CL and Piva E. Influence of chain extender length of aromatic dimethacrylates on polymer network development. Dental Materials, 2008; 24: 165-171.

Okamoto A, Sekiya K, Fukushima M and Iwaku M *In vivo* wear pattern of an experimental light-cured hybrid composite resin. Dental Materials Journal, 1993; 12: 225-232.

Opdam NJM, Roeters JJM, Joosten M and Veeke O. Porosities and voids in Class I restorations placed by six operators using a packable or syringable composite. Dental Materials, 2002; 18: 58-63.

Opdam NJM, Loomans BAC, Roeters FJM and Bronkhorst. Five-year clinical performance of posterior resin composite restorations placed by dental students. Journal of Dentistry, 2004; 32: 379-383.

Opdam NJM, Bronkhorst EM, Roeters JM and Loomans BAC. A retrospective clinical study on longevity of posterior composite and amalgam restorations. Dental Materials, 2007; 23: 2-8.

Ortengren U, Andersson F, Elgh U, Terselius B, Karlsson S. Influence of pH and storage time on the sorption and solubility behaviour of three composite resin materials. Journal of Dentistry, 2001; 29: 35-41.

Øysæd H and Ruyter IE. Water sorption and filler characteristics of composites for use in posterior teeth. Journal of Dental Research, 1986; 65: 1315-1318.

Paffenbarger GC, Nelsen RJ and Sweeney WT. Direct and indirect filling resins: a review of some physical and chemical properties. Journal of the American Dental Association, 1953; 47: 516-524.

Pain S. Quicksilver quacks. New Scientist, 2001; 2317; 52-53.

Palin WM, Fleming GJP and Marquis PM. An evaluation of the technique of a hydrothermal low-fusing dental ceramic. Journal of Dentistry, 2001; 29: 443-449.

Palin WM, Fleming GJP, Burke FJT, Marquis PM and Randall RC. Monomer conversion versus flexure strength of a novel dental composite. Journal of Dentistry, 2003a; 31: 341-351.
Palin WM, Fleming GJP, Burke FJT, Marquis PM and Randall RC. The reliability in flexural strength testing of a novel dental composite. Journal of Dentistry, 2003b; 31: 549-557.

Palin WM, Fleming GJP, Nathwani H, Burke FJT and Randall RC. *In vitro* cuspal deflection and microleakage of maxillary premolars restored with novel low-shrink dental composites. Dental Materials, 2005a; 21: 324-335.

Palin WM, Fleming GJP, Burke FJT, Marquis PM, Pintado MR, Randall RC and Douglas WH. The frictional coefficients and associated wear resistance of novel low shrink resin-based composites. Dental Materials, 2005b; 21: 1111-1118.

Palin WM, Fleming GJP, Burke FJT, Marquis PM and Randall RC. The influence of short and medium-term water immersion on the hydrolytic stability of novel low-shrinkage dental composites. Dental Materials, 2005c; 21: 852-863.

Palin WM, Fleming GJP and Marquis PM. The reliability of standardized flexure strength testing procedures for a light activated resin-based composite. Dental Materials, 2005d; 21: 911-919.

Palin WM, Senyilmaz DP, Marquis PM and Shortall AC. Cure width potential for MOD resin composite molar restorations. Dental Materials, 2008; In Print.

Pallav P, de Gee AJ, Davidson CL, Erickson RL and Glasspoole EA. The influence of admixing microfiller to small-particle composite resin on wear, tensile strength, hardness and surface roughness. Journal of Dental Research, 1989; 68: 489-490.

Papadogiannis Y, Lakes RS, Palaghias G, Antoniades MH and Papadogiannis D. Fatigue of dental composites. Dental Materials, 2006; 23: 235-242.

Pearson J. Long-term water sorption and solubility of composite filling materials. Journal of Dentistry, 1979; 7: 64-68.

Pereira SG, Osorio R, Toledano M, Cabrerizo-Vilchez MA, Nunes TG and Kalachandra S. Novel light-cured resins and composites with improved physiochemical properties. Dental Materials, 2007; 23: 1189-1198.

Petrovic LM and Atanackovic TM. A model for shrinkage strain in photo polymerization of dental composites. Dental Materials, 2008; 24: 556-560.

Peuman M, Kanumilli P, Munck JD, Landuyt KV, Lambrechts P and Meerbeek BV. Clinical effectiveness of contemporary adhesives: a systemic review of current clinical trails. Dental Materials, 2005; 21: 864-881.

Peutzfeldt A. Resin composites in dentistry: the monomer systems. European Journal of Oral Science, 1997; 105: 97-116.

Peutzfeldt A and Asmussen E. The effect of postcuring on quantity of remaining double bonds, mechanical properties and *in vitro* wear of two resin composites. Journal of Dentistry, 2000; 28: 447-452.

Philips RW. Skinner's Science of Dental Materials. WB Saunders Company, 1991; (9th Edition): Chapters 1, 17 and 18.

Piddock V, Marquis PM and Wilson HJ. The mechanical strength and microstructure of all-ceramic crowns. Journal of Dentistry, 1987; 15: 153-158.

Polydorou O, Trittler R, Hellwig E and Kummerer K. Elution of monomers from two conventional dental composite materials. Dental Materials, 2007; 23: 1535-1541.

Powers JM and Sakaguchi RL. Craig's Restorative Dental Materials. Mosby Elsevier, 2007; (12th Edition): Chapter 1.

Price RBT, Felix CA and Andreou P. Third-generation vs a second generation curing light: effect on knoop microhardness. Compendium, 2006; 27: 490-497.

Quance SC, Shortall AC, Harrington E and Lumley PJ. Effect of exposure and post-cure temperature storage on hardness of contemporary photo-activated composites. Journal of Dentistry, 2001; 29: 553-560.

Rawls HR, Wellinghoff VT, Norling BK, Leamon SH, Swynnerton NF and Wellinghoff ST. Low shrinkage resin from liquid crystal disacrylate monomers. Polymer Preprints, 1997; 38: 167-168.

Ritchie RO. Mechanics of fatigue crack propagation in metals, composites and ceramics: role of crack-tip shielding. Materials Science and Engineering, 1988; 103A: 15-28.

Ritter JE. Predicting lifetimes of materials and material structures. Dental Materials, 1995a; 11: 142-146.

Ritter JE. Critiques of test methods for lifetime predictions. Dental Materials, 1995b; 11: 147-151.

Ritter JE, Grayeski W and Lardner TJ. Cyclic fatigue-crack growth along polymer/glass interfaces. Polymer Engineering Science, 1996; 36: 2382-2388.

Robin C, Scherrer SS, Wiskot HWA. Rijk WG and Belser UC. Weibull parameters of composite resin bond strengths to porcelain and noble alloy using the Rocatec system. Dental Materials, 2002; 18: 389-395.

Roesler FC. Brittle fractures near equilibrium. Proceedings of the Physical Society (London), 1956; B69, 55: 981- 992.

Roeters FJM, Opdam NJM and Loomans BAC. The amalgam free dental school. Journal of Dentistry, 2004; 32: 371-377.

Rokicki G. Aliphatic cyclic carbonates and spiroorthocarbonates as monomers. Progress in Polymer Science, 2000; 25: 259-342.

Roulet JF. Degradation of dental polymers. Basal, Karger; New York, 1987; (1st Edition): Chapter 2.

Roulet JF. Benefits and disadvantages of tooth-coloured alternatives to amalgam. Journal of Dentistry, 1997; 25: 459-473.

Roeters FJM, Opdam NJM and Loomans BAC. The amalgam free dental school. Journal of Dentistry, 2004; 32: 371-377.

Rudnick A, Hunter AR and Holden. An analysis of the diametral-compression test. Materials Research and Standards, 1963; 3: 283-289.

Rueggeberg FA, Ergle JW and Lockwood PE. Effect pf photoinitiator level on properties of a light-cured and post-cure heated model resin system. Dental Materials, 1997; 13: 360-364.

Rueggeberg FA, Ergle JW and Mettenburg DJ. Polymerisation depths of contemporary light-curing units using microhardness. Journal of Esthetic Dentistry, 2000; 12: 340-349.

Rueggeberg FA. From vulcanite to vinyl, a history of resins in restorative dentistry. Journal of Prosthetic Dentistry, 2002; 87: 364-379.

Ruyter IE and Svendsen SA. Composition of dental resins and composite materials. Acta Odontology Scandinavia, 1978; 36: 75-82.

Ruyter IE and Øysæd H. Conversion in different depths of ultraviolet and visible light activated composite materials. Acta Odontology Scandinavia, 1982; 40: 179-192.

Sabbagh J, Vreven J and Leloop G. Dynamic and static moduli of elastic of resin-based materials. Dental Materials, 2002; 18: 64-71.

Sabbagh J, Ryelandt L, Bacherius L, Biebuyck JJ, Vreven J, Lambrechts P and Leloup G. Characterization of the inorganic fraction of resin composites. Journal of Oral Rehabilitation, 2004; 31: 1090-1101.

Sanda F, Takata T and Endo T. Synethsis and radical polymerisation of spiroorthocarbonates bearing *exo*-methylene groups. Marcomolecules, 1993; 26: 737-743.

Sarkar NK. Internal corrosion in dental composite wear: its significance and simulation. Journal of Biomedical Materials Research, 2000; 53: 371-380.

Sawyer WG, Freudenberg KD, Bhimaraj P and Schadle LS. A study on the friction and wear behaviour of PTFE filled with alumina nanoparticles. Wear, 2003; 254:573-580.

Schreiber CK. Polymethylmethacrylate reinforced with carbon fibres. British Dental Journal, 1971; 130: 29-30.

Schneider LFJ, Moraes RR, Cavalcante LM, Sinhoreti MAC, Correr-Sobrinho L and Consani S. Cross-link density evaluation through softening tests: effect of ethanol concentration. Dental Materials, 2008; 24: 199-203.

Schwartz JI and Söderholm KJM. Effects of filler size, water and alcohol on hardness and laboratory wear of dental composites. Acta Odontology Scandinavia, 2004; 62: 102-106.

Seefeld F, Wenz H-J, Ludwig K and Kern M. Resistance to fracture and structural characteristics of different fiber-reinforced post systems. Dental Materials, 2007; 23: 265-271.

Seventh International Conference on Mercury as a Global Pollutant (7th ICMGP), 2004; Solvenia.

Shetty DK, Rosenfield AR, McGuire P and Duckworth WH. Biaxial flexure tests for ceramics. Ceramic Bulletin, 1980; 59: 1193-1197.

Shintani H, Inoue T and Yamaki M. Analysis of camphorquinone in visible light cured composite resins. Dental Materials, 1985; 1: 124-126.

Shirai K, Yoshida Y, Nakayama Y, Fujitani M, Shintani H, Wakasa K, Okazaki M, Snauwaert J and Van Meerbeek B. Journal of Biomedical Materials Research, 2000; 53; 204-210.

Shiu C, Zhang Z and Thomas CR. A novel technique for the study of bacterial cell mechanical properties. Biotechnology Techniques, 1999; 13: 707-713.

Shortall ACC, Palin WM and Burtscher P. Refractive index mismatch and monomer reactivity influence composite curing depth. Journal of Dental Research, 2008; 87: 84-88.

Sideridou I, Tserki V and Papanastasiou G. Effect of chemical structure on degree of conversion in light-cured dimethacrylate-based dental resins. Biomaterials, 2002; 23: 1819-1829.

Sideridou I, Tserki V and Papanastasiou.. Study of water sorption, solubility and modulus of elasticity of light cured dimethacrylate-based dental resins. Biomaterials, 2003; 24: 655-665.

Smith DC. Recent developments and prospects in dental polymer. Journal of Prosthetic Dentistry, 1962; 12: 1066-1078.

Söderholm KJM. Degradation of glass filler in experimental composites. Journal of Dental Research, 1981; 60: 1867-1875.

Söderholm KJM. Leaking of fillers in dental composites. Journal of Dental Research, 1983; 62: 126-130.

Söderholm KJM, Zigan M, Ragan M, Fischlschweiger W and Bergman M. Hydrolytic degradation of dental composites. Journal of Dental Research, 1984; 63: 1248-1254.

Söderholm KJM and Roberts MJ. Influence of water exposure on the tensile strength of composites. Journal of Dental Research, 1990; 69: 1812-1816.

Söderholm KJM and Shang SW. Molecular orientation of silane at the surface of colloidal silica. Journal of Dental Research, 1993; 72: 1050-1054.

Söderhom KJM, Achanta S and Olsson S. Variables affecting the depth of cure of composites (abstract). Journal of Dental Research, 1993; 72 (Special Issue); 138.

Söderholm KJM, Mukherjee R and Longmate J. Filler leachability of composites stored in distilled water or artificial saliva. Journal of Dental Research, 1996; 75: 1692-1699.

Söderholm KJM and Richards ND. Wear resistance of composites, a solved problem? General Dentistry, 1998; 46: 256-263.

Söderholm KJM and Mariotti A. BisGMA based resins in dentistry: are they safe? Journal of the American Dental Association, 1999; 130: 201-209.

Söderholm KJM, Yang MCK and Garcea I. Filler particle leachability of experimental dental composites. European Journal of Oral Science, 2000; 108: 555-560.

Spencer AJ. Dental amalgam and mercury in dentistry. Australian Dental Journal, 2000; 46: 60-61.

Stanford JW. The current status of restorative resins. Dental Clinics of North America, 1971; 15: 166-173.

Stanley P, Fessler H and Sivill AD. An engineer's approach to the prediction of failure probability of brittle components. Proceedings of the British Ceramic Society, 1973; 22: 452-487.

Stansbury JW, Dickens B and Liu DW. Preparation and characterization of cyclopolymerisable resin formulations. Journal of Dental Research, 1995; 74: 1110-1115.

Stokes AN, Hood JAA and Tidmarsh BG. Effect of 6-month water storage on silane-treated resin/porcelain bonds. Journal of Dentistry, 1988; 16: 294-296.

Sugden KC. Nicholas Dubois de Chemant and the disputed invention of mineral teeth. British Dental Journal, 1983; 155: 202.

Sun G and Zhang Z. Mechanical strength of microcapsules made of different wall materials. International Journal of Pharmacology, 2002; 242: 307-311.

Suzuki S, Leinfelder KF, Kawai K and Tsuchitani Y. Effect of particle variation on wear rates of posterior composites. American Journal of Dentistry, 1995; 8: 173-178.

Takeshige F, Kawakami T, Hayashi M and Ebisu S. Fatigue behaviour of resin composites in aqueous environments. Dental Materials, 2007; 23: 893-899.

Tanoue N, Koishi Y, Matsumura H and Atsuta M. Curing depth of different shades of a photo-activated prosthetic composite material. Journal of Oral Rehabilitation, 2001; 28: 618-623.

Tay FR, Pashley DH and Yoshiyama M. Two modes of nanoleakage expression in single-step adhesives. Journal of Dental Research, 2002; 81: 472-476.

Tay FR, Hashimoto M, Pashley DH, Peters MC, Lai SCN, Yiu CKY and Cheong C. Aging affects two modes of nanoleakage expression in bonded dentin. Journal of Dental Research, 2003a; 82: 537-541.

Tay FR and Pashley DH. Water treeing- a potential mechanism for degradation of dentin adhesives. American Journal of Dentistry, 2003b; 16: 6-12.

Tayal A and Khan SA. Degradation of a water-soluble polymer: molecular weight changes and chain scission characteristics. Macromolecules, 2000; 33: 9488-9493.

Tetric EvoCeram, Scientific Documentation, 2006. Ivoclar Vivadent.

Thoman DR, Bain LE and Ante CE. Inferences on the parameters of the Weibull distributions. Technometrics, 1969; 2: 445-460.

Thompson JY, Anusavice KJ, Nama A and Morri HF. Fracture surface characterization of clinically failed all-ceramic crowns. Journal of Dental Research, 1994; 73: 1824-1832.

Thostenson. Nanocomposites in context: review. Composites Science and Technology, 2005; 65: 491-516.

Tian M, Gao Y, Liao Y, Hedin NE and Fong H. Fabrication and evaluation of BisGMA/TEGDMA dental resins/composites containing nano fibrillar silicate. Dental Materials, 2008; 24: 235-243.

Tilbrook DA, Clarke RL, Howle NE and Braden M. Photocurable epoxy-polyol matrices for use in dental composites I. Biomaterials. 2000; 21: 1743-1753.

Timoshenko S and Woinowsky-Krieger S. Symmetrical bending of circular plates. In: Theory of Plates and Shells. McGraw-Hill; New York, 1959; (2nd Edition).

Toledano M, Osorio R, Osorio E, Fuentes V, Prati C and Garcia-Godoy F. Sorption and solubility of resin-based restorative dental materials. Journal of Dentistry, 2003; 31: 43-50.

Tolle TB and Anderson DP. Morphology development in layered silicate thermoset nanocomposites. Composites Science and Technology, 2002; 63: 1033-1041.

Torbjorner A, Karlsson S, Odman PA. Survival rate and failure characteristics for two post designs. Journal of Prosthetic Dentistry, 1995; 73: 439-444.

Torry SA, Campbell A, Cunliffe AV and Tod DA. Kinetic analysis of organosiliane hydrolysis and condensation. International Journal of Adhesion and Adhesives, 2006; 26: 40-49

Trustrum K and Jayatilaka A. On estimating Weibull modulus for a brittle material. Journal of Materials Science, 1979; 14: 1080-1084.

Turssi CP, Ferracane JL and Vogel K. Filler features and their effects on wear ad degree of conversion of particulate dental resin composites. Biomaterials, 2005; 26: 4932-4937.

Turssi CP, Ferracane JL and Ferracane LL. Wear and fatigue behaviour of nano-structured dental resin composites. Journal of Biomedical Materials Research Part B: Applied Biomaterials, 2006; 78B: 196-203.

Tyas MJ, Jones DW and Rizkalla AS. The evaluation of resin composite consistency. Dental Materials, 1998; 14: 424-428.

Vanlandingham MR, Eduljee and Gillespie JW. Moisture diffusion in epoxy systems. Journal of Applied Polymer Science, 1999; 71: 787-798.

Van Dijk MA, Orrit TM, Lippitz M, Berciaud S, Lasne D, Cognet L and Lounis B. Absorption and scattering microscopy of single metal nanoparticles. Physical Chemistry Chemical Physics, 2006; 8: 3486-3495.

Van Noort R. Introduction to Dental Materials. Mosby Publications, 2007; (3rd Edition): Chapeter 2.2.

Venhoven BA, de Gee AJ, Werner A and Davidson CL. Silane treatment of filler and composite blending in a one-step procedure for dental restoratives. Biomaterials, 1994; 14: 1152-1156.

Venz S and Dickens B. NIR-spectroscopic investigation of water sorption characteristics of dental resins and composites. Journal of Biomedical Materials Research, 1991; 25: 1231-1248.

Visvanathan A, Ilie N, Hickel R and Kunzelmann K-H. The influence of curing times and light curing methods on the polymerization shrinkage stress of a shrinkage optimized composite with hybrid-type prepolymer fillers. Dental Materials, 2007; 23: 777-784.

Wahl N. Orthodontics in three millennia. Chapter 1: antiquity to the mid-19th century. American Journal of Orthodontics and Dentofacial Orthopedics, 2005; 127: 255-259.

Wang CX, Cowen C, Zhang Z and Thomas CR. High-speed compression of single alginate microparticles. Chemical Engineering and Science, 2005; 60: 6649-6657.

Watanabe H, Khera SC, Vargas MA and Qian F. Fracture toughness comparison of six resin composites. Dental Materials, 2008; 28: 418-425.

Watts DC, Amer O and Combe EC. Characteristics of visible-light-activated composite systems. British Dental Journal, 1984; 156: 209-215.

Watts DC and Hindi AA. Intrinsic 'soft-start' polymerisation shrinkage-kinetics in an acrylate-based resin-composite. Dental Materials, 1999; 15: 39-45.

Whitters CJ, Strang R, Brown D, Clarke RL, Curtis RV, Hatton PV, Ireland AJ, Lloyd CH, McCabe JF, Nicholson JW, Scrimgeour SN, Setcos JC, Sherroff M, Noort RV, Watts DC and Wood D. Dental materials:1997 Literature Review. Journal of Dentistry, 1999; 27: 401-435.

Willems G, Lambrechts P, Braem M, Celis JP and Vanherle G. A classification of dental composites according to their morphological and mechanical characteristics. Dental Materials, 1992; 8: 310-319.

Wegner LD and Gibson LJ. The fracture toughness behaviour of interpenetrating phase composites. International Journal of Mechanical Sciences, 2001; 43: 1771-1791.

Wei RP and Simmons GW. Recent progress in understanding environment assisted fatigue crack growth. International Journal of Fracture, 1981; 17: 235-247.

Weibull W. A statistical distribution function of wide applicability. Journal of Applied Mechanics, 1951: 293-297.

Weinmann W, Thalacker C and Guggenberger R. Siloranes in dental composites. Dental Materials, 2005; 21: 68-74.

Whitters CJ, STrang R, Brown D, Clarke RL, Curtis RV, Hatton PV, Ireland AJ, Lloyd CH, McCabe JF, Nicholson JW, Scrimgeour SN, Setcos JC, Sherroff M, Noort RV, Watts DC and Wood D. Dental materials:1997 literature review. Journal of Dentistry, 1999; 27: 401-435.

Williams PD and Smith DC. Measurement of the tensile strength of dental restorative materials by use of a diametral compression test. Journal Dental Research, 1971; 50: 436-442.

Willems G, Lambrechts P, Braem M, Celis JP and Vanherle G. A classification of dental composites according to their morphology and mechanical characteristics. Dental Materials, 1992; 8: 310-319.

Wilson NHF. Curricular issues changing from amalgam to tooth-coloured materials. Journal of Dentistry, 2004; 32: 367-369.

Wilson KS, Zhang K, Atonucci JM. Systematic variation of interfacial phase reactivity in dental noancomposites. Biomaterials, 2005; 26: 5095-5103.

Wright PJF. Comments on an indirect tensile test on concrete cylinders. Magazine of Concrete Research, 1955; 1: 87-96.

Wu W, Sadehipour K, Boberick K and Baran G. Predictive modelling of elastic properties of particulate-reinforced composites. Materials Science and Engineering, 2002; A332: 362-370.

Xu X and Burgess JO. Compressive strength, fluoride release and recharge of fluoride-release materials. Biomaterials, 2003; 24: 2451-2461.

Yang L, Wang J, Hong J, Santerre JP and Pilliar RM. Synthesis and characterization of a novel polymer-ceramic system for biodegradable composite applications. Journal of Biomedical Research, Part A, 2003; 66: 622-632.

Yap AUJ. Post-irradiation hardness of resin-modified goass ionomer cements and a polyacid-modified composite resin. Journal of Materials Science, 1997; 8: 413-416.

Yap AUJ, Lee HK and Sabapathy R. Release of methacrylic acid from dental composites. Dental Materials, 2000; 16: 172-179.

Yap AUJ, Chew CL, Ong LFKL and Teoh SH. Environmental damage and occlusal contact wear of composite restorations. Journal of Oral Rehabilitation, 2002; 29: 87-97.

Yap AUJ, Lim LY, Yang TY, Ali A and Chung SM. Influence of dietary solvents on strength of nanofill and ormocer composites. Operative Dentistry, 2005; 30: 129-133.

Yoshida K and Greener EH. Effect of photoinitiator on degree of conversion of unfilled light-cured resin. Journal of Dentistry, 1994; 22: 296-299.

Yoshida U, Meerbeek BV, Nakayama Y, Okazaki M Snauwaert J, Hellemans K, Lambrechts P, Vanherle G and Wakasa K. Evidence of chemical bonding at biomaterial-hard tissue interfaces. Journal of Dental Research, 2000; 79: 709-714.

Yip HK and Samaranayaka LP. Caries removal techniques and instrumentation: a review. Clinical Oral Investigations, 1998; 2: 148-154.

Youdelis WV. Dental amalgam, 1967; US Patent No. 3305356.

Zeschky J, Lo J, Höfner T and Greil. Mg alloy infiltrated Si-O-Si ceramic foams. Materials Science and Engineering A, 2005; 403: 215-221.

Zhang Z, Ferenczi MA, Lush AC and Thomas CR. A novel micromanipulation technique for measuring the bursting strength of single mammalian cells, 1991. Applied Microbiology and Biotechnology; 36: 208-210.

Zhang Z, Ferenczi MA and Thomas CR. A micromanipulation technique with a theoretical cell model for determining mechanical properties of single mammalian cells. Chemical Engineering and Science, 1992; 47: 1347-1354.

Zhang YZ, Su B, Ramakrishna S and Lim T. Chitosan nanofibers from an easily electrospinable UHMWPEO-doped chitosan solution system. Biomacromolecules, 2008; 9: 136-141.

## APPENDIX OF PRELIMINARY STUDIES

### Appendix 1 Micromanipulation of supplied FSB and silanated GR

'Nanocluster' filler particulates separated from the resin matrix using the dissolution method and irregular fillers supplied by the manufacturer coated with a silane coupling agent were tested using the micromanipulation technique (Section 3.2.1). The hypothesis was;

1. The fracture mechanisms of the 'nanoclusters' separated using the dissolution technique (Section 3.2.1.1) would be comparable with those of 'nanoclusters' supplied by the manufacturer.
2. The mechanical properties of the silanated and unsilanated irregular particulates (GR) would be comparable.

Kruskal-Wallis & Mann Whitney U tests highlighted no significant difference between the force at fracture of the 'nanoclusters' supplied by 3M (FSB) and those separated from the unpolymerized resin matrix ($FSB_{(sep)}$) (P>005) (Figure A1a). Z-tests of the fractures did not highlight a significant difference between the occurrences of multiple fractures (P=0.76). Likewise, statistical analysis and z-tests of the silanated and unsilanted irregular filler failed to highlight a significant difference (P>0.05). Furthermore, comparison of the pseudo-modulus of stress of the supplied and separated 'nanoclusters' and of the silanated and unsilanated irregular fillers highlighted no significant difference (P>0.05) (Figure A1b).

Consequently, both hypotheses were accepted and it was concluded the fillers selected for the investigation were representative of the failure mechanisms fillers underwent.

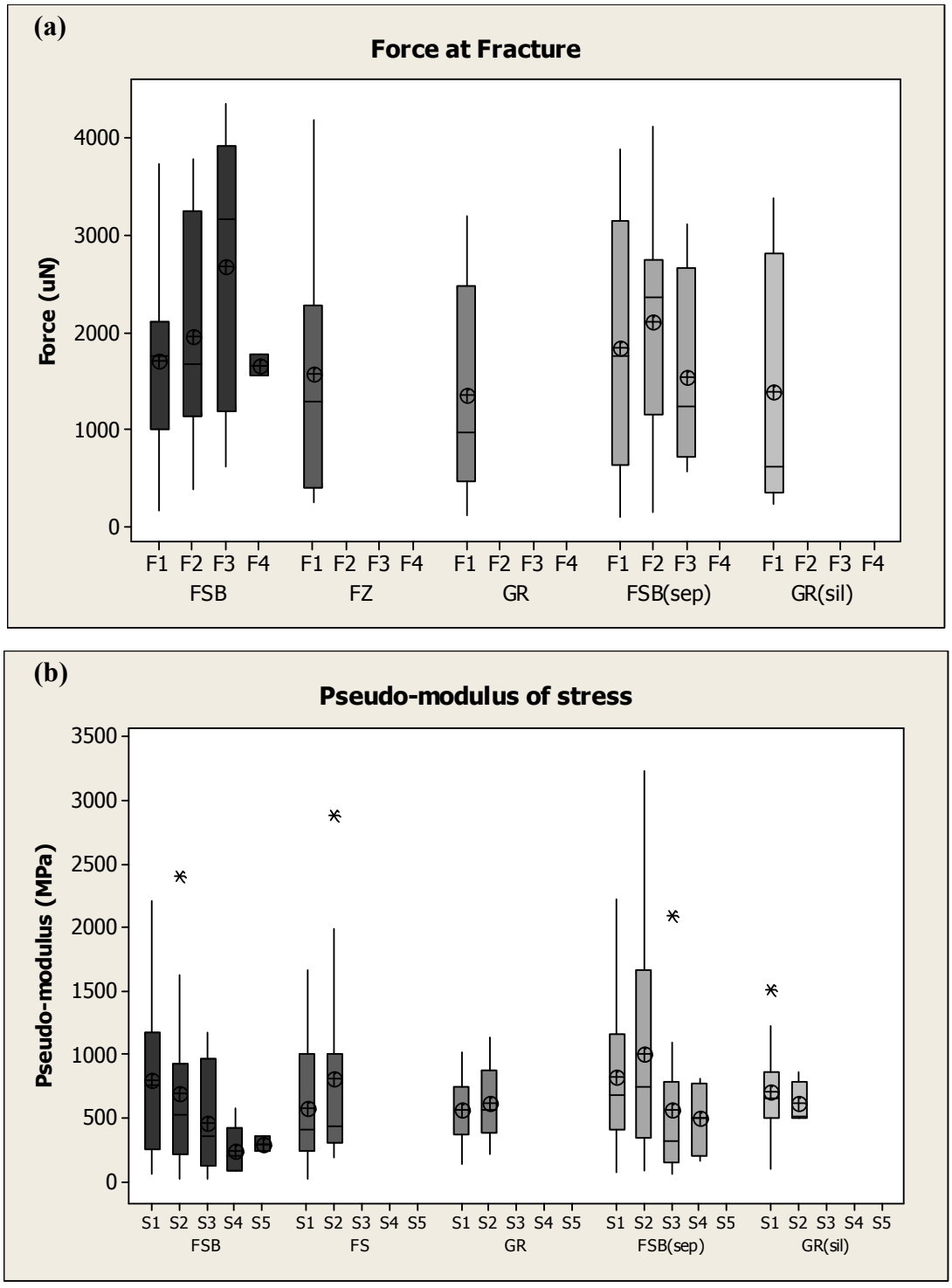


**Figure A1. Box and whisker plots highlighting the range and mean (a) force at fracture (µN) and (b) pseudo-modulus of stress of FSB, FZ, GR fillers and also FSB fillers separated by dissolution and silanated GR fillers following analysis using the micromanipulation technique.**

## Appendix 2 Oven-LCU

The Vickers surface hardness of disc-shaped specimens of FZ following the recommended 20s irradiation period using a handheld-LCU was identified to be 94±4.2. Subsequently, to attain a comparable degree of cure for the beam-shaped specimens produced using the oven-LCU an approximately equivalent surface hardness was sought.

| Curing time (mins) | 1 | 4 | 8 | 11 | 14 | 18 |
|---|---|---|---|---|---|---|
| Surface hardness (VHN) | 33 (2.7) | 62 (3.3) | 82 (1.9) | 88 (3.4) | 93 (3.1) | 92 (3.9) |

**Table A1. Vickers surface hardness of FZ specimens following selected curing periods within the oven-LCU to obtain a compared degree of cure to that of the handheld Optilux 501 LCU.**